

Fracture Coalescence in Natural Rocks

by

Ariel R. Martinez

Ingeniero Civil
Universidad de Buenos Aires, Argentina, 1996

SUBMITTED TO THE DEPARTMENT OF CIVIL AND ENVIRONMENTAL
ENGINEERING IN PARTIAL FULFILLMENT OF THE REQUIREMENTS
FOR THE DEGREE OF

MASTER OF SCIENCE IN CIVIL AND ENVIRONMENTAL ENGINEERING
AT THE
MASSACHUSETTS INSTITUTE OF TECHNOLOGY

FEBRUARY 1999

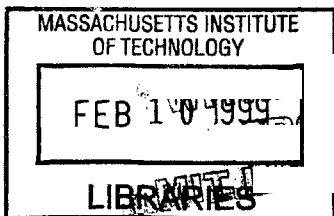
© 1999 Massachusetts Institute of Technology.
All rights reserved.

Signature of Author: _____
Ariel R. Martinez
Department of Civil and Environmental Engineering
January, 15 1999

Certified by: _____
Herbert H. Einstein
Professor of Civil and Environmental Engineering
Thesis Supervisor

Handwritten signature

Accepted by: _____
Andrew, J. Whittle
Chairman, Departmental Committee on Graduate Studies



Fracture Coalescence in Natural Rocks

by

Ariel R. Martinez

Submitted to the Department of Civil and Environmental Engineering
on January 15, 1999 in Partial Fulfillment of the
Requirements for the Degree of Master Of Science
in Civil and Environmental Engineering

ABSTRACT:

Crack initiation, propagation, and coalescence is being investigated in uniaxial compression tests on granite and marble. The specimens contain two parallel flaws, cut through the thickness, which are arranged at different distances and angles. These pre-existing fractures or "flaws" are cut with a water jet in the prismatic specimens (6" height, 3" wide, and 1.25" thick). The basic measurements and observations include crack initiation stress, coalescence stress, failure stress, crack initiation angle, and crack pattern, focusing particularly on the coalescence mechanisms of the two flaws. Under uniaxial static loading, two types of cracks emanate from the flaws: wing cracks, which are tensile cracks, and shear cracks. Two ways of assessing the crack type are employed: (1) observing the relative displacement when the fracture is created, which is done with a high-speed camera, and (2) fractography. Wing cracks are generally stable and tend to align with the direction of maximum compression. Shear cracks also initiate in a stable manner but in a direction coplanar to the flaw. Coalescence is produced by an unstable propagation of either internal crack type (i.e. wing or shear). Results in granite and marble show that five types of coalescence occur for non-overlapping geometries, namely: (I) Coalescence of internal shear cracks emanating from the tips. (II) Coalescence of internal shear cracks through a tension crack. (III) Coalescence of an internal wing crack and an internal shear crack. (IV) Coalescence of two internal wing cracks and (IVB) coalescence through only one internal wing crack. These results are consistent with preceding research results on molded gypsum.

Thesis Supervisor: Herbert H. Einstein

Title: Professor of Civil and Environmental Engineering

Acknowledgments

The writing of this page, left on purpose for the end, means a closure of a phase. I want to express my sincere gratitude to:

Prof. Herbert Einstein for extending his great advice and support further than the research aspects.

Beatriz Fidalgo-Valverde, who worked in this project as part of her Master's Degree requirements (for Camborne School of Mines, UK). Her mineralogy studies, as well as the fractography pictures and some of the analyses in granite are included in this thesis.

Prof. Charles Ladd, Dr. J. Germaine and Prof. Whittle for teaching and showing me the principles of "academic life".

Stephen Rudolph in the Civil Engineering Department, Tony Caloggero in the Edgerton Lab and Gerald Wentworth in the LMP for their technical advice and patience when I was developing the lab procedure and learning how to use their equipment.

All of my grad students "colleagues" for making a nice working environment.

Cynthia Stewart for her support and concern about my "sleeping time".

My friends at MIT and around the world for sharing both the "good stuff" and "the load" in the not-so-nice times of grad school. I have to mention Miguel here who has been an always-accessible ear (plus a good cook), and Bea (for the second time in this page) for "not turning off the light at the end of the tunnel".

My family: my brother Ivan, my nephew Iñaki (brave hot-dog eater), and my father; my grandparents (Romeo y María) for teaching me "good" life habits; my mom for showing me through her example that every problem can be tackled and solved (por el medio, de frente y con fuerza), teaching me that the world is wide, and of course, supporting my "extra-MIT" expenses. Iva, who has been an excellent "life-mate" always supporting all of my plans and showing me a different perspective of life in general. Alberto, my "souls" godfather for helping me realize that everything is possible.

Prof. Eduardo Nuñez in Buenos Aires, for introducing me into the "geotech" field and teaching me "not to accept easy problems".

To all of you, and everyone else, who encouraged me, thanks.

Para Ma...

Table of Contents

Title Page	1
Abstract	2
Acknowledgments	3
Dedication	4
Table of Contents	5
List of Tables	9
List of Figures	10
Chapter 1: INTRODUCTION	21
1.1 General Overview	21
1.2 Objective and organization of this dissertation	22
Chapter 2: BACKGROUND AND FORMER RESULTS	27
2.1 Fracture Mechanics	27
2.2 Specimens with a single flaw	29
2.3 Specimens with multiple flaws	33
Chapter 3: SPECIMEN CHARACTERISTICS AND EXPERIMENTAL PROCEDURE	58
3.1 Specimen geometry	58
3.2 Overview of Granite and Marble Specimen Preparation	59
Chapter 4: EXPERIMENTAL RESULTS	64
4.1 Introduction	64
4.2 Material Properties	65
4.2.1 Granite properties.....	65
4.2.2 Marble properties.....	66

4.2.3 Other material properties.....	67
4.3 Fracture coalescence.....	67
4.3.1 General coalescence types.....	68
4.3.2 Fracture coalescence in granite.....	71
4.3.3 Fracture coalescence in marble.....	72
4.4 Sequence and pattern of crack growth.....	72
4.4.1 Granite results.....	73
4.4.2 Marble results.....	81
4.5 Relationship between failure stress and coalescence stress.....	87
4.5.1 Granite results.....	87
4.5.2 Marble results.....	87
4.6 Fractography.....	88
4.6.1 Introduction.....	88
4.6.2 Background.....	88
4.6.3 Former Results in Gypsum.....	89
4.6.4 Fractography Observations in Granite	90
4.6.5 Fractography Observations in marble.....	93
4.6.6 Sources of error.....	93
4.7 Influence of flaws in stiffness.....	94
Chapter 5: CONCLUSION.....	169
5.1 General results.....	169
5.2 Granite results.....	171
5.3 Marble results.....	173
5.4 Comparison with gypsum and former results.....	173
5.5 Guidelines for further research.....	175
Appendix A: LAB PROCEDURE.....	177
A.1 Cutting Rock.....	177
A.1.1 Overhead Saw.....	177

A.1.2	Cutting with the overhead saw.....	178
A.1.3	Precision Saw.....	180
A.1.4	Cutting with the precision saw.....	181
A.1.5	Belt Sander (For marble)	183
A.1.6	Polishing Marble Specimens.....	183
A.2	Making Gypsum Specimens.....	184
A.2.1	Molding.....	185
A.2.2	Polishing.....	191
A.2.3	Cutting.....	193
A.2.4	Curing.....	193
A.3	Cutting the Flaws.....	194
A.3.1	Water Jet Machine.....	194
A.3.2	Cutting with the water jet machine.....	199
A.4	Load Testing.....	208
A.4.1	TV, VCR, Camera, Microscope, and Light.....	208
A.4.2	Baldwin 200 Kips Loading Machine.....	210
A.4.3	Other Issues Affecting Load Testing.....	212
A.4.4	Load Testing.....	214
A.4.5	High Speed Camera.....	220
A.4.6	Using the High Speed Camera.....	223
A.4.7	Processing data.....	228
A.4.8	Image Processing.....	230
Appendix B:	STRESS-STRAIN PLOTS IN GRANITE.....	294
Appendix C:	STRESS-STRAIN PLOTS IN MARBLE.....	309
Appendix D:	LAB EQUIPMENT IMPROVEMENT ALTERNATIVES.....	323
D.1	Introduction.....	323
D.2	Overview of existing equipment.....	323
D.3	Equipment to be acquired.....	324

D.3.1 High-speed camera.....	324
D.3.2 PC.....	326
D.3.3 (Post-mortem) Image processing software.....	326
D.4 Alternatives.....	327
D.4.1	327
D.4.2	328
D.4.3	328
D.4.4	329
D.4.5	329
D.5 Accessories	330
References.....	337
Biographical note.....	341

List of Tables

Table 3.1:	Flaw geometries for granite and marble specimens.....	61
Table 3.2:	Steps to prepare and test prismatic pre-cracked specimens.....	62
Table 4.1:	Coalescence and failure stress on granite specimens.....	96
Table 4.2:	Coalescence and failure stress on marble specimens.....	99
Table 4.3:	Other material properties.....	101
Table 4.4:	Coalescence modes for different flaw geometries.....	102
Table 4.5:	Relationship between spacing/continuity and coalescence type. After Bobet (1997)	102
Table 4.6:	Relationship between ligament length and coalescence stress for granite specimens with coplanar geometries (show type I coalescence)	103
Table 4.7:	Relationship between ligament length and coalescence stress for granite specimens with non-coplanar geometries that show type II coalescence ...	103
Table 4.8:	Order of appearance of the different cracks and stress levels observed in granite specimens.....	104
Table 4.9:	Order of appearance of the different cracks and stress levels observed in marble specimens.....	105
Table A.1:	Mold number and geometry for gypsum specimens.....	233
Table D.1:	Recording time [sec] and frame storage capacity of Motion Scope 1,000S Motion System.....	331

List of Figures

Figure 1.1a:	Rock slope with coalescence of non-persistent joints forming a failure surface.....	24
Figure 1.1b:	Sides slopes controlled by joints in an open channel excavation, from Eshwaraiah and Upadhyaya (1990)	25
Figure 1.2a:	Critical block in an underground opening formed by fracture coalescence.....	25
Figure 1.2b:	Example of critical block in a shallow tunnel, from Karaca (1995).....	26
Figure 2.1:	Length of stable crack propagated from an elliptical flaw under compressive stress conditions, from Hoek (1967).....	37
Figure 2.2:	Crack propagation in tension, from Atkinson (1987)	38
Figure 2.3:	Fracture propagation in compression. Shear across the bridge, from Rock Mechanics Principles, Coates D.	39
Figure 2.4:	Types of cracks according to mode of loading.....	40
Figure 2.5:	Prismatic rock specimens with flaws cut through the thickness.....	41
Figure 2.6:	Single flaw specimens of plaster of Paris, from Lajtai (1974)	42
Figure 2.7:	Single flaw specimen of limestone, Ingraffea and Heuze (1980)	42
Figure 2.8:	Single flaw specimens of sandstone, after Petit and Barquins (1988)	43
Figure 2.9:	Single flaw specimen of marble, from Jiefan et. al. (1990)	43
Figure 2.10:	Single flaw specimen of marble, from Chen et. al. (1992)	44
Figure 2.11:	Wrapping in a single 3-D flaw specimen, from Dyskin et. al. (1995)	45
Figure 2.12:	Wing crack growth pattern, from “The Fracture of Rock”.....	46
Figure 2.13:	Crack patterns in Carrara marble (3 to 5 flaw specimens), from Chen et. al. (1992)	47

Figure 2.14: Crack development and failure of kaolinite specimens subjected to direct shear, from L. Vallejo (1987)48

Figure 2.15: Patterns of crack coalescence observed by Wong and Chau (1998).....49

Figure 2.16: Flaw geometry used by Reyes (1991) and Shen et. al. (1995)50

Figure 2.17 Non-overlapping and overlapping geometries.....50

Figure 2.18: Crack pattern in gypsum specimens in uniaxial compression for overlapping geometries, after Reyes (1991)51

Figure 2.19: Crack pattern in gypsum specimens in uniaxial compression for non-overlapping geometries, after Shen et. al. (1995)52

Figure 2.20: Dimensions and shape of specimens used by Bobet (1997) and in the present research.....53

Figure 2.21: Types of coalescence, from Bobet (1997). The results for overlapping geometries are from Reyes (1991)54

Figure 2.22: Coalescence type I in gypsum specimens,, from Bobet (1997)55

Figure 2.23: Coalescence type II in gypsum specimens,, from Bobet (1997)56

Figure 2.24: Coalescence type III in gypsum specimens,, from Bobet (1997)57

Figure 3.1: Flaw geometry in a two flaw specimen.....63

Figure 3.2: Flaw geometry in a jointed slope.....63

Figure 4.1: Coalescence modes in granite and marble specimens.....106

Figure 4.2: Stress-strain plots for granite intact (no flaws) specimens..... 107

Figure 4.3: Failure of an intact granite specimen.108

Figure 4.4: Different rock failure modes, from Gramberg (1989)108

Figure 4.5: Failure due to horizontal cracks.....109

Figure 4.6: Stress-strain plots for marble intact (no flaws) specimens..... 109

Figure 4.7: Failure of an intact marble specimen. Failure by shearing.....110

Figure 4.8:	Failure due non-centered load and/or bending moment.....	110
Figure 4.9:	Variation of coalescence stress with ligament length for all the specimens (granite and marble)	111
Figure 4.10:	Variation of coalescence stress with ligament length for coplanar geometries in granite (geometries with coalescence type I)	112
Figure 4.11:	Variation of coalescence stress with ligament length for non-coplanar geometries in granite (geometries with coalescence type II)	112
Figure 4.12:	Variation of coalescence stress with ligament length for coplanar geometries in marble (geometries with coalescence type I)	113
Figure 4.13:	Variation of coalescence stress with ligament length for non-coplanar geometries in marble (geometries with coalescence type II)	114
Figure 4.14:	Crack pattern for granite geometry 45-0-a.....	115
Figure 4.15:	Crack pattern for granite geometry 60-0-a.....	117
Figure 4.16:	Crack pattern for granite geometry 60-0-2a.....	118
Figure 4.17:	Crack pattern for granite geometry 30-0-a.....	119
Figure 4.18:	Crack pattern for granite geometry 30-0-2a.....	120
Figure 4.19:	Crack pattern for granite geometry 45-0-2a.....	121
Figure 4.20:	Crack pattern for granite geometry 60-0-3a.....	123
Figure 4.21:	Crack pattern for granite geometry 30-a-a.....	124
Figure 4.22:	Crack pattern for granite geometry 30-a-2a.....	125
Figure 4.23:	Crack pattern for granite geometry 45-a-2a.....	126
Figure 4.24:	Crack pattern for granite geometry 60-a-2a.....	127
Figure 4.25:	Crack pattern for granite geometry 45-2a-2a.....	128
Figure 4.26:	Crack pattern for granite geometry 30-2a-2a.....	129
Figure 4.27:	Crack pattern for granite geometry 45-a-a.....	130

Figure 4.28:	Crack pattern for marble geometry 45-0-a.....	131
Figure 4.29:	Crack pattern for marble geometry 60-0-a.....	132
Figure 4.30:	Crack pattern for marble geometry 60-0-2a.....	133
Figure 4.31:	Crack pattern for marble geometry 30-0-a.....	134
Figure 4.32:	Crack pattern for marble geometry 30-0-2a.....	135
Figure 4.33:	Crack pattern for marble geometry 45-0-2a.....	136
Figure 4.34:	Crack pattern for marble geometry 30-a-2a.....	137
Figure 4.35:	Crack pattern for marble geometry 30-2a-2a.....	138
Figure 4.36:	Crack pattern for marble geometry 30-a-a.....	139
Figure 4.37:	Crack pattern for marble geometry 60-a-2a.....	140
Figure 4.38:	Crack pattern for marble geometry 45-2a-2a.....	141
Figure 4.39:	Crack pattern for marble geometry 45-a-2a.....	142
Figure 4.40:	Crack pattern for marble geometry 45-a-a.....	143
Figure 4.41:	Coalescence stress Vs. failure stress for granite specimens with flaw inclination angle $\beta = 30$	144
Figure 4.42:	Coalescence stress Vs. failure stress for granite specimens with flaw inclination angle $\beta = 45$	144
Figure 4.43:	Coalescence stress Vs. failure stress for granite specimens with flaw inclination angle $\beta = 60$	145
Figure 4.44:	Coalescence stress Vs. failure stress for marble specimens with flaw inclination angle $\beta = 30$	146
Figure 4.45:	Coalescence stress Vs. failure stress for marble specimens with flaw inclination angle $\beta = 45$	147
Figure 4.46:	Coalescence stress Vs. failure stress for marble specimens with flaw inclination angle $\beta = 60$	147
Figure 4.47:	Plumose Structure, from Ameen, M (1995)	148

Figure 4.48:	Twinned (striated) crystals of feldspar.....	149
Figure 4.49:	Surface morphology on gypsum, from Reyes (1991).....	150
Figure 4.50:	Principal minerals composing granite.....	151
Figure 4.51:	Example of zonation in granite, from Pusch (1997)	152
Figure 4.52:	Example of tension fracture.....	153
Figure 4.53:	Tension crack surface in granite specimen.....	154
Figure 4.54:	Tension crack surface in granite specimen.....	155
Figure 4.55:	Tension crack surface in granite specimen.....	156
Figure 4.56:	Example of shear fractures.....	157
Figure 4.57:	Shear crack surface in a granite specimen.....	158
Figure 4.58:	Shear crack surface in a granite specimen.....	159
Figure 4.59:	Parting planes indicating direction of slippage.....	159
Figure 4.60:	Calcite, principal mineral component of marble.....	160
Figure 4.61:	Tensile crack surface in marble.....	160
Figure 4.62:	Shear crack surface in marble.....	161
Figure 4.63:	Coalescence fracture surface in marble (type II)	161
Figure 4.64:	Coalescence fracture surface in marble (type III)	162
Figure 4.65:	Coalescence surface in granite (type III)	163
Figure 4.66:	Coalescence surface in granite (type II)	164
Figure 4.67:	Sequence of steps leading to observe a tensile-like surface in a shear crack.....	165
Figure 4.68:	Coalescence type I surface on granite.....	166
Figure 4.69:	Stress-strain plot showing a jump due to coalescence.....	167

Figure 4.70:	Representation of E/E_{INT} for granite.....	168
Figure 4.71:	Representation of E/E_{INT} for marble.....	168
Figure 5.1:	Coalescence modes in granite and marble specimens.....	176
Figure A.1.1:	Overhead saw – Main parts.....	234
Figure A.1.2a:	Detail of the cuts done in granite specimens with the overhead saw.....	235
Figure A.1.2b:	Second and third cut to be done in marble.....	236
Figure A.1.3:	Set-up of specimen in the overhead saw. (Ready for the first cut)	237
Figure A.1.4:	Measuring and leveling to make the first cut.....	238
Figure A.1.5:	Making the second cut.	238
Figure A.1.6:	Precision saw – Main parts.....	239
Figure A.1.7:	Setting the guide in the precision saw.....	240
Figure A.1.8:	Setting the specimen to cut in the precision saw.....	241
Figure A.1.9:	Oil drop device in the precision saw.....	242
Figure A.1.10:	Steps to cut with the precision saw.....	242
Figure A.1.11	Belt sander. Main components.....	243
Figure A.2.1:	Gypsum mold.....	244
Figure A.2.2:	Plate sets.....	245
Figure A.2.3:	Screw sizes.....	246
Figure A.2.4:	Mixer used to mix gypsum and celite.....	247
Figure A.2.5:	Plexiglas pattern/plates.....	248
Figure A.2.6:	Plexiglas pattern.....	249
Figure A.2.7:	Taping base of mold.....	250
Figure A.2.8:	Correct way to assemble Plexiglas covering.....	251

Figure A.2.9: Vibrating table.....252

Figure A.2.10: Mold set to dry.....252

Figure A.2.11: Specimen set after unmolding.....253

Figure A.2.12: Polishing table.....253

Figure A.2.13: How to place gypsum specimens in the oven when curing.....254

Figure A.2.14: Timelines for gypsum specimens fabrication, curing and testing.....255

Figure A.3.1: Operation principle of a water-abrasive jet.....256

Figure A.3.2: Jet lag defects.....256

Figure A.3.3: Taper. Effect of machining speed.....257

Figure A.3.4: Main parts of the OMAX water-abrasive jet.....257

Figure A.3.5: OMAX control system.....258

Figure A.3.6: Precision X-Y table.....258

Figure A.3.7: Abrasive jet system.....259

Figure A.3.8: Welcome screen on the water jet controller.....260

Figure A.3.9: Layout screen on the water jet controller.....261

Figure A.3.10: Notation used to identify geometry, from Bobet (1997).....262

Figure A.3.11: Spreadsheet done to compute the flaw tips coordinates.....263

Figure A.3.12: Correction of the flaw length for granite and marble.....264

Figure A.3.13: Correction of the flaw length for gypsum.....264

Figure A.3.14: Summary of the necessary steps to draw the geometry.....265

Figure A.3.15: Typical cut path finished.....265

Figure A.3.16: Setting screen in the water jet controller.....266

Figure A.3.17: “Make” screen in the water jet controller.....267

Figure A.3.18:	Correction of the lag effect by setting an “off delay”	267
Figure A.3.19:	Adjusting the height of the nozzle (standoff distance)	268
Figure A.3.20:	Buttons on the make screen used to coordinate the actual position of the specimen in the X-Y table and the drawing.	268
Figure A.3.21:	Setting the specimen on the X-Y table. Plan View.....	269
Figure A.4.1:	Schematic of the set-up for loading test, from Bobet (1997)	270
Figure A.4.2:	Detail of the loading test set-up.....	271
Figure A.4.3:	Set-up for loading test.....	272
Figure A.4.4a:	Load testing machine. Movement of the different parts when testing from Bobet (1997)	273
Figure A.4.4b:	Main component of a universal loading machine, from SATEC catalogue.....	274
Figure A.4.5:	Data collected on compression tests in a dummy (steel piece)	274
Figure A.4.6:	Direction of the load in uniaxial testing.....	275
Figure A.4.7:	Set-up of specimens and steel platens for uniaxial load testing.....	275
Figure A.4.8:	Mtest2 screen.....	276
Figure A.4.9:	Mtest2 chart area.....	276
Figure A.4.10:	Mtest2 – Left bar after pressing “Utils”	277
Figure A.4.11:	Mtest2- Left bar after pressing “Setup”	277
Figure A.4.12:	Mtest2- New window that appears to search for the setting file after pressing “Recall Setup”	277
Figure A.4.13:	Loading process.....	278
Figure A.4.14:	Amplification needed to identify fractures.....	278
Figure A.4.15:	Examples of identification needed to identify fractures, from Bobet (1997)	279

Figure A.4.16:	Data sheet used for gypsum, from Bobet (1997)	280
Figure A.4.17:	Granite data sheet.....	281
Figure A.4.18:	Mtest2- Left bar after pressing “Store”	281
Figure A.4.19:	Mtest2- Left bar after pressing “Servo”	281
Figure A.4.20:	Mtest2- Segmented displacement rate parameters (or segmented servo parameters) for granite.....	282
Figure A.4.21:	Mtest2- Segmented displacement rate parameters (or segmented servo parameters) for gypsum.....	283
Figure A.4.22a:	Main parts of the Kodak Ektapro (high-speed camera + motion analyzer.....	284
Figure A.4.22b:	Main parts of a motion analyzer.....	284
Figure A.4.23:	Example of recorded images.....	285
Figure A.4.24:	Keypad to operate the motion analyzer.....	285
Figure A.4.25:	Connections to make.....	286
Figure A.4.26:	Lenses, close ups and amplifiers.....	287
Figure A.4.27:	Adjusting the image due to loading machine movement.....	288
Figure A.4.28:	Video display.....	288
Figure A.4.29:	Format of the “text only” file created by the Mtest2 controlling software.....	289
Figure A.4.30:	Processed data in the “new” Excel [®] template.....	290
Figure A.4.31a:	Plotted data for granite specimens.....	291
Figure A.4.31b:	Plotted data for gypsum specimens.....	291
Figure A.4.31c:	Plotted data for marble specimens.....	292
Figure A.4.32:	Connecting the VCR to the PC to use the frame grabber.....	293
Figure A.4.33:	Screen window in the frame grabber.....	293

Figure A.4.34a:	Frame grabber- Adjusting the image.....	231
Figure A.4.34b:	Frame grabber- Capturing pictures and movies.....	232
Figure B. 1:	Stress-strain curves for granite specimens with geometry 30-0-a.....	295
Figure B. 2:	Stress-strain curves for granite specimens with geometry 30-0-2a.....	296
Figure B. 3:	Stress-strain curves for granite specimens with geometry 30-2a-2a.....	297
Figure B. 4:	Stress-strain curves for granite specimens with geometry 30-a-a.....	298
Figure B. 5:	Stress-strain curves for granite specimens with geometry 30-a-2a.....	299
Figure B. 6:	Stress-strain curves for granite specimens with geometry 45-0-a.....	300
Figure B. 7:	Stress-strain curves for granite specimens with geometry 45-0-2a.....	301
Figure B. 8:	Stress-strain curves for granite specimens with geometry 45-2a-2a.....	302
Figure B. 9:	Stress-strain curves for granite specimens with geometry 45-a-2a.....	303
Figure B. 10:	Stress-strain curves for granite specimens with geometry 45-a-a.....	304
Figure B. 11:	Stress-strain curves for granite specimens with geometry 60-0-a.....	305
Figure B. 12:	Stress-strain curves for granite specimens with geometry 60-0-2a.....	306
Figure B. 13:	Stress-strain curves for granite specimens with geometry 60-0-3a.....	307
Figure B.14:	Stress-strain curves for granite specimens with geometry 60-a-2a.....	308
Figure C. 1:	Stress-strain curves for marble specimens with geometry 30-0-a.....	310
Figure C. 2:	Stress-strain curves for marble specimens with geometry 30-0-2a.....	311
Figure C. 3:	Stress-strain curves for marble specimens with geometry 30-2a-2a.....	312
Figure C. 4:	Stress-strain curves for marble specimens with geometry 30-a-a.....	313
Figure C. 5:	Stress-strain curves for marble specimens with geometry 30-a-2a.....	314
Figure C. 6:	Stress-strain curves for marble specimens with geometry 45-0-a.....	315
Figure C. 7:	Stress-strain curves for marble specimens with geometry 45-0-2a.....	316

Figure C. 8:	Stress-strain curves for marble specimens with geometry 45-2a-2a.....	317
Figure C. 9:	Stress-strain curves for marble specimens with geometry 45-a-2a.....	318
Figure C. 10:	Stress-strain curves for marble specimens with geometry 45-a-a.....	319
Figure C. 11:	Stress-strain curves for marble specimens with geometry 60-0-a.....	320
Figure C. 12:	Stress-strain curves for marble specimens with geometry 60-0-2a.....	321
Figure C.13:	Stress-strain curves for marble specimens with geometry 60-a-2a.....	322
Figure D.1:	Data flow with the existent equipment.....	332
Figure D.2:	Kodak SR1,000. High-speed motion system.....	333
Figure D.3:	Multi channel data link.....	334
Figure D.4:	Alternative showing the use of the standard camera and a high-speed camera simultaneously.....	335
Figure D.5:	Lab data flow using the Kodak Sr1,00 high-speed motion system and the multi-channel data link.....	336

Chapter 1: INTRODUCTION

1.1 General Overview

The strength and deformability of a rock mass is controlled by both the intact rock and the characteristics of discontinuities such as fractures, particularly their persistence and orientation. Furthermore, the rock mass behavior depends not only on the existing fractures but also on how these fractures originate, propagate, and coalesce.

Discontinuities are common structural features of rock masses. Tectonic movements alter equilibrium sufficiently to activate movements along pre-existing fractures and may also generate new fractures resulting in earthquakes. Understanding of the mechanics of rock fracture is also of general importance to the solution of many engineering problems, e.g. failure in rock slopes and dam abutments, or fracture generating processes such as hydraulic fracturing and blasting.

The fundamental questions that arise are:

- How can one predict deformation and strength of these discontinuous structures?
- What combination of load and discontinuity geometry lead to failure?
- What material parameters is the fracture process governed by?

The existence, initiation, and propagation of fractures affect geology, and design and construction of engineering structures. Understanding of the fracturing process will give the possibility to engineers and geologists of accurately predicting rock mass behavior. Specifically, it is essential to know how existing fractures coalesce to form continuous fracture surfaces that lead to failure (figures 1.1A, and 1.2A). This process involves the failure of intact rock between joints (rock bridges). Figure 1.1B and 1.2B further illustrate the generation of unstable blocks in discontinuous rock masses.

What is usually called “intact” rock is not a uniformly coherent material, but contains defects that occur as visible or microscopic linear or planar discontinuities associated with certain minerals. Defects include microfractures, grain boundaries, mineral

cleavages, twinning planes, inclusions, and elongated shell fragments. As is to be expected defects influence the ultimate strength of a rock and may act as surfaces of weakness, which control the direction in which failure occurs.

At a small scale, fracture initiation, propagation, and coalescence inside or at the contact between grains of the rock determine the strength and deformability of intact rock, since the failure of most rocks at any scale involves crack and fracture propagation. Hence, the fracturing process at the small scale can be seen as a model for the larger scale problem of fracturing in rock masses.

1.2 Objective and organization of this thesis

This research studies propagation and coalescence of discontinuities in intact natural rock.

Prismatic specimens are tested in uniaxial compression, and the fracture growth pattern is observed and recorded with a high-speed camera. The main goal is to find similarities and differences for fracture coalescence patterns in different types of rocks. Former researchers have tested molded gypsum {Reyes (1992), Bobet (1997)}; and artificial sandstone {Wong et al. (1998)}. The present work describes results of tests on natural granite and marble.

Specifically, the materials used are:

- Barre granite quarried by the Rock of Ages Corporation. The granite is obtained in blocks of 14" x 13" x 4", and with sawn surfaces.
- Danby Marble blocks acquired from the Vermont Marble Company, Proctor VT. The marble blocks are 12" x 12" x 6".

All the blocks were cut in a quarry with the same grain orientation to maintain uniformity. It is important to note that these blocks have been stored for several years. To ensure that the blocks being used have not been damaged during prior handling and/or

storage, intact specimens are cut and tested before preparing specimens with cut flaws for coalescence tests.

This thesis is organized as follows: Chapter 2 introduces some fracture mechanics concepts and summarizes former results for rock. Chapter 3 shows the rock specimen characteristics and gives a brief overview of the experimental procedure to prepare and test them. Chapter 4 presents the results of uniaxial compression tests run on granite and marble specimens, their interpretation, and fractography analyses performed for both granite and marble specimens. Chapter 5, conclusion, summarizes and compares results of crack pattern growth and fracture coalescence in different natural and molded rocks. Appendix A describes details of the lab procedures for preparing and testing rock specimens (for gypsum, granite, and marble). Appendix B and C contain the stress strain plots of the load tests on granite and marble specimens, respectively. Appendix D discusses different alternatives for improvement of the equipment used to test and observe the fracture growth pattern in the MIT Rock Mechanics Lab.

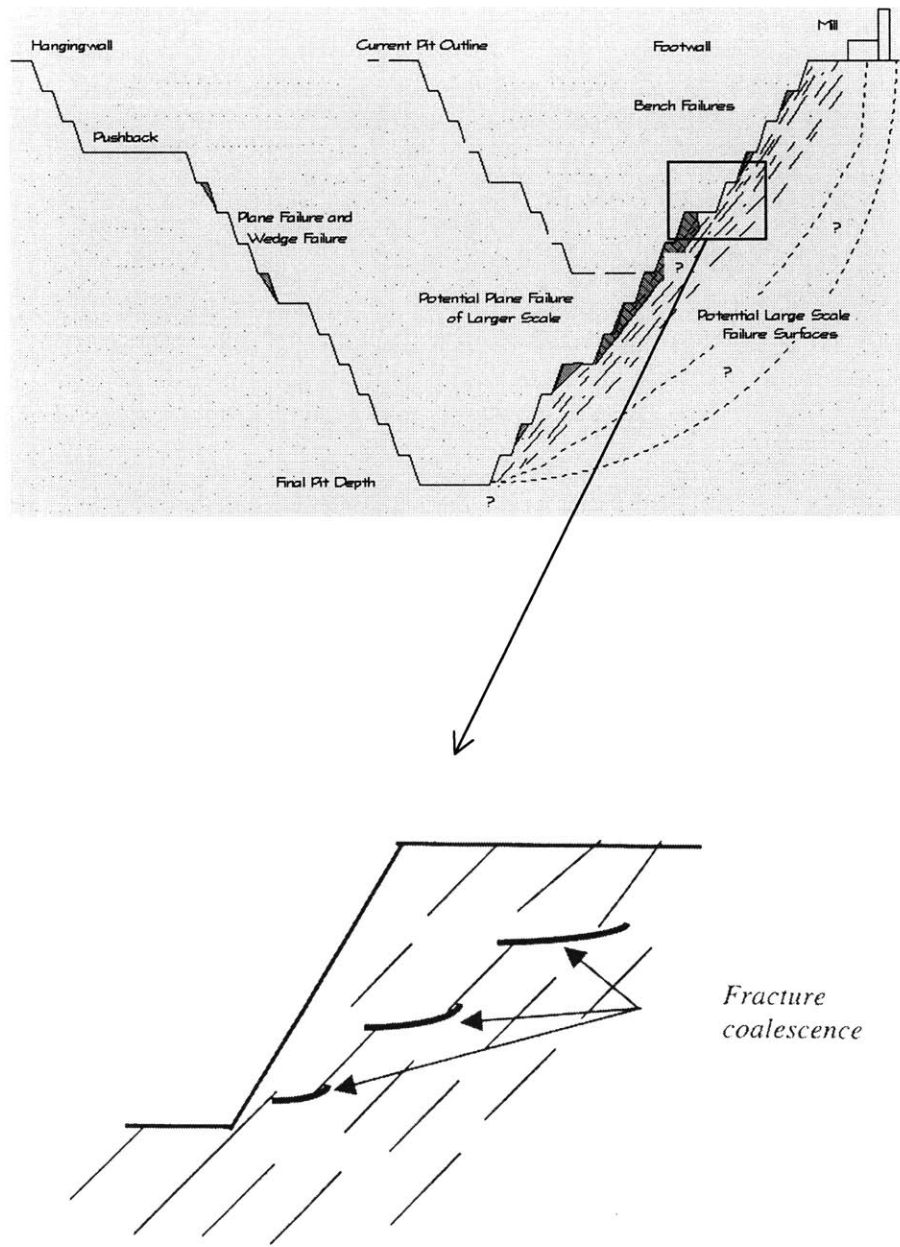


Figure 1.1a: Rock slope with coalescence of non-persistent joints forming a failure surface.

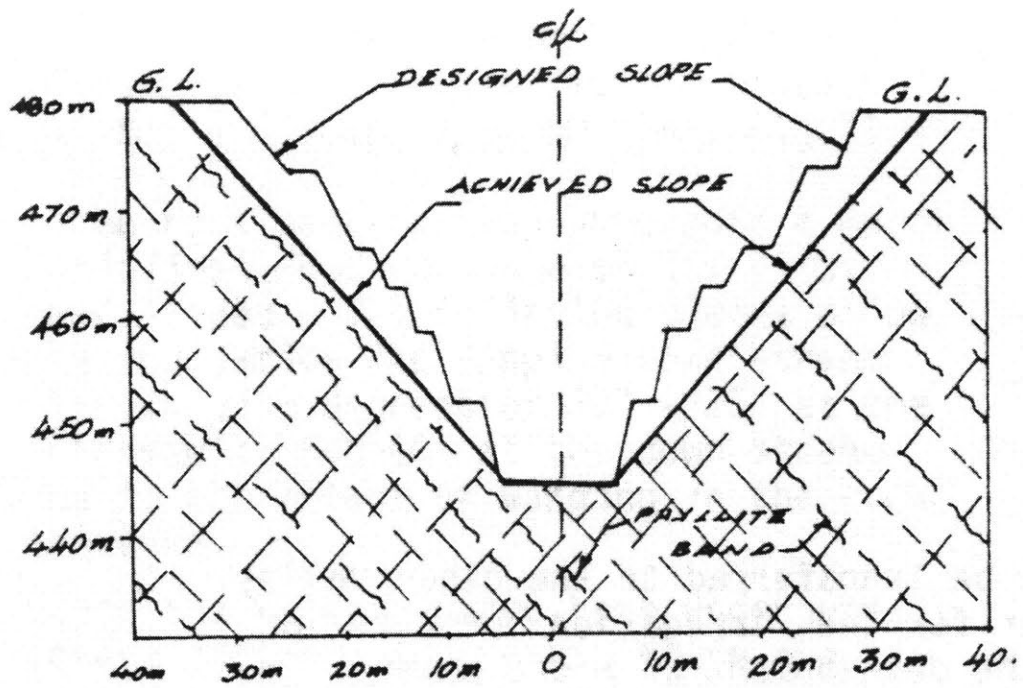


Figure 1.1b: Side slopes controlled by joints in an open channel excavation.
 From Eshwaraiah and Upadhyaya (1990)

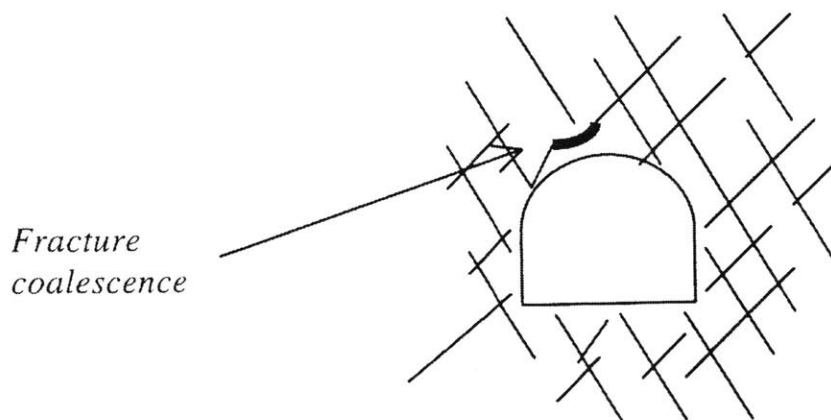


Figure 1.2a: Critical block in an underground opening formed by fracture coalescence.



Figure 1.2b: Example of critical block in a shallow tunnel, from Karaca et al. (1995)

Chapter 2: BACKGROUND AND FORMER RESULTS

Extensive research has been done on crack propagation on many materials and under different loading modes. The literature about crack propagation in different materials is quite extensive.

This chapter introduces the basic concepts of rock fracture mechanics and gives an overview on former experimental research; it focuses on fracture initiation and propagation in general, and on fracture coalescence in particular.

2.1 Fracture Mechanics

As was mentioned in chapter 1, rocks contain cracks. Griffith (1920) showed that because of the presence of these minute cracks or flaws, the measured tensile strengths of most brittle materials is much less than the real strength that would be inferred from the values of their interparticle forces. Griffith demonstrated that very high tensile stresses occur at the boundaries of these openings (assuming elliptical shapes) even under compressive stress conditions. Cracks propagate from boundaries of one of these existing cracks (flaws) when the local stress exceeds the strength of the material.

When the principal stresses applied to a flawed rock specimen are compressive, the crack that is initiated on the boundary of the flaw will only propagate a short distance, which depends on the ratio of the minor to the major principal stress (σ_3/σ_1) as shown in figure 2.1. Experimental evidence shown by Hoek & Bieniawski (1965) suggests that further propagation of these cracks occurs when the applied load is increased.

It is hence clear that in tension the propagation process starts from only one flaw (see figure 2.2). On the other hand, in compression the propagation process is the result of the interaction between two or more discontinuities (see figure 2.3), and only the coalescence of several propagated cracks leads to failure.

In fracture mechanics, three different fracturing modes are characterized:

- i) Tensile fracturing of rock (Mode I): the plane of the crack carries no shear traction. In this case the crack simply opens (Figure 2.4a).
- ii) Shear fracture of rock (Modes II and III): the plane of the crack undergoes lateral movement parallel to the crack plane (Figures 2.4b and 2.4c).

Fractures in rock can be divided into tension fractures and shear fractures. The upper crust contains both types of fractures. Usually, tension fractures are named joints and shear fractures are named faults.

Rock fracture mechanics studies the discrete initiation and propagation of an individual crack or cracks in rock subjected to a particular stress field. The individual crack or cracks can be pre-existing or newly introduced due to increased loading. Very important in this sense is the ability to establish a relationship between rock fracture strength and the geometry of cracks. Fracture tests differ from ordinary strength tests in rock mechanics by requiring specimens with accurately defined cracks, which are either pre-introduced or induced during increased loading.

A distinction must be made between fracture initiation, and fracture propagation. According to Bienawski (1967), fracture initiation is defined as the process by which the pre-existing single crack or cracks start to extend or grow. Fracture propagation is defined as the failure process by which the pre-existing crack or cracks continue to grow subsequent to fracture initiation. Fracture initiation indicates the onset of crack extension and is confined to the vicinity of the crack tips. Fracture propagation represents the process of crack extension from the crack tips to other cracks and eventually to the boundaries of the material, which leads to failure of the stressed material.

The next two sections review results of previous experimental research involving testing of rock specimens (see figure 2.5). Specifically, they cover: (1) studies on crack propagation in rock specimens with a single pre-existing flaw with different inclination angles (Section 2.2), and (2) studies on specimens with two or more flaws (Section 2.3).

2.2 Specimens with a single flaw

Lajtai (1974) tested prismatic specimens made of Plaster of Paris with dimensions 6" x 6" x 3", having single flaws with inclination angles varying from 0° to 90° at 5° intervals. The crack formation sequence was as follows:

- i. Tensile Fractures formed first. They appeared suddenly and with noise (figure 2.6a). The load versus vertical strain diagram did not show any indication of the formation of these cracks. As the load increased, the cracks propagated in a stable manner along a curved path tending to become parallel to the load direction.
- ii. Normal (to the loading direction) Shear Fractures followed closely, extending in a stable manner. These cracks were in the horizontal direction as shown in figure 2.6b. Note that these cracks initiated in a clearly compressive stress area at the flaw tip. As these fractures initiate, the stress vs. vertical strain diagram showed a lower slope indicating that the material began to yield.
- iii. With further increase of the axial load, both tensile and shear fractures extended. Damage of the material is visible close to the normal shear fractures; a shear zone appeared in this area through additional normal shear and perhaps tensile fractures (figure 2.6c).
- iv. The shear zone expanded in the axial direction (i.e. it grew vertically), producing large volumes where the material becomes granulated. At this point, Inclined Shear Fractures appeared in the shear zone (figure 2.6d).

Ingraffea and Heuze (1980) performed uniaxial compression tests on limestone and granodiorite specimens with single inclined flaws. The crack growth sequence was reported as follows:

- i. Cracks initiated from tensile stress concentration points near the flaw tips, and they were called "Primary Cracks".
- ii. Primary Cracks propagated slowly along a curvilinear path towards the direction of maximum compressive load (vertical in figure 2.7).

- iii. A second set of cracks called “Secondary Cracks” initiated at the compressive stress concentration points near the flaw tips.
- iv. The secondary cracks propagated in an unstable manner leading to the specimen failure, at a stress 3 to 5 times greater than the crack initiation stress.

Petit and Barquins (1988) tested prismatic single flaw specimens of sandstone. They used both a low porosity (4%) and a high porosity (18%) sandstone for their experiments. The specimen dimensions were 50 mm x 50 mm x 5 mm.

- i. Both types of specimens showed axisymmetric “Branch Fractures” with a curvilinear trajectory approaching asymptotically the central loading axis. (cracks labeled “*bf*” in figure 2.8). These so-called Branch Fractures were less developed in the high porosity sandstone.
- ii. The development of a Shear Zone was observed during most of the loading test (“*sz*” in figure 2.8); this Shear Zone was marked by en-echelon microcracks, which initiated from the flaw tip. With further increase of the load, this Shear Zone developed even more, causing the specimen to fail.

Jiefan et al. (1990) tested Fangshan marble specimens in uniaxial compression. The prismatic specimens were 104 mm x 80 mm x 6 mm, with a single inclined flaw about 20 mm long. The observed crack sequence was (See the referenced numbers in figure 2.9):

- i. Crack (1): PFTCs (Primary Forward Tensile Cracks). They appeared when the compressive stress was about 40% of the peak strength. They initiated close to flaw tips.
- ii. Cracks (2), (4), and (5): SFTC (Secondary Forward Tensile Cracks), FSBs (Forward Shear Belts), BSBs (Backwards Shear Belts). As the load further increased, another pair of wing cracks (2 in figure 2.9) appeared at the flaw tips. Meanwhile, dark areas corresponding to the FSBs (4) in figure, and BSBs (5) developed from the flaw tips towards the four corners of the specimen.

- iii. Crack (3): BTC (Backward Tensile Crack). As the load was increasing, a pair of BTCs initiated at the flaw tips and propagated very rapidly along the loading direction. As the load increased more, the tensile cracks lengthened and the shear zones were intensified; but no new cracks initiated.
- iv. Failure. Three different failure mechanisms were observed, splitting along tensile cracks. Shear fracture along shear belts. Combination of the two aforementioned mechanisms.

Chen et al. (1992) tested in uniaxial compression prismatic marble specimens with a single flaw. The specimen dimensions were 110 mm x 80 mm x 100 mm, and the central single flaw had a 30° inclination angle. The crack growth process was (see also figure 2.10):

- i. First, a pair of primary cracks close to the flaw tips (but slightly offset from it, see figure 2.10b). As the load was increased, the cracks propagated perpendicular to the flaw with a straight trajectory. These were classified as tensile cracks.
- ii. Secondary Cracks appeared from the flaw tips in the compressive stress area, and propagated both up and downwards along the direction of loading (major principal stress direction). These secondary cracks were longer and propagated faster than the tensile cracks, however they were also stable (see figure 2.10c).
- iii. As the load increased more, and after the secondary crack had propagated for a while they stopped growing. Then an X shape black band appeared from the flaw tips (figure 2.10d) and approached the boundary of the specimen as the load increased. The propagation of this X band led the specimen to fail.

Dyskin et al. (1995) ran compression tests on PMMA (casting resin), and in sandstone to prove that the real crack growth mechanisms are more complex than stated by the aforementioned researchers. They stated that existing discontinuities in rocks are in nature three-dimensional, and that under increasing applied load a single 3-D crack does not grow extensively and that interaction between adjacent cracks is responsible for its

unstable growth. Figure 2.13 shows the crack pattern observed in a specimen with a 13-mm 3-D flaw inclined 30° to the axis of the load that was tested in uniaxial compression; typically, two wing cracks emerged from both flaw tips. They then grew in a stable manner (stepwise) and the wings started to wrap around the initial crack, which eventually stopped the wing growth. The authors also studied interaction between several 3-D crack configurations. They stated that the obtained coalescence patterns differ from the ones typically observed in 2-D tests (plates and prismatic specimens with flaws cut through the thickness). However, there are two problems with this research. The number of tests is not large enough to reach a definitive conclusion, and some of the flaws in the resin samples have been cut with a laser, that might produce micro-cracks, which would affect the results.

Although the patterns that were found by the aforementioned researchers differ to some extent, there are some common characteristics:

- In compression tests, and according to Griffith's theory, crack propagation initiates always near the flaw tips. Shear cracks initiate in a compressive stress field close to the crack tips; tension cracks initiate in a tension field close to the flaw tips.
- In compression tests, tensile cracks propagate along a curved path, tending asymptotically toward the load direction.

Some fracture mechanics books, however, show crack patterns that differ from the ones described and observed above. Figure 2.12 summarizes the growth pattern for tensile cracks (or wing cracks) in uniaxial compression. Note that the fracturing process starts with closure of the flaw, and that the specimen failure is caused by the wing cracks reaching the borders of the specimen. Also some sliding of the flaw occurs prior to the development of the wing cracks.

2.3 Specimens with multiple flaws

Chen et al. (1992) performed uniaxial compression tests on prismatic specimens of Carrara marble. The specimens had arrays of either three or five flaws (see figure 2.13). Note that the flaws were not always parallel. They could distinguish four different fracture coalescence stages (figure 2.13):

- i. Relatively independent fracture stage. The primary cracks (or wing cracks) appeared at each flaw tip and initiated in a direction perpendicular to the flaws (figures 2.13a and b).
- ii. Coalescence stage. Primary cracks or secondary cracks propagated and connected the flaws. The primary cracks appeared first, and cause coalescence for most of the specimens (figures 2.13c and d). Whenever the primary tensile cracks could not link the flaw, the secondary cracks made them coalesce (figures 2.13g).
- iii. Fracturing of the whole flaw system. After coalescence occurred, all the flaws acted as a single discontinuity. The cracks at the extreme end of the flaw system propagated as the load increased, and the internal cracks stopped growing (figures 2.13j).
- iv. Failure. An X shaped microcrack band (not shown in figure 2.15), similar to the X band observed in the specimens with a single flaw (see figure 2.10d), appeared at both ends of the flaw system, and propagated, leading to the specimen failure.

L.E. Vallejo (1987) studied the effect of fissures on failure of stiff clay when subjected to direct shear. Figure 2.14 shows his fractured prismatic specimens of kaolinite. Note that a single flaw specimen is shown in “a” and “b”, and a two-flaw specimen shown in “c” and “d”. He observed shear cracks initiating and propagating from the tip of the flaws and coplanar with them. He also observed tensile fractures starting at the tip of the flaws with initiation angles close to 90° to the flaws. The origin of fractures (shear or tension) was also assessed by running numerical simulations using linear elastic fractures mechanics theory.

Wong and Chau (1998) investigated the pattern of crack coalescence of sandstone-like molded material. Their prismatic specimen dimensions were 60 mm x 120 mm x 25 mm, and had two parallel inclined frictional cracks. They tested both overlapping and non-overlapping geometries. The flaws had different friction coefficients: $\mu = 0.6, 0.7,$ and 0.9 that correspond to $\phi = 31^\circ, 35^\circ,$ and 41° .

Figure 2.15 summarizes the observed coalescence pattern. They found three different main modes of crack coalescence: (1) Shear crack coalescence (S-mode in figure 2.15a), (2) mixed crack coalescence crack pattern (M-mode in figure 2.15b and c), and (3) wing tensile crack coalescence (W-mode in figure 2.15 d to i).

Reyes (1991) and Shen et al. (1995) tested prismatic molded gypsum specimens, with dimensions 6" x 3" x 1.25" and two parallel flaws*. The length of the flaws was always 0.5" = 12.7 mm. The flaw arrangement is shown in figure 2.16; the varied parameters were the flaw angle β , and the ligament angle α . The flaw angles were $30^\circ, 45^\circ,$ and 60° , and the ligament angle ranged from 30° to 150° changing in intervals of 15° . For ligament angles $\alpha < 90^\circ$, the flaw arrangement is defined as "non-overlapping geometry" since the flaws do not overlap in the direction of the load; for $\alpha > 90^\circ$ the flaws overlap in the loading direction (see figure 2.17).

Reyes (1991) clearly demonstrated that for overlapping geometries, the leading coalescence mechanism is the linkage of wing cracks with the flaws (see figure 2.18). Shen et al (1995) obtained for non-overlapping geometries the crack pattern shown in figure 2.19. They both observed two different crack types, tensile cracks (primary, or wing cracks), and secondary cracks. Primary cracks appeared first; they started from both internal and external flaw tips, and propagated in a stable manner towards the maximum compression direction. On the other hand, secondary cracks appeared suddenly and propagated fast and unstably.

* Flaws are cracks that are made through the specimen thickness before the loading test. In the case of gypsum the cracks are made when molding the specimens. In the case of the present research, where natural rock (granite and marble) specimens are tested, the flaws are cut before load testing with a high- pressure water-abrasive jet. For further details on lab procedures refer to Appendix A.

Bobet (1997) investigated crack coalescence in gypsum specimens with two pre-existing parallel flaws in uniaxial and biaxial compression. Flaws were either open or closed. In both cases, similar behavior was observed. The specimens were prismatic (Figure 2.20), with dimensions $152.4 \times 76.2 \times 30$ mm (6" \times 3" \times 1.25"). He tested only non-overlapping geometries. Figure 2.20 also shows the geometrical parameters he chose: flaw inclination angle β° , spacing s , and continuity c . The flaw angle β was 30° , 45° and 60° . Note that these parameters are related to the ligament angle (α) used by Reyes (1992) and Shen (1995). The "s" and "c" parameters are expressed in multiples of "a", which is half of the flaw length. In Reyes (1991), Bobet (1997) and the present research, the flaw length always equals 0.5" and hence "a" = 0.25" = 12.7 mm.

Bobet observed that tensile wing cracks appear at both the internal and external tips of the flaws. Shear cracks, both internal and external, also initiate at the tips of the flaws, and propagate in stable manner, always in the plane of the flaws. He also observed that internal and external wing cracks appear simultaneously for all geometries and that they propagate in a stable manner following a curvilinear path that aligns itself with the direction of compressive load.

Fracture coalescence occurred by the linkage of two internal cracks. Figure 2.21 shows five coalescence types that were observed (for overlapping and non-overlapping geometries) by Bobet and Reyes.

Coalescence type I occurred through the linkage of internal shear cracks (Figure 2.22). It only occurred for a ratio of spacing to continuity (s/c) of less than $1/3$, i.e. coplanar or close to coplanar flaws.

Coalescence type II was produced when two internal shear cracks were linked by a tensile crack (Figure 2.23). It occurred when the ratio s/c was greater than $1/3$.

Coalescence type III was produced by the propagation of an internal shear crack from one of the flaws until it reached the internal wing crack of the other flaw (Figure 2.24). It was

observed that this type of coalescence occurred when the ligament angle was around 90° (i.e., the ratio $s/c = 1$).

The present research continues the research done by Bobet (1997). The specimen geometries are the same (non-overlapping geometries and also the same parameters: “ β ”, “s”, and “c”). However, the materials being tested are natural rocks (granite and marble).

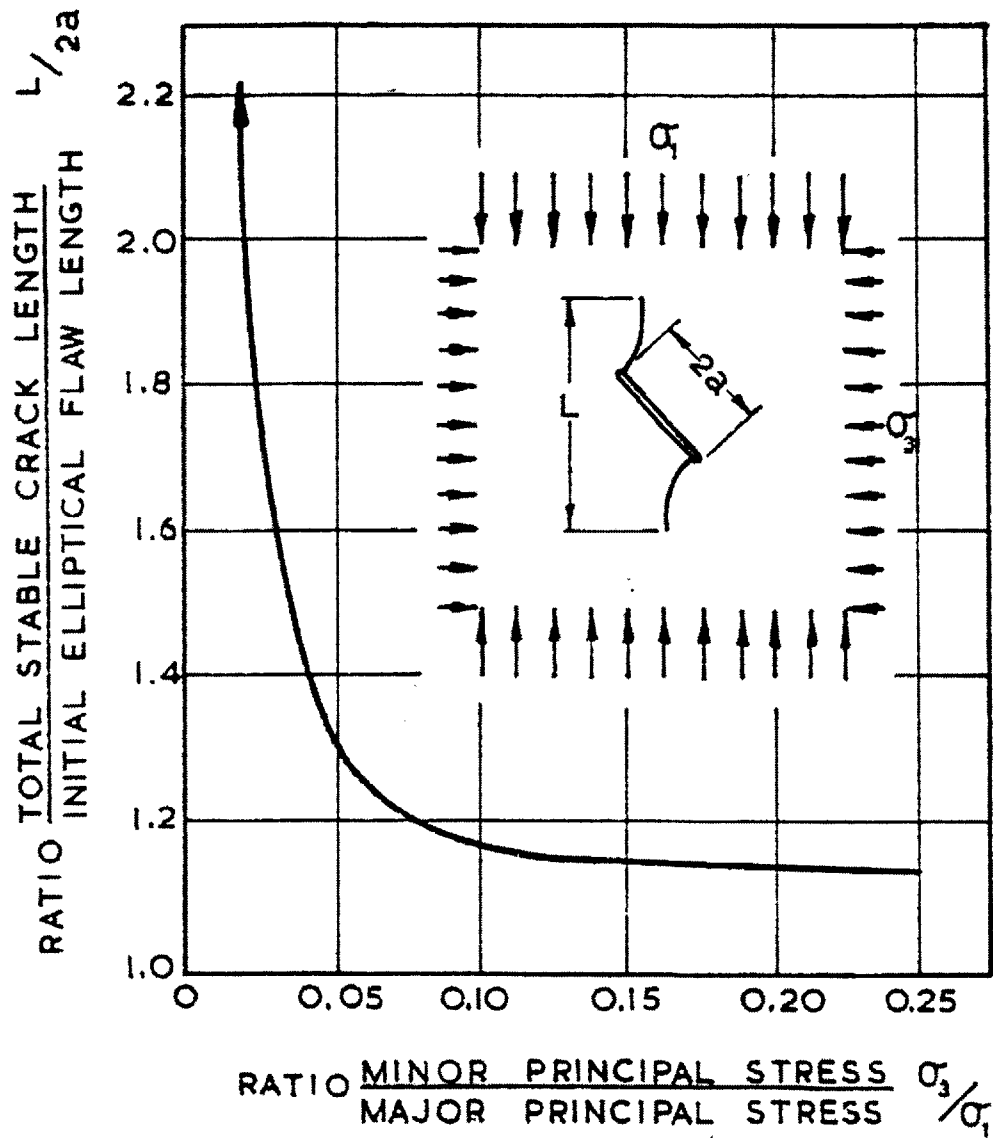


Figure 2.1: Length of stable crack propagated from an elliptical flaw under compressive stress conditions. Hoek 1967, after Hoek and Bieniawski.

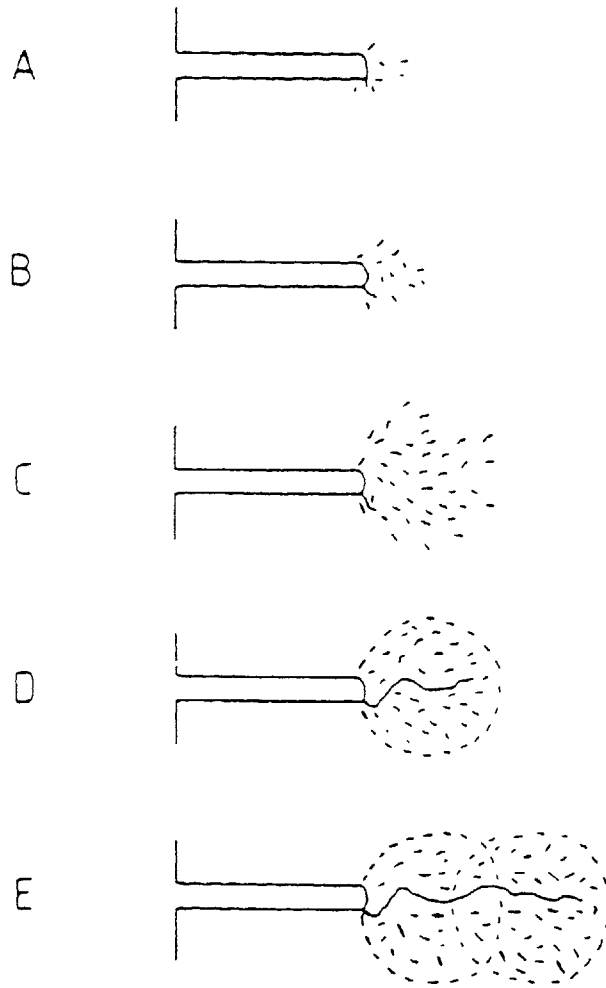


Figure 2.2: Crack Propagation in tension. (From B.T. Atkinson, 1987).

- a) Few isolated microcracks induced by loading.
- b) Microcracking begins
- c) Microcracking becomes more intense
- d) Microcracking extends by linkage of microcracks

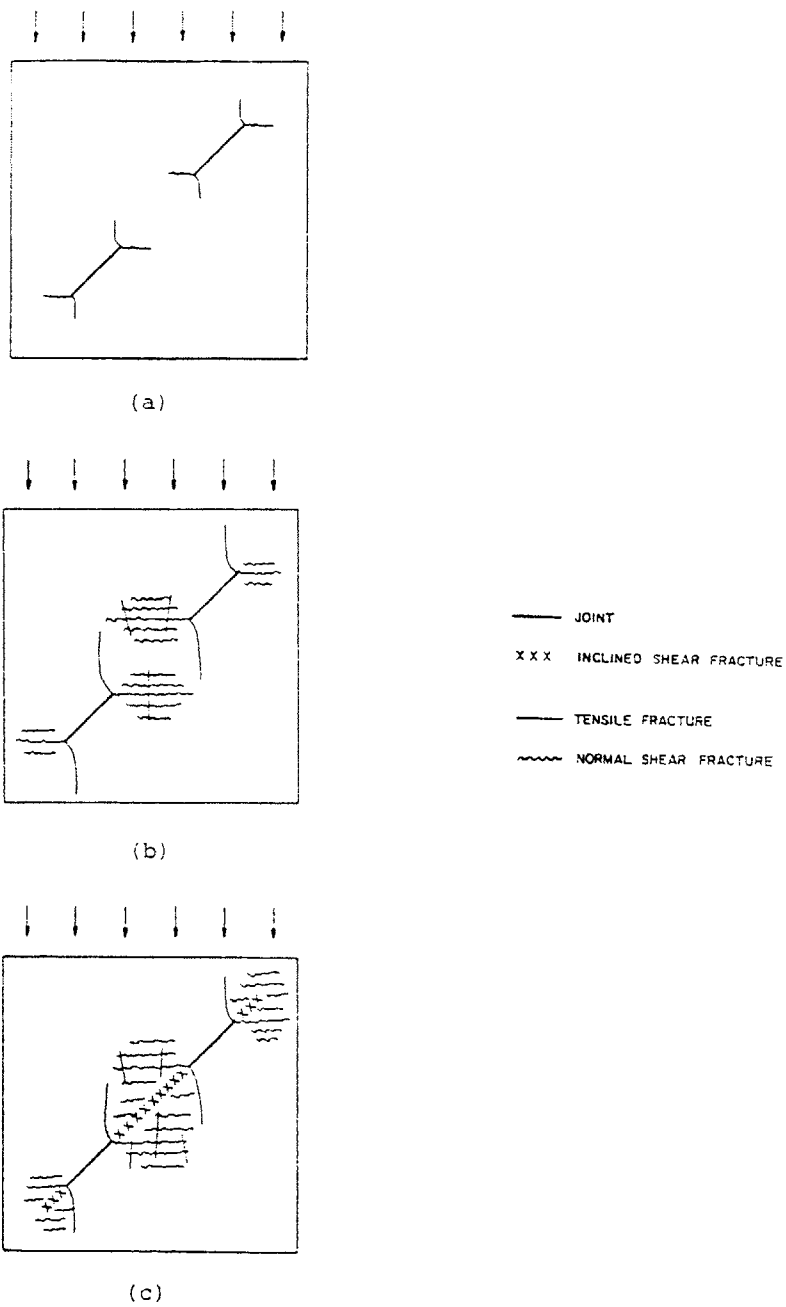


Figure 2.3: Fracture propagation in compression. Shear across the bridge (from Rock Mechanics Principles, D. F. Coates).

- a) Initial tensile and normal shear fractures around individual fractures.
- b) Fracture zone expands in the rock bridge.
- c) Inclined shear fractures complete the ultimate failure surface.

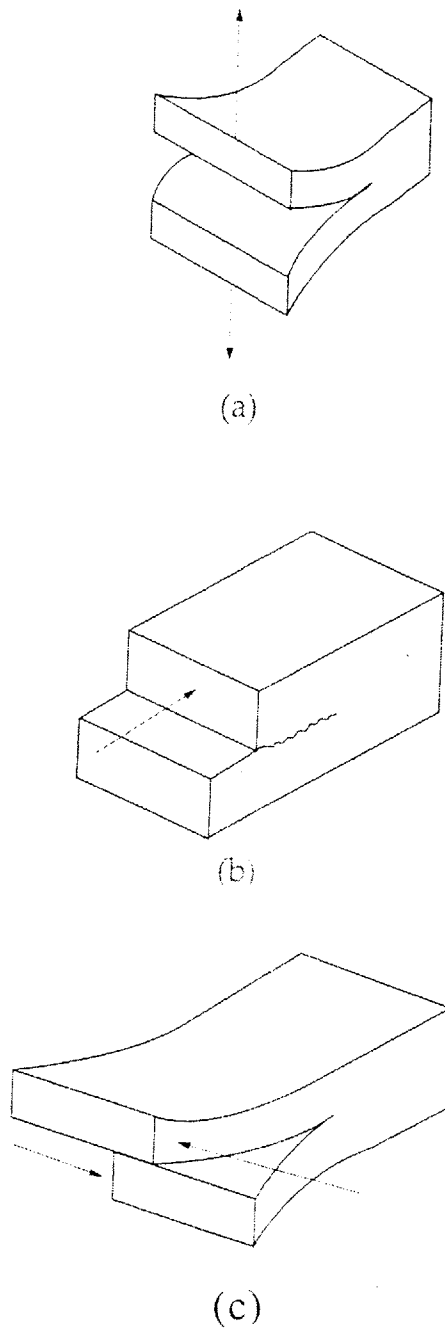
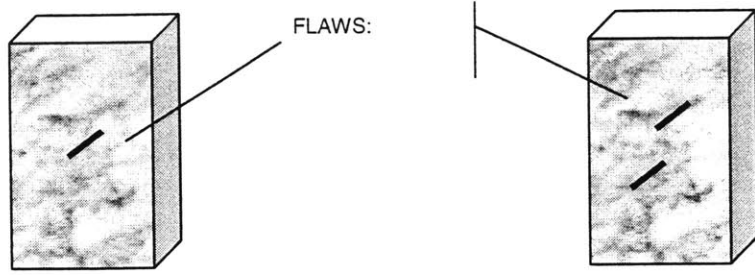


Figure 2.4: Types of cracks according to mode of loading.

- a) Tensile fracturing of rock (Mode I).
- b) Shear fracturing of rock (Mode II).
- c) Shear fracturing of rock (Mode III).



ONE FLAW SPECIMEN

TWO FLAW SPECIMEN

Figure 2.5: Prismatic rock specimen with flaws cut through the thickness

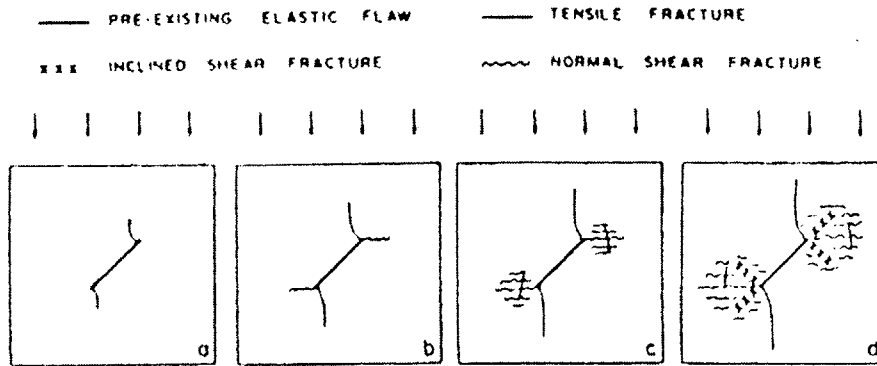


Figure 2.6: Single flaw specimens of Plaster of Paris, Lajtai (1974)

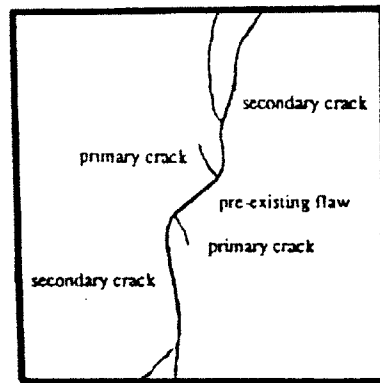
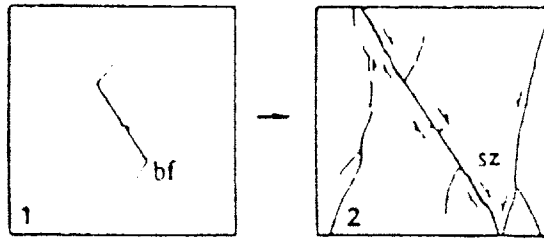
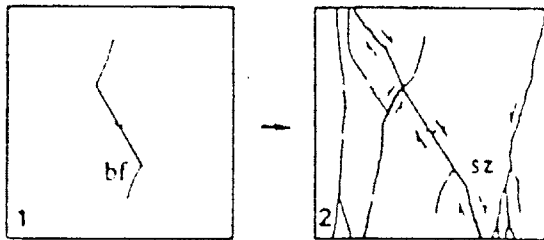


Figure 2.7: Single flaw specimens of Limestone, Ingraffea and Heuze (1980)



high porosity sandstone



low porosity sandstone

Figure 2.8 Single flaw specimens of Sandstone, Petit and Barquins (1988).
 “bf”: Brach Fracture.
 “sz”: Shear Zone.

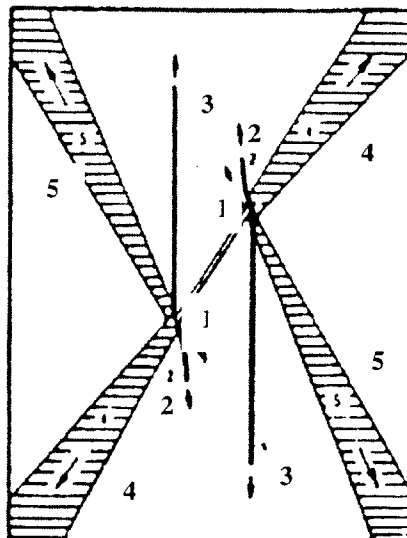


Figure 2.9 Single flaw specimen of Marble, Jiefan et al. (1990).

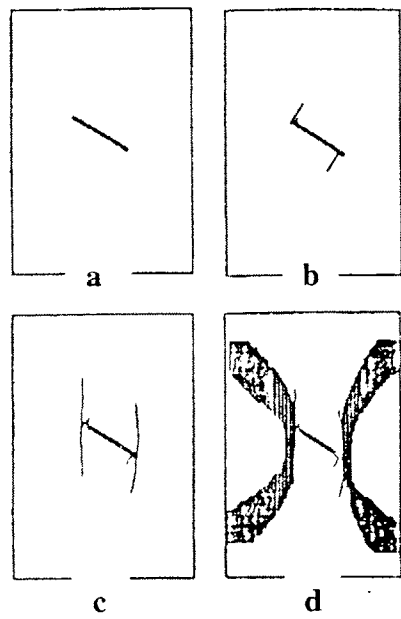


Figure 2.10: Single flaw specimens of Marble, Chen et al. (1992).

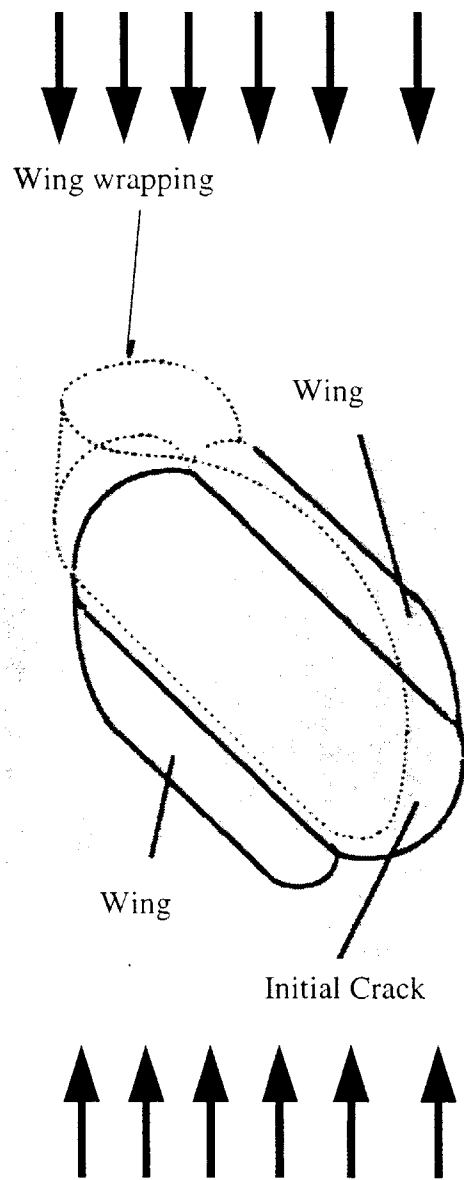


Figure 2.11: Wrapping in a single 3-D flaw specimen. From Dyskin et al. (1995).

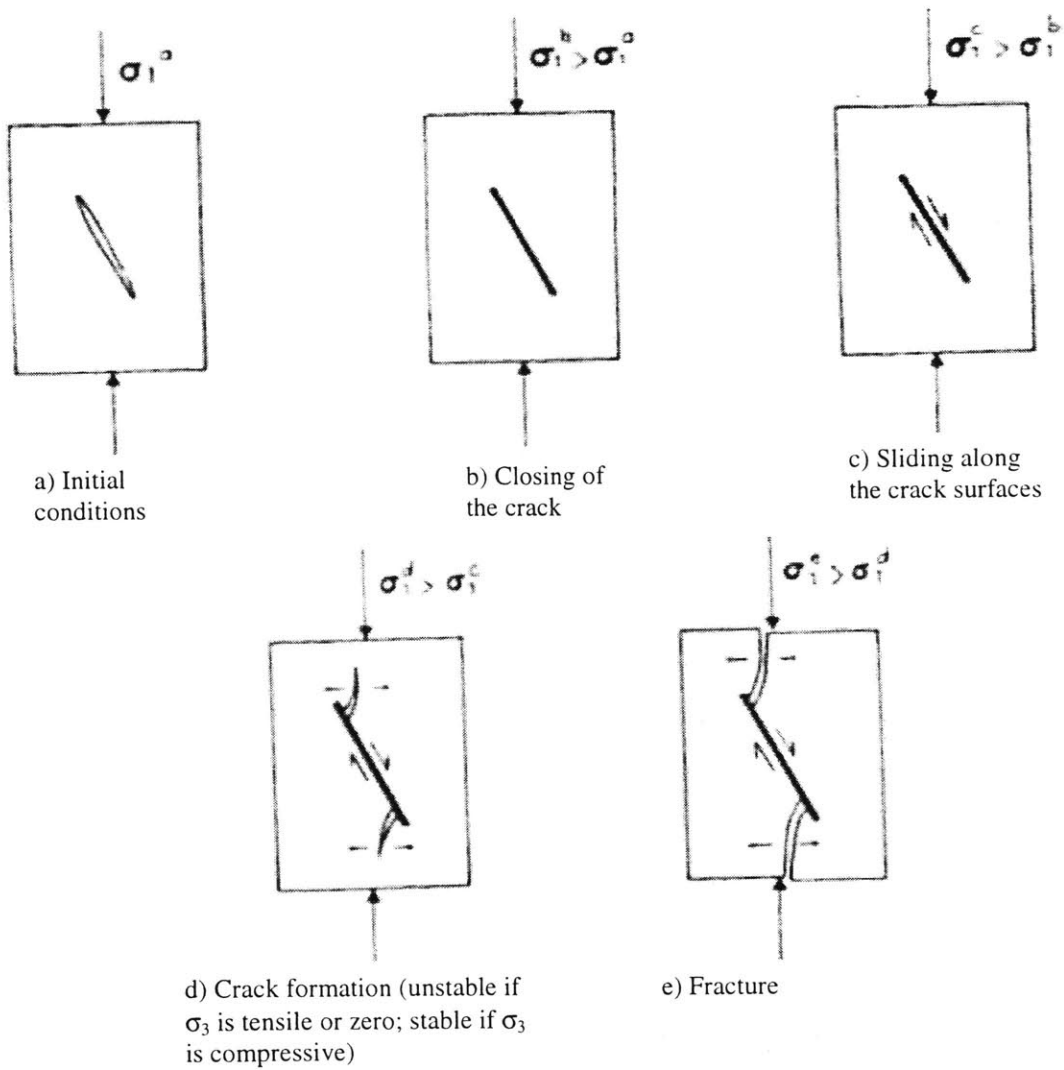


Figure 2.12: Wing crack growth pattern, after Blés & Feuga in “The Fracture of Rocks”.

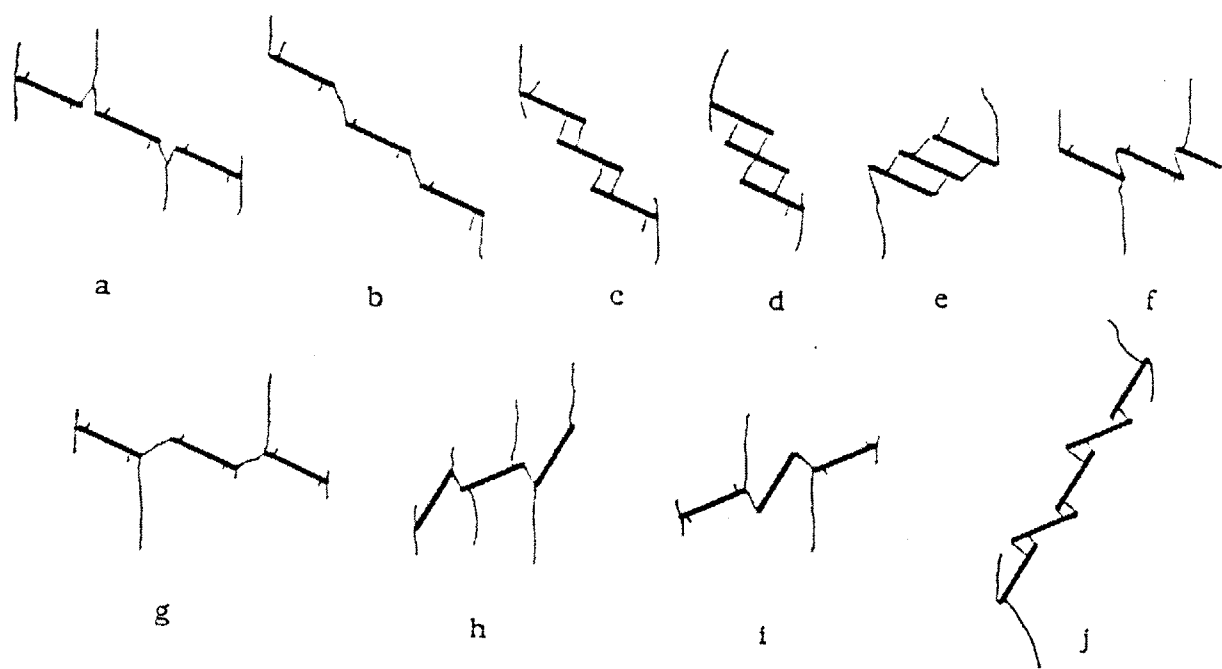


Figure 2.13: Crack Patterns in Carrara Marble (3 to 5 flaw specimens). Chen et al. (1992)

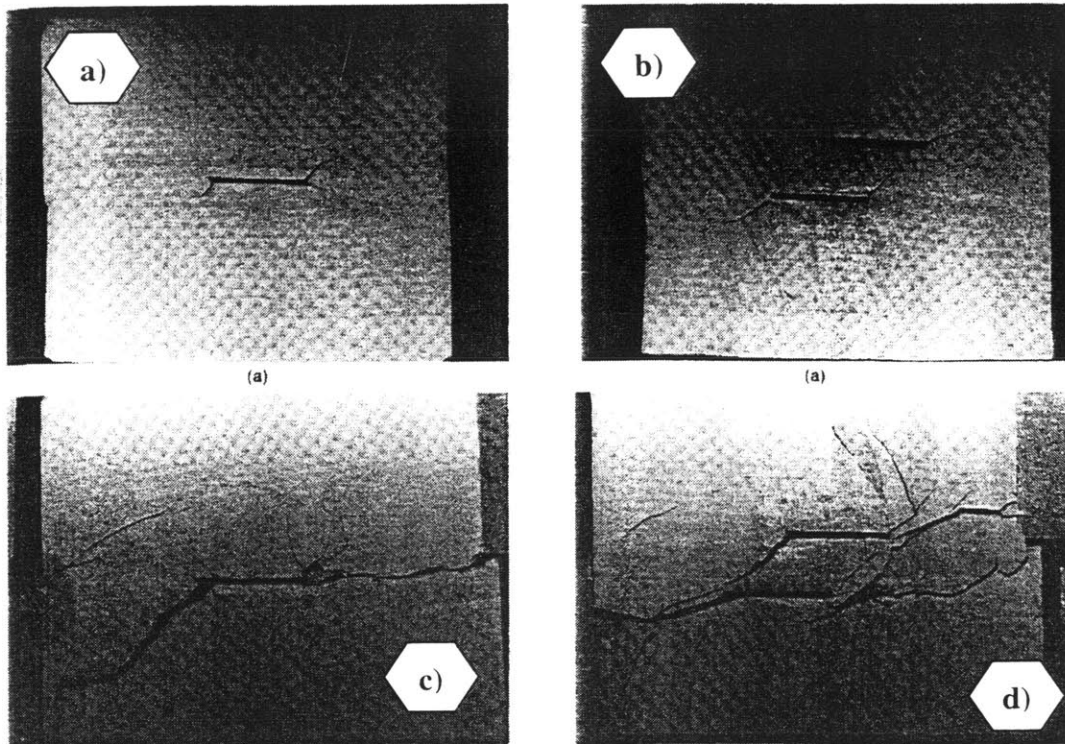


Figure 2.14: Crack development and failure of kaolinite specimens subjected to direct shear.
From L.E. Vallejo (1987).

- a) Secondary crack development in a sample with a single horizontal crack.
- b) Final failure of a specimen with a single horizontal crack.
- c) Secondary crack development in a sample with two horizontal cracks.
- d) Final failure of a specimen with two horizontal cracks.

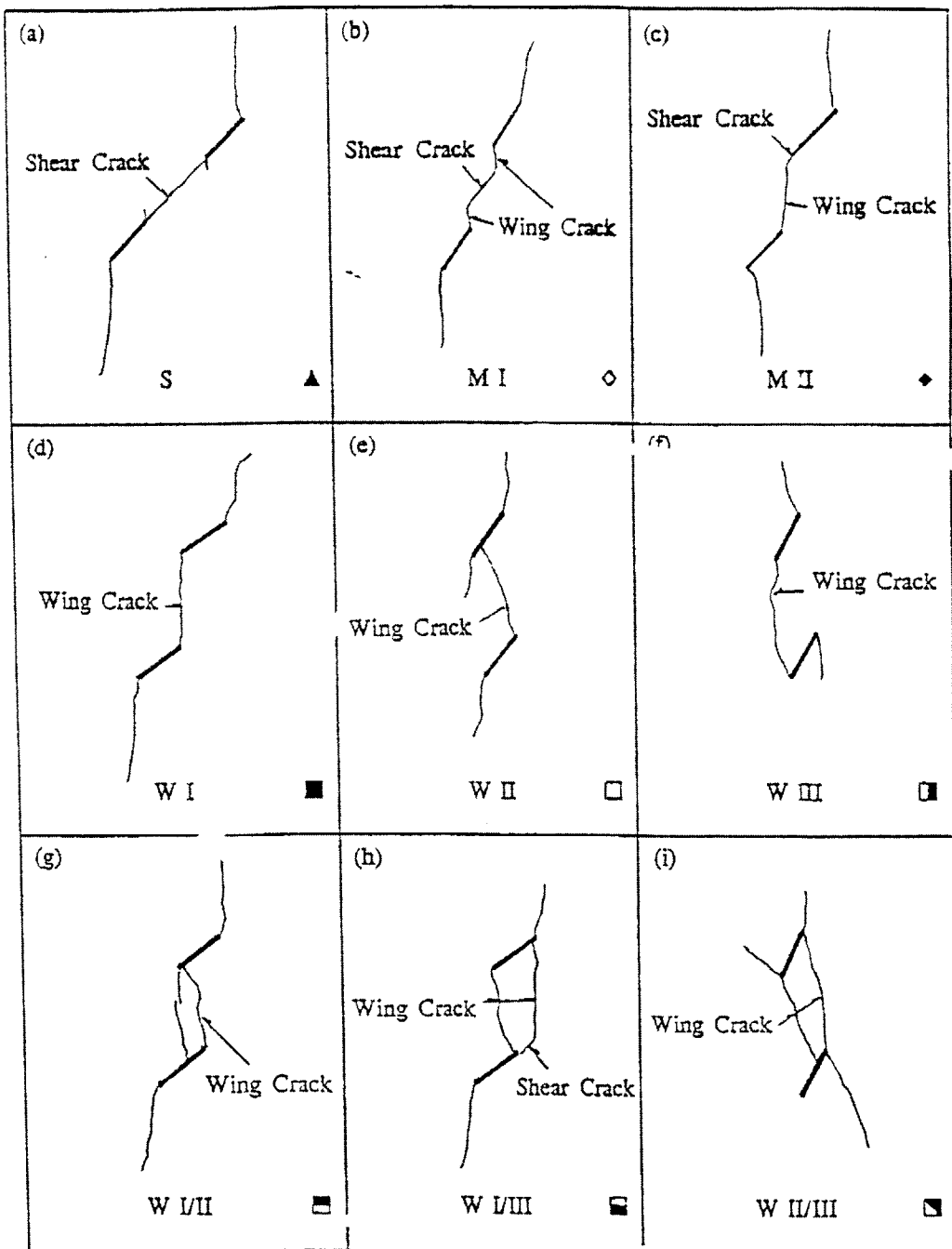


Figure 2.15: Patterns of crack coalescence observed by Wong and Chau (1998)

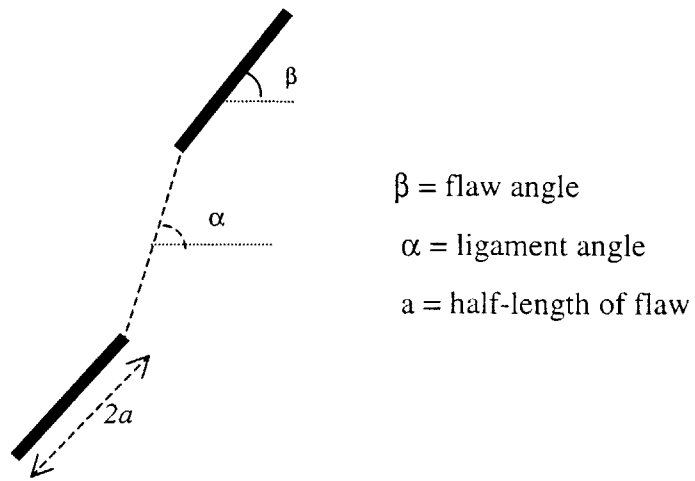


Figure 2.16: Flaw geometry used by Reyes (1991) and Shen et al. (1995)

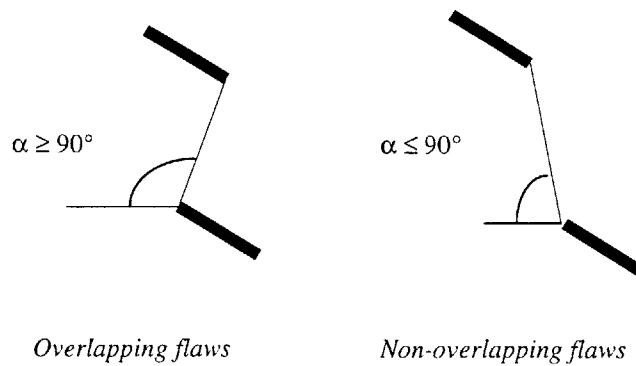


Figure 2.17: Non-overlapping and overlapping geometries

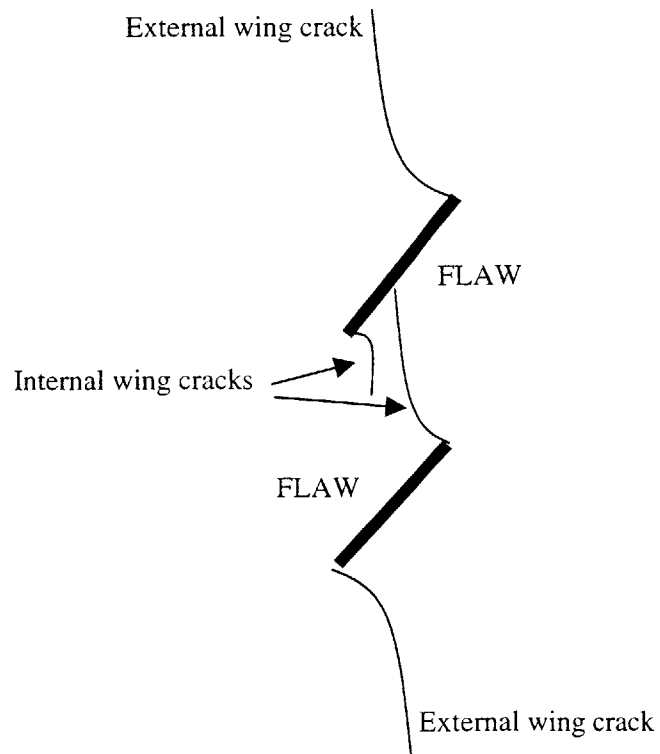


Figure 2.18: Crack pattern in gypsum specimens in uniaxial compression for overlapping geometries. Reyes (1991)

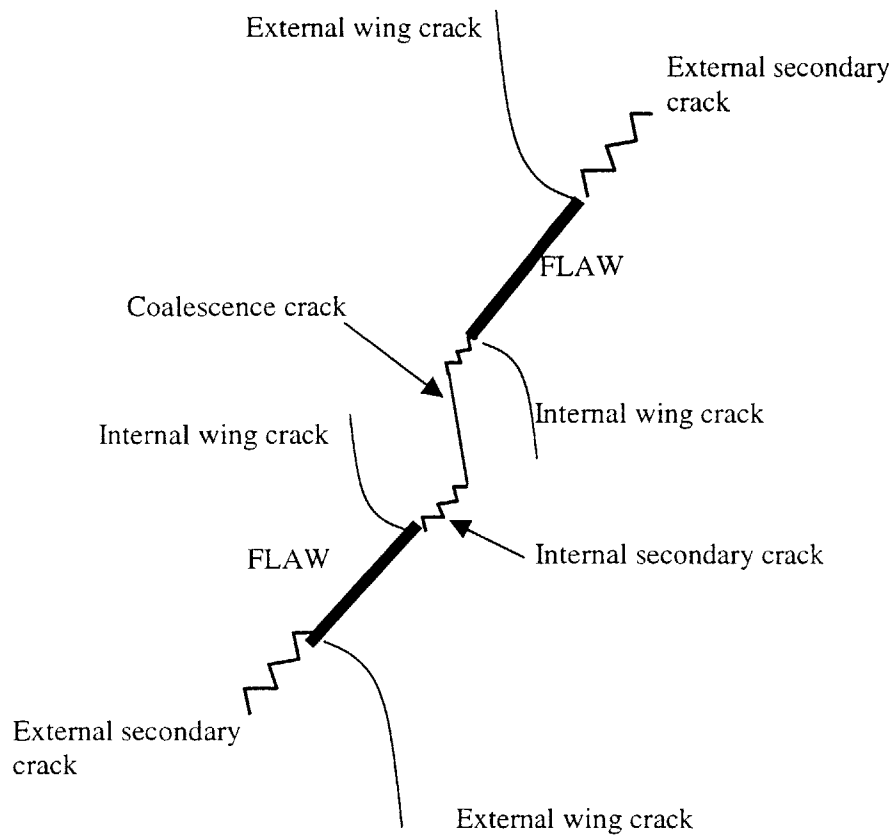


Figure 2.19: Crack pattern in gypsum specimens in uniaxial compression for non-overlapping geometries. Shen et al. (1995)

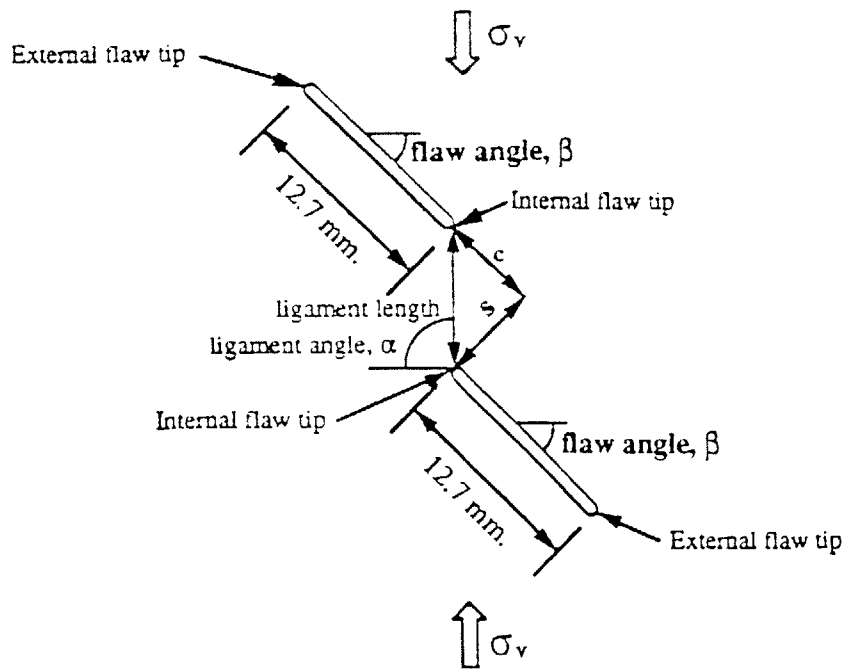
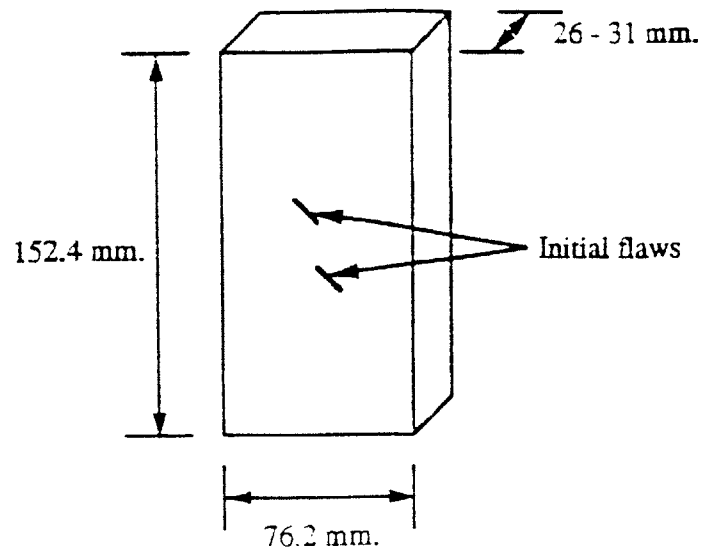


Figure 2.20: Dimensions and shape of specimen used by Bobet (1997) and in the present work.






Type	Schematic path of Coalescence	Description of Coalescence	Mode of Coalescence
I		Type of coalescing fracture: secondary shear crack. Initiation position: preexisting flaw tips. Crack surface characterization: rough, with many small kink steps; contains crushed gypsum	Shearing
II		Type of coalescing fracture: secondary shear and tensile cracks. Initiation position: preexisting flaw tips. Crack surface characterization: some parts are clean and smooth while other parts are rough with crushed gypsum	Shearing + tension
III		Type of coalescing fracture: secondary shear crack and wing crack. Initiation position: preexisting flaw tips. Crack surface characterization: some parts are clean and smooth while other parts are rough with crushed gypsum	Shearing + tension
IV		Type of coalescing fracture: wing crack. Initiation position: preexisting flaw tips. Crack surface characterization: smooth and clean.	Tension
V		Type of coalescing fracture: secondary crack. Initiation position: preexisting flaw tips. Crack surface characterization: very rough, coated with a lot of crushed gypsum	Shearing ?

Figure 2.21: Types of coalescence, from Bobet (1997). The results for overlapping geometries are from Reyes (1991)

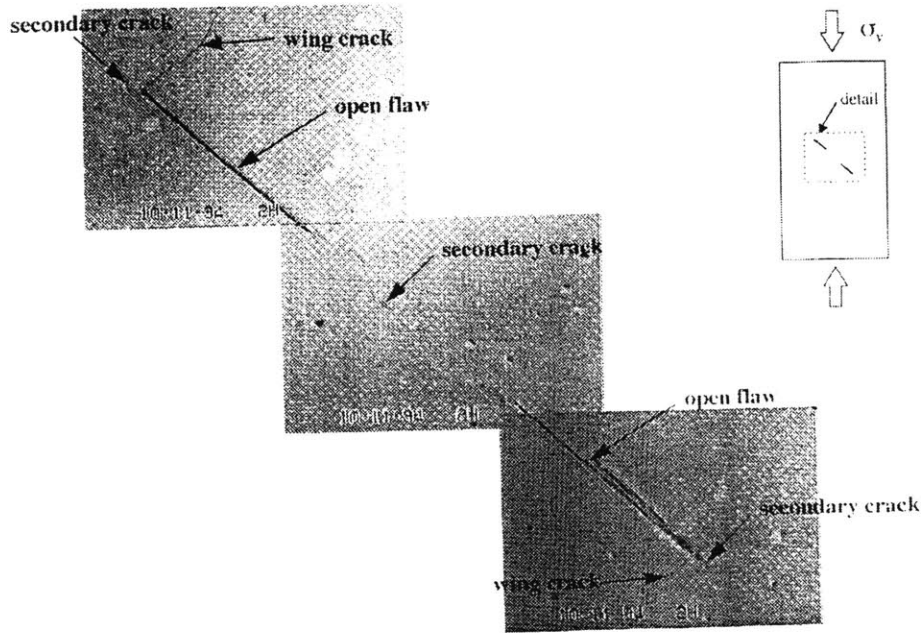


Figure 2.22: Coalescence type I in gypsum specimen. After Bobet (1997)

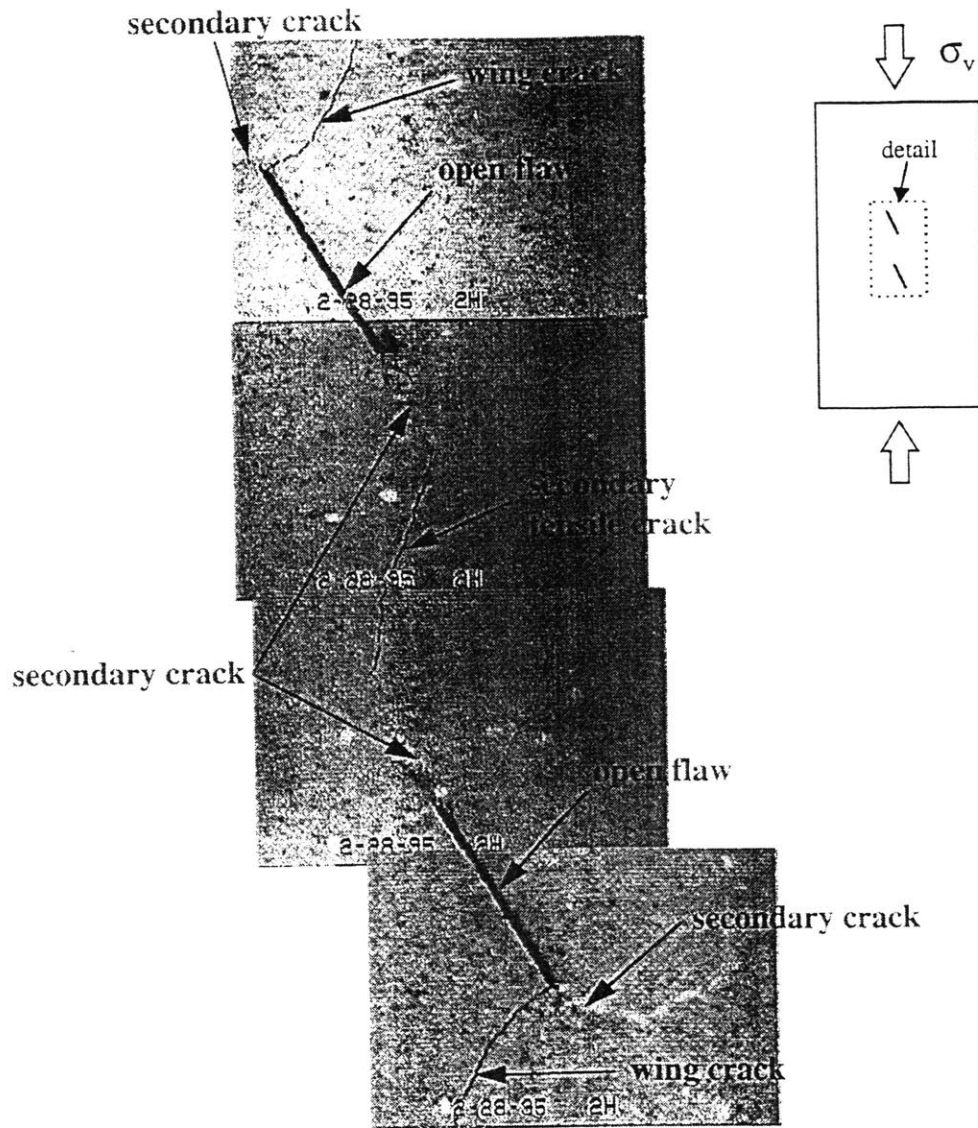


Figure 2.23: Coalescence type II in gypsum specimen. After Bobet (1997)

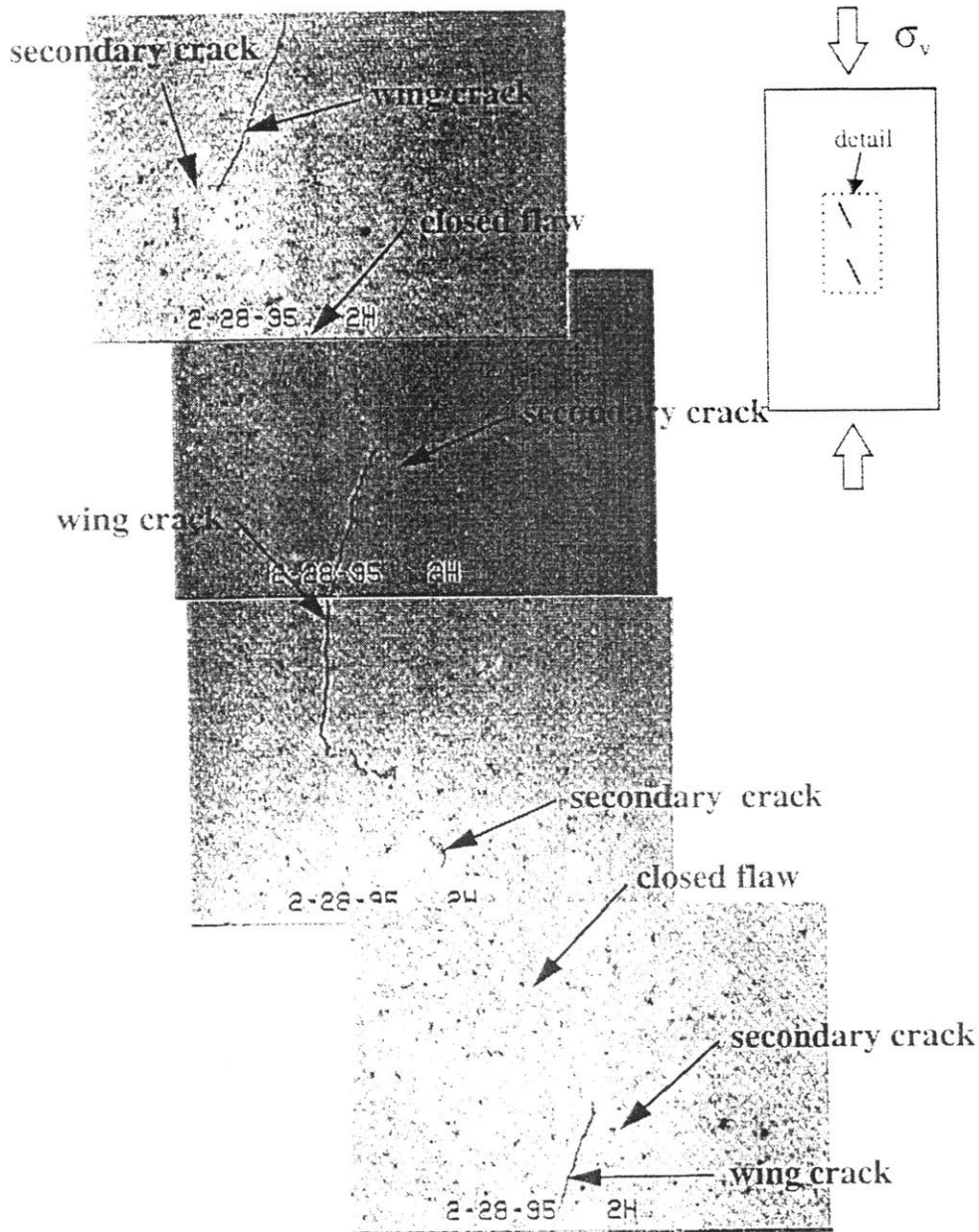


Figure 2.24: Coalescence type III in gypsum specimen, after Bobet (1997)

Chapter 3: SPECIMEN CHARACTERISTICS AND EXPERIMENTAL PROCEDURE

Uniaxial compression tests are performed on granite and marble specimens. The specimens are prismatic and have two parallel flaws cut through the thickness. The specimen geometries (flaw arrangement) are similar to those used by Bobet (1997); there are 14 different geometries, but always with non-overlapping arrangements ($\alpha < 90^\circ$). More than 90 granite specimens and 50 marble specimens have been tested.

3.1. Specimen geometry

The specimens used are prismatic, with dimensions 6" x 3" x 1.25" (152×76.2×31.7 mm.), with two flaws through the thickness and perpendicular to the specimen face. Flaw geometries are defined by the basic parameters: flaw inclination angle β° , spacing s , and continuity c in this order (See figure 3.1). For example, 60-a-2a correspond to a specimen, with a flaw angle of 60° , spacing of " $a = 0.25'' = 6.35 \text{ mm}$ " and continuity of " $2a = 0.5'' = 12.7 \text{ mm}$ ". Figure 3.2 shows the same notation for fractures in a rock mass.

These parameters are varied in the following ranges:

- Flaw angle: $\beta = 30^\circ, 45^\circ, \text{ and } 60^\circ$.
- Spacing: $s = 0 \text{ to } 3a$. ($a = 0.25'' = 6.35 \text{ mm}$)
- Continuity: $c = a \text{ to } 2a$. ($a = 0.25'' = 6.35 \text{ mm}$)

Table 3.1 lists the geometries used for this study in both granite and marble specimens and their corresponding ligament length, (l) and ligament angle, (α). Five to eight granite specimens and three to five marble specimens have been tested per geometry.

3.2. Overview of Specimen Preparation:

This section gives only a general overview of the specimen preparation. Appendix A provides a very detailed description of the equipment used and explains the preparation of specimens and the testing procedure. Note that Appendix A includes detailed specimen preparation instructions for gypsum, granite, and marble specimens. It covers every step from cutting the original rock blocks to load testing and data processing, including also the observation techniques using either a standard camera or a high-speed camera. Table 3.2 lists these steps and the respective sections in Appendix A.

The following is a brief description of the necessary steps for prismatic natural rock (granite and marble) specimen preparation and uniaxial compression testing:

- a) Cutting the specimens from the original block. The cuts to make with the overhead saw depend on the material since the original blocks come in different sizes.
 - For Granite: the original block size is 14" x 13" x 4". Three cuts are necessary. (1) Cut a slab to a slab with 1.25" thickness (i.e. 14"x4"x1.25"). (2) Reduce the width of the slab to 3". (3) Cut the slab in half. In the case of granite two specimens are obtained per slab.
 - For Marble: The original block is 12" x 12" x 6". Make three cuts with the overhead saw. (1) Cut a 1.25" thick slab (i.e. 12"x6"x1.25"). (2) Cut the slab in two 3" wide pieces. (3) Cut each of these slabs in two 3" x 6" pieces. Note that in this case four specimens are obtained per slab.

- b) The second step also depends on the material:
 - For Granite: Cut each of the obtained pieces with the precision saw. Two cuts, which will be the loaded faces, are necessary per specimen. This step ensures that the faces to load are smooth and parallel.

- For Marble: Polish the faces to load. This is so done by using a belt sander. This step is necessary to ensure that the faces to load are smooth and parallel (In this case, the specimen is not cut with the precision saw since the specimen already has the specified dimensions after step a).
- c) Cut the flaws with the water abrasive jet. First, draw the geometry. Then place the specimen on the water-jet table and set the cutting quality and parameters (material and thickness to be cut). Make the cut. See Appendix A for details.
 - d) Test the specimens in uniaxial compression. First set up the camera, lights, image processor, monitor and VCR. Set the specimen and steel platens. Turn on the PC (controller of the loading machine) and start the Mtest2 controlling software, choose the appropriate loading file (according to the material being tested). Start testing. Also start recording with either the high-speed or the standard camera + microscope. Observe the fracture growth in the high-resolution monitor; write down the load at which the fractures initiate. After the specimen fails, draw the final fracture pattern on the data sheet.
 - e) Process the stress strain data from the controlling PC. Using the Excel template to transform the “.raw” file into the final stress strain data. Indicate in the stress strain chart when the fractures have developed, as well as the coalescence stress (if coalescence occurs).
 - f) Process the videotape data. By using the frame grabber, take images that show clearly the fracture pattern in the specimen. Having clear images directly from the frame grabber is almost impossible; extra image processing is generally required. Use Adobe Photoshop or Kodak Photo Enhancer (both available at the Edgerton Lab Image Processing Center at MIT).

The specimens are numbered in the order they have been tested, and not by geometry. These numbers are those found in chapter 4 and in the charts in Appendices B and C. The key letters GR are used to indicate that the specimen is a granite rock specimen, and MA is used for marble specimens.

Geometry	Ligament angle	Ligament length
30-0-a	30	a
30-0-2a	30	2a
30-2a-2a	75	2.83a
30-a-a	75	1.41a
30-a-2a	56.6	2.24a
45-0-a	45	a
45-0-2a	45	2a
45-2a-2a	90	2.83a
45-a-a	90	1.41
45-a-2a	71.6	2.24a
60-0-a	60	a
60-0-2a	60	2a
60-a-2a	86.6	2.24a

a = 0.25" = 12.7 mm. (Half of the flaw length)

Table 3.1: Flaw geometries for granite and marble specimens.

GYP SUM		GRANITE (ALWAYS CUT FLAWS)	MARBLE (ALWAYS CUT FLAWS)
Prefabricated Flaws	Cut Flaws		
Mold Specimen with shims A.2.1	Mold Specimen A.2.1	Cutting with the overhead saw A.1.2	Cutting with the overhead saw A.1.2
Polish the face to observe A.2.2	Polish the face to observe A.2.2	Cutting with the precision saw A.1.4	Polishing the faces to load A.1.6
Curing in the oven A.2.4	Cut the flaws (water-jet) A.2.3 / A.3.2	Cutting the flaws with the water-jet A.3.2	Cutting the flaws with the water-jet A.3.2
Testing with the standard camera A.4.4	Curing in the oven A.2.4	Testing with the standard or high speed camera A.4.4 or A.4.7	Testing with the standard or high speed camera A.4.4 or A.4.7
Processing data A.4.7	Testing with the standard camera A.4.6	Processing data A.4.7	Processing data A.4.7
Processing images A.4.8	Processing data A.4.7	Processing images A.4.8	Processing images A.4.8
	Processing images A.4.8		

Note: Bold numbers refer to the sections in the Appendix A.

Table 3.2: Steps to prepare and test prismatic pre-cracked rock specimens

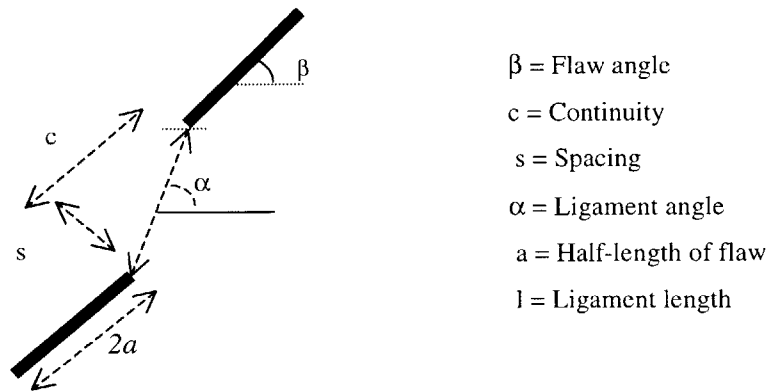


Figure 3.1: Flaw geometry for a specimen with two flaws.

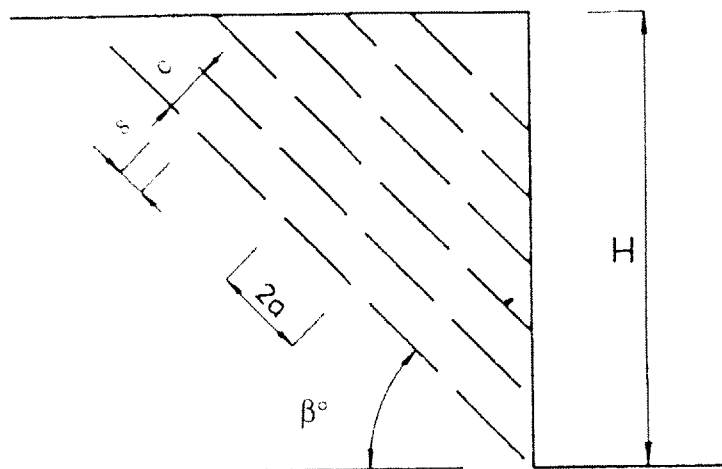


Figure 3.2: Flaw geometry in a jointed slope

Chapter 4: EXPERIMENTAL RESULTS

4.1 Introduction

This chapter describes the observations made in uniaxial compression loading tests run on prismatic granite and marble specimens with two parallel flaws cut through the thickness. For specimen characteristics, preparation, and lab testing refer to chapter 3 and Appendix A. The basic measurements and observations made include crack initiation stress, coalescence stress, failure stress, crack initiation angle, and crack pattern, focusing particularly on the coalescence mechanism of the two flaws.

While analyzing the results, it is important to have in mind that lab tests are an approximation of real rock behavior since the sudden failure of brittle rock specimens is associated with the nature of the loading machine itself. When compressive stress is applied, the loading machine deforms and stores elastic energy that is released near the failure threshold, causing the specimen to break suddenly. This is clearly observed when testing granite specimens, although the feedback control of the machine restricts the released elastic energy.

Table 4.1 lists the results obtained in uniaxial compression tests on granite specimens and table 4.2 the results from tests run on marble specimens. These tables include coalescence type, coalescence stress, and failure stress (peak); also coalescence and failure stress averages are computed for all of the geometries. The observed fracture coalescence patterns in granite and marble specimens are summarized in figure 4.1.

Section 4.2 introduces the granite and marble properties. Section 4.3 describes the observed coalescence types in general and discusses particular observations made in granite and marble specimens. Section 4.4 shows in detail the crack growth pattern for both granite and marble specimens. Section 4.5 compares and relates the coalescence stress with the stress level at failure. Section 4.6 summarizes the fractography observations made on granite and marble specimens. Section 4.7 shows the influence of

the flaws on the stress-strain plots in general and on the material stiffness (Young's Modulus) in particular.

4.2 Material Properties

4.2.1 Granite Properties

Granite is an igneous rock composed of about 25-35% quartz and 50% feldspar; other common constituents of granite are dark silicate (biotite mica) and muscovite (mica).

Intact (no flaws) specimens from every block are tested in uniaxial compression in order to assess the uniformity of the material. Figure 4.2 shows the stress-strain plots for these intact granite specimens. The noticeable difference in compressibility among the tests might be due to machine compressibility. The measured strain represents the system "specimen + loading machine". Appendix A (Lab Procedure) includes a discussion and a quantification of this machine compressibility.

One block out of approximately seven was discarded due to a very low strength and a failure mode showing splitting. This splitting is also observed in several specimens with flaws. The average strength after eliminating non-consistent tests is 139.58 MPa, with a standard deviation of 21.88 MPa (15.7 %).

Regarding failure modes, it is not easy to recover specimens after failure in only two halves as it was common for gypsum specimens. Usually, failure in granite specimens occurs very violently with many pieces "shooting" or falling as shown in figure 4.3. As described by Gramberg (1989), granite specimens often fail by buckling and peeling off that result from axial cataclasis, scaling and spalling (Type II in figure 4.4).

In some granite specimens (about 5%) horizontal cracks initiate tangentially to the external wing cracks. They propagate until they reach the sides, causing the specimen to fail (see figure 4.5).

4.2.2 Marble properties.

Marble is a nonfoliated metamorphic rock; it is a coarse, crystalline rock whose parent rock was limestone or dolostone. Pure marble is white and composed essentially of calcite. Often the limestone from which marble forms contains impurities that color the marble. Thus, marble can be pink, gray, green, or even black. Also, when impure limestone is metamorphosed, it may yield a variety of accessory minerals including chlorite, mica, garnet, and commonly wollastonite. When marble forms from limestone interbedded with shales, it will appear banded. Occasionally, marble will split along these bands and reveal the mica minerals that recrystallized from clay minerals.

The marble blocks used in the present research have some colored bands. However, these bands have no effect on the failure mode of either the intact or the flawed specimens. When observing the fracture surfaces one can see that these colored bands contain muscovite mica crystals.

As in granite, intact (no flaws) marble specimens from every block are tested in uniaxial compression in order to assess the uniformity of the material. Figure 4.6 shows the stress strain plots for these intact specimens. Again, the plotted strain includes the loading machine compressibility. It is noticeable in this chart and from the failure stresses of flawed marble specimens in table 4.2 that one of the blocks was stronger than the others. However, the failure pattern for intact specimens was consistent and hence the block was not discarded. The average strength of intact (no flaws) marble specimens is 43.57 MPa, with a standard deviation of 7.31 MPa (16.8 %).

Figure 4.3 shows the typical mode of failure for intact marble specimens (called type III by Gramberg). In this case, the specimens fail by shearing. This is also clearly seen in figure 4.7. Splitting is not generally observed in marble specimens.

Some specimens (for both granite and marble) show a failure mode that develops due to a combination of compressive force and bending moment, causing a “break head” (see figure 4.8), which is probably caused by incorrectly aligned and lubricated end platens. If the specimen fails in such a way the test and its data have to be discarded.

4.2.3 Other Material Properties.

Other material properties for both granite and marble are listed in Table 4.3. There are two sets of values for each rock; the values from the source (where the rocks came from) and the ones measured in the present research.

4.3 Fracture Coalescence

The coalescence types observed in the present research for both granite and marble are to some extent the same as the ones observed by previous researchers. As discussed later, a new coalescence type that was observed by neither Reyes (1991) nor Bobet (1997) has been found in granite specimens; it is called type IVB (see figure 4.1). However, this coalescence type is not completely new, since Wong and Chau (1998) observed it in their tests on molded sandstone.

For non-overlapping geometries and in both granite and marble specimens, coalescence always occurs due to internal cracks. Furthermore, the coalescence type depends on the flaw geometry. Specimens with coplanar flaws coalesce due to only internal shear cracks. On the other hand, in specimens with non-coplanar flaws, coalescence occurs through different combinations of internal shear cracks, internal wing cracks, and tension cracks[Ⓞ].

Ⓞ Wing cracks are tension cracks that initiate at (or near to, in some marble specimens) the flaw tips and tend to align with the load direction (vertical). The term “tension crack” is used to address other cracks originated under tensile stress (e.g. the vertical tension crack in the case of coalescence type II).

The particular fracture initiation and propagation patterns and failure mechanisms for the different tested geometries in granite and marble are discussed in Section 4.4. This section focuses on the crack coalescence mechanisms. Subsection 4.3.1 describes the coalescence modes shown in figure 4.1; particular issues of fracture coalescence, as well as stress levels, in granite and marble specimens are addressed in subsections 4.3.2 and 4.3.3 respectively.

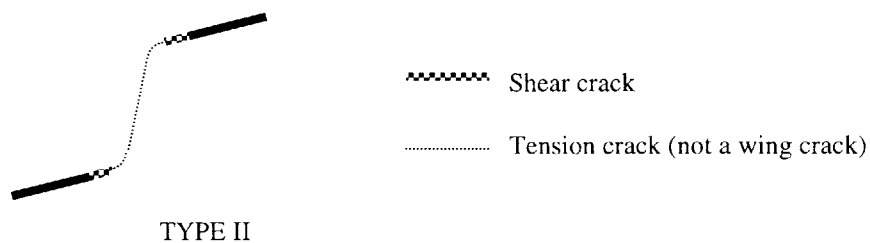
4.3.1 General coalescence types

Next, a description of the observed coalescence types follows. This information is summarized in Figure 4.1.

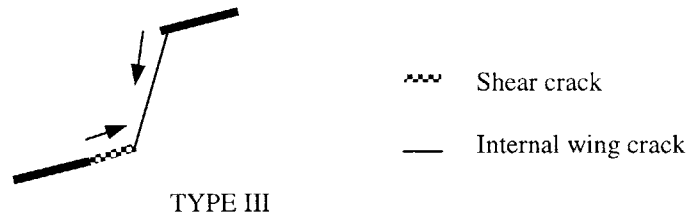
Type I occurs by either the linkage of two or the propagation of one internal shear crack. It is always observed in specimens with coplanar flaws.



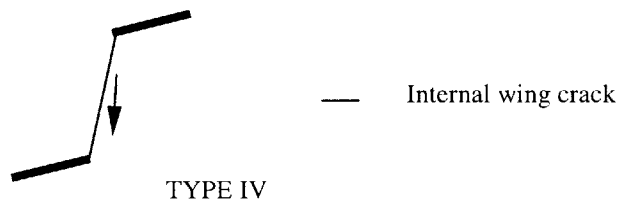
Coalescence **type II** is produced by the linkage of two internal shear cracks by a tension crack (note that this is a crack that originates in tension, but it is not a wing crack), which is almost vertical, and thus parallel to the main principal compression stress.



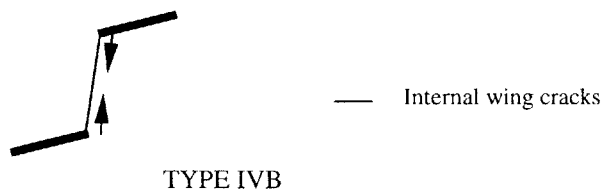
Coalescence **type III** develops when an internal shear crack from one of the flaws reaches the internal wing crack originated at the other flaw.



Coalescence **type IV** occurs by the propagation of an internal wing crack from one flaw until it reaches the other flaw.



Coalescence **type IVB** occurs by the linkage of two internal wing cracks that propagate until they join.



Wong et al (1998) observed this type of coalescence in specimens with flaw geometries having a ligament angle $90^\circ < \alpha < 75^\circ$. In the present research, this coalescence type is

observed for a geometry with ligament angle (α) equal to 90° , which is the boundary between overlapping and non-overlapping flaws. Type IVB is a coalescence type very close to type IV. In this case, the two internal wing cracks encounter each other half-way, completing the coalescence. It is hence called type IVB due to its similarity with type IV and should be expected to appear for both non-overlapping and overlapping flaw geometries.

Table 4.4 shows the observed coalescence types for both granite and marble specimens with different flaw geometries; the coalescence types observed in gypsum specimens are also included for purposes of comparison (both molded and cut flaws). The results in gypsum specimens with molded specimens are from Bobet (1997) and the ones with cut flaws are an unpublished series of test results. The only observable differences in coalescence modes between granite and marble specimens are for coplanar geometries (Geometries indicated with an arrow in table 4.4). Coplanar geometries with flaw angle $\beta = 30$ do not show coalescence for marble. Some granite specimens with flaw geometry 45-0-2a (also coplanar) appear to have no coalescence. However, when observed at a slower speed it is clear that these granite specimens (45-0-2a) have coalescence type I very close to failure, this is discussed in more detail in Section 4.4.

Bobet (1997) found a relationship between the ratio spacing/continuity (s/c) and the coalescence type, which is shown in table 4.5. The observations made on both granite and marble specimens support these values.

Figure 4.9 shows the variation of coalescence stress versus ligament length for both granite and marble specimens. The greater scatter in the granite results is evident. It is also seen that the general trend is an increase for granite but a slight decrease for marble specimens (see plotted regression lines). Next, the particular aspects of fracture coalescence in granite and marble are described (4.3.2 and 4.3.3 respectively).

4.3.2 Fracture coalescence in Granite.

Coalescence type I develops in granite specimens with geometries 30-0-a, 30-0-2a, 45-0-a, 60-0-a and 60-0-2a. This indicates that this type of coalescence predominates in geometries with coplanar flaws, and it does not depend on the flaw angle β . Table 4.6 lists ligament length and the corresponding coalescence stress averages for granite specimens with coplanar geometries. Figure 4.10 plots these data, showing the variation of the coalescence stress with the ligament length, which is expressed in terms of the half-flaw length (a). It can be seen that the coalescence stress increases with the ligament length. It is noticeable that specimens with a flaw inclination angle $\beta = 45^\circ$ coalesce at a higher stress level than the other geometries ($\beta=30$ and $\beta =60$).

Coalescence type II is observed for geometries 30-a-a, 30-a-2a, 30-2a-2a, 45-2a-2a, 45-a-2a, 45-a-a, and 60-a-2a. Table 4.7 lists the ligament length and average coalescence stress for the geometries with coalescence type II. Figure 4.11 plots these data and shows how the ligament length for these non-coplanar geometries affects coalescence stress. Note that both specimens with flaw angle $\beta = 45^\circ$ and with $\beta = 30^\circ$ show a slight decrease in coalescence stress when the ligament length increases. However, this decreasing trend could be due to the data scatter (greater for specimens with flaw angle $\beta = 45$). Bobet (1997) and Reyes (1991) generally observed a trend of the coalescence stress to increase with the ligament length for their molded gypsum specimens. The coalescence stresses and the coalescence types for all the tested granite specimens are shown in table 4.1.

Coalescence type III is observed in a few specimens with flaw geometries 30-2a-2a and 45-2a-2a. Hence, type III can occur when the ratio spacing/ continuity is $s/c = 1$.

Coalescence types IV and IVB occur for granite specimens with flaw geometry 45-a-a, which has a ligament angle (α) of 90° .

4.3.3 Fracture coalescence in marble.

Table 4.2 lists coalescence stresses and coalescence types for marble specimens; also coalescence stress average is computed and shown for each geometry.

Coalescence type I is observed in marble specimens with coplanar flaw geometries 45-0-a, 45-0-2a, 60-0-a, and 60-0-2a. It is noticeable that the coplanar geometries with flaw angle $\beta = 30$ (30-0-a and 30-0-2a) do not coalesce in the case of marble. Figure 4.12 shows the variation of the coalescence stress with the ligament length for marble specimens that present coalescence type I. As was observed for granite specimens with coplanar flaw geometries, the coalescence stress slightly increases as the ligament length increases.

Marble specimens with non-coplanar flaw geometries show either coalescence type II or type III. Coalescence type II is always observed in marble for geometries 30-2a-2a, 30-a-a, and 60-a-2a. On the other hand, marble specimens with flaw geometries 30-a-2a, 45-2a-2a, 45-a-2a, 45-a-a have either coalescence type II or type III (see table 4.2 for the observed coalescence type and coalescence stress for each of the tested marble specimens).

Figure 4.13 shows the variation of coalescence stress versus ligament length for marble specimens with non-coplanar flaw geometries. It can be seen that the coalescence stress is almost constant for specimens with flaw angle $\beta = 30$ and slightly decreases for specimens with $\beta = 45$.

4.4 Sequence and pattern of crack growth

Fracture initiation and propagation patterns are consistent for specimens with the same flaw geometry (i.e. the tests are reproducible). However, both the fracture growth pattern and the coalescence type depend on the flaw geometry. This, as well as the corresponding stresses and observations on fracture surface characteristics are now discussed in detail.

4.4.1 Granite results

Table 4.8 summarizes the observations on over 90 granite specimens with 2 parallel flaws cut through the thickness. For each geometry, the numbers in the first row of this table indicate the order in which the cracks develop, and the numbers shown in the second row are the stresses at which the cracks initiate, the specimens coalesce, or fail. Also the coalescence type (I, II, III, IV, IVB, or NO) is included in the coalescence column.

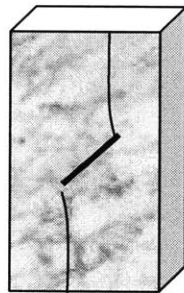
Figures 4.14 to 4.27 for granite and 4.28 to 4.40 for marble are pictures of the specimens during the load tests which are taken with a high-speed video camera and then digitized from the videotapes with a frame grabber as explained in Appendix A. The pictures in these figures (4.14 to 4.27 and 4.28 to 4.40) are taken from different specimens as indicated in the figure legends; on the other hand, each figure usually shows several of the features (steps) in the propagation and coalescence process. Typically, for granite, the same picture is shown both in raw and enhanced form (the cracks are highlighted); this is indicated by an arrow.

Below is a detailed description of the fracture pattern sequences for the different geometries follows. The text describes what is summarized in table 4.8 and makes reference to the pictures taken during load testing (figures 4.14 to 4.27).

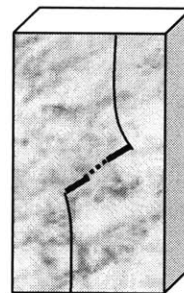
- 45-0-a
 - External wing cracks initiate (45 MPa).
 - Internal shear cracks initiate (60 MPa).
 - Internal shear cracks propagate until coalescence type I is complete (90 MPa. See 1 in figures 4.14a, 4.14b, and 4.14c). In general, both internal shear cracks develop until they coalesce. However, in some cases coalescence is accomplished by only one internal shear crack. In preceding research, the equipment did not allow one to state that these coalescence cracks were actually created in shear and the term “secondary cracks” rather than “shear cracks” was used. In this research, by using the high speed camera, relative movement can be seen when playing the event 500 or 1,000 times slower (the coalescence crack develops in a time of

approximately 1/30 to 1/100 seconds, but sometimes it develops stepwise). For an example of fracture propagation times see the text box at the bottom of figure 4.14c.

- Around coalescence (90 MPa) the specimens generally show flaking and/or loose grains in the observed surface (see 2 in figures 4.14a, figures 4.14b, and 4.14c)
- For some specimens, internal wing cracks initiate right before (90 MPa) or right after coalescence (95 MPa). They usually do not take part in the failure mechanism (i.e. they do not cause the specimen to fail). 3 in figure 4.14c indicates an internal wing crack (The picture was taken at failure).
- The specimens fail (100 MPa. See 4 in figures 4.14a and 4.14c) by propagation of the external wing cracks (i.e. when the external wing cracks reach the boundaries of the specimen). This is very reasonable, since after coalescence occurs for these coplanar geometries, the specimens behave as if they were specimens with only one flaw.



Single Flaw Specimen



Two Flaw Specimen with type I coalescence

▪ 60-0-a

The fracture pattern is very similar to the one observed on specimens with 45-0-a flaw geometry.

- External wing cracks initiate (50 MPa).
- Internal shear cracks initiate (60 MPa) and propagate very fast to make coalescence type I (60 MPa); 1 in figures 4.15a and 4.15b. At this same stress level the specimens show spalling (2 in figures 4.15a and 4.15b).
- Only one specimen (GR39, which is shown in figure 4.15a) had internal wing cracks initiated at around the coalescence stress (60 MPa). 3 in figure 4.15a

indicates this particular internal wing crack. Note that the initiation angle respect to the flaw is not around 90° as is usual.

- The specimens fail at a high stress (115 MPa) due to propagation of the external wing cracks. (4 in figure 4.15b).

- 60-0-2a

The fracture pattern is again very similar to the one observed on specimens with 45-0-a flaw geometry.

- External wing cracks initiate (at 50 MPa) and propagate stably.
- In some specimens, internal wing cracks initiate (60 MPa) but they do not propagate.
- Internal shear cracks initiate (60MPa).
- Internal shear cracks propagate producing coalescence type I (75 MPa. See 1 in figure 4.16). The coalescence stress (75 MPa) is higher than the one for specimens with 60-0-a since the ligament length is greater.
- A lot of spalling is typically visible in these specimens (See 2 in figure 4.16).
- Failure (at 100 MPa) is caused by propagation of external wing cracks.

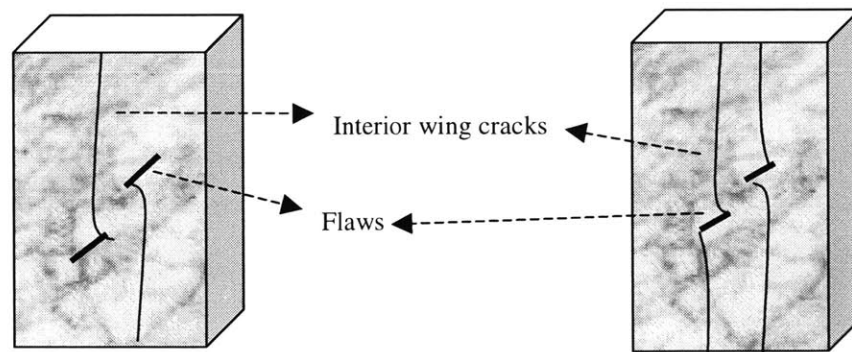
- 30-0-a

- Internal shear cracks initiate (45 MPa).
- Internal shear cracks propagate producing coalescence type I (70 MPa. See 1 in figures 4.17a and 4.17b).
- Internal wing cracks initiate (75 MPa See 2 in figures 4.17a and 4.17b) where the internal shear crack and the flaw merge.
- External wing cracks initiate in some specimens (80 MPa) before failure, but they do not propagate and hence they do not make the specimens fail in any case
- As the load further increases, the internal wing cracks propagate, causing the specimens to fail (85 MPa. See 3 in figure 4.17b).

- 30-0-2a

- Internal shear cracks initiate (50 MPa).

- In some specimens external wing cracks initiate (55 MPa. See 1 in figure 4.18), but they do not propagate further before coalescence.
 - Internal shear cracks propagate making the specimens to have coalescence type I (80 MPa. See 2 in figure 4.18). The coalescence stress is higher than the one observed in 30-0-a specimens (70 MPa). This is logical since the ligament length is greater.
 - Internal wing cracks initiate (85 MPa)
 - The specimens generally fail (85 MPa) due to a very fast propagation of internal wing cracks.
- 45-0-2a
- Internal wing cracks initiate (85 MPa. See 1 in figure 4.19b).
 - Internal shear cracks initiate (105 MPa).
 - Internal shear cracks propagate very fast making the specimen coalesce (type I) at 105 MPa. See 2 in figures 4.19a, 4.19c, and 4.19d.
 - Failure (115 MPa) does not seem to be influenced by coalescence. Two facts are clearly visible from the high-speed images: first, the specimens coalesce in shear (type I), since relative displacement is visible (3 in figure 4.19b); second, failure is due to propagation of internal wing cracks, which initiate prior to coalescence (4 in figure 4.19d). The specimens literally split in two or three vertical parts.



Note that this failure mechanism is very different from the one observed in 45-0-a specimens, where after coalescence the specimens behave as if they had only one larger flaw. It is also important to note that this mechanism could not be observed

when testing with the normal speed camera. In those cases “No Coalescence” was recorded. This seems to be the reason why this behavior was not observed in earlier research at MIT.

Another important feature to be observed in figure 4.19 is that the same fracture pattern can be observed on both faces of the specimens (the pictures in the left are from one face and the ones in the right column, which have a black frame, are from the other face). Hence, figures 4.19a and 4.19b are the two faces of the same specimen. The same holds for figures 4.19c and 4.19d. This fact is important since some researchers argue that the fracture process is in fact 3-D and hence the fracture pattern cannot be observed completely by looking at only the face of the specimen. This issue was addressed by Dyskin et al. (1995) and is discussed in Section 2.2.

- 60-0-3a

This geometry has the longest ligament length ($= 3a = 1.5''$) of all the geometries tested in the present research.

- External wing cracks initiate (85 MPa).
- In some specimens, internal wing cracks initiate (90 MPa) but they do not propagate.
- External wing cracks propagate until they make the specimen fail (115 MPa).
- Coalescence occurred for only one in five specimens at 118 MPa (note that this is the coalescence stress for this particular specimen and not an average stress as the other values shown in this chapter). This specimen is shown in figure 4.20; It had coalescence type I (see 1 in figure 4.20), with a general crack pattern similar to the one observed in the 45-0-a specimens. It is clear (and consistent with previous studies) that there is a limit for coalescence to occur, as the ligament length increases.
- All the specimens show spalling (2 in figure 4.20).

- 30-a-a

- External wing cracks initiate (70 MPa).

- Interior shear cracks initiate (80 MPa). In some specimens, and due to spalling (see 1 in figure 4.21), it is very easy to mistake these interior shear cracks for internal wing cracks. However, the spalling indicates that the dominant stress is compression.
- Only one specimen (the one shown in figure 4.21) really had an internal wing crack (see 2 in figure 4.21)
- The specimens generally coalesce (80 MPa) due to an almost vertical tension crack that links both internal shear cracks (type II. See 3 in figure 4.21). Note that this vertical tension crack is not a wing crack.
- The specimens fail (90 MPa. See 4 in figure 4.21) due to the propagation of external wing cracks. During failure, the coalescence crack can behave in two very different modes: it can slip or open wider as in figure 4.21.

- 30-a-2a

The general fracture growth pattern is similar to the one observed in 30-a-a specimens.

- External wing cracks initiate (60 MPa).
- Internal shear cracks initiate (70 MPa).
- These internal shear cracks are immediately linked by a vertical tension crack producing coalescence type II (70 MPa. See 1 in figure 4.22a).
- Specimens typically show spalling (see 2 in figure 4.22b).
- The specimens fail (110 MPa) due to propagation of the external wing cracks.

- 45-a-2a

The fracture growth pattern is again very similar to the one described for 30-a-a specimens.

- External wing cracks initiate (50 MPa).
- In some specimens, internal wing cracks initiate (65 MPa), but do not propagate further.
- Internal shear cracks initiate (100 MPa) and are linked by a vertical tension crack (type II at 100 MPa. See 1 in figure 4.23a and 4.23b). Note that the coalescence

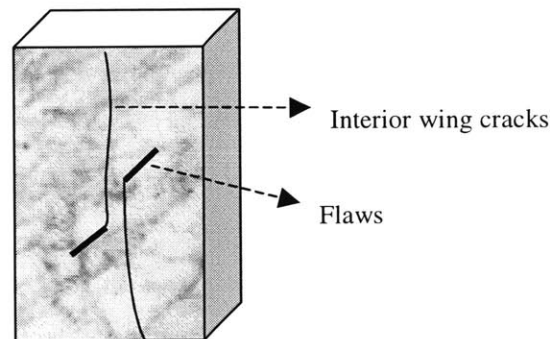
stress is higher than for other geometries. 2 and 3 in figure 4.23b (taken with the high-speed camera) clearly show that this vertical tension crack first opens in tension and then, at failure, slips. Hence a shear-like surface results as a product of the post-coalescence slippage of the coalescence crack. Fractography analysis did not allow one to draw a definitive conclusion about this mechanism, although Reyes (1991) stated that shear after tensile failure was a possibility (see also Section 4.6).

- The specimens fail (110 MPa) due to propagation of the external wing cracks.

- 60-a-2a

The fracture growth pattern is again very similar to the one described for 30-a-a specimens.

- External wing cracks initiate (60 MPa).
- Internal shear cracks initiate (90 MPa).
- Coalescence type II occurs (90 MPa. See 1 in figure 4.24).
- Specimens typically show spalling (see 2 in figure 4.24)
- Failure is due to propagation of external wing cracks.
- 3 out of 5 specimens did not coalesce. When the specimens do not coalesce, the failure is due to internal wing cracks that initiated at around 90 MPa:



- 45-2a -2a

- External wing cracks initiate (55 MPa).
- Internal shear cracks initiate (60 MPa).
- The internal shear cracks are immediate linked by a vertical tension crack (coalescence type II at 60 MPa. See 1 in figure 4.25b).

- One specimen had coalescence type III at a similar stress level (see 2 in figure 4.25a)
- Failure (95 MPa) is due to propagation of external wing cracks.

- 30-2a-2a

The general crack pattern is the same as the one formerly described for geometry 45-2a-2a.

- External wing cracks initiate (65 MPa).
- Internal shear cracks initiate (70 MPa. See 1 in figure 4.26a and 4.26b).
- Coalescence is either type II (2 in figure 4.26b) or III (3 in figure 4.26a) at around 75 MPa. In the case of specimens with coalescence type III, an internal shear crack develops from one tip, and coalescence is completed through an internal wing crack, which develops from the other flaw tip (4 in figure 4.26a).
- Some specimens develop internal wing cracks (75 MPa). 5 in figure 4.26a indicates an internal wing cracks that does not start at the flaw tip. This is not common in the case of granite.
- Specimens fail (85 MPa) due to propagation of external shear cracks.

- 45-a-a

The general crack pattern is again similar to the one formerly described for geometries 45-2a-2a and 30-2a-2a.

- External wing cracks initiate (45 MPa).
- In some specimens, internal shear cracks initiate (50 MPa).
- In most of the specimens, the internal shear cracks are immediate linked by a vertical tension crack (coalescence type II at 60 MPa).
- For at least three specimens (out of 6) the coalescence mechanism (or coalescence type) is different. In these cases, coalescence type IV (1 in figure 4.27b) and the new type IVB (2 in figure 4.27a) are observed.
- Failure (85 MPa. See 3 in figure 4.27b) is always caused by propagation of external wing cracks.

4.4.2 Marble results

Fracture growth patterns and coalescence types are very consistent in marble specimens with different flaw geometries. Table 4.9 summarizes observations made on over 50 marble specimens with two parallel flaws cut through the thickness. Note that specimens with exactly the same flaw geometries as in granite have been tested. For each geometry, the numbers in the first row of this table indicate the order in which the cracks initiate or develop, and the numbers shown in the second row are the stress levels in MPa at which the cracks initiate, the specimens coalesce, or fail. Also the coalescence type is included in the coalescence column.

The video images (taken generally at 250 frames per second) are much clearer than in the case of granite. This is due to the high contrast between the material color (white) and the fractures (black). However, the existence of glare sometimes masks the fracture growth pattern observations and limits the amount of light that can be used to record the fracture process. Figures 4.28 to 4.40 are such raw pictures in which no cracks are drawn to enhance the images.

Next, a detailed description of the fracture pattern sequences for the different tested geometries follows. The text describes what is summarized in table 4.8 and make reference to the pictures taken during load testing (figures 4.28 to 4.40).

- 45-0-a
 - First, external wing cracks develop at the tip of the flaws (18 MPa. See 1 in figure 4.28a).
 - Internal wing cracks initiate (20 MPa. See 2 in figure 4.28b). Both internal and external wing cracks initiate perpendicular to the flaws.
 - Internal shear cracks initiate coplanar to the flaws (29 MPa).
 - These internal shear cracks propagates very fast. As in granite, some specimens coalesce (type I at 29 MPa. See 3 in figures 4.28a and 4.28b) with only one

internal shear crack and some coalesce by the joining of two internal shear cracks (each of them initiated at each flaw).

- In some specimens, an external shear crack initiates in one of the flaws (30 MPa. See 4 in figure 4.28a), which initiate right after coalescence.
- The specimens fail (32 MPa) when either the external wing cracks or the external shear cracks reach the boundaries. The failure in marble specimens is not as violent as in granite; the marble specimens rarely explode.

Generally, the specimens show spalling at both the external and the internal tips of the flaws. This is an indication that the dominant stress is compression. This spalling is not clearly visible in figure 4.28. During the test, and before the spalling is visible, a brighter (more white) area is clearly seen. This effect is also visible in granite. However, in that case, the grains and the color confuse the image. The development of this brighter area may indicate that the surface is about to be detached.

- 60-0-a

- External wing cracks initiate (25 MPa. See 1 in figure 4.29b).
- Internal shear cracks initiate (28 MPa).
- External shear cracks initiate coplanar to the flaws (29 MPa. See 2 in figures 4.29a and 4.29b).
- As the load further increases, the specimens coalesce (type I at 30 MPa. See 3 in figures 4.29a and 4.29b).
- Failure (36 MPa) is caused by the propagation of the external shear cracks. The failure pattern is very similar to the one shown by intact specimens (shearing, as explained in Section 4.2.2 and shown in figure 4.7).

- 60-0-2a

The crack pattern and sequence is very similar to the ones observed in 60-0-a specimens.

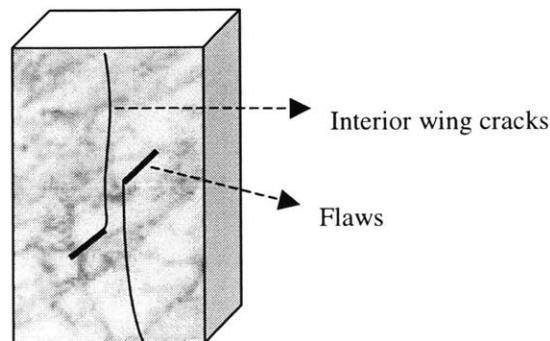
- External wing cracks initiate (30 MPa. See 1 in figure 4.30a).
- Internal shear cracks initiate (30 MPa).

- External shear cracks initiate coplanar to the flaws (30 MPa. See 2 in figure 4.30 and 4.30b). Note that all of these cracks (external wing, internal and external shear) are initiating almost at the same time (or for the same stress).
- As the load further increases, the specimens coalesce (type I at 31 MPa. See 3 in figure 4.30a and 4.30b). Note that the coalescence stress is almost the same as the one for 60-0-a specimens, despite the difference in ligament length (“a” = 0.5” and “2a” = 1”, respectively).
- Failure (37 MPa) is caused by the propagation of the external shear cracks.

▪ 30-0-a / 30-0-2a

These two geometries are described together since the fracture pattern is very similar. None of these geometries have coalescence (see 1 in figures 4.31a, 4.31b, 4.32a, and 4.32b).

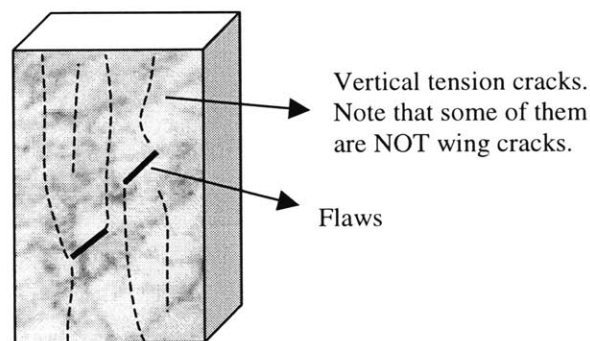
- External wing cracks initiate (16 MPa for 30-0-a and 18 MPa for 30-0-2a) perpendicular to the flaws (see 2 in figure 4.31b). Two of the specimens have shown wing cracks that develop in the middle of the flaws (instead of at the flaw tips), see 3 in figure 4.32b
- Internal wing cracks initiate (23 MPa for 30-0-a and 20 for 30-0-2a) but do not propagate further. At that moment the area between the flaws becomes brighter (see 4 in figure 4.31a) and shows spalling for some specimens. However, no coalescence crack did develop for any of the tested specimens.
- Failure is generally caused by internal wing cracks (at 32 MPa for 30-0-a, and at 33 MPa for 30-0-2a); this is similar to the observed failure mode for some granite specimens with coplanar geometries (see 5 in figure 4.32a).



In this failure mode the specimens behave as if the two flaws were completely independent. Flaw closure is typically observed during failure (see 6 in figure 4.31b and 4.32b).

▪ 45-0-2a

- Internal wing cracks initiate (22 MPa. See 1 in figure 4.33a).
- External wing cracks initiate (26 MPa).
- In some specimens, external shear cracks initiate (26 MPa).
- Internal shear cracks initiate (32 MPa).
- In most of the specimens, the internal shear cracks propagate very fast, producing coalescence type I (32 MPa. See 2 in figure 4.33a and 4.33b). The specimens usually become brighter in the coalescence area.
- Some specimens fail (34 MPa. See 3 in figure 4.33a) due to the propagation of external wing or external shear cracks.
- Some specimens fail (34 MPa) due to the development of vertical tensile cracks, which are not wing cracks (see 4 in figure 4.33b). During failure these vertical tension cracks are slipped.



▪ 30-a-2a

- Internal wing cracks initiate (18 MPa. See 1 in figures 4.34a and 4.34b)
- External wing cracks initiate (22 MPa. See 2 in figures 4.34a and 4.34b). Both internal and external wing cracks initiate perpendicular to the flaws and at their tips.
- Internal shear cracks initiate (25 MPa) in the plane of the flaws but they do not propagate farther.

- Coalescence (25 MPa) is produced by a tensile crack that links both internal shear cracks, producing coalescence type II (at 25 MPa. See 3 in figure 4.34b).
 - One out of three specimens had coalescence type III (at around 21 MPa. See 4 in figure 4.34a).
 - The specimens fail (25 MPa) due to propagation of the external wing cracks. Note that coalescence and failure are very close in time (and hence in stress). 5 in figure 4.34b shows a vertical crack that's being opened while the specimen is failing.
- 30-2a-2a / 30-a-a
 - External wing cracks initiate (20 MPa for both geometries. See 1 in figures 4.35a and 4.36b). For these geometries the external wing cracks do not always initiate at the flaw tips (see 2 in figure 4.36a).
 - Internal shear cracks initiate (24 MPa for 30-2a-2a, and 22 MPa for 30-a-a).
 - The internal shear cracks are immediately linked by a vertical tension crack, producing coalescence type II (at 24 MPa for both geometries. See 3 in figures 4.35b and 4.36a).
 - One specimen with flaw geometry 30-a-a had an external shear crack that initiated (28 MPa) prior to failure.
 - Failure (At 35 MPa for 30-2a-2a, and at 30 MPa for 30-a-a) generally occurs due to the propagation of the external wing cracks. 4 in figure 4.35a indicates an example of a vertical crack opening during failure in a 30-2a-2a marble specimen. 5 in figure 4.36b indicates flaw closure, which is typically observed in specimens with flaw angle $\beta = 30$ prior to the failure.
- 60-a-2a
 - Internal shear cracks initiate (29 MPa) in the plane of the flaws.
 - Typically, in only one of the flaws, an external wing crack initiates (30 MPa. See 1 in figures 4.37a and 4.37b) perpendicular to the flaw and at its external tip.
 - Typically, in only one of the flaws, an external shear crack initiates (30 MPa. See 2 in figures 4.37a and 4.37b).

- A tensile crack that links both internal shear cracks propagates, producing type II coalescence (31 MPa. See 3 in figures 4.37a and 4.37b).
 - The specimens fail (34 MPa) due to propagation of either the external wing cracks or the external shear cracks.
- 45-2a-2a / 45-a-2a

Both geometries show a similar crack pattern.

 - External wing cracks initiate (16 MPa for 45-2a-2a and 20 MPa for 45-a-2a. See 1 in figures 4.38a, 4.39a and 4.39b); in some specimens these external wing cracks do not initiate at the flaw tips (See 2 in figure 4.38b).
 - Internal shear cracks initiate (22 MPa for 45-2a-2a and 20 MPa for 45-a-2a) in the plane of the flaws.
 - Coalescence happens (at 22 MPa for 45-2a-2a, and at 24 MPa for 45-a-2a). Both type II (See 3 in figures 4.38a and 4.39b) and type III (see 4 in figures 4.38b and 4.39a) are observed.
 - Failure (at 30 MPa for 45-2a-2a, and at 31 MPa for 45-a-2a) of the specimens is caused by the external wing cracks reaching the specimen boundaries. 5 in figure 4.39b indicates a common observation in marble specimens, which is that during the failure process there is a lot of slippage.
- 45-a-a
 - Internal shear cracks initiate (26 MPa) in the plane of the flaws.
 - Either type II (see 1 in figures 4.40a and 4.40b) or type III coalescence happens (26 MPa).
 - External wing cracks initiate (30 MPa. See 2 in figure 4.40b). Note that this is the only geometry in which coalescence is observed prior to external wing crack initiation.
 - Typically a lot of spalling at the external tips of the flaws is observable (See 3 in figure 4.40b).
 - In some specimens, external shear cracks initiate (30 MPa. See 4 in figure 4.40b).

- The specimens generally fail (33 MPa) by propagation of either external wing cracks or external shear cracks. In some specimens vertical cracks, which are not wing cracks, open during failure (see 5 in figure 4.40a)

4.5 Relationship between failure stress and coalescence stress

As a general trend and for both granite and marble specimens the failure stress increases as the coalescence stress increases. This is consistent with previous results in gypsum specimens from Bobet (1997).

4.5.1 Granite Results

Figures 4.41, 4.42, and 4.43 show the variation of coalescence stress with failure stress for granite specimens with flaw inclination angle $\beta = 30^\circ$, 45° , and 60° respectively. The shaded areas represent the zone where coalescence stresses would be greater than failure stress, something physically impossible. The upper boundary of the shaded area indicates where the coalescence stress would be equal to the failure stress. Linear regression lines for the data are also shown. Generally, the coalescence stresses increase as the failure stresses increase for specimens with flaw angles of 30° and 45° . However, geometries 30-a-2a, 45-2a-2a, 60-0-2a, and 60-a-2a show that the failure stress decreases for an increase in the coalescence stress. This unlikely result may be due to the small number of tested specimens (note that one of the curves has only two points).

4.5.2 Marble Results

Figures 4.44, 4.45, and 4.46 show the variation of coalescence stress with failure stress for each flaw inclination angle ($\beta = 30^\circ$, 45° , and 60°) in marble specimens. It is clear from these charts that the dispersion of the results is much smaller than in the case of

granite. The lines are linear regression plots on the data. As a general trend, the coalescence stress increases with the failure stress. The only exception to this general trend is for specimens with flaw geometry 30-a-a as shown in figure 4.44.

4.6 Fractography

4.6.1 Introduction

Fracture origin and propagation can be analyzed by using a high-speed video camera to record the loading process of the specimen in a VCR and observing the relative movements during initiation and propagation of fractures. All of these observations are made at the same time as the cracks develop (i.e. while testing).

Another way to identify the type of fracture is to perform fractography analyses, i. e. studying the crack surface after failure. Surface morphologies are studied and linked with the mode of crack propagation. Fractography can be classified into macrofractography, which studies fractures using the naked eye or a hand lens and microfractography, which studies fracture surface features with optical or electron microscopes.

In this research, macrofractography is used as a secondary tool to identify crack origin (the primary tool used for this is the high-speed camera, which provides the possibility to observe the fracture initiation process up to 1,000 times slower, allowing one to clearly identify relative displacement of the crack surfaces).

4.6.2 Background

The main factors that distinguish shear and tension surfaces are the presence of powder on fracture surfaces, roughness, brightness, modes of breaking of the minerals composing the rock in the case of granite, etc. Furthermore, there are some typical surface morphologies: (1) tension cracks have a distinctive surface morphology called plumose

structure (figure 4.47a and 4.47b), which consists of an axis and striations marking the direction of fracture propagation; (2) shear cracks generally have slickensides; the surface is often polished and striated.

Natural rocks are typically composed of mineral grains. While analyzing fracture surfaces one observes different mineral grains. Generally, minerals composing the rock show one of the following three types of breaking:

- Cleavage is the tendency of minerals to break along weak planes that are consequence of the atomic packing. When minerals break with cleavage the observable result is a planar surface. Cleavage can be observed in feldspars, with cleavage planes forming 90° angles.
- Fracture: in some minerals, such as quartz, the strength of bonds is approximately the same in all directions. In this case, minerals do not follow a particular crystallography direction when breaking. There are different types of fracture; conchoidal fracture is the most common type in quartz.
- Parting: when minerals break along planes of structural weakness, they have parting. Parting is not observed in all minerals, but only in those that are twinned, such as feldspars (Figure 4.48). A twinned crystal is actually composed of two or more crystals of the same substance which are intergrown in such a way as to exhibit partial parallelism in some directions and reverse positions in others. Hence, a twinned crystal is a single crystal divided into two (or more) parts in which the crystal lattice of one part is differently oriented with respect to the next one.

4.6.3 Former results in gypsum

Reyes (1991) concluded that there are three different types of fracture surfaces in gypsum specimens (see figure 4.49): (1) the dotted region is characterized by absence of powder,

and smooth when observed by the naked eye. These characteristics are typical of wing crack surfaces (tensile) in gypsum. (2) The dashed region is characterized by traces of pulverized gypsum, and the surface is rougher than in the tensile cracks. (3) The shaded region is characterized by significant amounts of pulverized gypsum and the surface is very rough. This can be seen as typical of a shear crack surface on gypsum.

As it is described later, the observations on natural rock crack surfaces are different, shear crack surfaces are smooth and tensile crack surfaces are rough. Powder, however is characteristic for shear surfaces both in gypsum and natural rock.

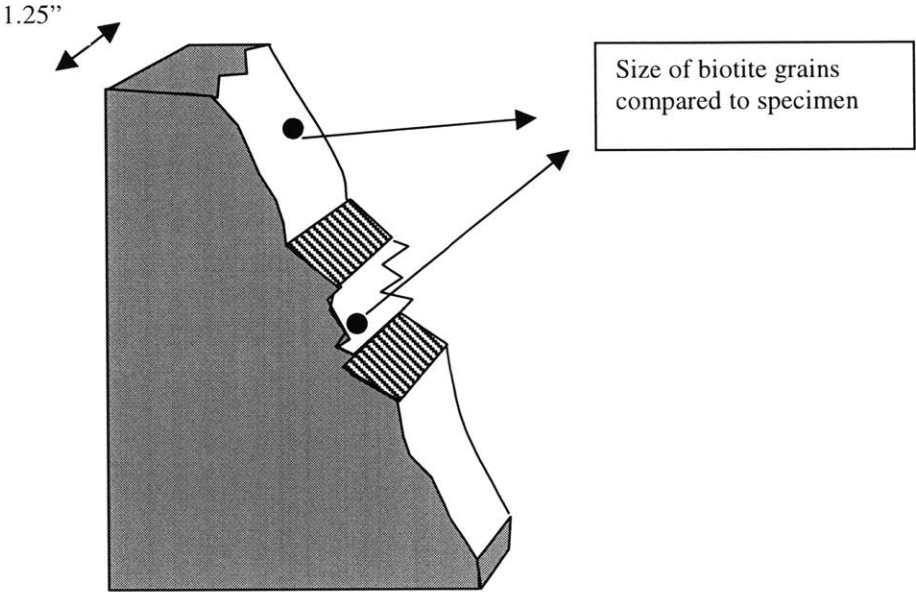
4.6.4 Fractography observations in granite

Figure 4.50 shows the three main minerals that compose granite, which are a) feldspar, b) quartz, and c) biotite. It is clear that mineral grains influence how cracks initiate and propagate.

It is generally observed at the front face of the specimen during load testing that cracks go through the grain boundaries. However, when analyzing some crack surfaces, grain breakage is observed; it is difficult to assess the cause of this grain breaking. There are three possible reasons. (1) The grain breakage is produced by the slippage of opened fractures during the loading process (this seems to be the most probable explanation). (2) The mineral fractures were present in the natural rock. (3) Fractures actually break the grains when they initiate (this has never been observed at the front face of the specimens during the loading process). Note that (3) refers to fracture initiation, while (1) refers to fracture slippage after fractures have initiated and propagated.

Another common observation during load testing is that cracks typically tend to initiate and propagate through biotite grains (they have a sheet-like shape and are weaker than the other minerals in granite). This process is called zonation {see figure 4.51 from Pusch (1977)}. Furthermore, when analyzing both shear and tensile crack surfaces, biotite grains can be seen on the surface; this is again indicating that the cracks propagate next to

them. However, it is important to realize that biotite grains do not extend through all the specimen thickness and hence one cannot say that the crack initiation location is only related to the biotite grain location.



- Tension cracks

The tension cracks studied here are: (1) external wing cracks, (2) internal wing cracks from coalescence cracks (types III, IV, or IVB), or (3) vertical tension cracks (not internal wing cracks) from coalescence cracks type II. The surfaces of tension cracks are typically bright and, in contrast to shear cracks, there is no powder or dust on them. The tendency of tension cracks is to segment or tilt with abrupt steps and then propagate for short distances within the cleavage planes and fracture surfaces of mineral grains. For this reason, tension crack surfaces are very rough (figure 4.52). Plumose structure can be observed only on very few specimens because the grains composing granite make this observation difficult.

In general, the different granite minerals (figure 4.50) grains can be easily recognized on a tensile crack surface:

- Quartz crystals can be found as either hexagonal prisms (see 1 in figure 4.53 and 4.54) bounded by a dipiramid or presenting conchoidal fracture (see 2 in figure 4.55).
 - As was mentioned before, biotite grains are generally observed loosely sticking to the surface (3 in figures 4.53, 4.54 and 4.55).
 - Feldspar grains present in a tension crack show cleavage, with cleavage planes at or around 90° (see 4 in figures 4.53 and 4.54). Atkinson (1987) observed that minerals with a well-defined cleavage, such as feldspars, generally crack parallel to cleavage planes. Furthermore, it can be said that failure of complete crystals along cleavage planes (in the case of feldspars) suggests the presence of tensile stresses.
- Shear cracks

The surfaces of shear cracks have powder and dust on them; even after cleaning the surface, there is still dust and the surface is opaque. During the shear crack propagation there is relative movement between both sides of the crack, involving friction (figure 4.56); this slippage produces smoother surfaces with some slickensides and striations parallel to the direction of the movement (see 1 in figure 4.57).

Regarding mineral grains, it is observed that:

- Few or no quartz crystals are observed.
- As in tension crack surfaces, biotite grains can be seen on the surface (2 in figure 4.57), but in the shear cracks they are even looser.
- In some specimens thin superposed planes of feldspar with a pointed shape can be observed (see 3 in figure 4.58 and also figure 4.59). The points are aligned with the direction of slippage. This kind of break is parting, since feldspar has twinning planes.

4.6.5 Fractography observations in marble

Marble is composed by calcite (figure 4.60) or dolomite. The analysis of fracture surfaces can be summarized as follows:

- Tension cracks

Tensile crack surfaces in marble specimens have no dust and are very bright (see figure 4.61). The marble used in the present research has some colored bands, formed of muscovite mica crystals. In tensile cracks, these mica crystals are very visible and bright. The surface is rough but not as rough as for granite specimens. Some external wing crack surfaces have plumose structures.

- Shear cracks

Shear crack surfaces are generally very dusty and with no bright areas at all (see figure 4.62). During load testing the generation of dust can be usually observed. This process is accentuated when the cracks slip during failure. Shear cracks have slickensides. However, there is no parting of minerals that could indicate the direction of movement as in granite.

Figures 4.63 and 4.64 show coalescence fracture surfaces in marble. Areas of tensile and shear fracturing can be distinguished. The crack shown in figure 4.63 belongs to a specimen that had coalescence type II, while figure 4.64 shows a coalescence crack surface type III.

4.6.6 Sources of error

It is generally possible to distinguish between shear and tension cracks, as in figures 4.65 and 4.66 for granite and figure 4.63 and 4.64 for marble. However, this difference is not that clear in specimens with small ligament length (around “ a ” = 0.5”).

The two principal sources of error in order of importance are (in order of importance):

- Observing shear-like characteristics in a crack surface does not allow one to make a definitive conclusion about the crack origin. For example, slickensides are observed in wing cracks (which are tension cracks) in some granite specimens with geometries 30-0-a, 30-a-2a, 45-0-2a and 60-a-2a. Hence, this shear surface structure is superposed on the tension crack surface by the subsequent slippage. The same posterior slippage causes shear-like crack surfaces on some marble wing cracks surfaces.
- There are some granite specimens in which a tensile like crack surface is observed in fractography analyses, but it is clear during testing (due to relative displacement) that the fracture developed in shear. The crack surfaces on these specimens appear to have a concave surface because material from the crack surface falls out after failure (see the sequence in figure 4.67).

For this reason, some shear cracks in granite present tensile like crack characteristics (see figures 4.68).

4.7 Influence of flaws in stiffness

Appendices B and C contain the stress-strain plots for specimens with different flaw geometries for granite and marble respectively. It is important to note that the strain data plotted in these charts are calculated from the displacements of the loading machine platens and hence the machine compressibility is included (i.e. it represents the strain of the system machine + specimen).

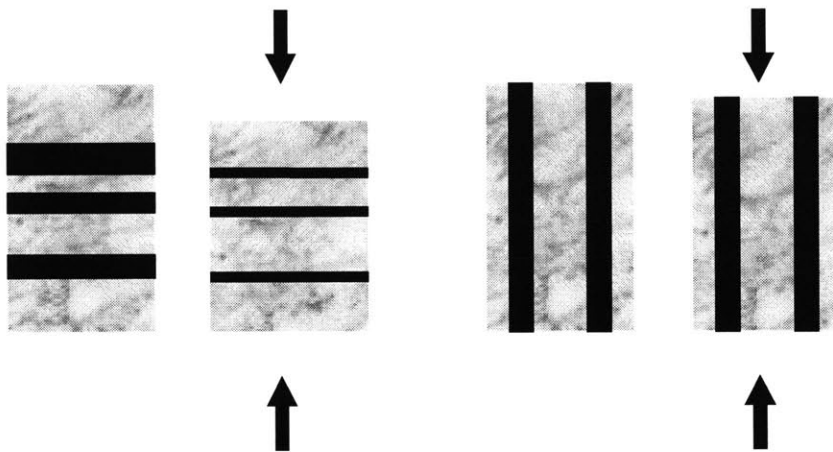
In general, the initiation of tension or shear fractures does not alter the shape of the stress-strain curves (no leap, or discontinuities) for both granite and marble. However, for a few tests the plots show a horizontal leap coincident with the coalescence stress (See figure 4.69).

It is observed that the introduction of flaws in the specimens makes them less stiff than the intact ones. Furthermore, the change in stiffness depends on the value of the flaw angle β .

In order to quantify this stiffness reduction, the E values were measured from the slopes of the stress-strain curves that are shown in Appendices B and C for the different geometries in granite and marble respectively. The results are represented for granite on figure 4.70 and for marble in figure 4.71. E is the Young's Modulus for the specimens with cut flaws (with the plotted flaw angle). These values are normalized by using E_{int} , which is the Young's Modulus measured in intact specimens.

Note that this result is also consistent with the observed flaw closure in marble specimens with flaw angle $\beta = 30^\circ$ and $\beta = 45^\circ$.

If the interpolation lines are extrapolated to $\beta = 0^\circ$ and $\beta = 90^\circ$, these charts reflect the fact that cracks perpendicular to the load produce a softer material (the cracks are being closed during loading, producing extra strain); while cracks parallel to the load have almost no influence on the material stiffness



Flaws perpendicular to the compression load yields a larger strain. (Mainly due to flaw closure).

Flaws parallel to the compression load yields a smaller strain

GEOMETRY	SPECIMEN	σ_{Coal} [Mpa]	σ_{Fail} [Mpa]	Coalescence type
30-0-a	GR62	63.05	80.32	I
	GR63	55.60	78.4	
	GR92	60.30	60.3	
	GR93	85.58	96.52	
	GR94	96.52	102.56	
	Average :	72.21	83.62	
30-0-2a	GR14 *	no	57.91	I
	GR15	87.95	87.95	
	GR66	93.84	93.84	
	GR67	85.74	85.74	
	GR72 *	no	107.58	
	GR83	56.74	65.54	
	GR84 *	no	98.75	
Average :	81.07	83.27		
30-2a-2a	GR23	78.60 (III)	86.32	II /some III
	GR24	88.25 (II)	89.67	
	GR41	53.74 (II)	71.69	
	GR68 *	75.37 (II)	?	
	GR69	81.87 (II)	82.56	
Average :	75.62	82.56		
30-a-a	GR10	108.90	111.64	II
	GR11	90.50	92.09	
	GR64	63.56	78.16	
	GR65	63.61	63.61	
	GR85	67.69	103.27	
	GR86	74.03	75.18	
Average :	78.05	87.33		
30-a-2a	GR12	82.59	107.39	II
	GR13 *	no	111.07	
	GR77 *	65.93	?	
	GR78	35.68	130.50	
	GR81	71.94	105.75	
	GR82	89.89	95.58	
Average :	70.03	109.81		
45-0-a	GR4	106.64	107.80	I
	GR5	99.28	110.30	
	GR59	63.69	85.40	
	GR60	106.64	113.75	
	GR61	79.06	84.98	
Average :	91.06	100.45		

Table 4.1: Coalescence and failure stress on **granite** specimens (it continues in next page)

*: Values not used to compute stress averages.

GEOMETRY	SPECIMEN	σ_{Coal} [Mpa]	σ_{Fail} [Mpa]	Coalescence type
45-0-2a	GR1 *	no	111.07	I / NO ? At high-speed Coalescence type I is observed for almost all of the specimens
	GR2	79.06	96.36	
	GR3 *	no	64.24	
	GR49	131.54	131.54	
	GR50 *	no	98.86	
	GR51 *	?	139.05	
	GR52 *	no	100.19	
	Average :	105.30	113.95	
45-2a-2a	GR25	78.67 (II)	92.65	II / some III
	GR26	72.20 (II)	81.66	
	GR42	39.47 (III)	89.92	
	GR43	64.35 (II)	94.43	
	GR87	54.04 (II)	116.43	
	GR88	41.90 (II)	97.58	
	Average :	58.44	95.45	
45-a-2a	GR18	130.18	131.45	II
	GR19	94.70	84.70	
	GR53	107.50	107.50	
	GR54	83.92	98.85	
	GR55	90.69	119.50	
	Average	101.40	108.40	
45-a-a	GR6 *	91.93 (II)	121.03	II / some IV / Some IVB
	GR7	79.06 (II)	111.61	
	GR44	39.88 (IVB ?)	72.15	
	GR45 *	45.48 (IVB)	68.60	
	GR46 *	47.80 (IV)	75.57	
	GR75 *	(II)	?	
	GR76	34.90 (II)	67.40	
	Average :	51.28	83.74	
60-0-a	GR39	43.50	125.60	I
	GR40	43.21	111.31	
	GR73 *	53.62	?	
	GR74	90.89	123.66	
	GR91	61.64	98.18	
	Average :	59.81	114.69	
60-0-2a	GR16	no	148.46	I
	GR17	74.54	124.07	
	GR56 *	59.96	73.71	
	GR57	81.41	87.11	
	GR58	73.11	92.50	
	Average :	76.35	101.23	

Table 4.1: Continued

GEOMETRY	SPECIMEN	σ_{Coal} [Mpa]	σ_{Fail} [Mpa]	Coalescence type
60-0-3a	GR27 *	no	130.75	NO
	GR28 *	no	110.29	
	GR89 *	118.05 (I)	139.13	
	GR90 *	no	85.55	
	Average :	**	**	
60-a-2a	GR20 *	no	62.93	II / some NO
	GR21 *	no	66.71	
	GR22	113.69	123.26	
	GR70 *	64.88	?	
	GR71	63.42	139.63	
	Average :	88.56	129.95	

Table 4.1: Continued

GEOMETRY	SPECIMEN	σ_{Coal} [Mpa]	σ_{Fail} [Mpa]	Coalescence type
30-0-a	MA35	No	38.60	NO
	MA36	No	34.20	
	MA04	No	28.19	
	MA05	No	29.01	
	Average :		32.50	
30-0-2a	MA06	No	28.18	NO
	MA07	No	22.53	
	MA37	No	36.37	
	MA38	No	45.72	
	Average :		33.20	
30-2a-2a	MA08	19.33	26.30	II
	MA09	25.71	34.71	
	MA30	28.24	38.43	
	MA31	24.09	38.52	
	Average :	24.34	34.49	
30-a-a	MA10	28.07	28.86	II
	MA11	13.09	30.88	
	MA40	29.91	30.31	
	Average :	23.69	30.02	
30-a-2a	MA12	20.40 (III)	20.60	II / III
	MA13	20.72 (II)	20.72	
	MA41	32.71 (II)	32.71	
	Average :	24.61	24.68	
45-0-a	MA14	23.71	26.22	I
	MA15	23.44	23.44	
	MA45	39.19	47.57	
	Average :	28.78	32.41	
45-0-2a	MA16	27.19 (I)	28.19	I
	MA17	25.88 (I)	28.02	
	MA44	44.54 (?)	44.54	
	Average :	32.54	33.58	
45-2a-2a	MA18	14.84 (II)	22.78	II / some III
	MA19	15.78 (III)	17.12	
	MA47	35.82 (II)	50.23	
	Average :	22.15	30.04	
45-a-2a	MA20 (III)	22.24 (III)	30.81	III / some II
	MA21 (II)	21.60 (II)	26.16	
	MA46 (III)	29.40 (III)	36.77	
	Average :	24.41	31.25	
45-a-a	MA22 (II)	24.57 (II)	26.20	II / III
	MA23 (II)	22.89 (II)	27.78	
	MA42 (III)	28.04 (III)	47.09	
	MA43 (III)	29.09 (III)	32.95	
	Average :	26.15	33.51	

Table 4.2: Coalescence and failure stress on **marble** specimens (it continues in next page)

GEOMETRY	SPECIMEN	σ_{Coal} [Mpa]	σ_{Fail} [Mpa]	Coalescence type
60-0-a	MA24	21.08	38.79	I
	MA25	31.48	33.27	
	MA33	41.47	41.47	
	MA34	27.68	31.66	
	Average :	30.43	36.30	
60-0-2a	MA26	31.60	38.58	I
	MA27	30.14	34.53	
	Average :	30.87	36.56	
60-0-3a	Not Tested			
60-a-2a	MA28	32.48	35.65	II
	MA29	29.84	32.88	
	Average :	31.16	34.27	

Table 4.2: Continued

	GRANITE		MARBLE	
Property	Value from source. After Kessler et al. (1940)	Measured values	Value from source. Obtained from the Vermont Marble Company	Measured values
Specific Gravity [g/cm ³]	2.61	N/A	2.73	N/A
Porosity [%]	1.51 – 1.62	N/A	0.48	N/A
Color	Light gray	Light gray	White	White (some color bands)
Absorption by weight. after 48 hours [%]	0.32	N/A	0.102	N/A
Compressive Strength [MPa]	170 (perpendicular to rift) 192.5 (parallel to rift)	140 (only available direction). Preserved constant	74	43.6
Modulus of Elasticity [MPa]	11,900 Minimum 23,100 Maximum	17,500 Average	51,800	11,500 Average
Tensile Strength [MPa]	N/A	N/A	16.1 Minimum	N/A

4.3: Other material properties.
Not Available

Specimen Geometry	COALESCENCE TYPE			
	GYPSUM		GRANITE	MARBLE
	Molded flaws	Cut flaws		
30-0- a	N/A	I	I	NO
30-0-2a	I	N/A	I	NO
30-2a-2a	II	II	II / some III	II
30-a- a	II	II	II	II
30-a-2a	II	II	II	II / III
45-0- a	N/A	I	I	I
45-0-2a	I	I	I / NO ?	I
45-2a-2a	II	N/A	II / some III	II / some III
45-a-2a	II	II	II	III / some II
45-a-a	II	II / III	II / IV / IVB	II/III
60-0-a	N/A	N/A	I	I
60-0-2a	I	N/A	I	I
60-0-3a	I	I	NO	Not Tested
60-a-2a	II	NO	II / some NO	II

N/A: Not Available.

Table 4.4: Coalescence modes for different flaw geometries. Gypsum results after Bobet (1997)

s/c ratio	Type of coalescence
$s/c < 1/3$	I
$1/3 < s/c < 1$	II
> 1	III

Table 4.5: Relationship between spacing / continuity ratio and coalescence type. After Bobet (1997)

Geometries	Ligament length (xa)	Coalescence stress (Mpa)
60 - 0 - a	1	59.81
60 - 0 - 2a	2	76.35
45 - 0 - a	1	91.06
45 - 0 - 2a	2	105.3
30 - 0 - a	1	72.21
30 - 0 - 2a	2	81.07

Table 4.6: Relationship between ligament length and coalescence stress for **granite** specimens with coplanar geometries (all the specimens show coalescence type I)

Geometries	Ligament length (xa)	Coalescence stress (MPa)
30-a-a	1.41	78.05
30-a-2a	2.23	70.03
30-2a-2a	4.13	75.62
45-a-a	1.41	51.28
45-a-2a	2.23	101.4
45-2a-2a	4.13	58.44


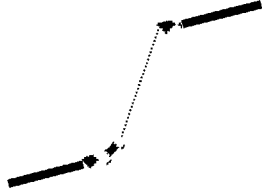
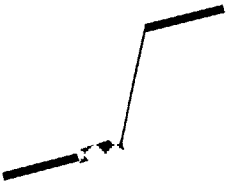
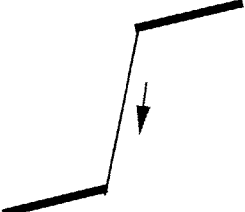
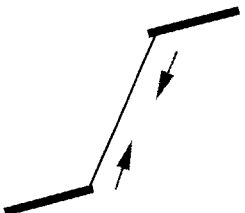
Table 4.7: Relationship between ligament length and coalescence stress for **granite** specimens with non-coplanar geometries that present coalescence type II

GEOMETRY		Internal Wings	External Wings	Int. Shear	Ext. Shear	Coalescence	Failure
45-0-a	Order	4	1	2	No	3 (I)	5
	Stress [MPa]	95	45	60	---	90	100
60-0-a	Order	No	1	2	No	3 (I)	4
	Stress [MPa]	---	50	60	---	60	115
60-0-2a	Order	2 (some)	1	3	No	4 (I)	5
	Stress [MPa]	60	50	60	---	75	100
30-0-a	Order	3	4 (some)	1	No	2 (I)	5
	Stress [MPa]	75	80	45	---	70	85
30-0-2a	Order	4	2 (some)	1	No	3 (I)	5
	Stress [MPa]	85	55	50	---	80	85
45-0-2a	Order	1	No	2	No	3 (I/NO)	4
	Stress [MPa]	85	---	105	---	105	115
60-0-3a	Order	2 (some)	1	No	No	NO	3
	Stress [MPa]	90	85	---	---	-----	115
30-a-a	Order	No	1	2	No	3 (II)	4
	Stress [MPa]	---	70	80	---	80	90
30-a-2a	Order	No	1	2	No	3 (II)	4
	Stress [MPa]	---	60	70	---	70	110
45-a-2a	Order	2 (some)	1	3	No	4 (II)	5
	Stress [MPa]	65	50	100	---	100	110
60-a-2a	Order	3 (some)	1	2	No	4 (II/NO)	5
	Stress [MPa]	90	60	90	---	90	130
45-2a-2a	Order	No	1	2	No	3 (II/III)	4
	Stress [MPa]	---	55	60	---	60	95
30-2a-2a	Order	3 (some)	1	2	No	4 (II/III)	5
	Stress [MPa]	75	65	70	---	75	85
45-a-a	Order	3 (some)	1	2 (some)	No	4(II/IV/IVB)	5
	Stress [MPa]	50	45	50	---	50	85

Table 4.8: Order of appearance of the different crack types and stress levels observed on **granite** specimens. "(some)" means that the type crack is observed only for some specimens with this geometry. Stress levels are ± 3 Mpa

GEOMETRY		Internal Wings	External Wings	Int. Shear	Ext. Shear	Coalescence	Failure
45-0-a	Order	2	1	3	5 (some)	4 (I)	6
	Stress [MPa]	20	18	29	30	29	32
60-0-a	Order	No	1	2	3	4 (I)	5
	Stress [MPa]	---	25	28	29	30	36
60-0-2a	Order	No	1	2	3	4 (I)	5
	Stress [MPa]	---	30	30	30	31	37
30-0-a	Order	2	1	No	No	NO	3
	Stress [MPa]	23	16	---	---	-----	32
30-0-2a	Order	2	1	No	No	NO	3
	Stress [MPa]	20	18	---	---	-----	33
45-0-2a	Order	1	2	4	3 (some)	5 (I)	6
	Stress [MPa]	22	26	32	26	32	34
30-a-2a	Order	1	2	3	No	4 (II/III)	5
	Stress [MPa]	18	22	25	---	25	25
30-2a-2a	Order	No	1	2	No	3 (II)	4
	Stress [MPa]	---	20	24	---	24	35
30-a-a	Order	No	1	2	4 (some)	3 (II)	5
	Stress [MPa]	---	20	22	28	24	30
60-a-2a	Order	No	2 (some)	1	3 (some)	4 (II)	5
	Stress [MPa]	---	30	29	30	31	34
45-2a-2a	Order	No	1	2	No	3 (II/III)	4
	Stress [MPa]	---	16	22	---	22	30
45-a-2a	Order	No	1	2	No	3 (III/II)	4
	Stress [MPa]	---	20	20	---	24	31
45-a-a	Order	No	4	1	3 (some)	2 (II/III)	5
	Stress [MPa]	---	30	26	30	26	33

Table 4.9: Order of appearance of the different crack types and stress levels observed on **marble** specimens. "(some)" means that the type crack is observed only for some specimens with this geometry. Stress levels are ± 1 Mpa.

TYPE I		Produced by the linkage of two internal shear cracks
TYPE II		Produced by the linkage of two internal shear cracks by a vertical tensile crack (not a wing crack)
TYPE III		Produced by the propagation of the internal shear crack from one of the flaws until it reaches the internal wing crack of the other flaw
TYPE IV		Produced by the propagation of an internal wing crack from one flaw until it reaches the other flaw. Observed only for granite.
TYPE IVB		Produced by the linkage of two internal wing cracks that propagate until they joint each other half-way. Observed only for granite.



Internal Shear crack
Internal wing crack
Tension crack (not wings)
Flaws

Figure 4.1: Coalescence modes in granite and marble specimens

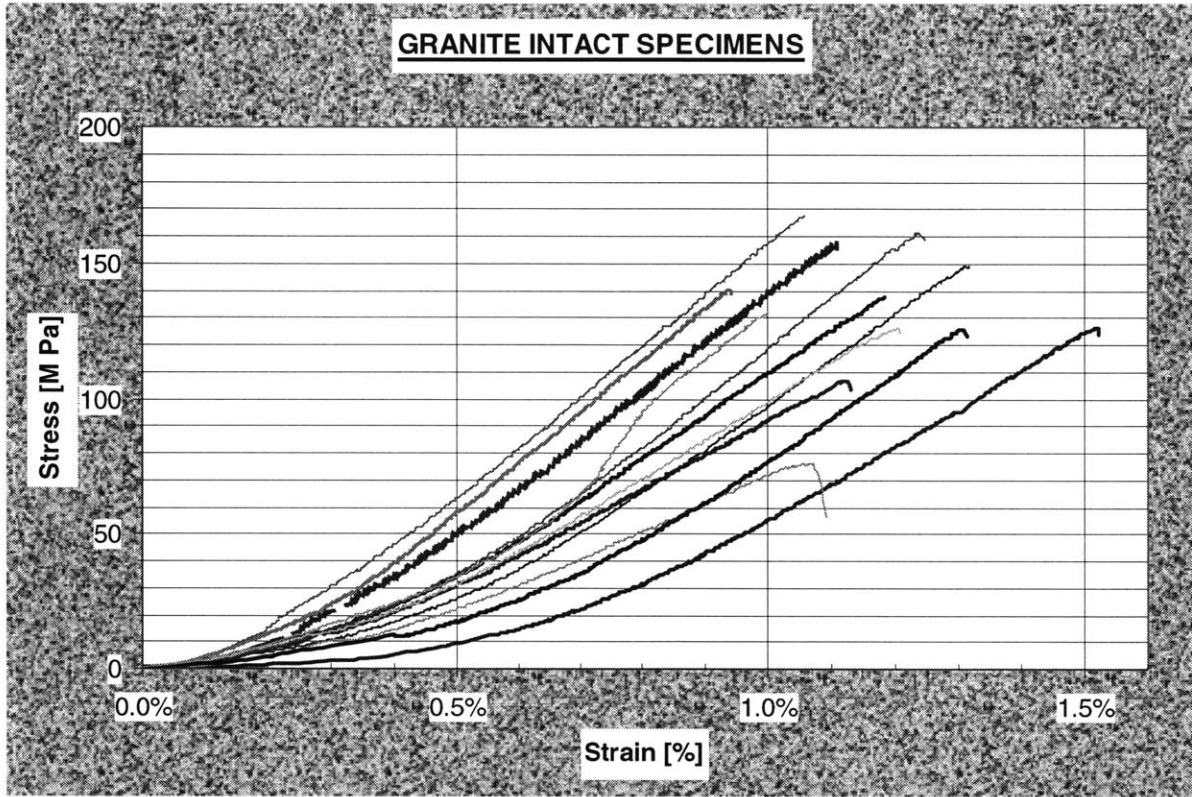


Figure 4.2: Stress strain plots for **granite** intact specimens

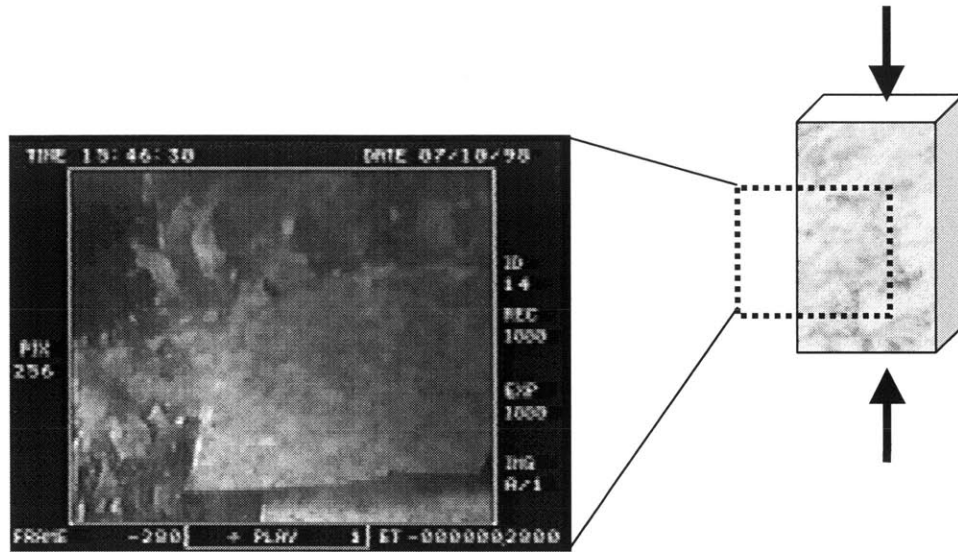


Figure 4.3: Failure of an intact **granite** specimen. Explosion recorded with high-speed camera and played back 1,000 times slower

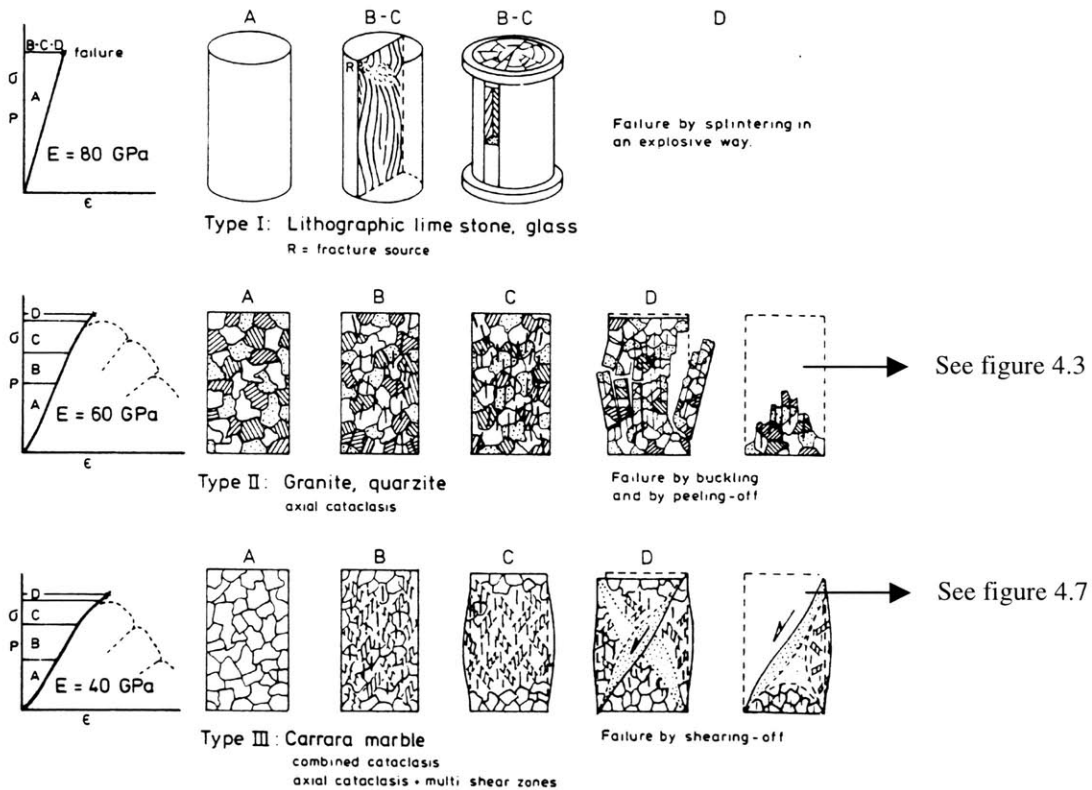


Figure 4.4 Different rock failure modes. From Gramberg (1989)
 Note type II for granite and type III for marble.

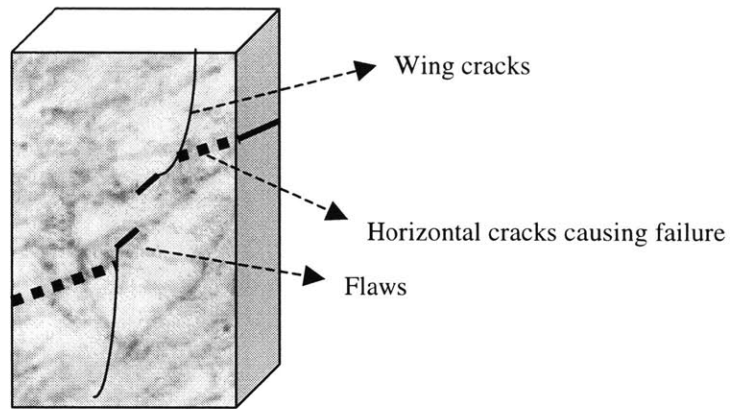


Figure 4.5: Failure due to horizontal cracks

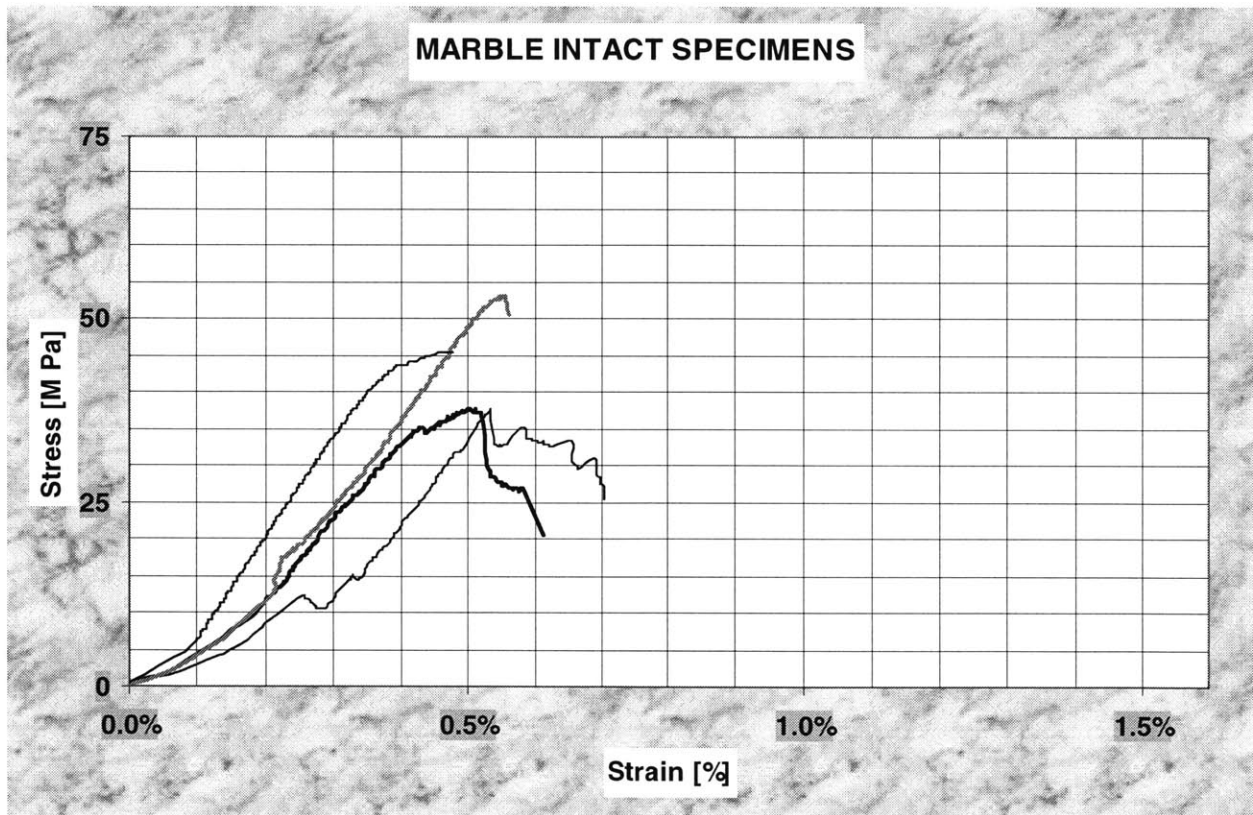


Figure 4.6: Stress strain plots for marble intact specimens

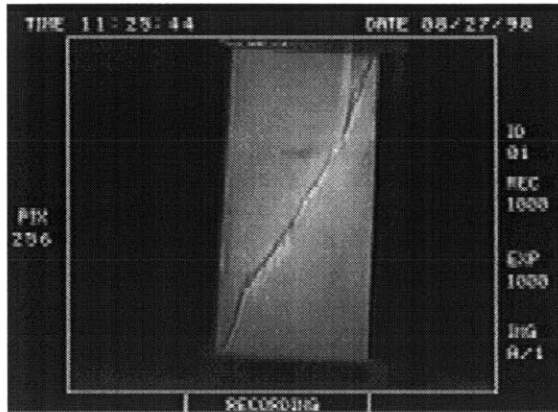


Figure 4.7: Failure of an intact **marble** specimen. Failure by shearing

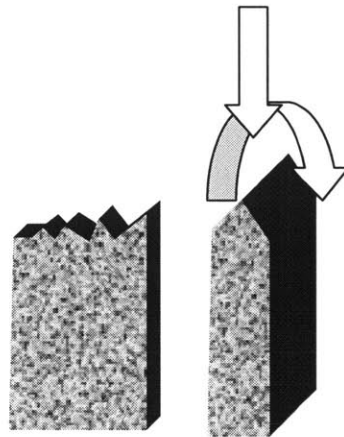


Figure 4.8: Failure due to non-centered load and or bending moment

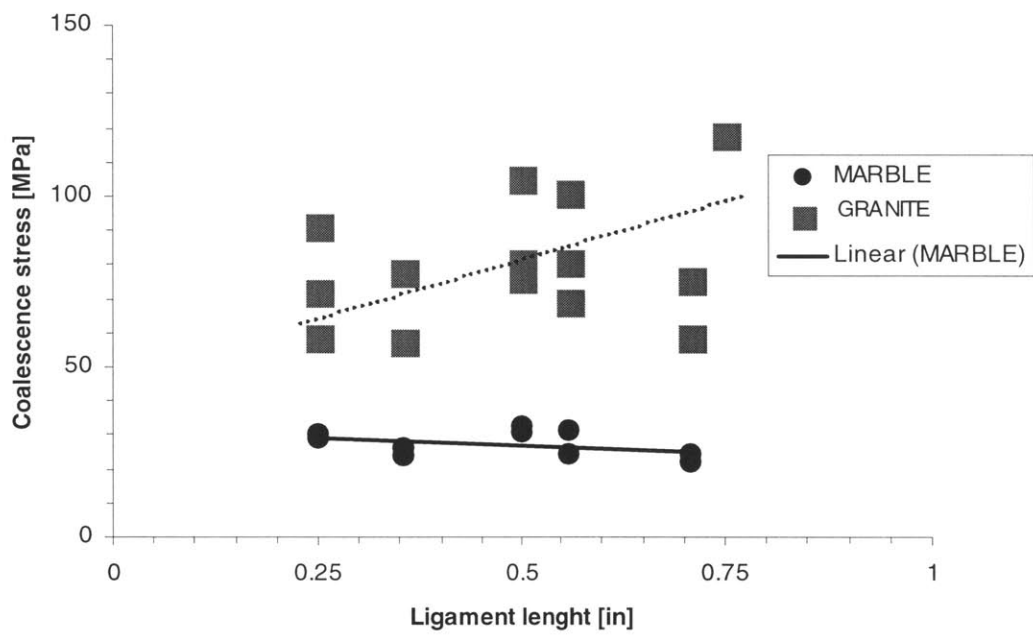


Figure 4.9: Variation of coalescence stress with ligament length for all the specimens (GRANITE + MARBLE)

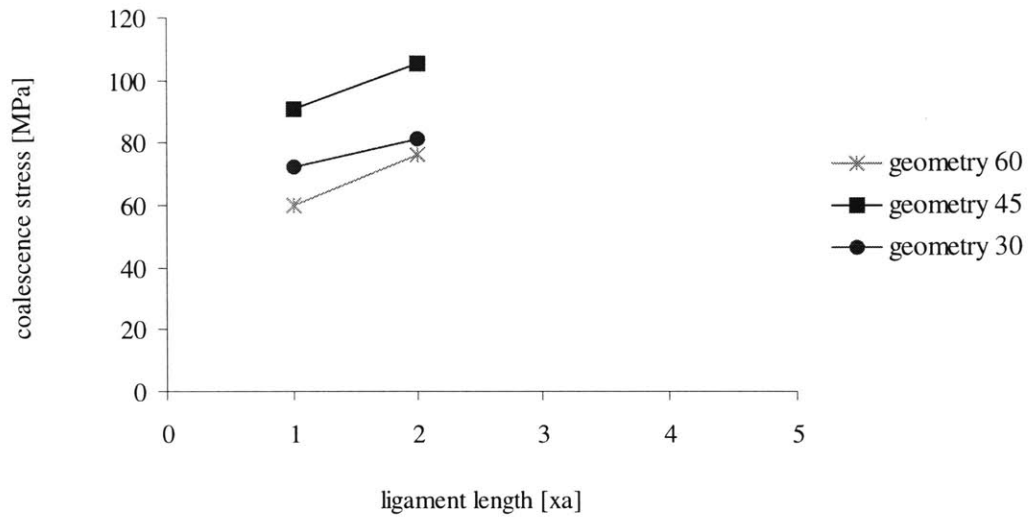


Figure 4.10: Variation of coalescence stress with ligament length for coplanar geometries in **granite**
 All of these geometries present coalescence **type I**

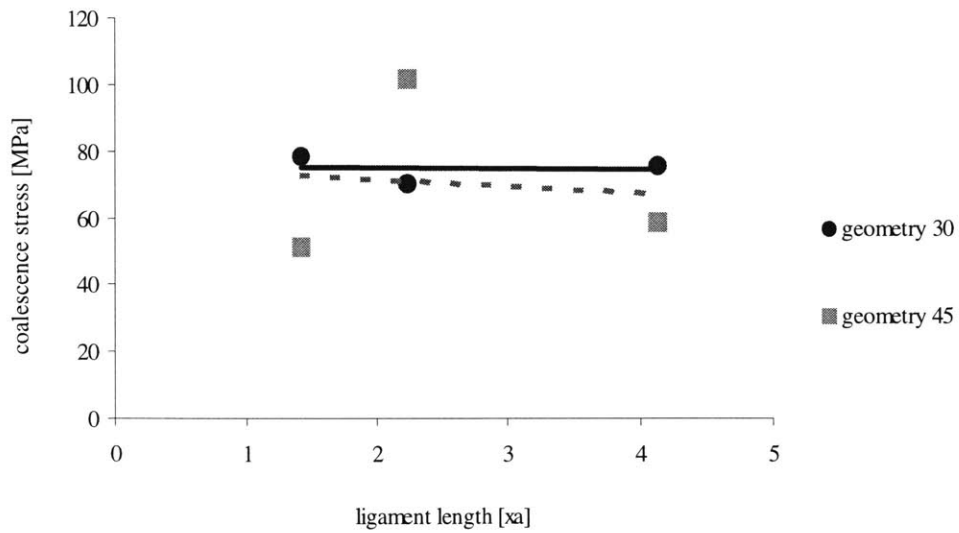


Figure 4.11: Variation of coalescence stress with ligament length for non-coplanar geometries in **granite**
 All of these geometries present coalescence **type II**

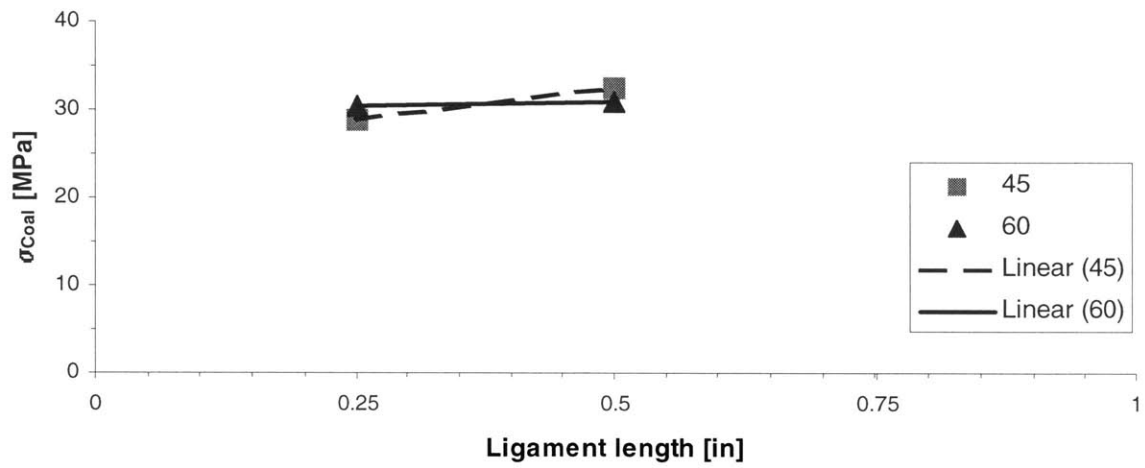


Figure 4.12: Variation of coalescence stress with ligament length for coplanar geometries in **marble**
 All of these geometries present coalescence **type I**

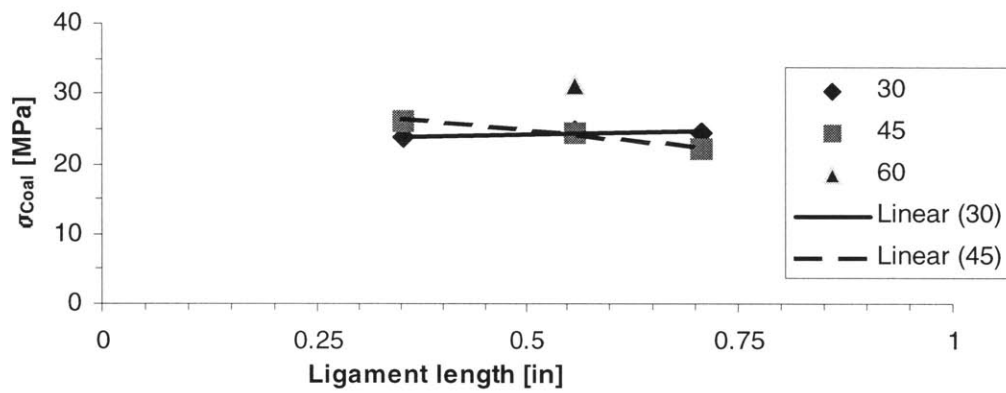


Figure 4.13: Variation of coalescence stress with ligament length for non-coplanar geometries in **marble**
 All of these geometries present coalescence **type II or type III**

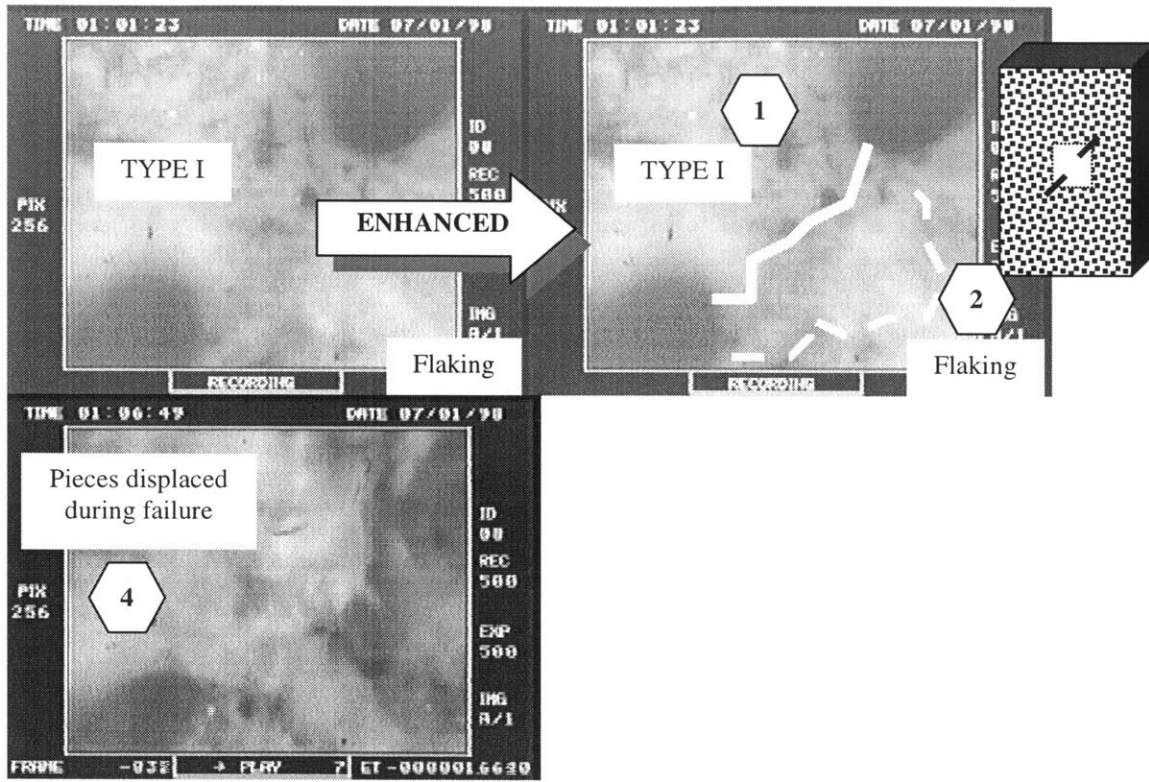


Figure 4.14a: Crack pattern for **granite** geometry 45-0-a. Specimen GR59

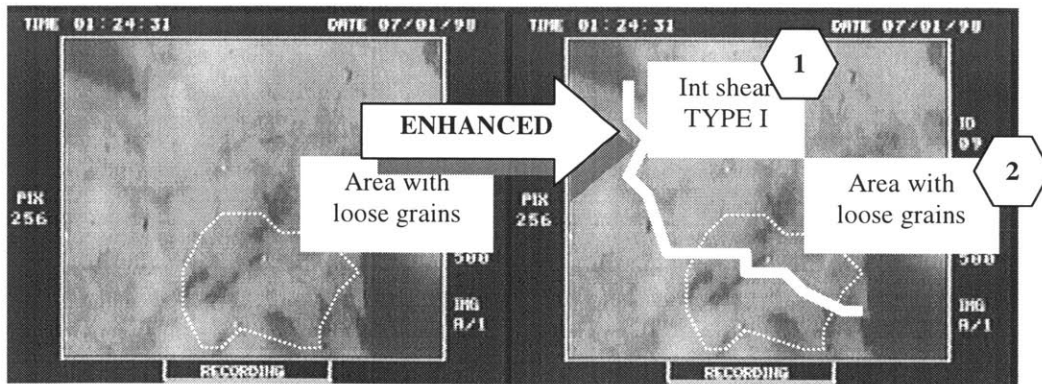
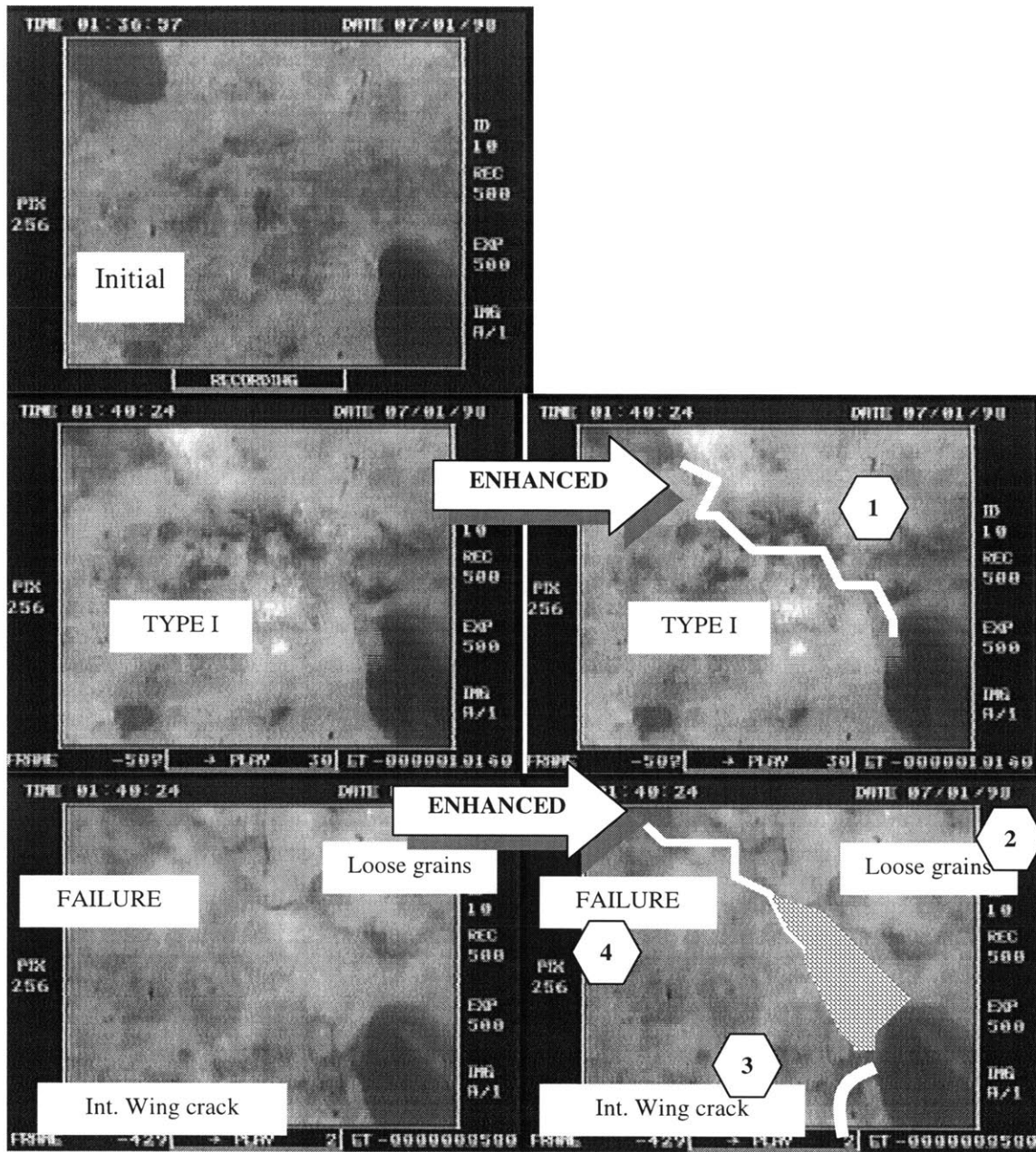


Figure 4.14b: Crack pattern for granite geometry 45-0-a. Specimen GR60



Note times between frames:

Time for the coalescence to develop:	3 seconds.
Time to failure:	0.1 seconds

Figure 4.14c: Crack pattern for **granite** geometry 45-0-a. Specimen GR61

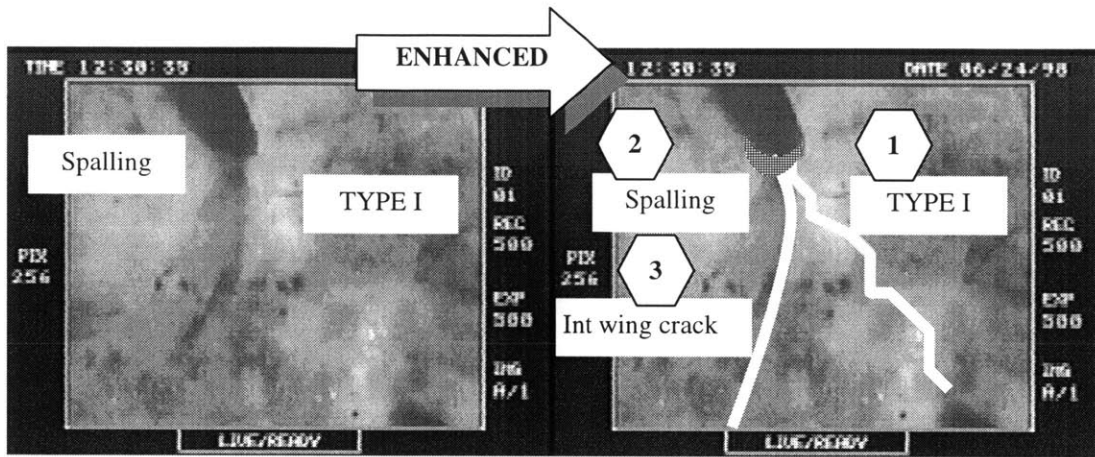


Figure 4.15a: Crack pattern for **granite** geometry 60-0-a. Specimen GR39

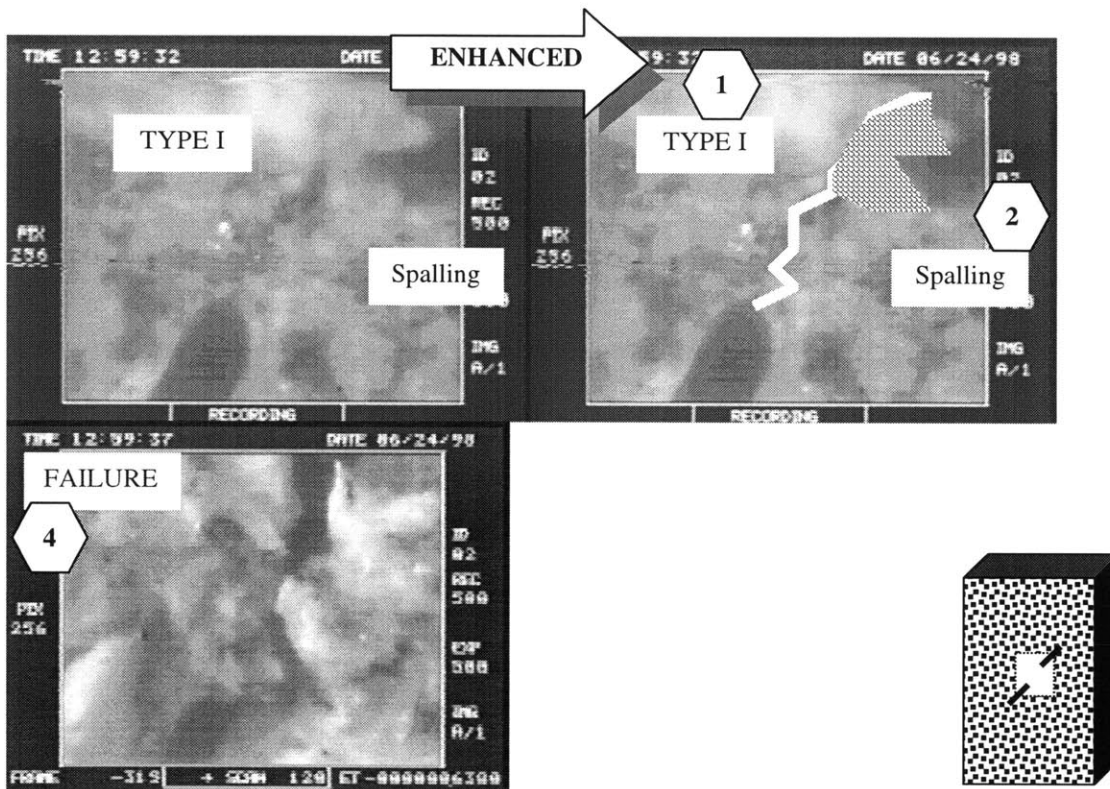


Figure 4.15b: Crack pattern for **granite** geometry 60-0-a. Specimen GR40

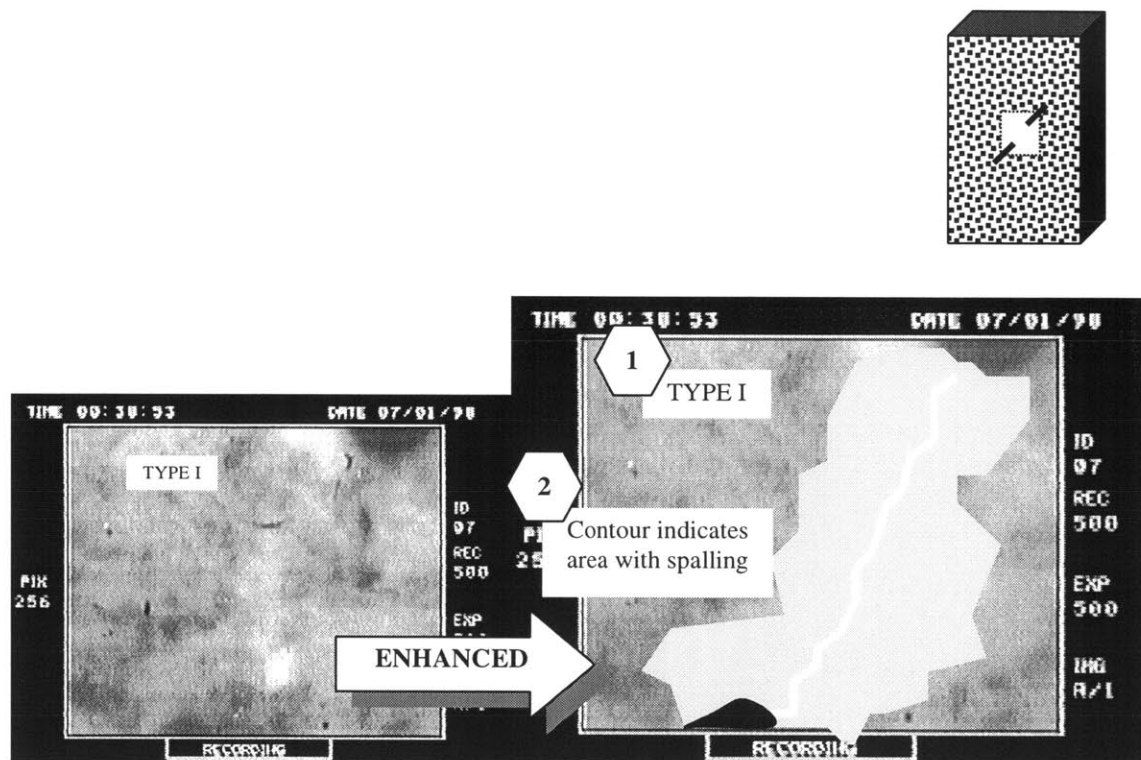


Figure 4.16: Crack pattern for **granite** geometry 60-0-2a. Specimen GR58

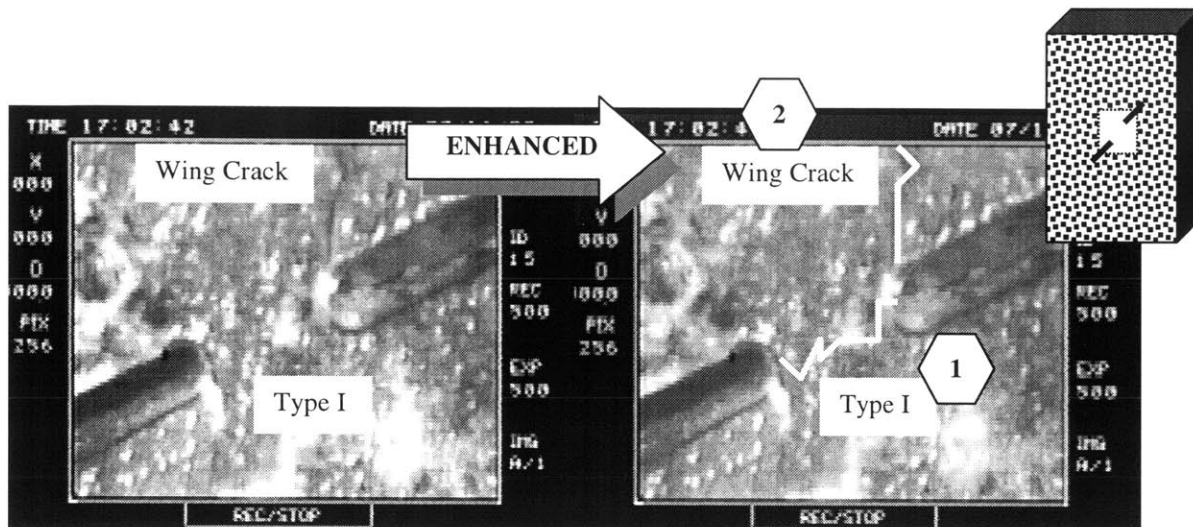


Figure 4.17a: Crack pattern for **granite** geometry 30-0-a. Specimen GR 92.

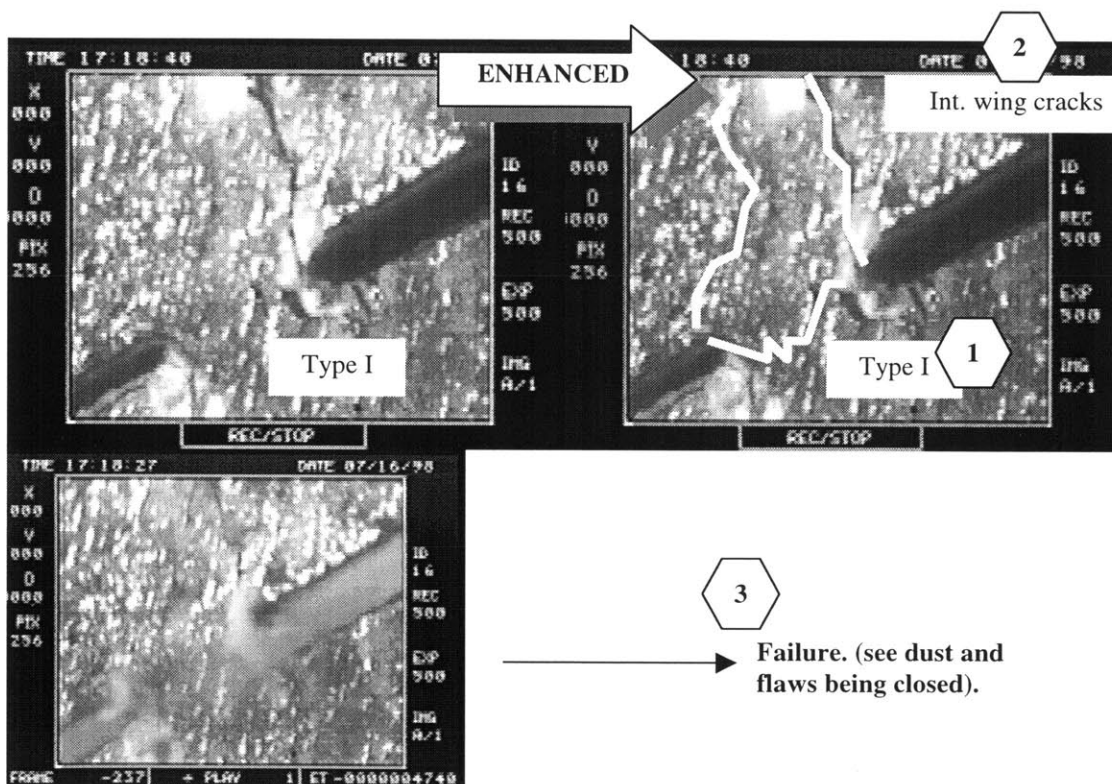


Figure 4.17b Crack pattern for **granite** geometry 30-0-a. Specimen GR 93.

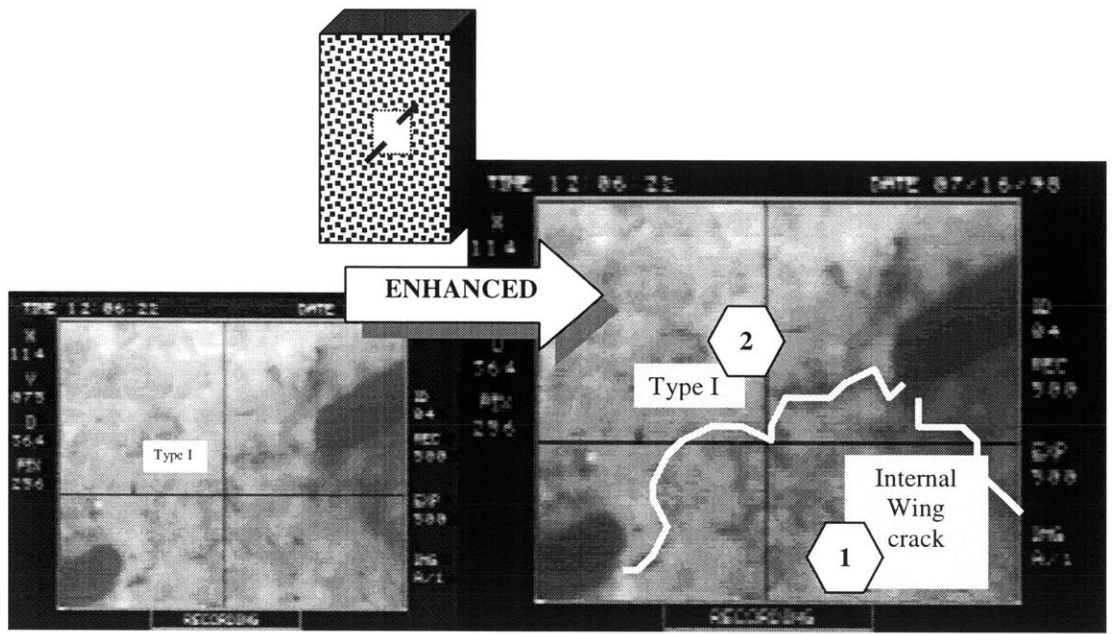


Figure 4.18: Crack pattern for **granite** geometry 30-0-2a. Specimen GR83

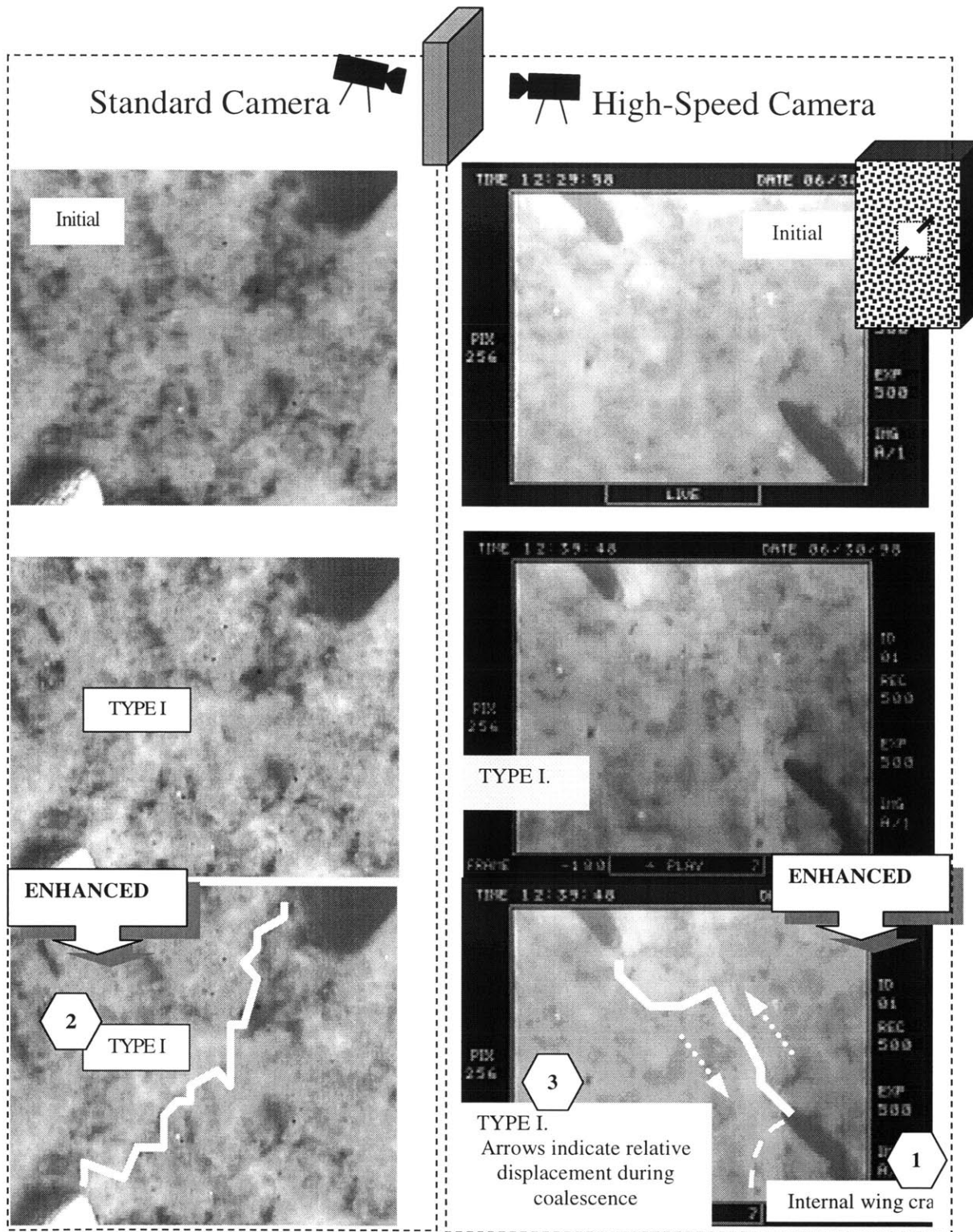


Figure 4.19a: Crack pattern for **granite** geometry 45-0-2a. Specimen GR49, face recorded with standard camera

Figure 4.19b: Crack pattern for **granite** geometry 45-0-2a. Specimen GR 49 , face recorded with the high-speed camera.

The two columns show two sides of the same specimen. One side was taken with a “normal” camera and the other one with the high-speed camera. The same process can be observed on both faces.

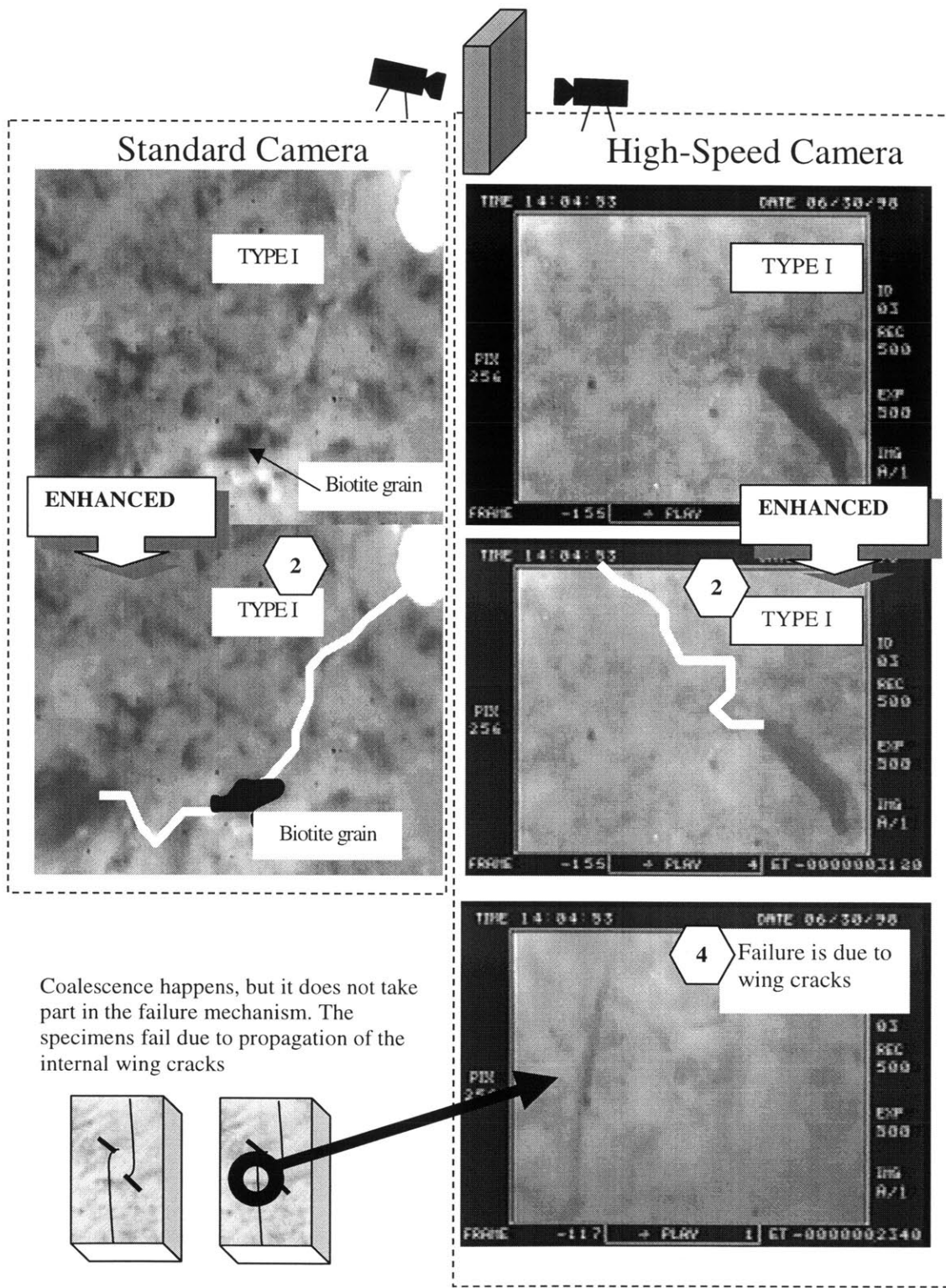


Figure 4.19c: Crack pattern for **granite** geometry 45-0-2a. Specimen GR51 (face recorded with standard camera)

Figure 4.19d: Crack pattern for **granite** geometry 45-0-2a. Specimen GR 51 (face recorded with the high-speed camera).

The two columns show two sides of the same specimen. One side was taken with a “normal” camera and the other one with the high-speed camera. The same process can be observed on both faces.

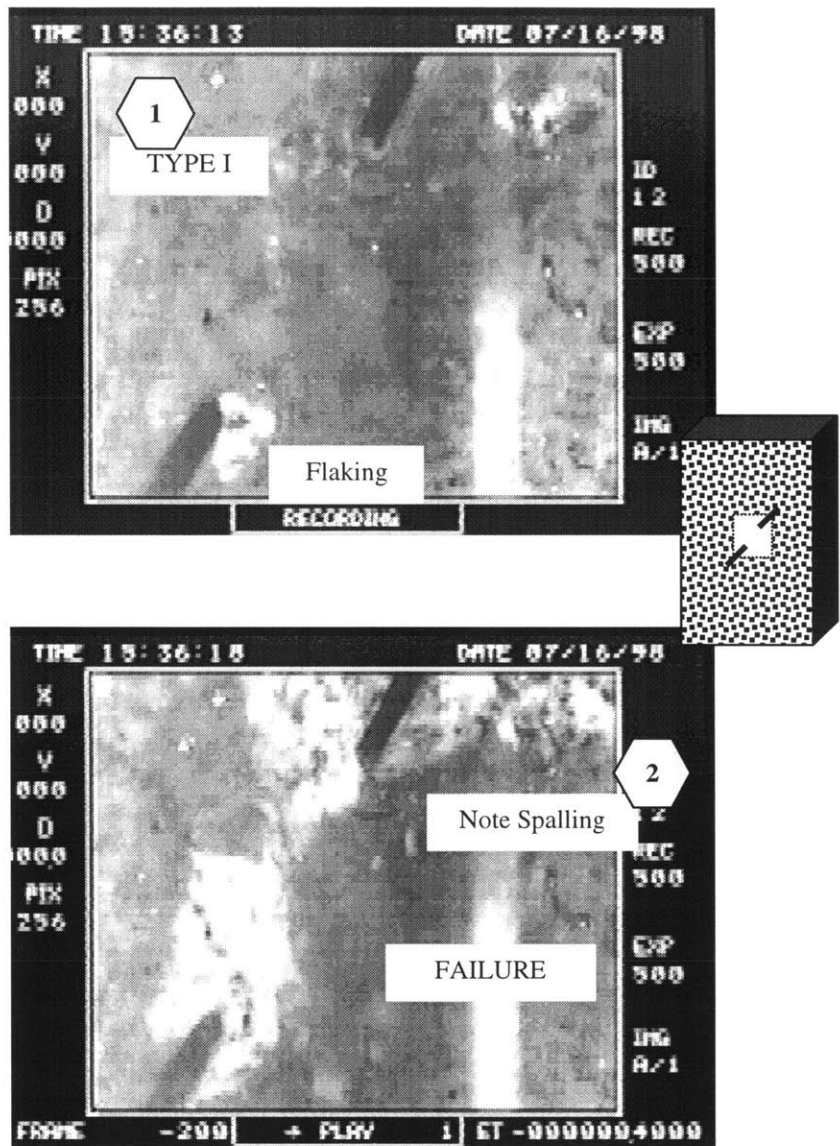


Figure 4.20: Crack pattern for **granite** geometry 60-0-3a. Specimen GR89.

Note that this geometry generally does NOT coalesce. However, 1 out of 5 showed coalescence right before failure. These pictures belong to that specimen.

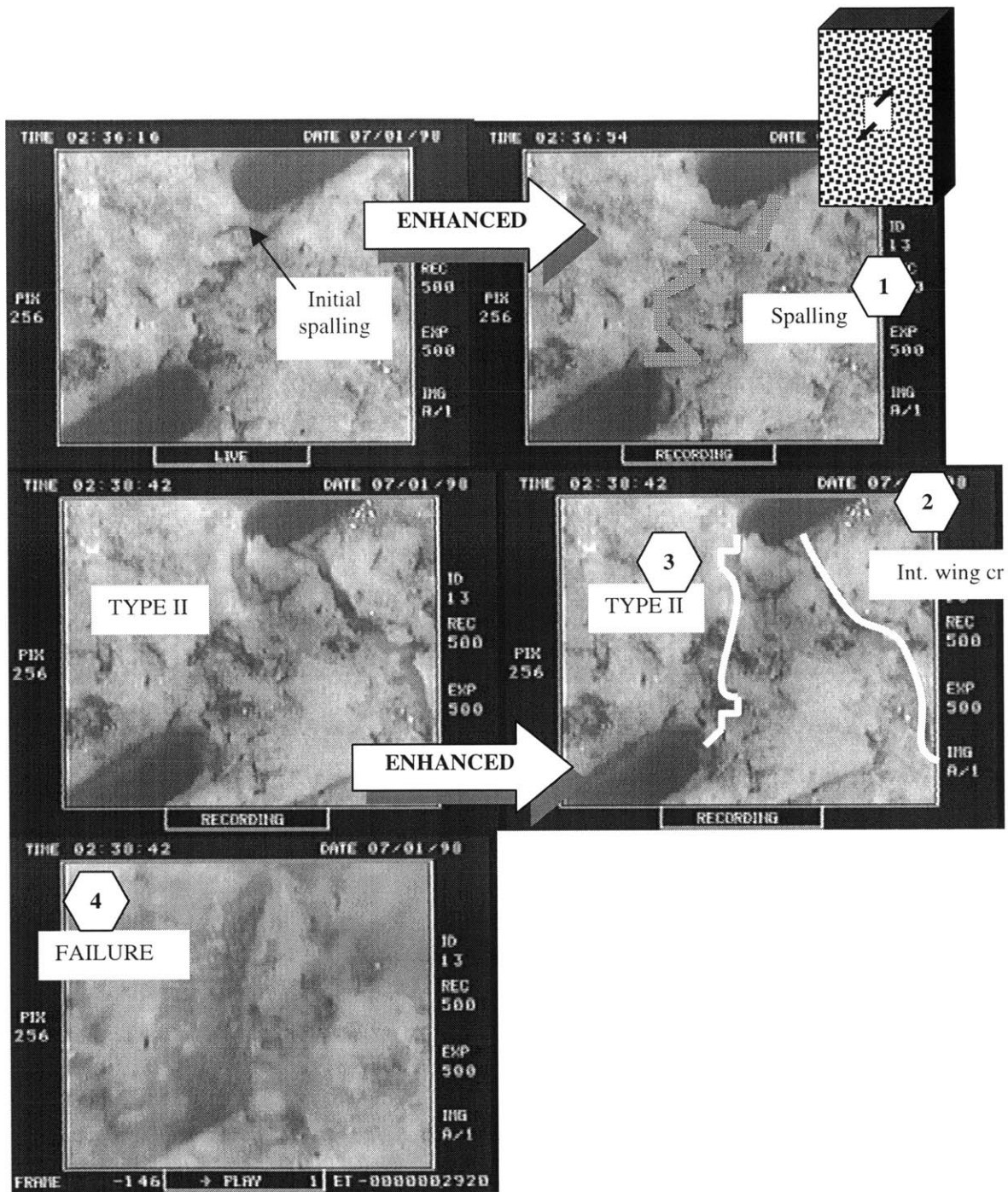


Figure 4.21: Crack pattern for **granite** geometry 30-a-a. Specimen GR64

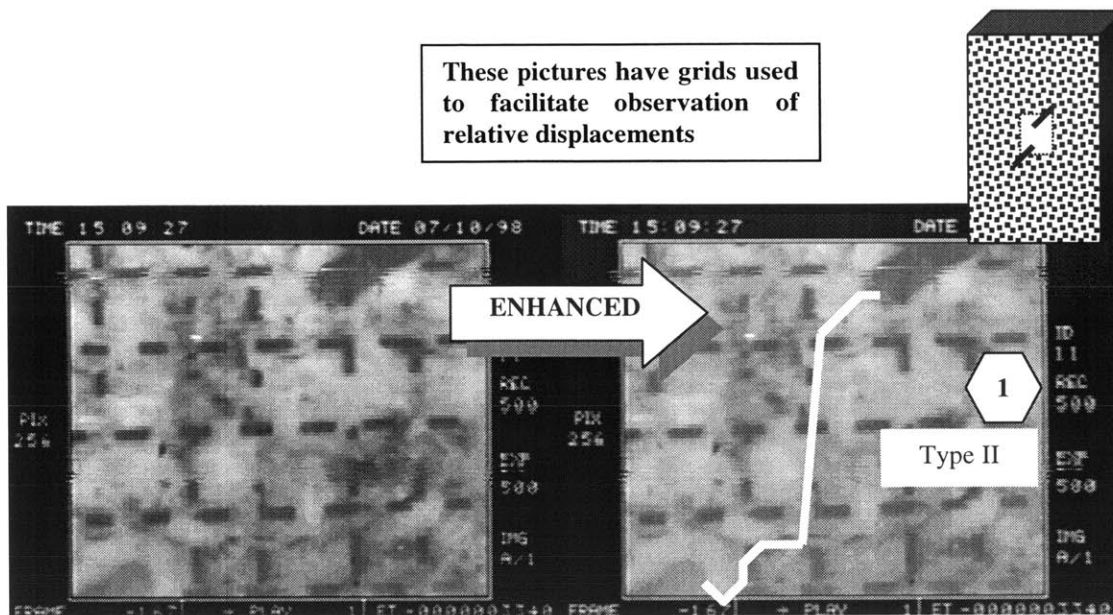


Figure 4.22a: Crack pattern for **granite** geometry 30-a-2a. Specimen GR77

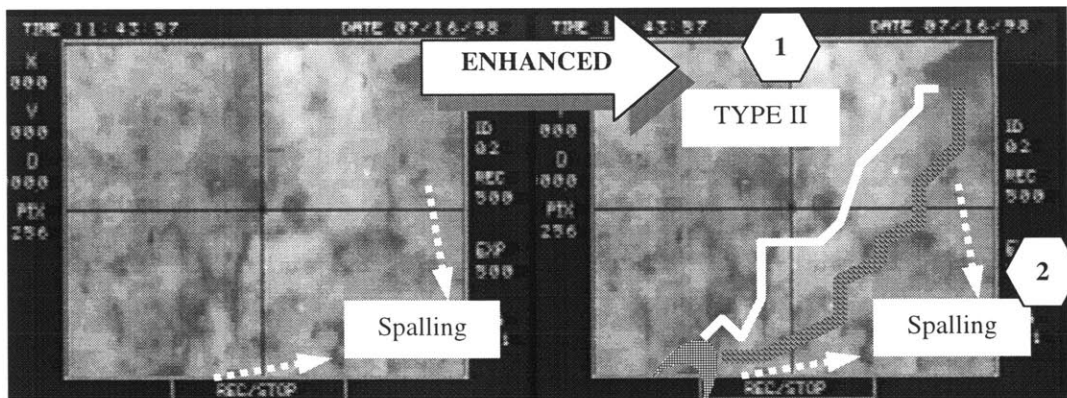


Figure 4.22b: Crack pattern for **granite** geometry 30-a-2a. Specimen GR82

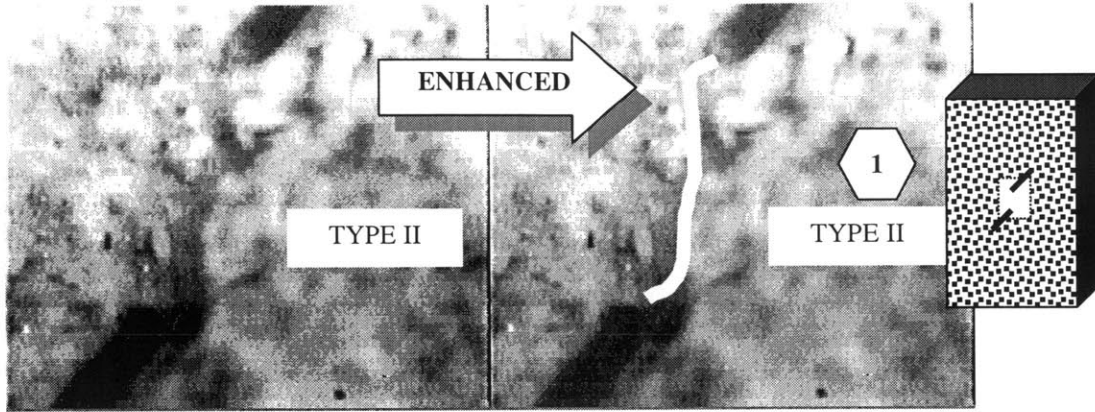


Figure 4.23a: Crack pattern for **granite** geometry 45-a-2a. Specimen GR54.

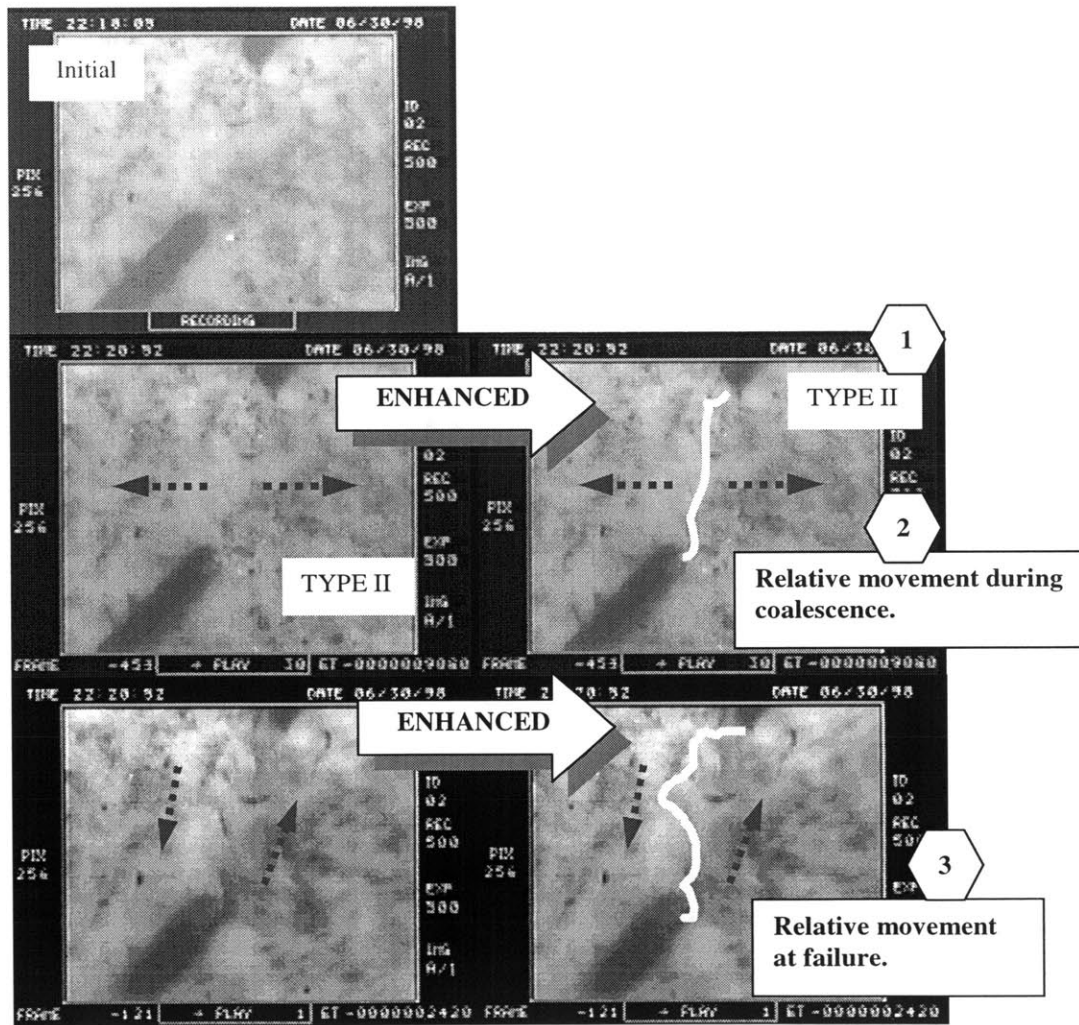


Figure 4.23b: Crack pattern for **granite** geometry 45-a-2a. Specimen GR53

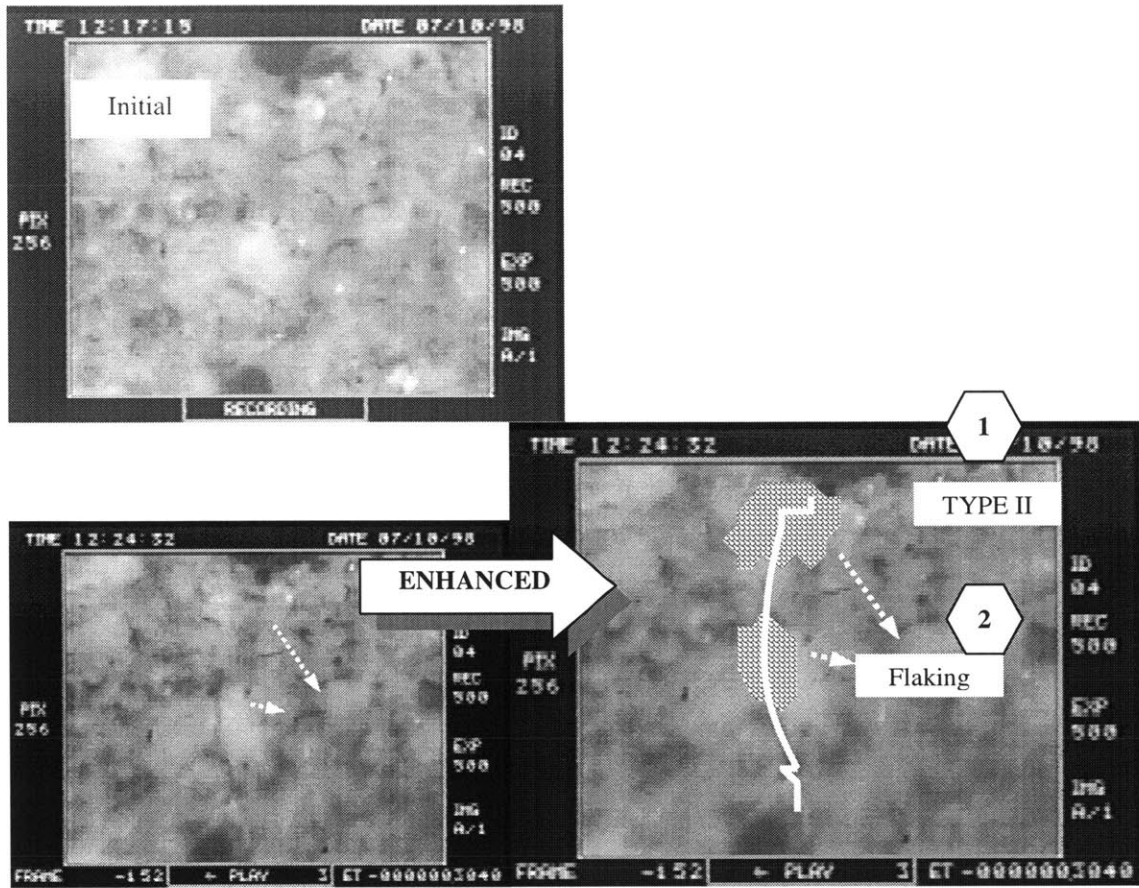


Figure 4.24: Crack pattern for **granite** geometry 60-a-2a. Specimen GR70

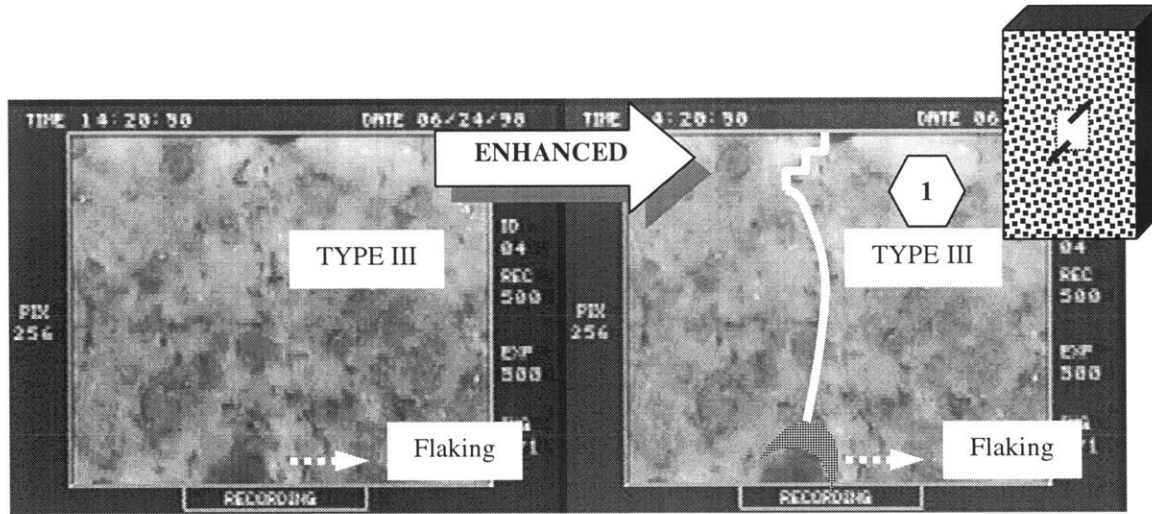


Figure 4.25a: Crack pattern for **granite** geometry 45-2a-2a. Specimen GR42

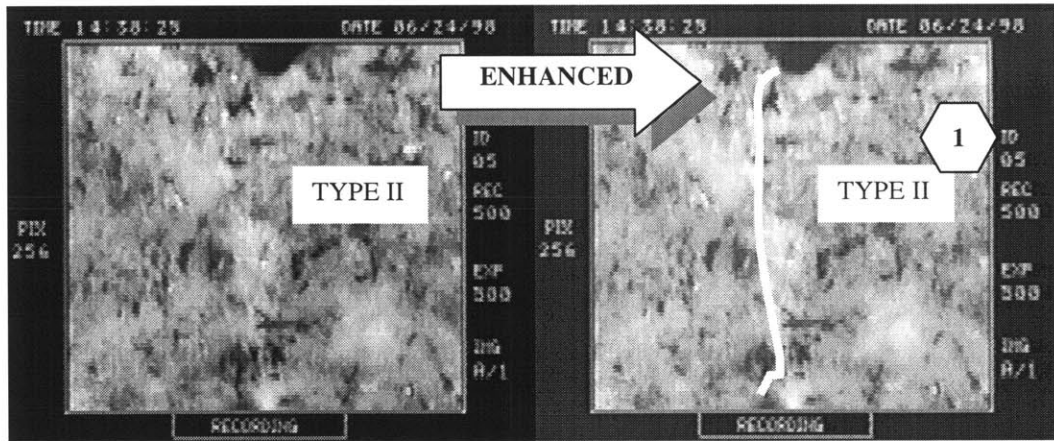


Figure 4.25b: Crack pattern for **granite** geometry 45-2a-2a. Specimen GR43.

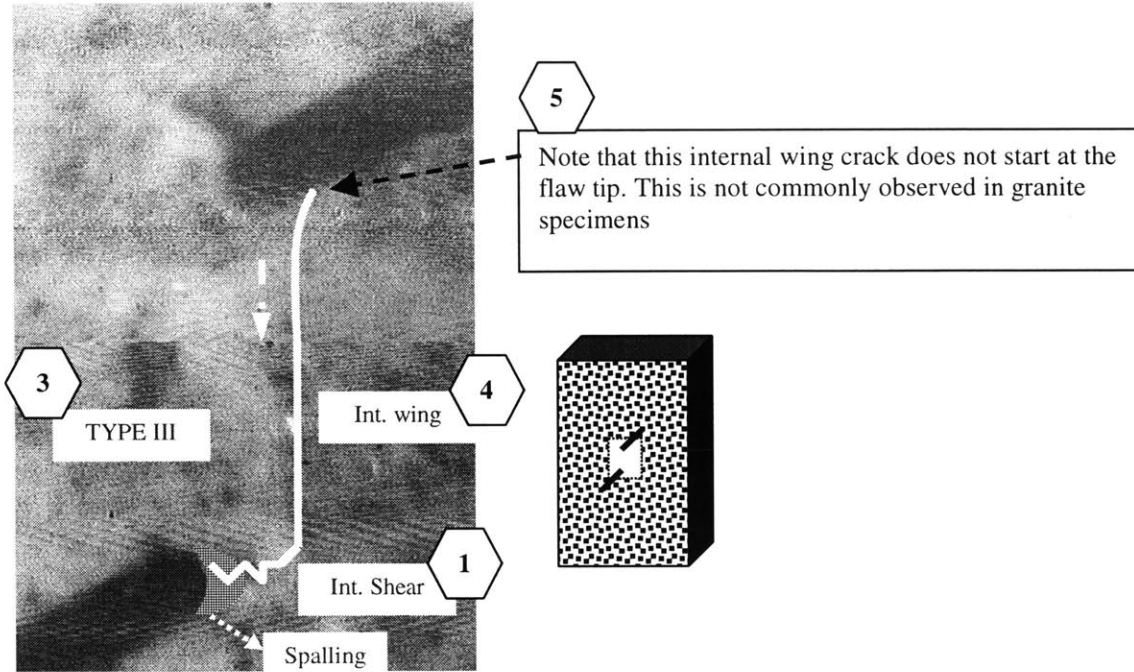


Figure 4.26a: Crack pattern for **granite** geometry 30-2a-2a. Specimen GR23

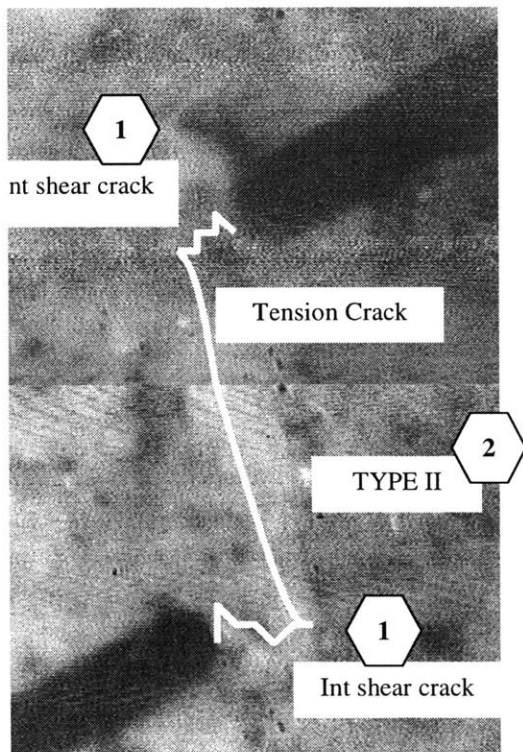


Figure 4.26b: Crack pattern for **granite** geometry 30-2a-2a. Specimen GR24

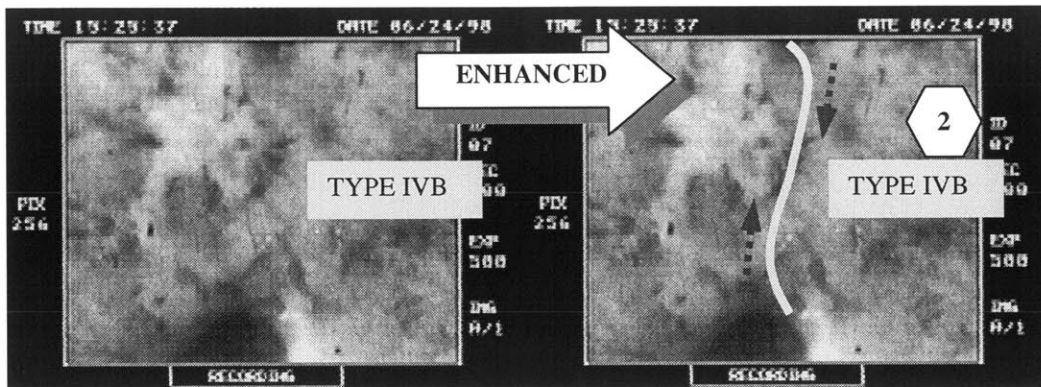


Figure 4.27a: Crack pattern for **granite** geometry 45-a-a. Specimen GR45 (IVB).

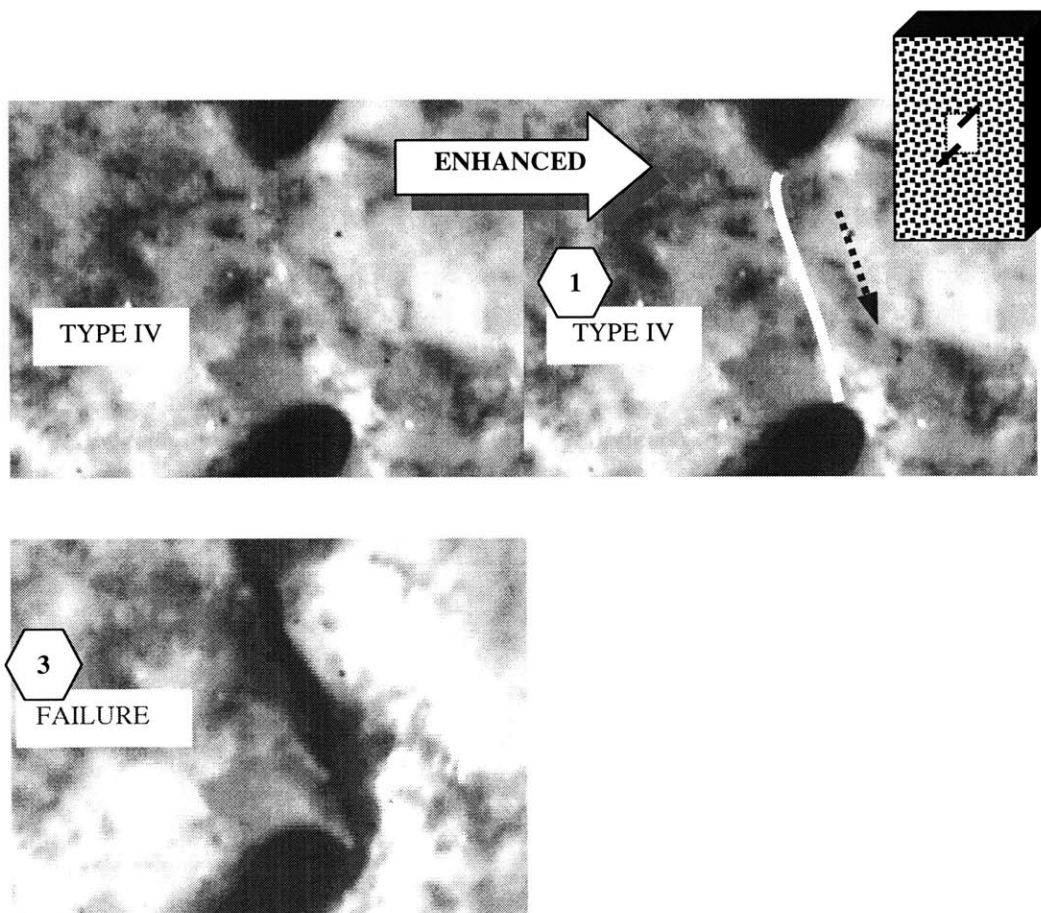


Figure 4.27b: Crack pattern for **granite** geometry 45-a-a. Specimen GR46 (IV).

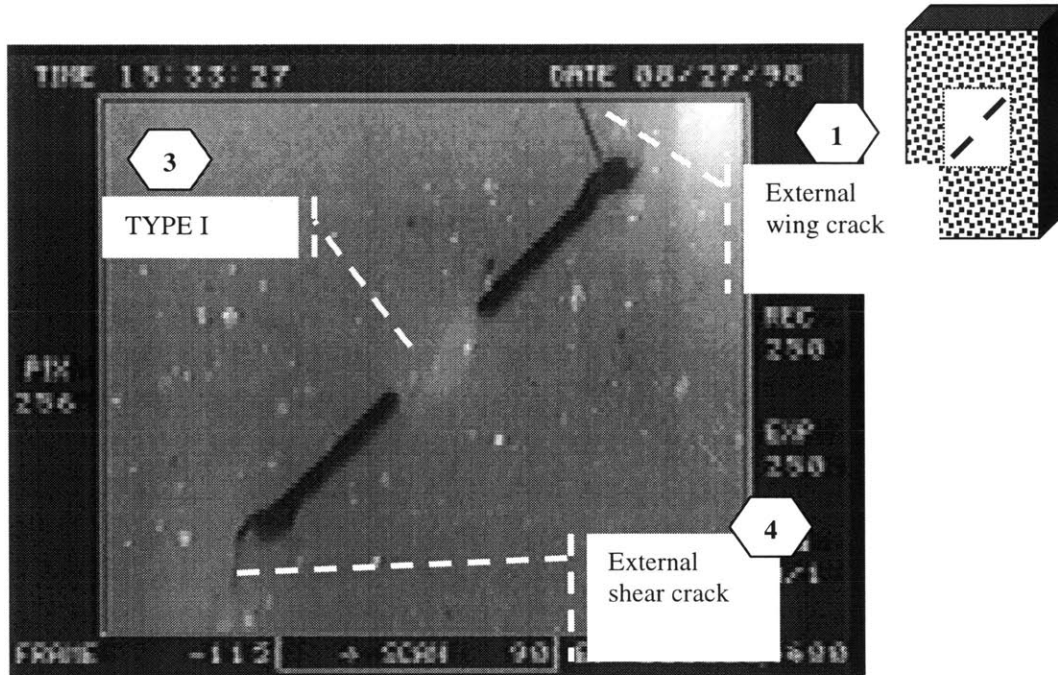


Figure 4.28a: Crack pattern for **marble** specimens with geometry 45-0-a. Specimen MA14

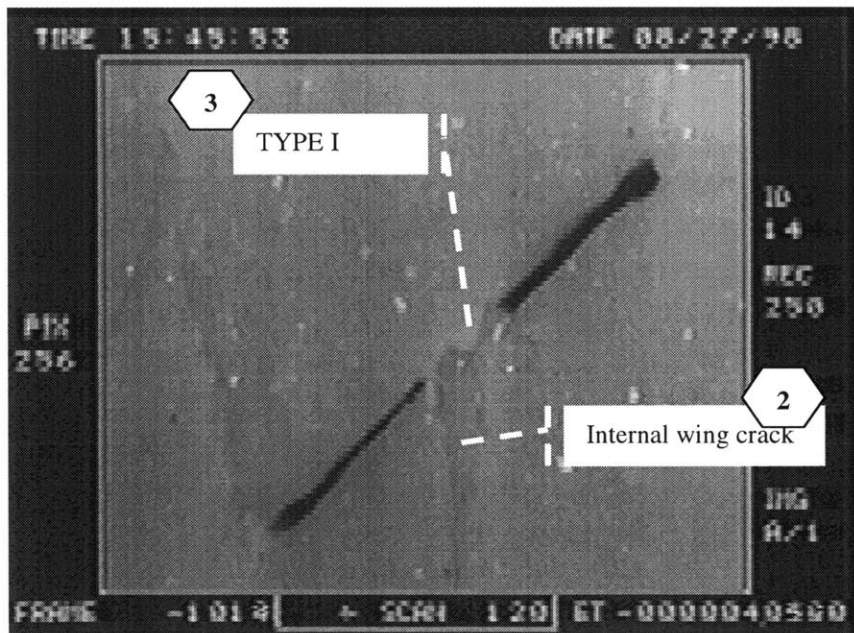


Figure 4.28b: Crack pattern for **marble** specimens with geometry 45-0-a. Specimen MA15

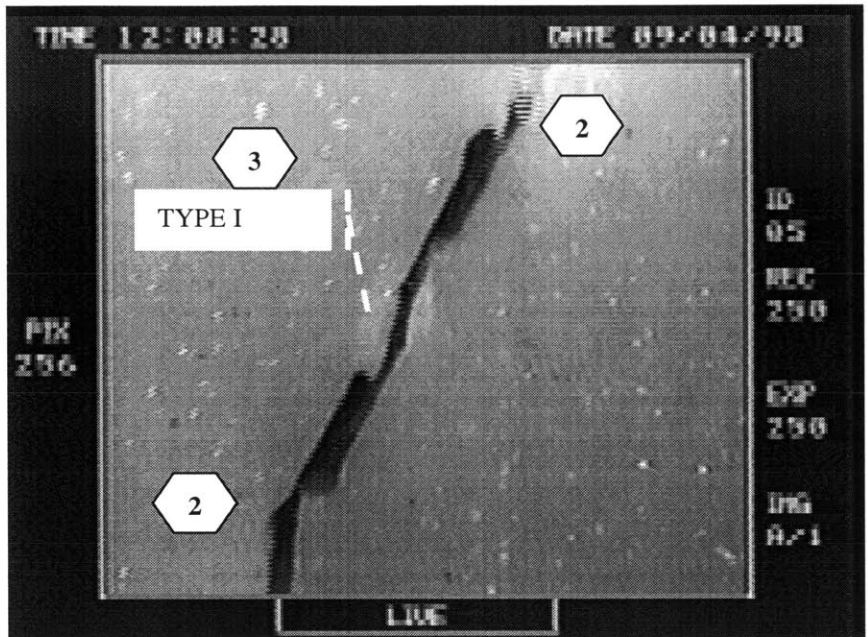


Figure 4.29a: Crack pattern for **marble** specimens with geometry 60-0-a. Specimen MA24

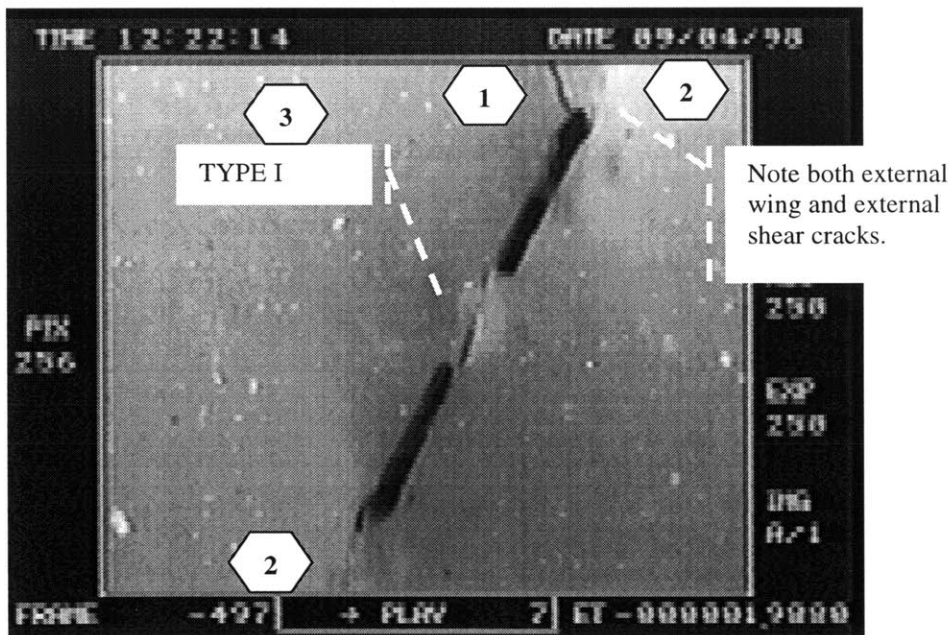


Figure 4.29b: Crack pattern for marble specimens with geometry 60-0-a. Specimen MA25

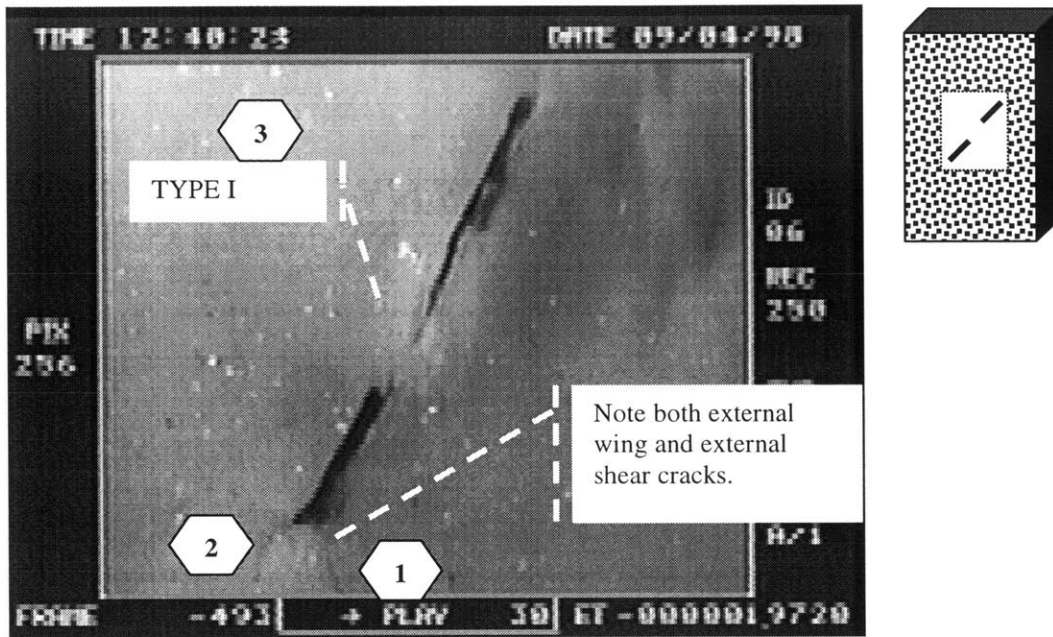


Figure 4.30a: Crack pattern for **marble** specimens with geometry 60-0-2a. Specimen MA26

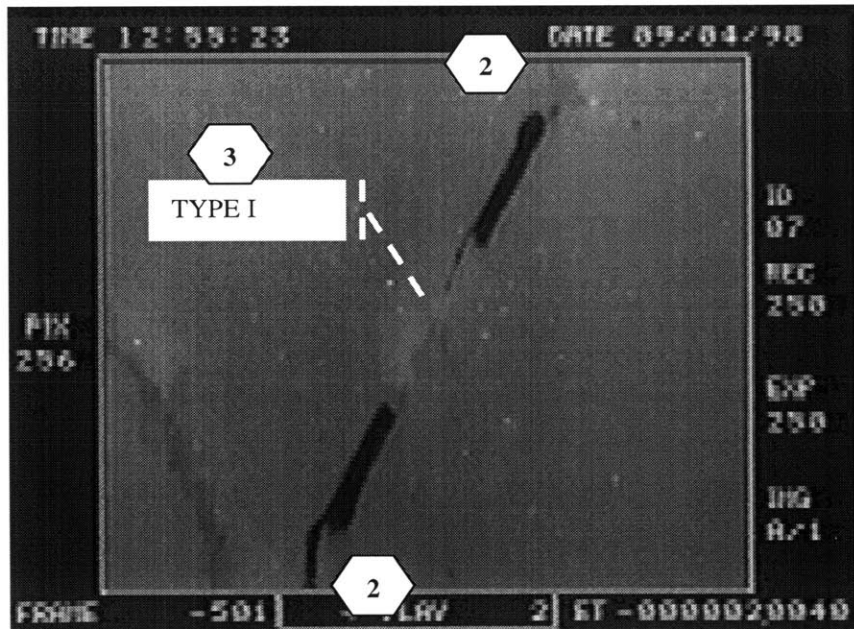


Figure 4.30b: Crack pattern for **marble** specimens with geometry 60-0-2a. Specimen MA27

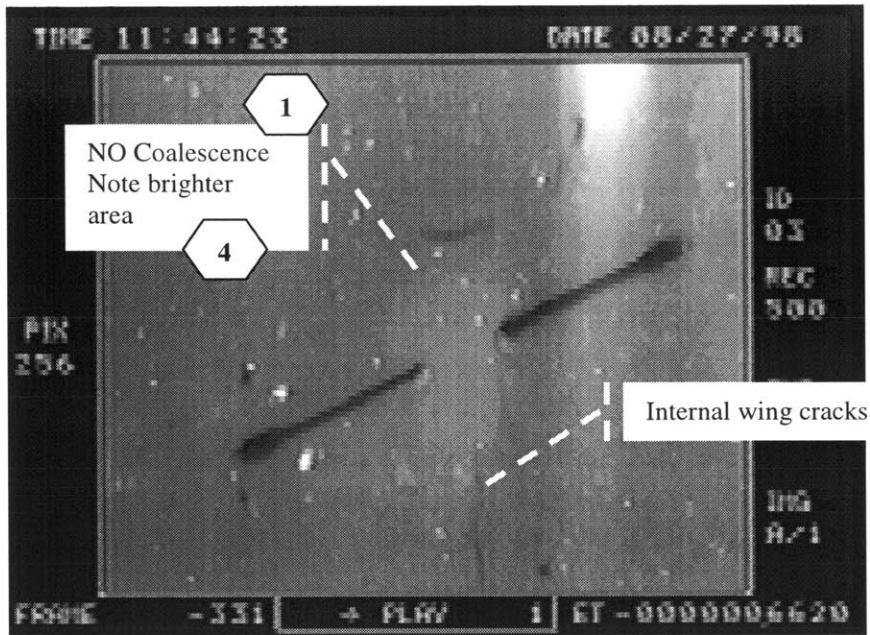


Figure 4.31a: Crack pattern for **marble** specimens with geometry 30-0-a. Specimen MA04

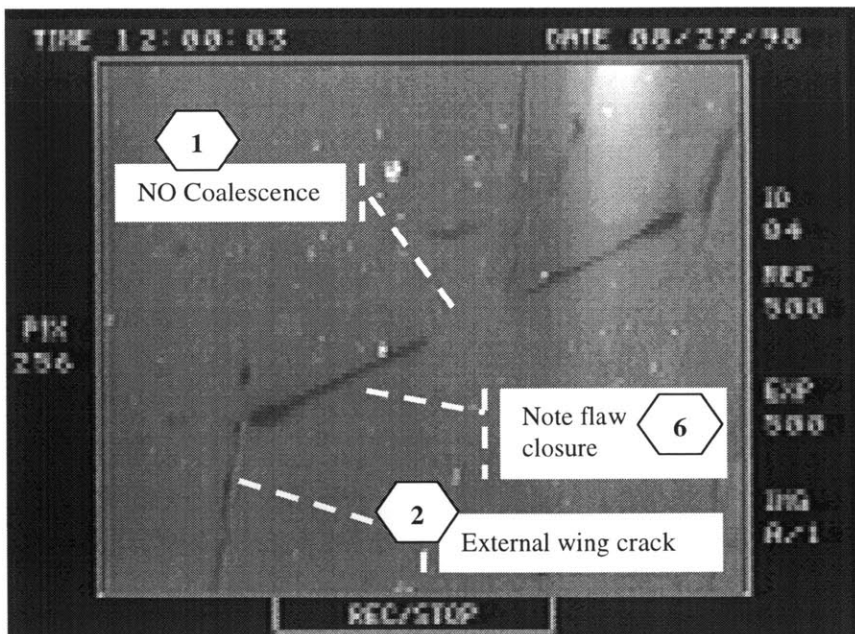


Figure 4.31b: Crack pattern for **marble** specimens with geometry 30-0-a. Specimen MA05

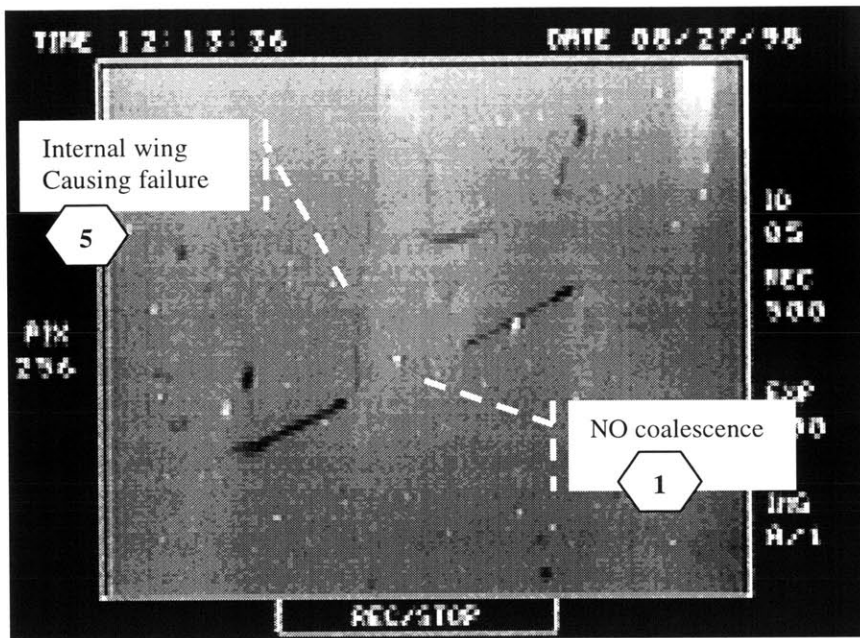


Figure 4.32a: Crack pattern for **marble** specimens with geometry 30-0-2a. Specimen MA07

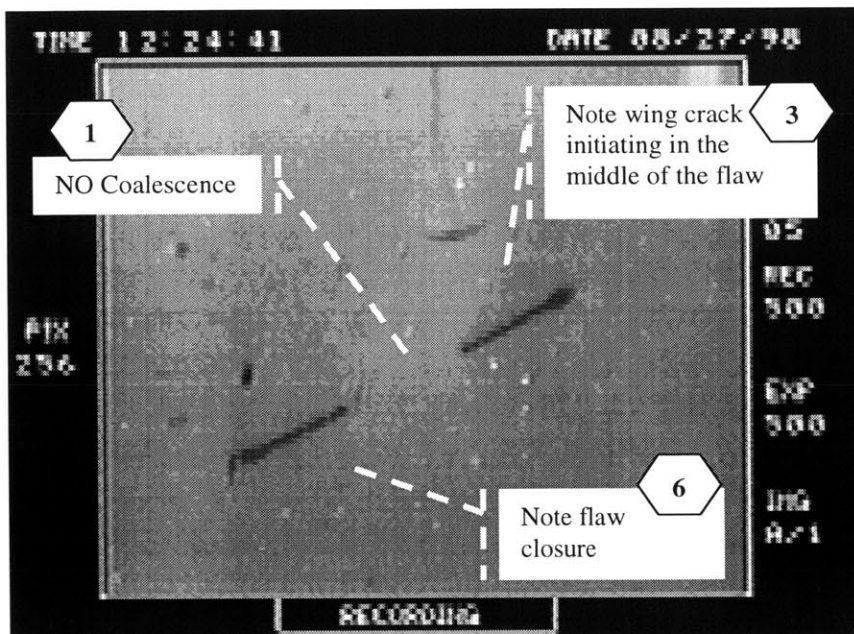


Figure 4.32b: Crack pattern for **marble** specimens with geometry 30-0-2a. Specimen MA08

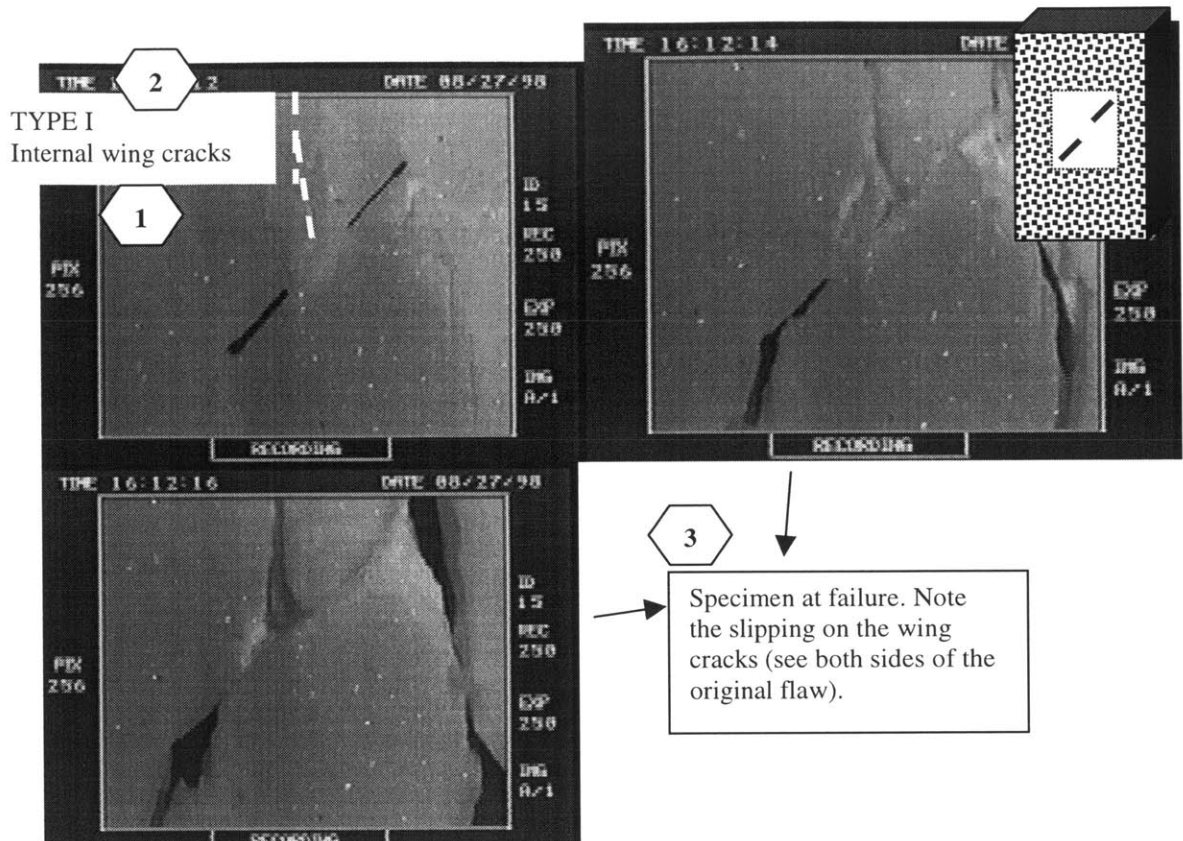


Figure 4.33a: Crack pattern for **marble** specimens with geometry 45-0-2a. Specimen MA16

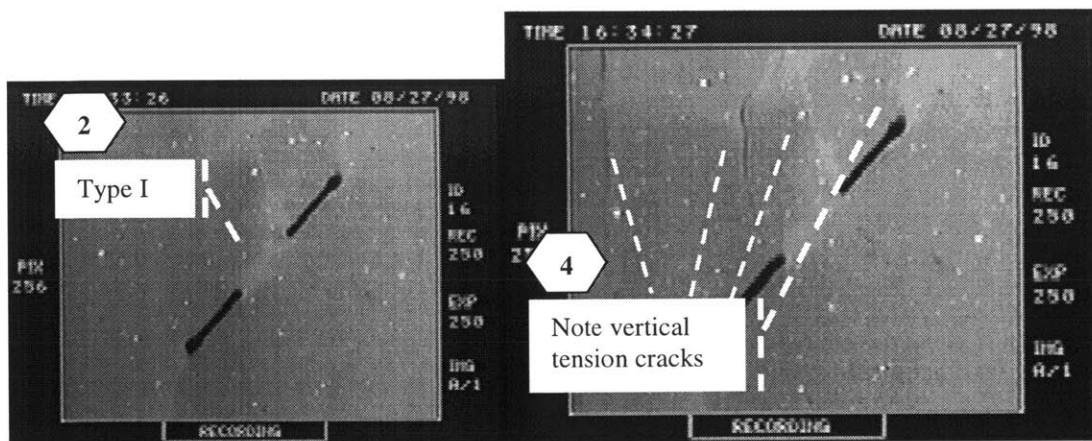


Figure 4.33b: Crack pattern for **marble** specimens with geometry 45-0-2a. Specimen MA17

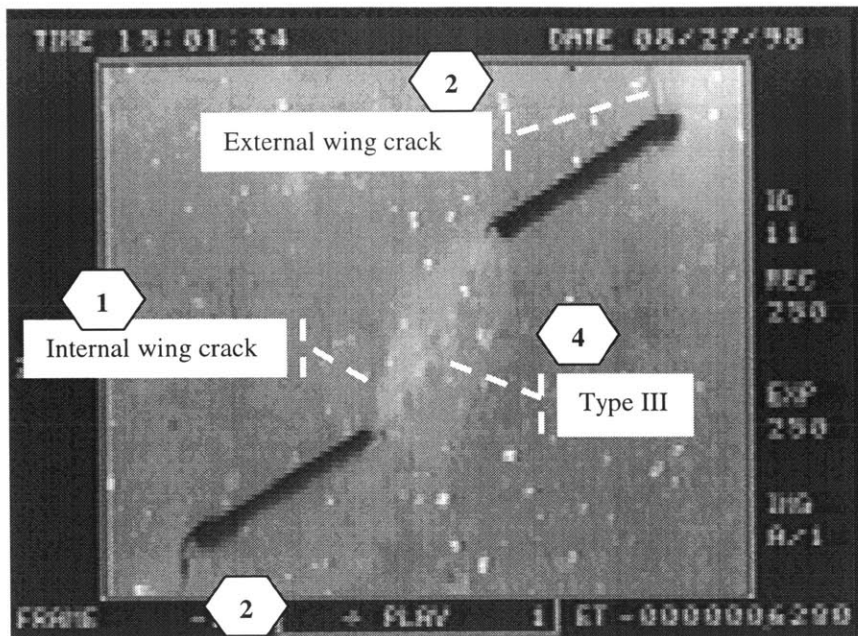


Figure 4.34a: Crack pattern for **marble** specimens with geometry 30-a-2a. Specimen MA12

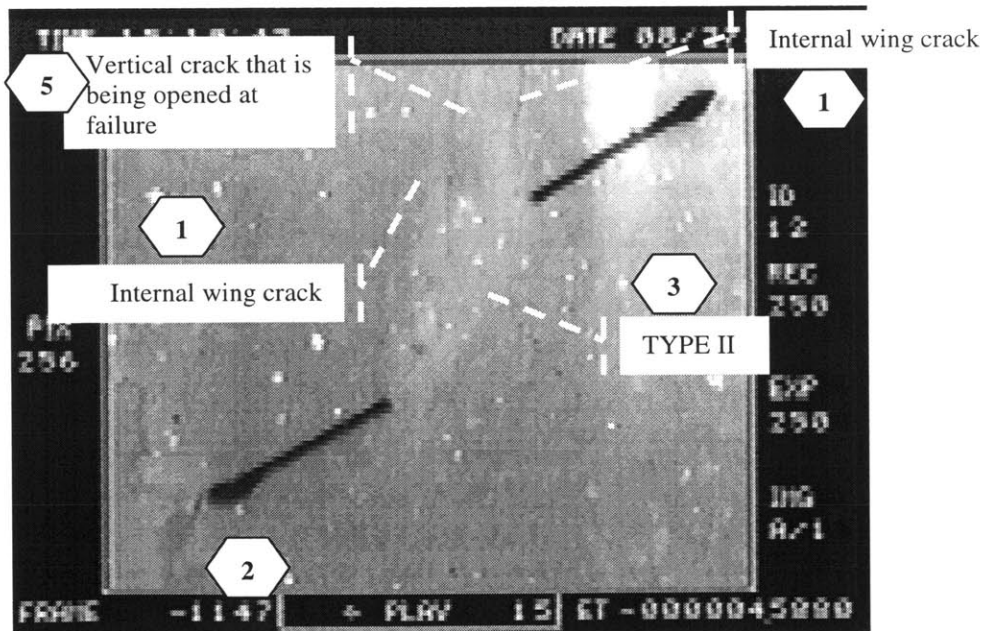


Figure 4.34b: Crack pattern for **marble** specimens with geometry 30-a-2a. Specimen MA13

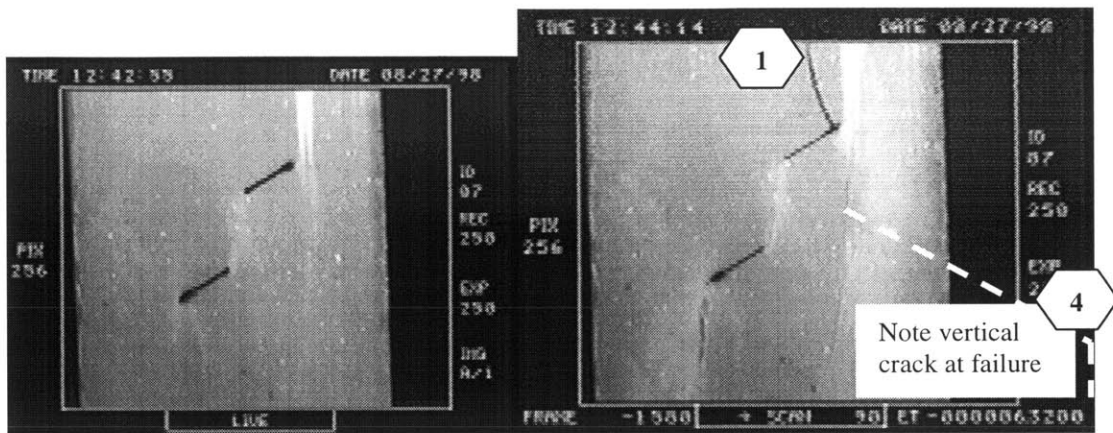


Figure 4.35a: Crack pattern for **marble** specimens with geometry 30-2a-2a. Specimen MA08

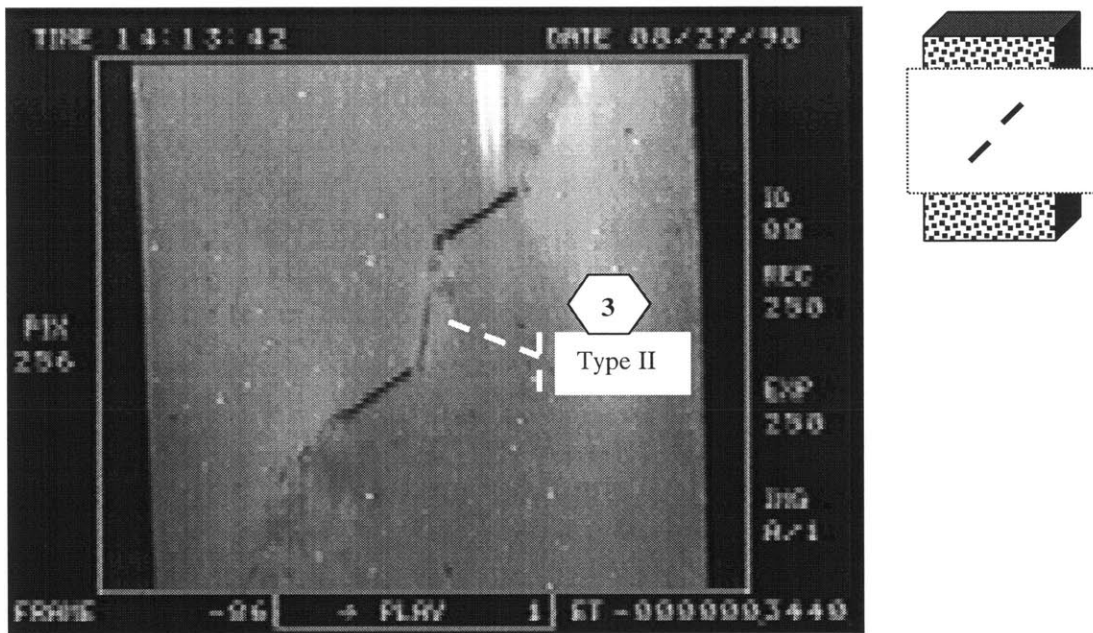


Figure 4.35b: Crack pattern for **marble** specimens with geometry 30-2a-2a. Specimen MA09

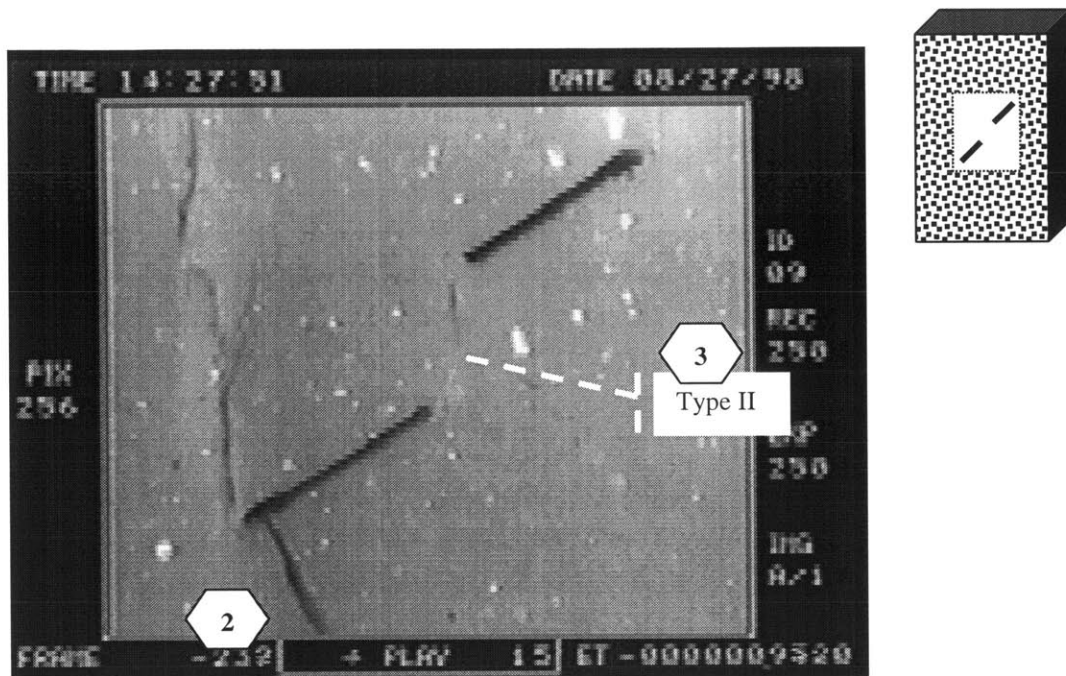


Figure 4.36a: Crack pattern for **marble** specimens with geometry 30-a-a. Specimen MA10

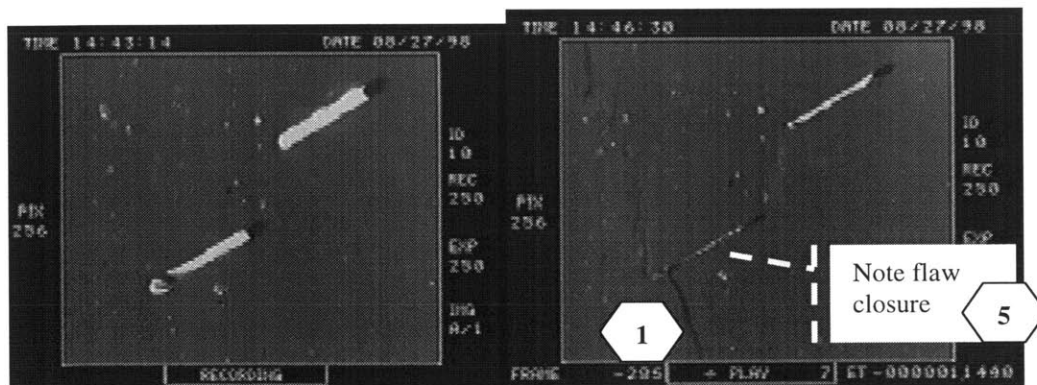


Figure 4.36b: Crack pattern for **marble** specimens with geometry 30-a-a. Specimen MA11

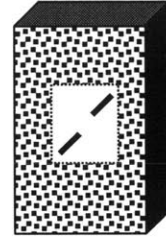
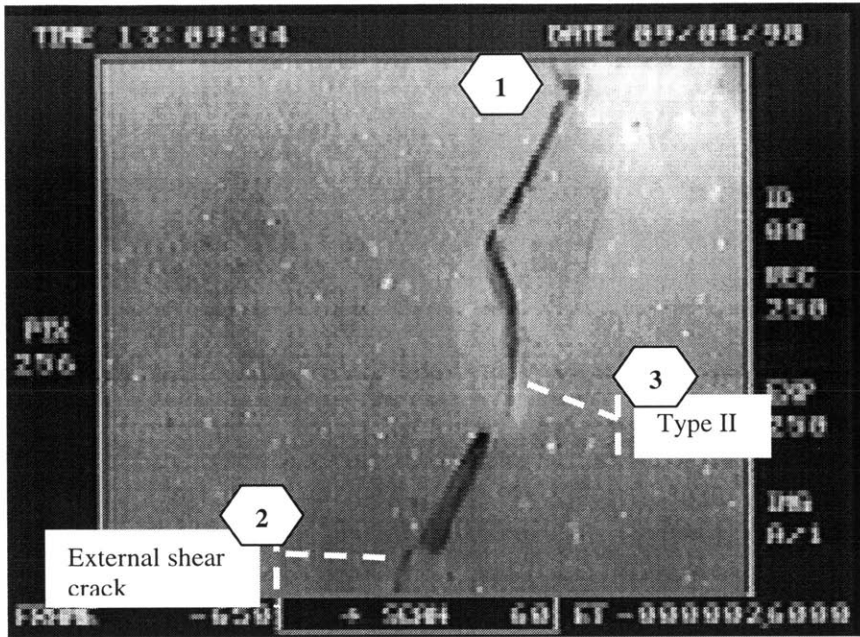


Figure 4.37a: Crack pattern for marble specimens with geometry 60-a-2a. Specimen MA28.

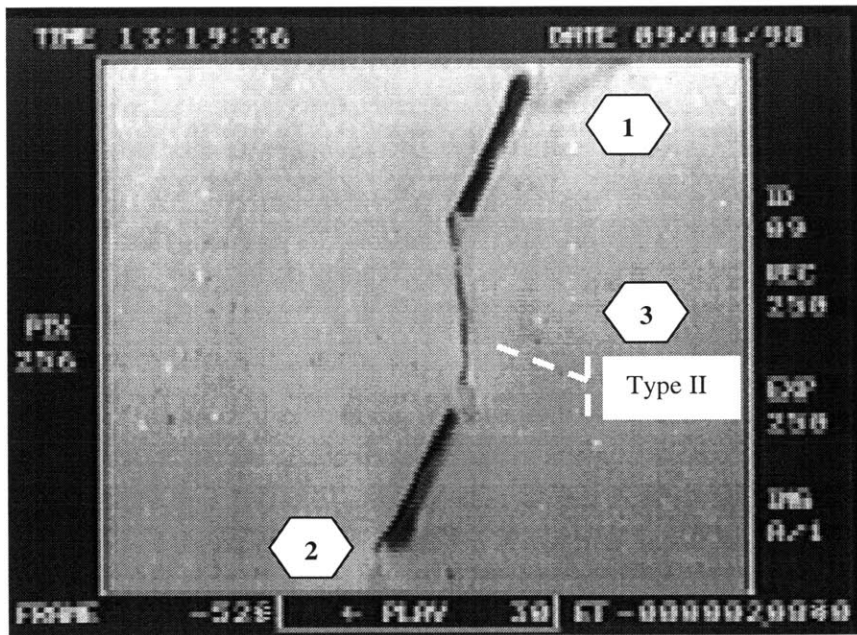


Figure 4.37b: Crack pattern for **marble** specimens with geometry 60-a-2a. Specimen MA29.

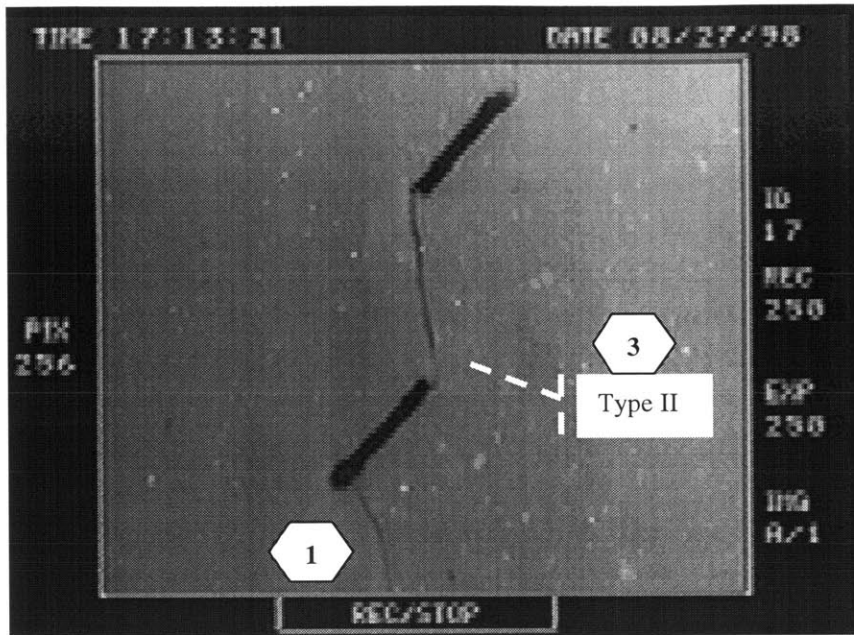


Figure 4.38a: Crack pattern for marble specimens with geometry 45-2a-2a. Specimen MA18

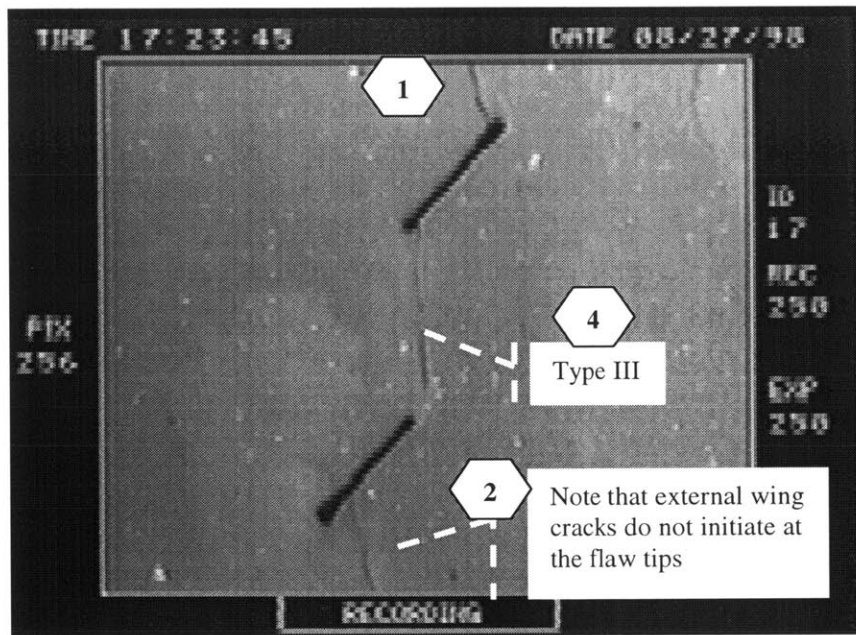


Figure 4.38b: Crack pattern for **marble** specimens with geometry 45-2a-2a. Specimen MA19

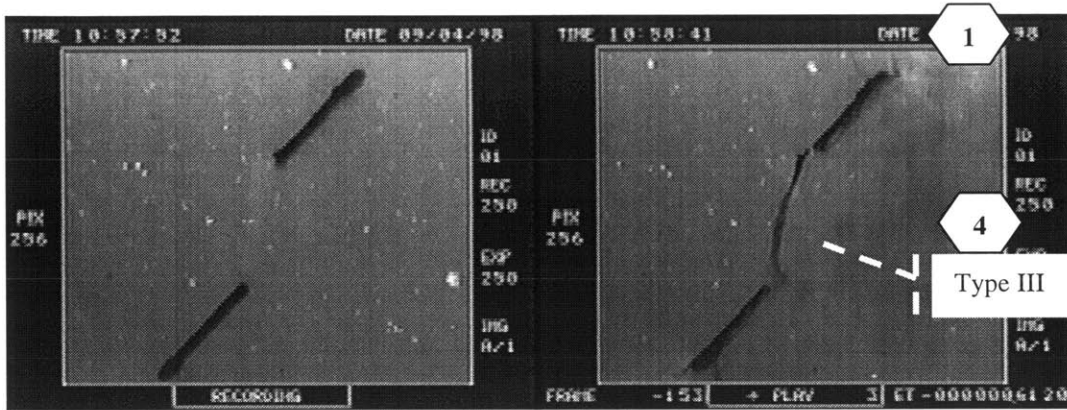


Figure 4.39a: Crack pattern for **marble** specimens with geometry 45-a-2a. Specimen MA20.

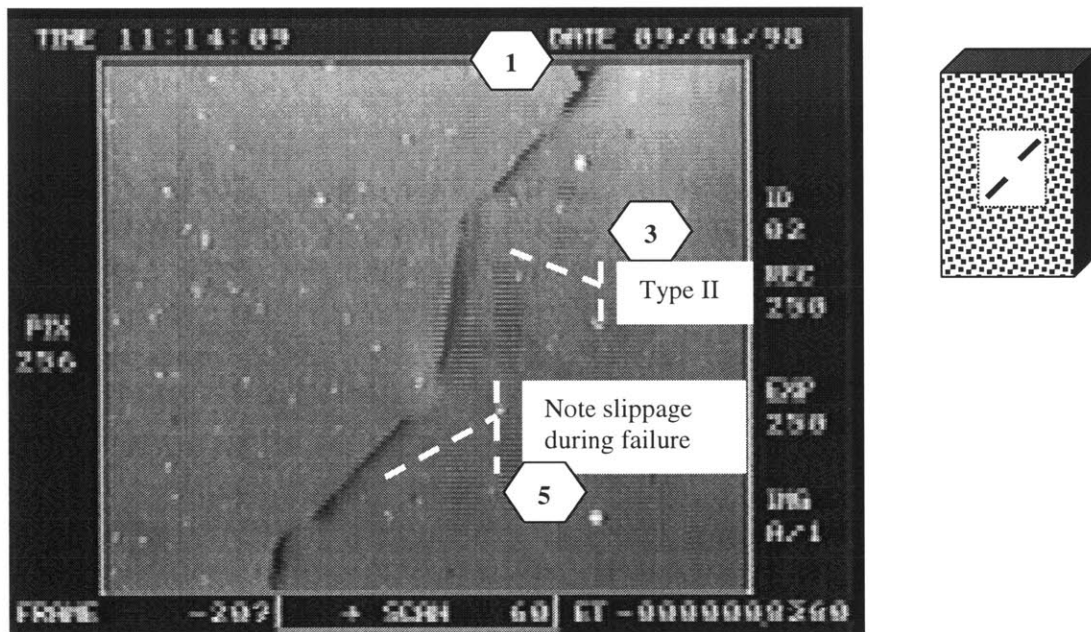


Figure 4.39b: Crack pattern for **marble** specimens with geometry 45-a-2a. Specimen MA21.

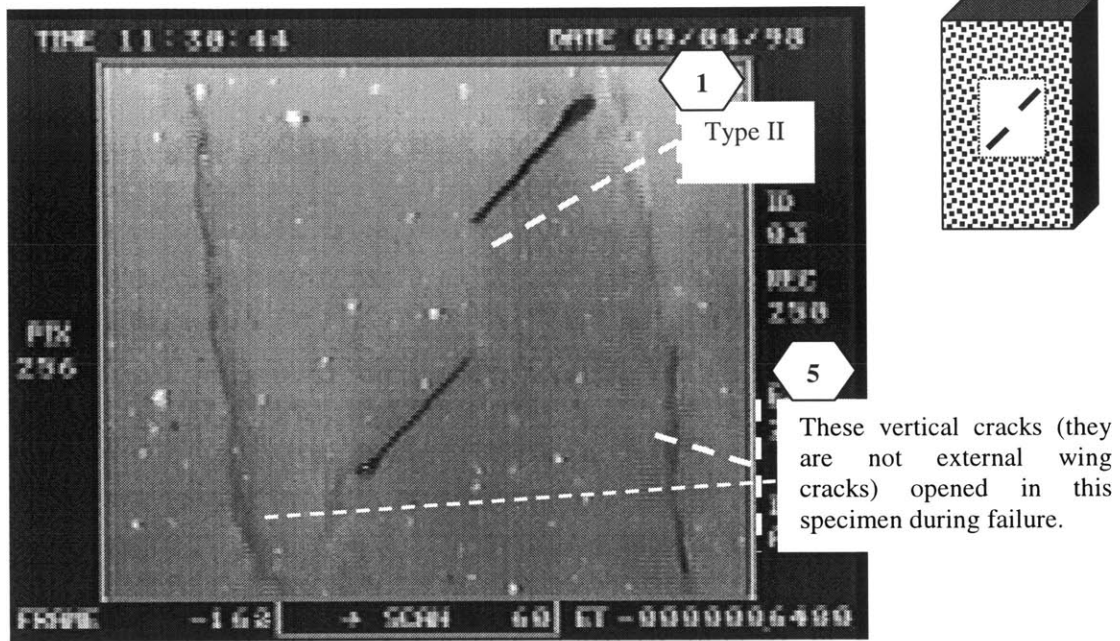


Figure 4.40a: Crack pattern for **marble** specimens with geometry 45-a-a. Specimen MA22

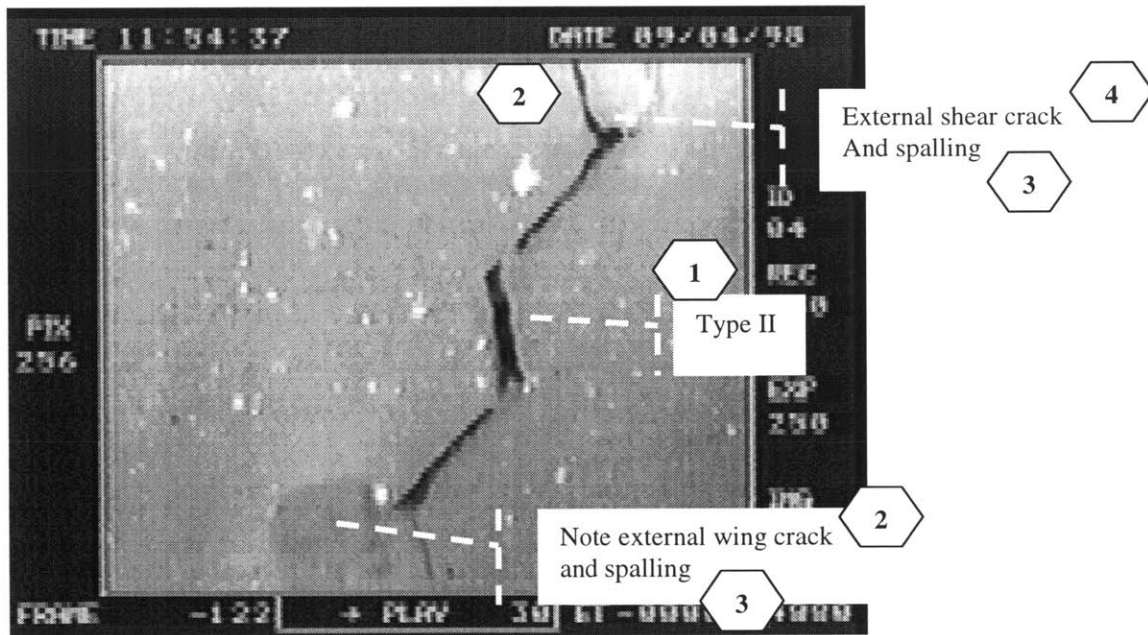


Figure 4.40b: Crack pattern for **marble** specimens with geometry 45-a-a. Specimen MA23

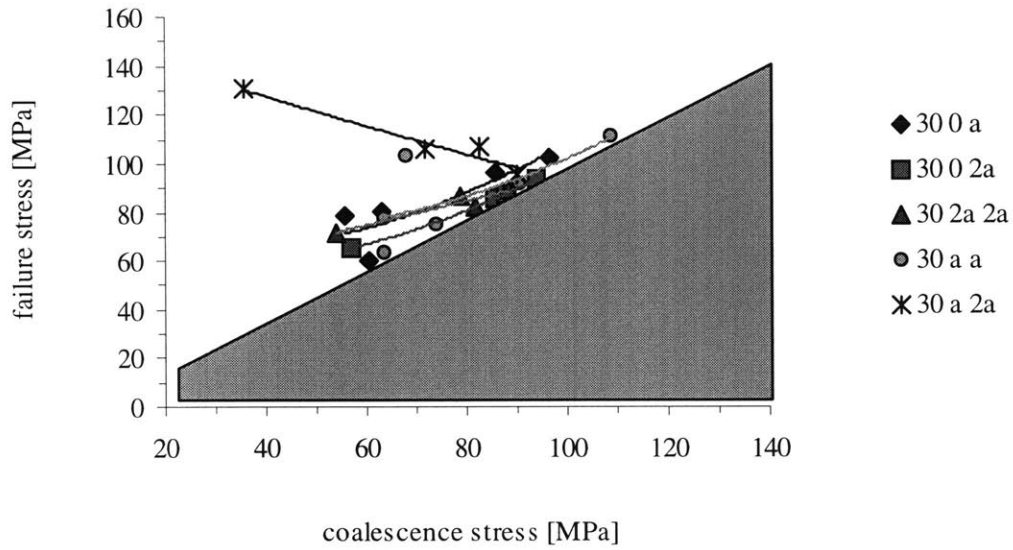


Figure 4.41: Coalescence stress vs failure stress for **granite** specimens with flaw inclination angle $\beta = 30^\circ$

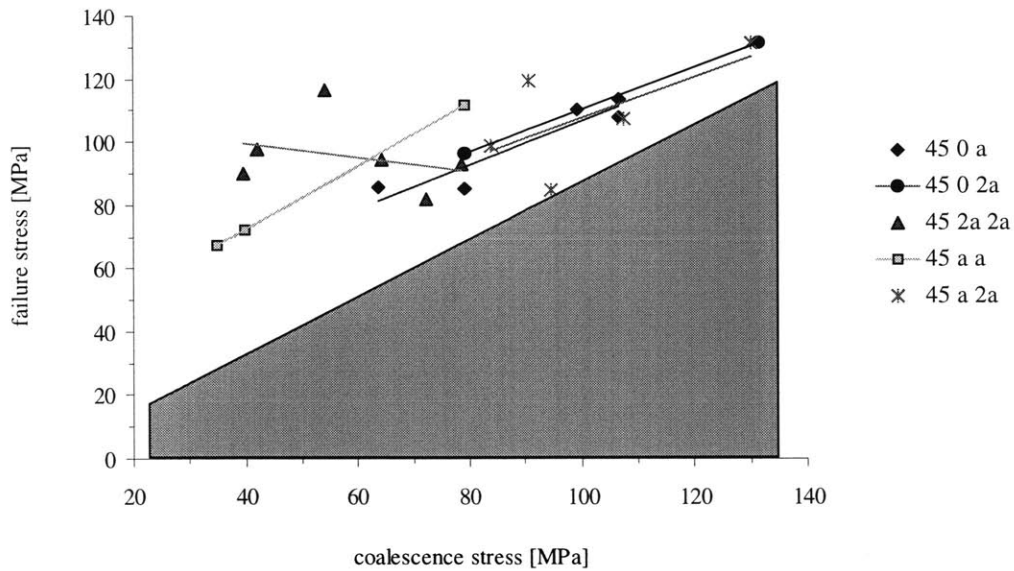


Figure 4.42: Coalescence stress vs failure stress for **granite** specimens with flaw inclination angle $\beta = 45^\circ$

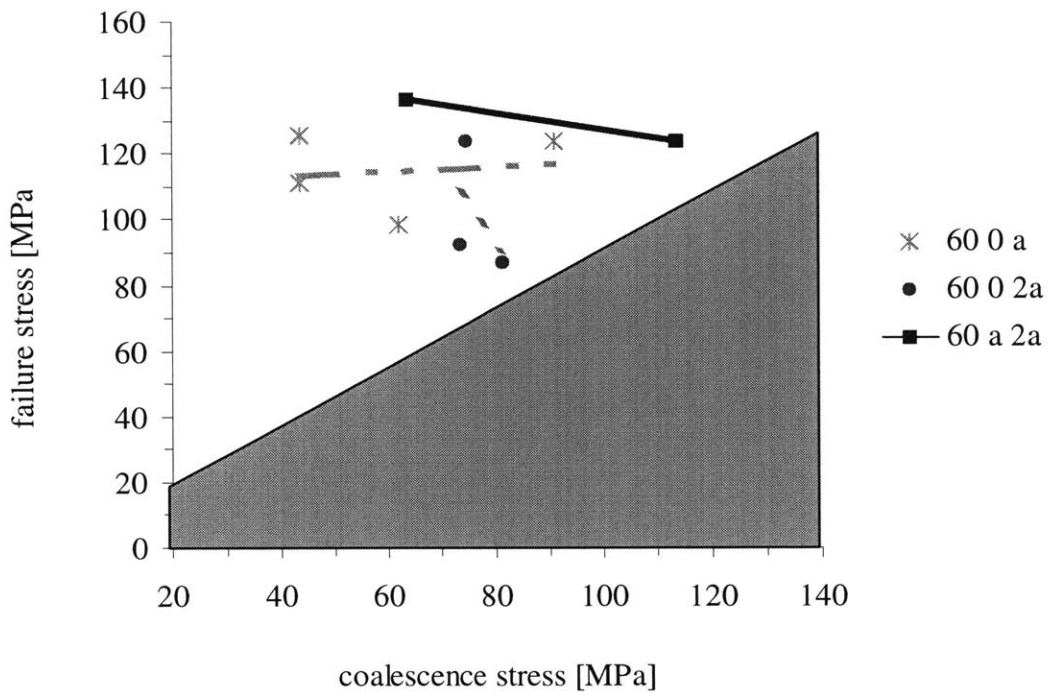


Figure 4.43: Coalescence stress vs failure stress for **granite** specimens with flaw inclination angle $\beta = 60^\circ$.

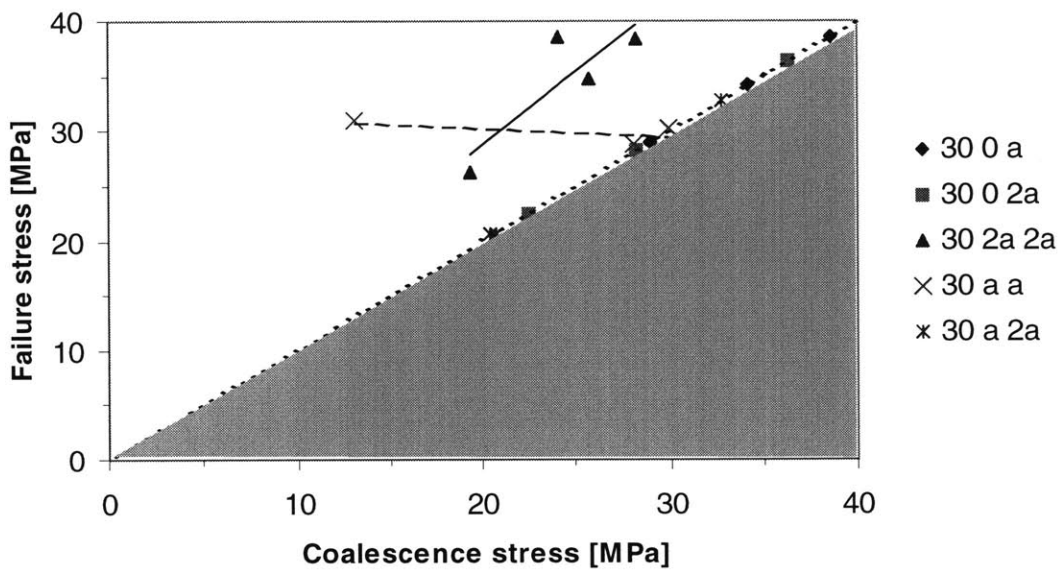


Figure 4.44: Coalescence stress vs failure stress for marble specimens with flaw inclination angle $\beta = 30^\circ$

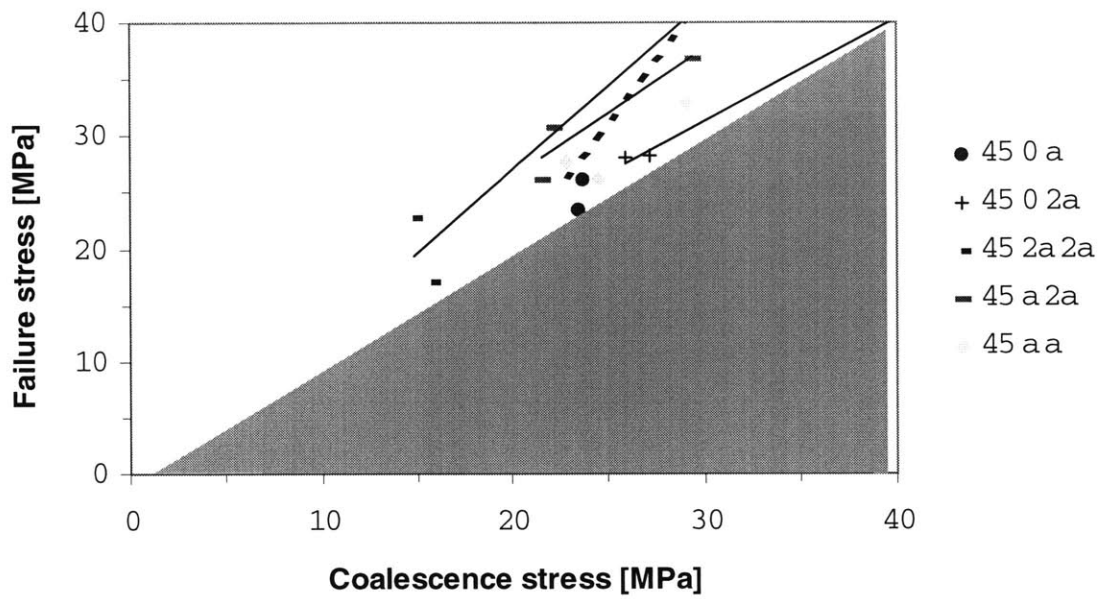


Figure 4.45: Coalescence stress vs failure stress for **marble** specimens with flaw inclination angle $\beta = 45^\circ$

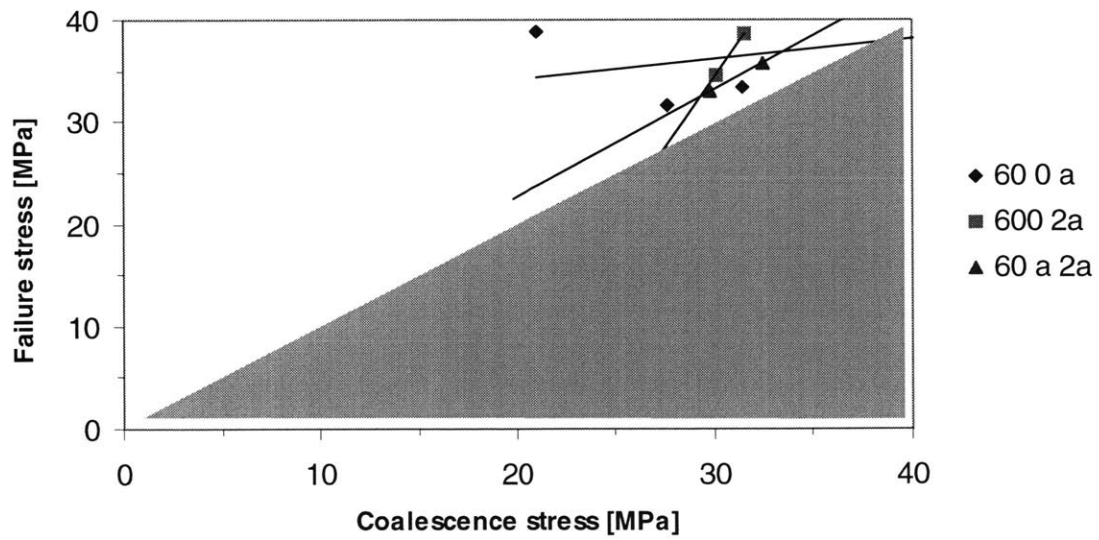


Figure 4.46: Coalescence stress vs failure stress for **marble** specimens with flaw inclination angle $\beta = 60^\circ$

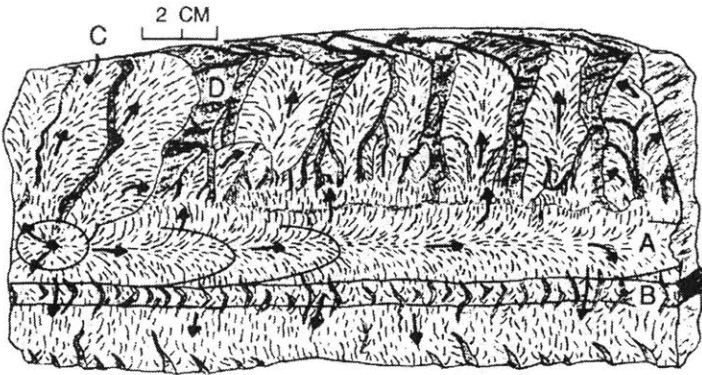
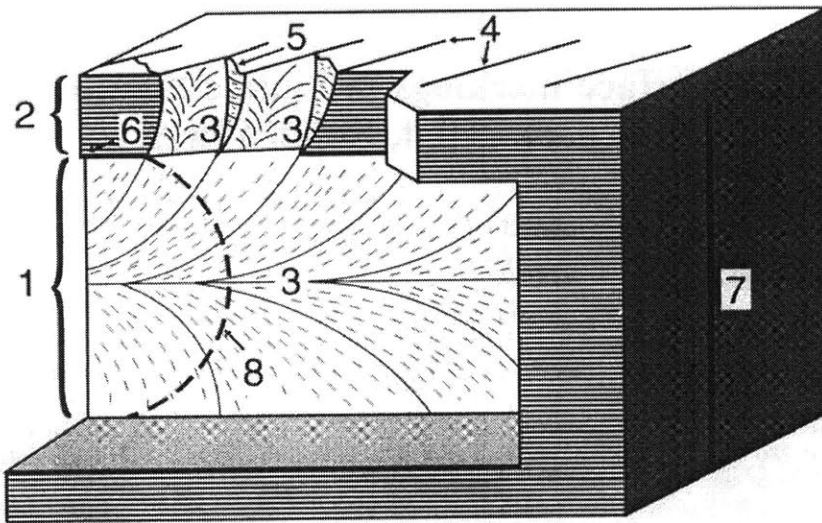


Figure 4.47a: Plumose structure- Sketch of joint in silstone, from Ameen,A.



Descriptive classification

- 1 Main joint face
- 2 Fringe
- 3 Plumose structure
- 4 F-Joints (B-Planes)
- 5 C-Fractures (straight medial)
- 6 Shoulder
- 7 Trace of main joint face
- 8 Arrest line

Genetic classification

- 1 Main fracture face
- 2 Twist-hackle fringe
- 3 Fracture plume
- 4 Twist-hackle face
- 5 Twist-hackle step
- 6 Plumose-coarse twist-hackle boundary
- 7 Tensional penetration
- 8 Arrest line

Figure 4.47b: Plumose structure- Component of fracture surface markings, from Ameen,A.

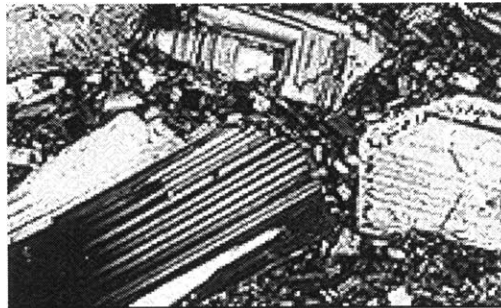
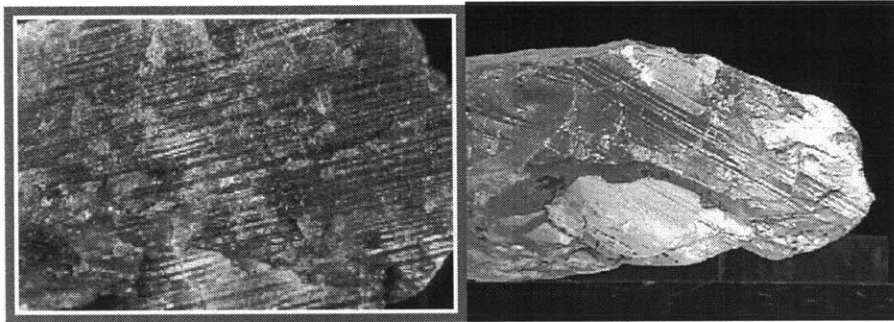


Figure 4.48: Twinned (striated) crystal of feldspar.

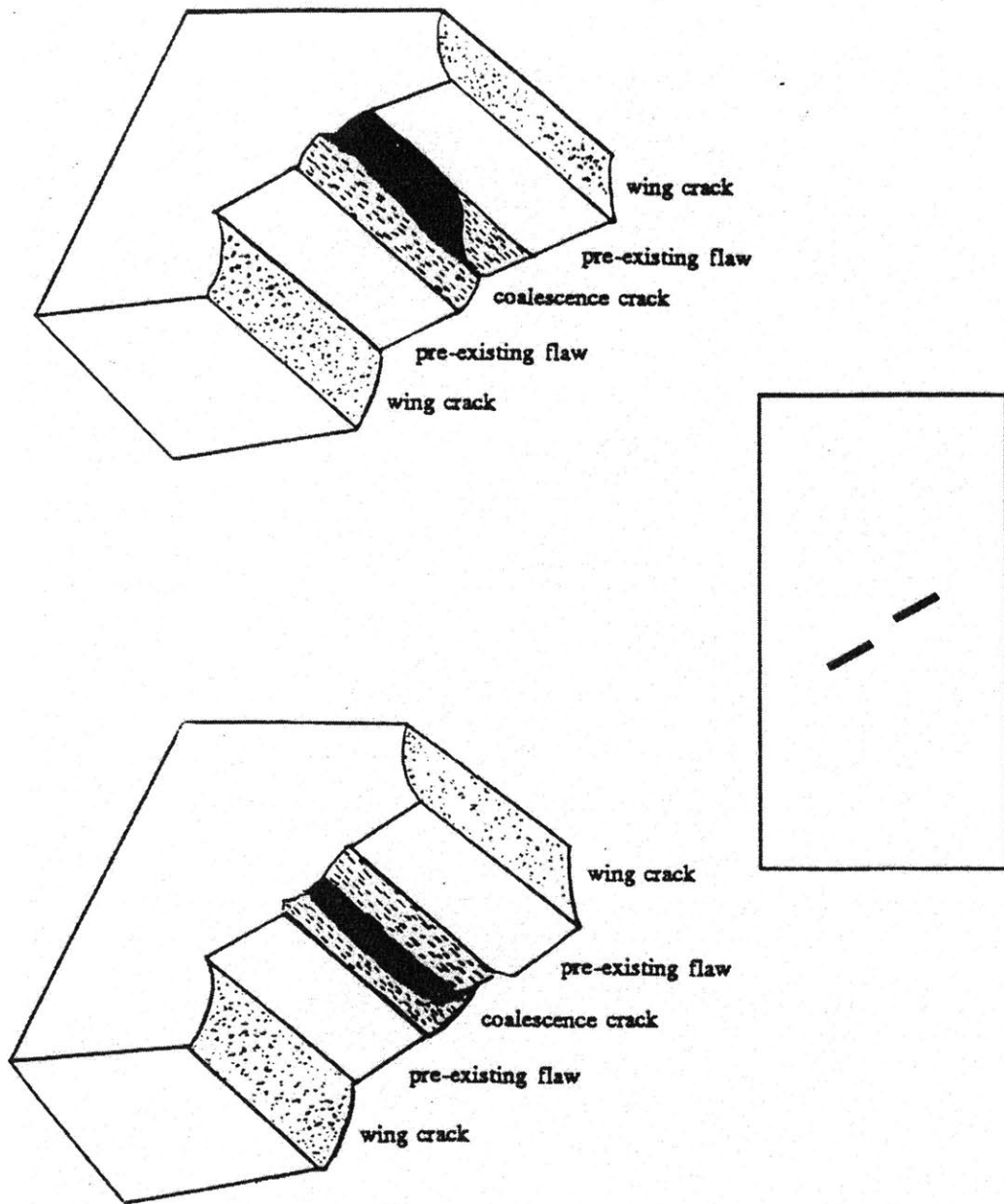


Figure 4.49: Surface morphologies on gypsum, from Reyes (1991)

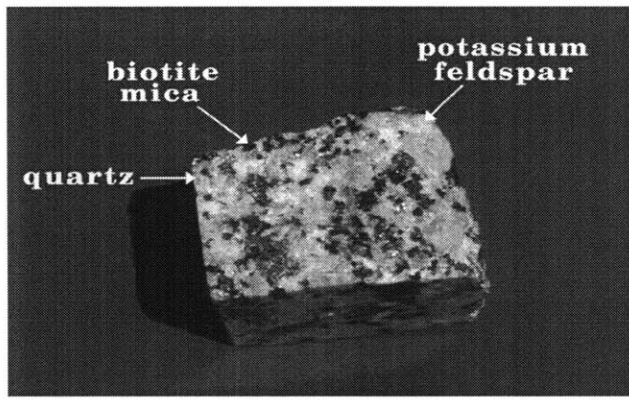
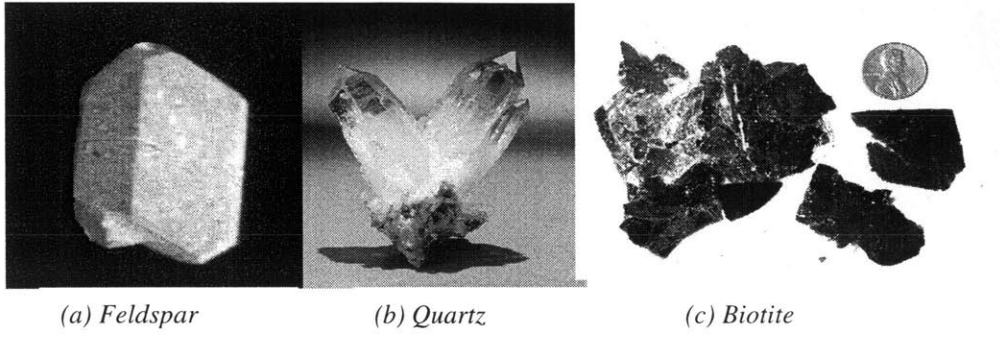


Figure 4.50: Principal minerals composing granite

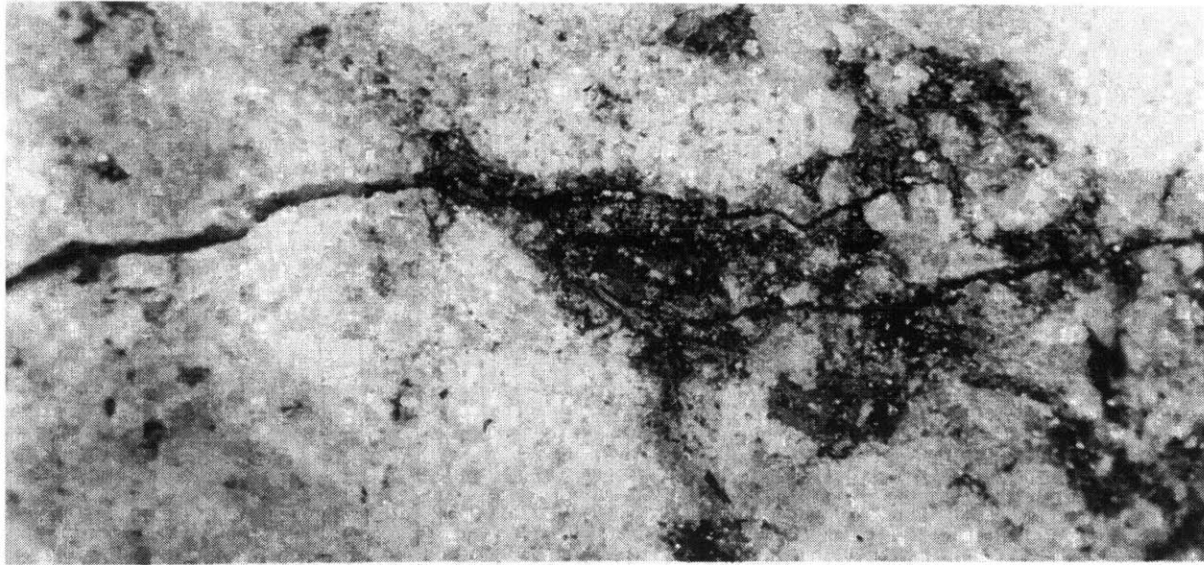


Figure 4.51: Example of zonation in granite (cracks tend to align with the weakest mineral).
From Pusch (1995)

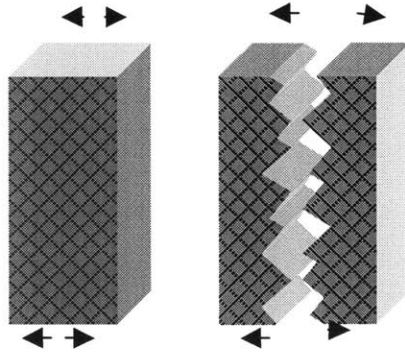


Figure 4.52: Example of a tension fracture.

- (a) *Fracture propagates along grain surfaces.*
- (b) *Both parts of specimen are separated due to tension forces. Roughness due to the grain exposure.*

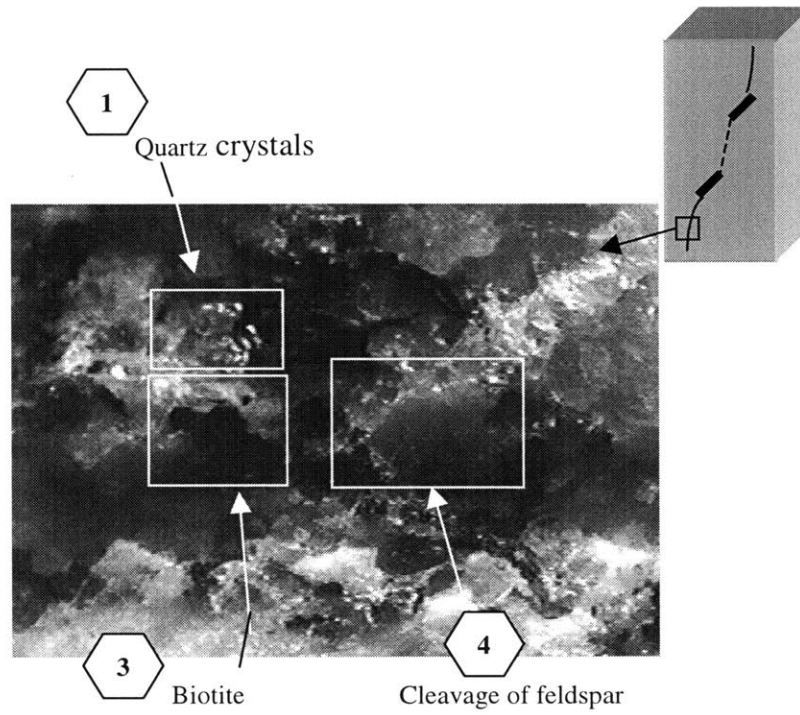


Figure 4.53: Tension crack in **granite** specimen GR 31 (45- 2a-2a)

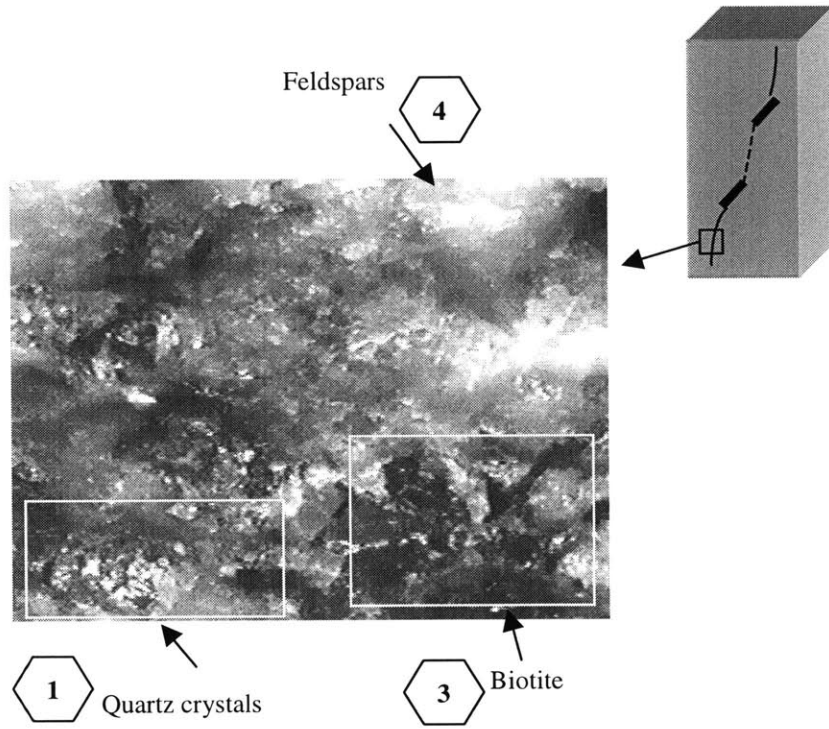


Figure 4.54: Tension crack in **granite** specimen GR 86 (30-a-a)

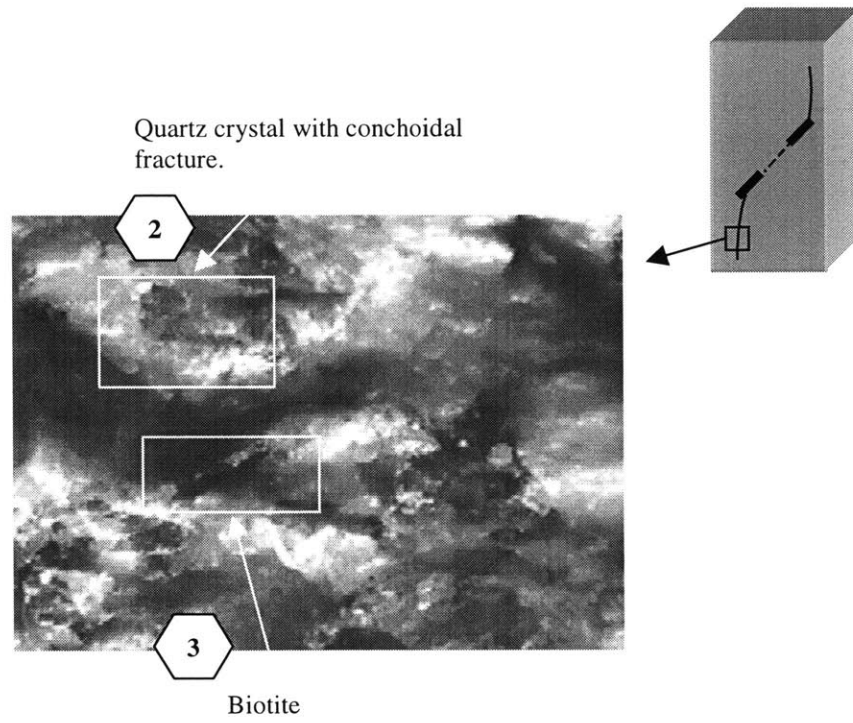


Figure 4.55: Tension crack in **granite** specimen GR 73 (60-0-a).

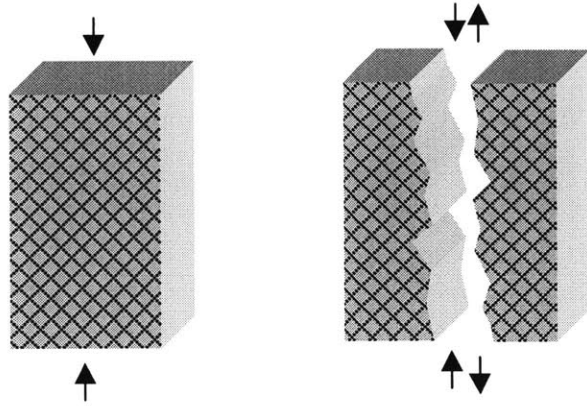


Figure 4.56: Example of a shear fracture.

(a) *Fracture propagates along grain surfaces.*

(b) *Friction between both parts due to shear forces.*

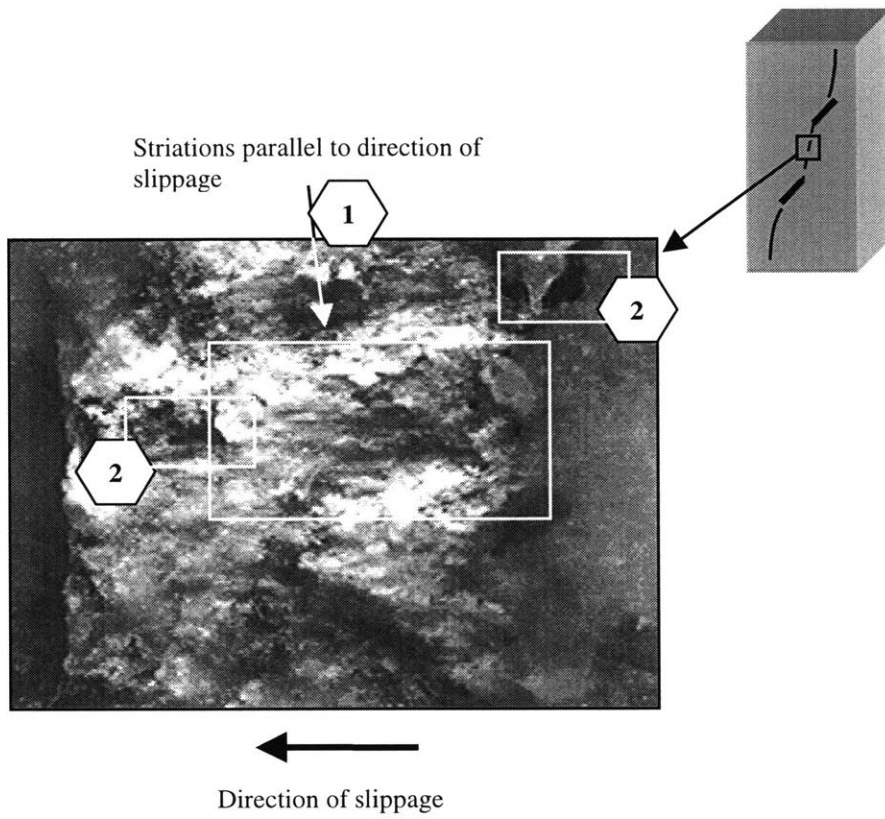


Figure 4.57: Shear crack in **granite**.

Note striations on the surface parallel to the direction of slippage.

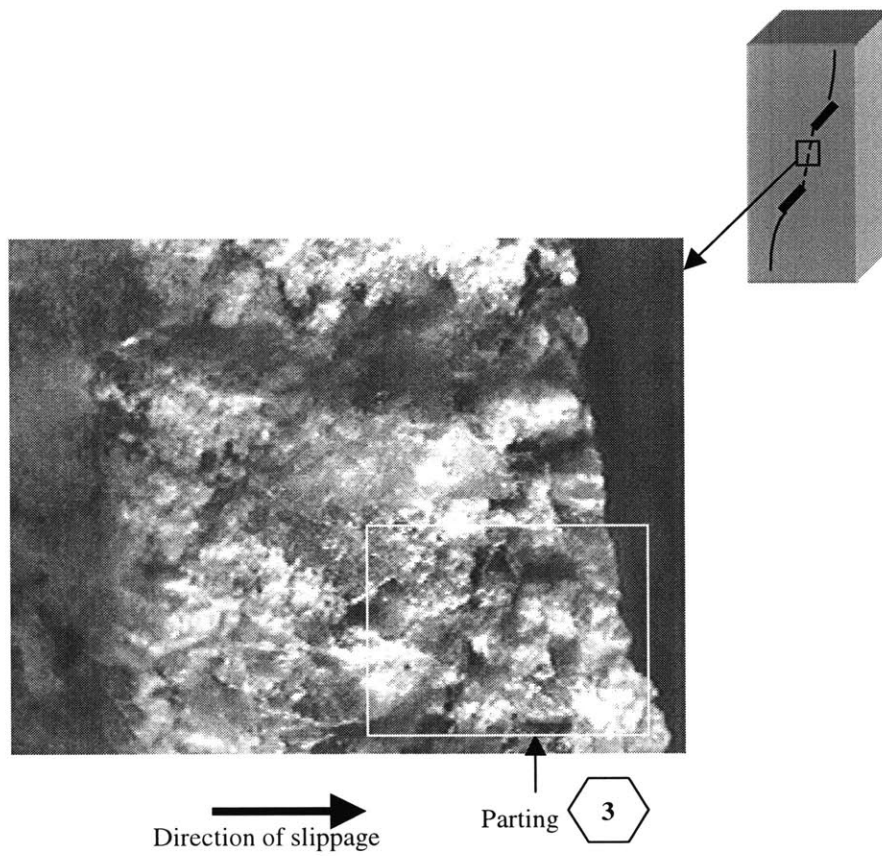


Figure 4.58: Shear crack in granite. Note sharp part of the parting planes indicating direction of slippage.

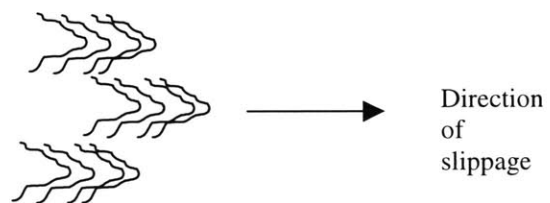


Figure 4.59: Parting planes indicating direction of slippage.

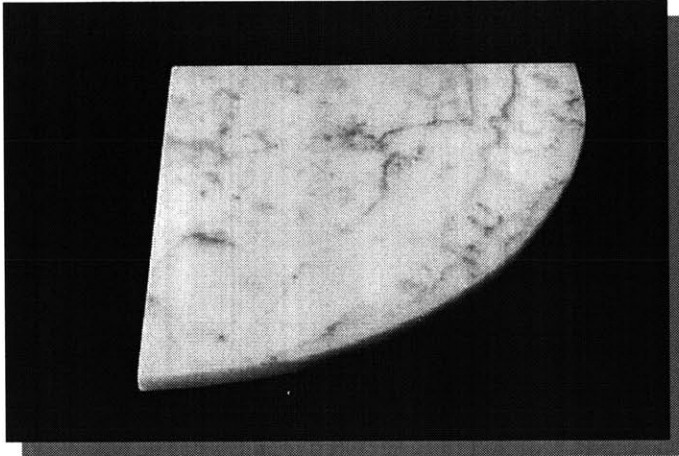


Figure 4.60: Calcite. Principal mineral component of marble

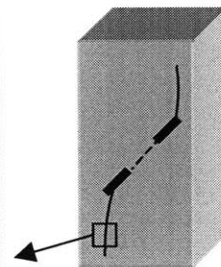
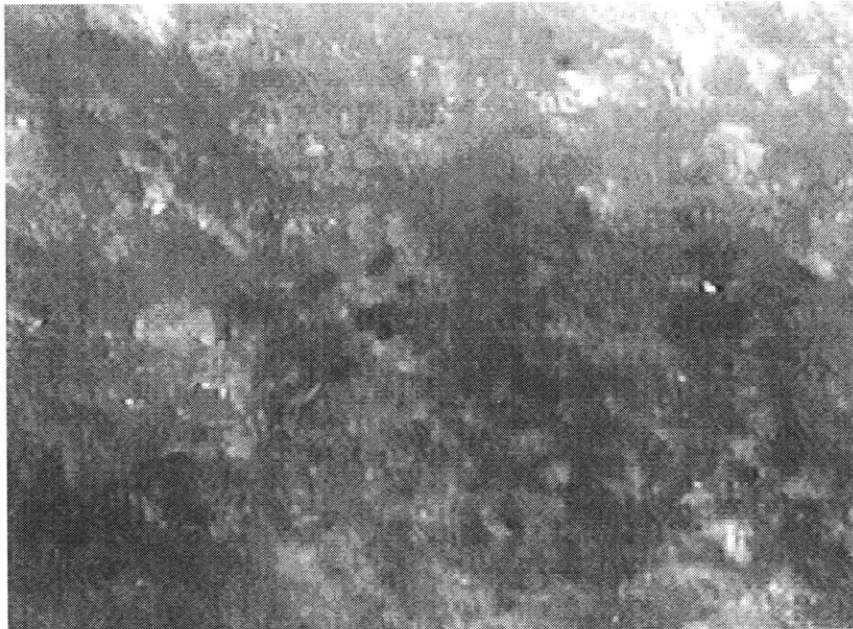


Figure 4.61: Tensile surface in **marble**

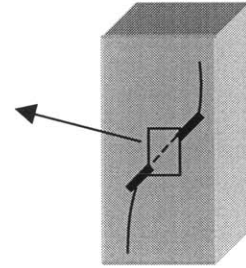
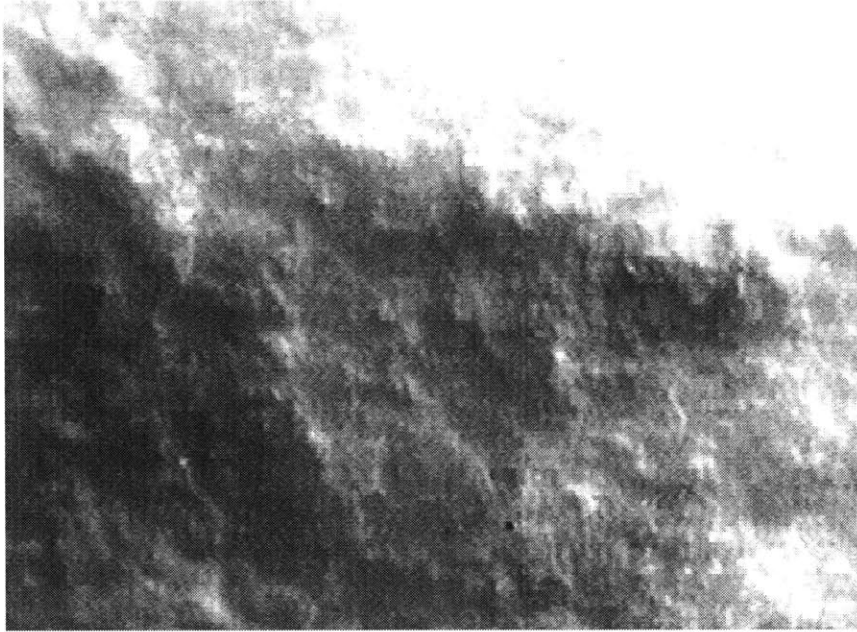


Figure 4.62: Shear surface in **marble**

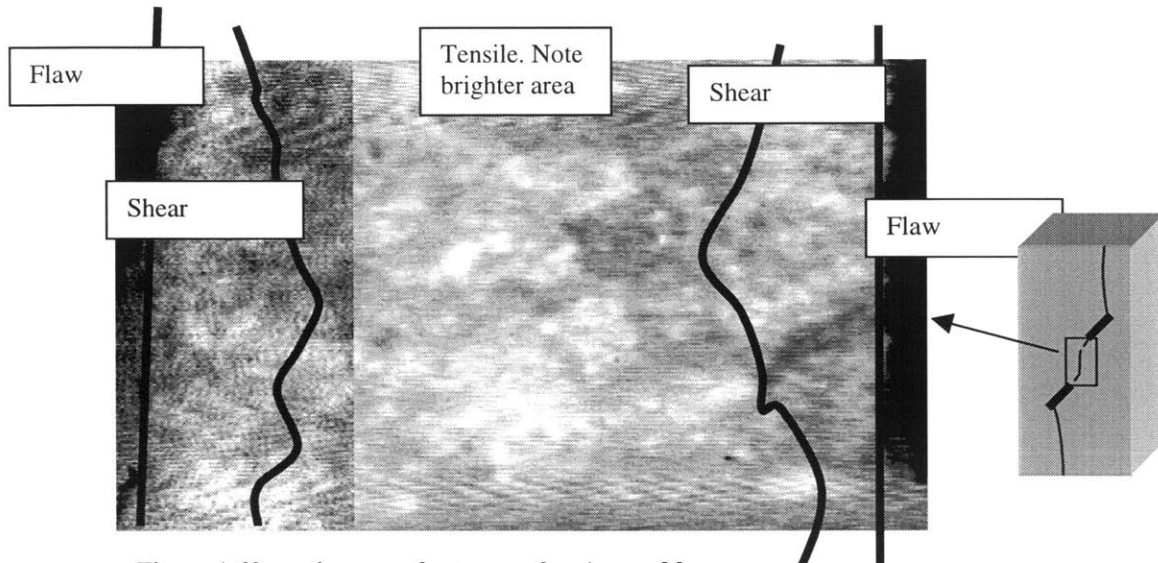


Figure 4.63: coalescence fracture surface in **marble** .
 Specimen MA 18 (45 2a 2a). Coalescence **TYPE II**

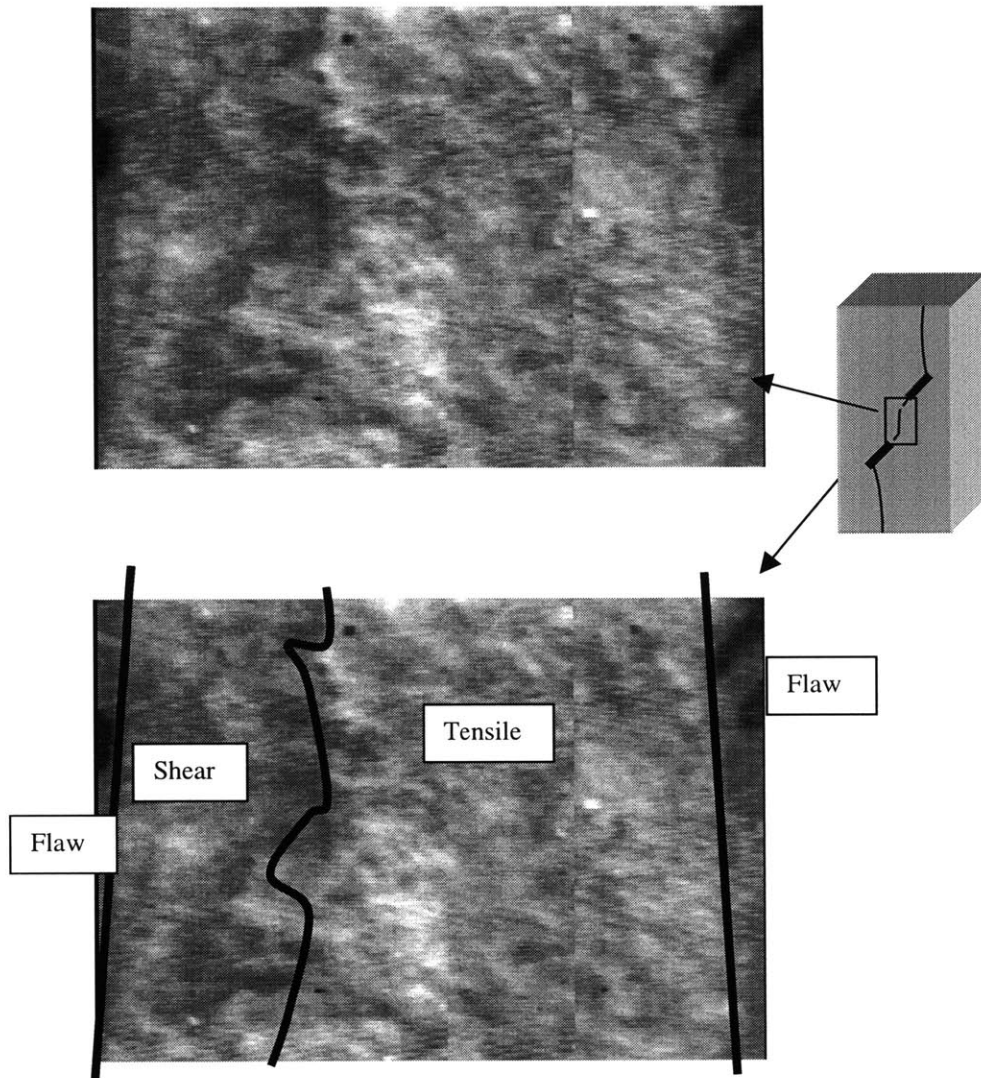


Figure 4.64: Coalescence fracture surface in **marble** .
 Specimen MA 12 (30-a-2a). Coalescence **TYPE III**.
 Upper: original picture.
 Lower: Enhanced picture showing the different fracture areas

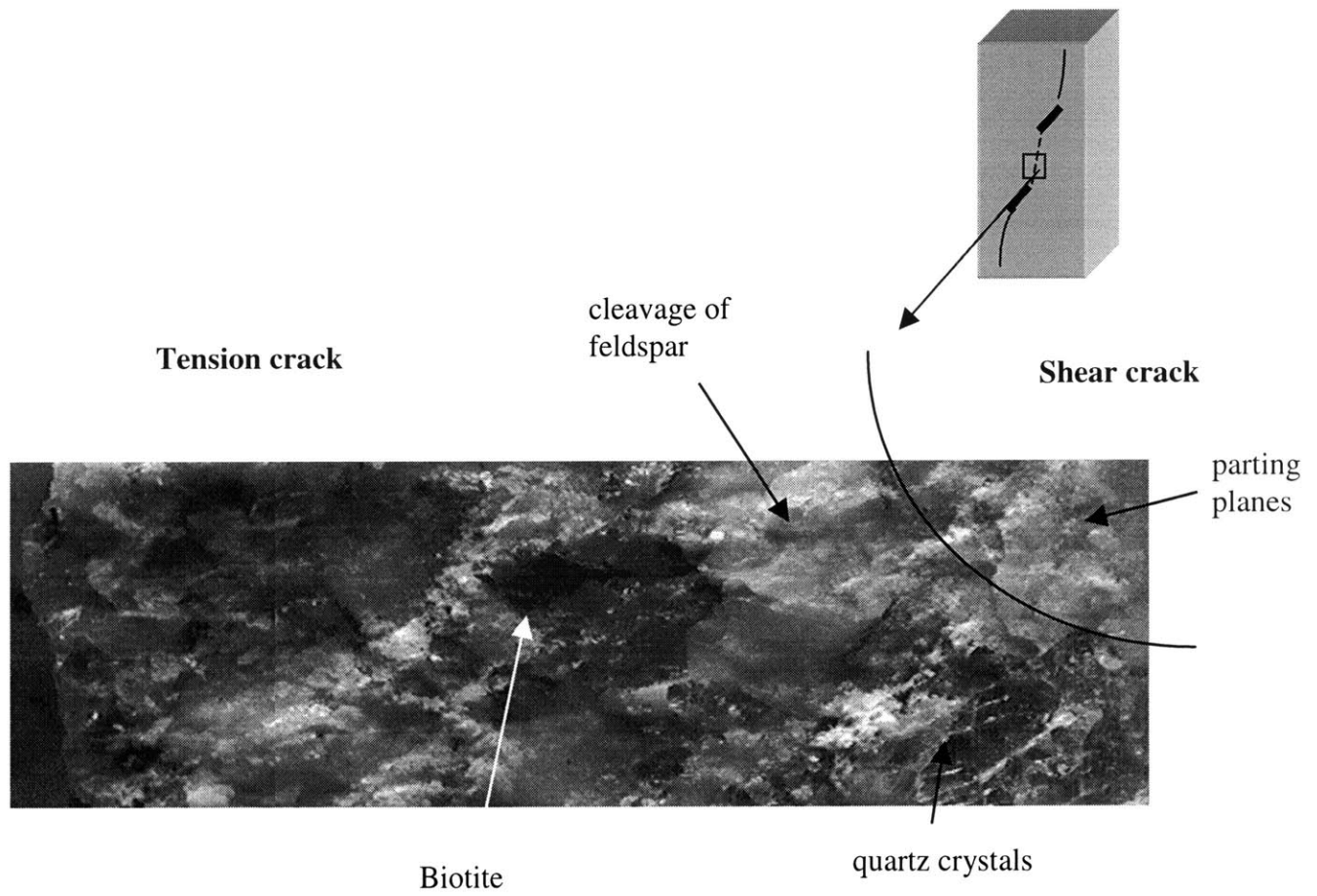


Figure 4.65: Coalescence surface of specimen GR 31 (45-2a-2a). Coalescence seems to take place as type III.

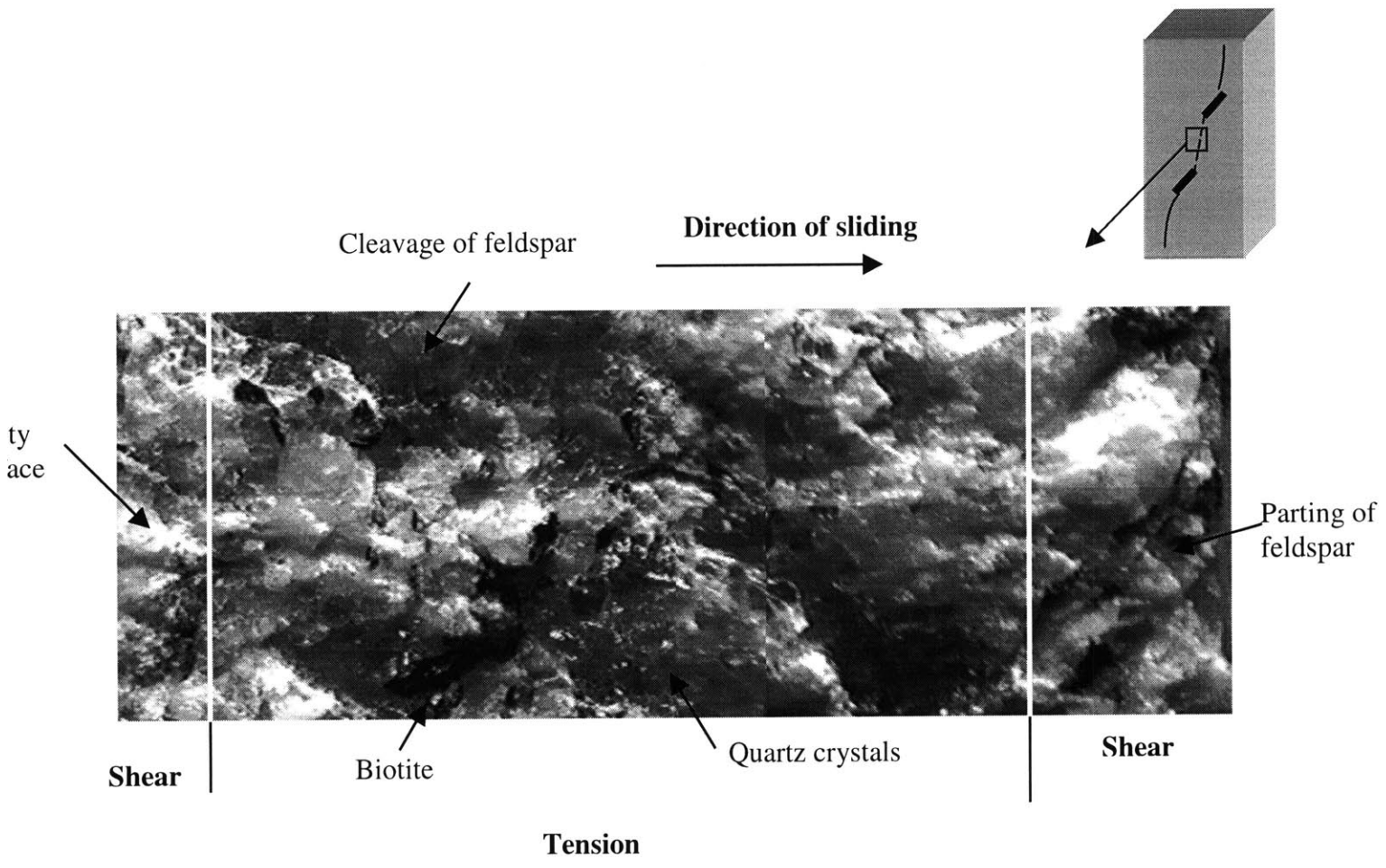


Figure 4.66: Coalescence surface of specimen GR 43 (45-2a-2a). Note changes from shear - tension - shear of coalescence type II.

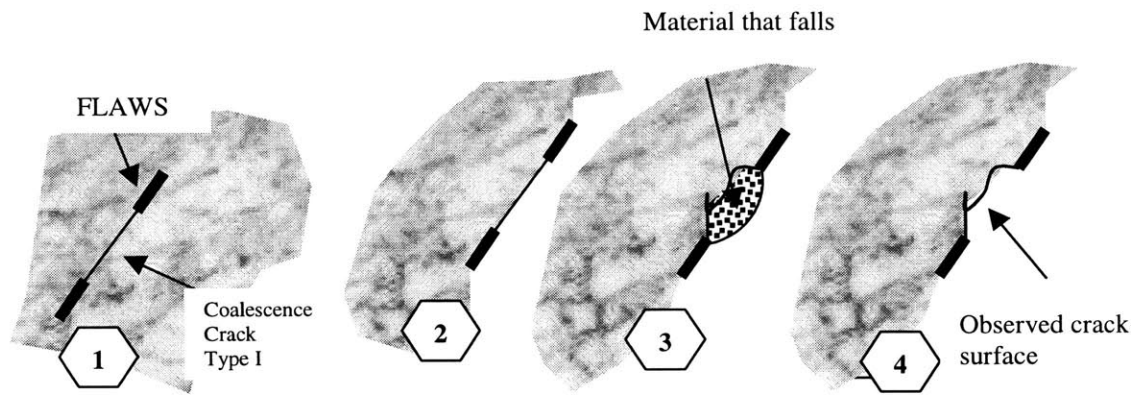


Figure 4.67: Sequence of steps leading to observe a tension-like crack surface in a shear crack.

- 1 Crack develops in shear (coalescence type I)
- 2 Specimen fails
- 3 Material loses after failure
- 4 A concave "tensile like" surface is observed in fractography analyses

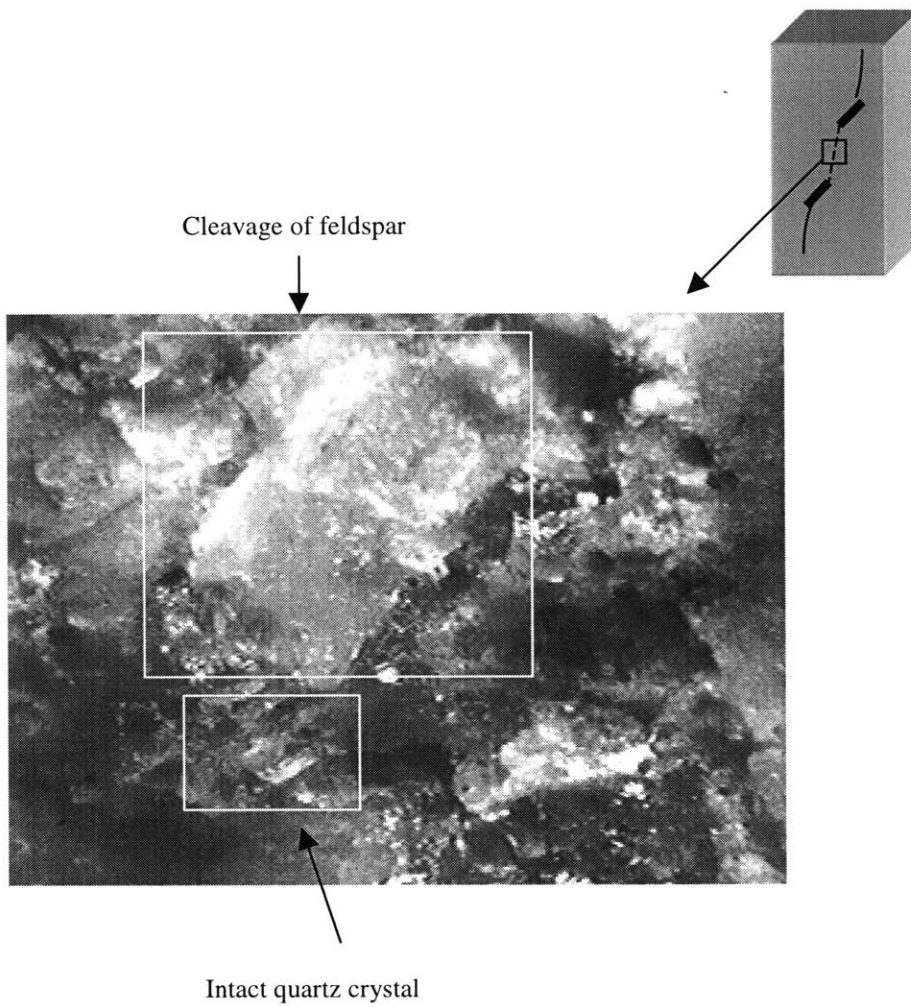


Figure 4.68: Coalescence surface of specimen GR 59 (45-0-a). This specimen has coalescence type I, but the picture shows the characteristics of tension fracture: rough and bright (due to the mechanism shown in figure 4.67)

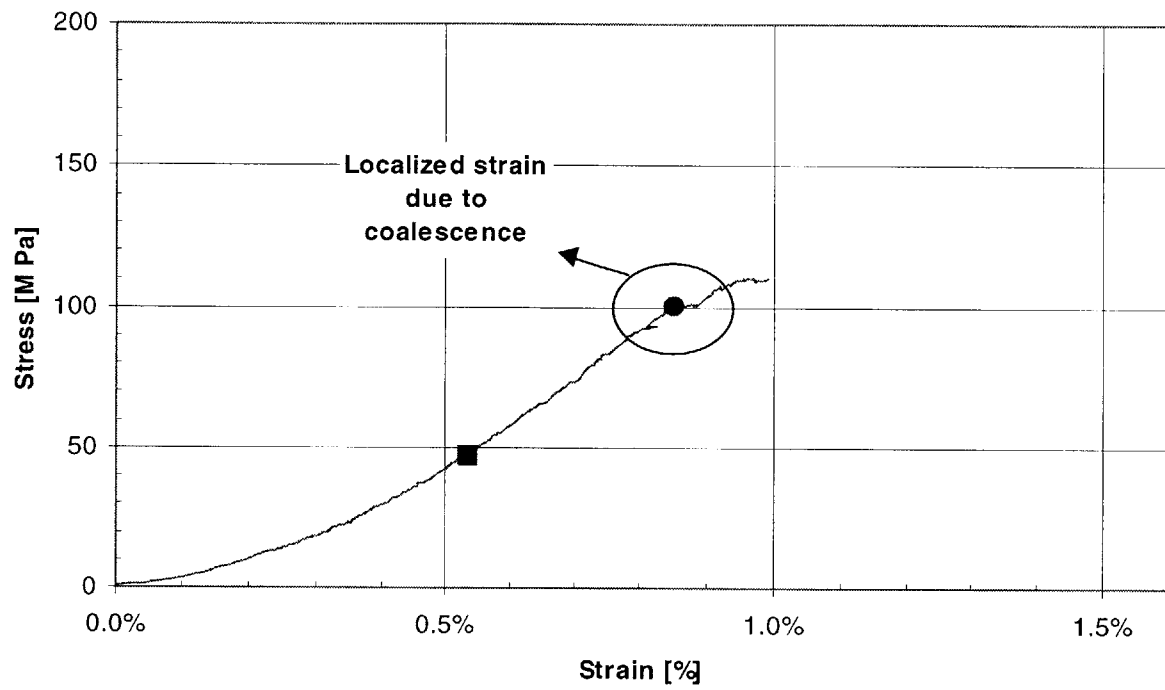


Figure 4.69: Stress strain plot showing a jump due to coalescence. Granite specimen with flaw geometry (45-0-a)

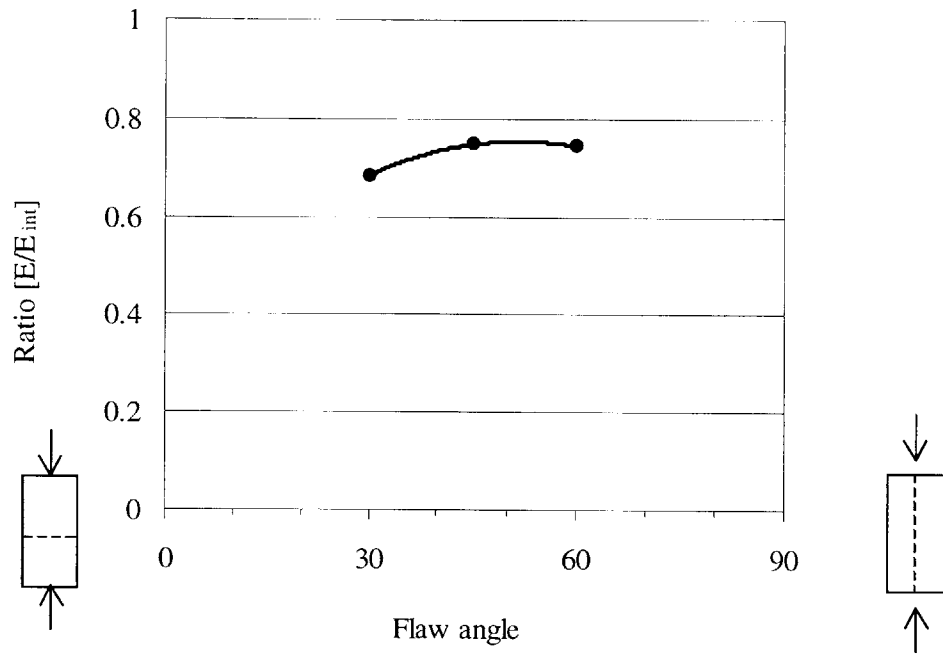


Figure 4.70: Representation of E/E_{int} versus flaw angle for **granite**

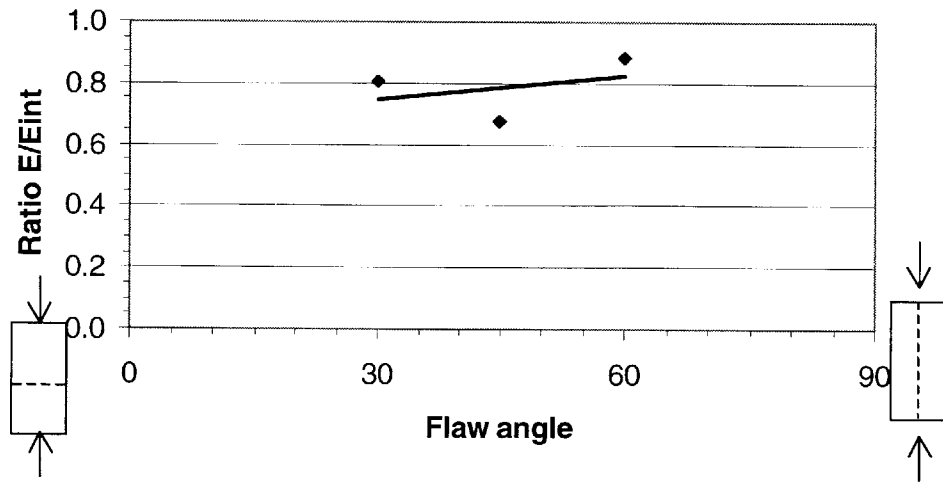


Figure 4.71: Representation of E/E_{int} versus flaw angle for **marble**

Chapter 5: CONCLUSION

Previous research in rock fracture mechanics has shown that fracture coalescence is a complicated process. Bobet (1997) conducted a very thorough experimental program on molded gypsum specimens and developed a numerical model that successfully predicted these experimental results. The present research focuses on obtaining experimental data on fracture coalescence in natural rocks. Prismatic specimens of granite and marble with two flaws cut through the thickness are tested in uniaxial compression. During the loading test one of the specimen faces is recorded with a high-speed video camera. The images are played-back at a lower speed in order to correctly understand the fracture initiation and propagation processes. Fractography analyses are performed on the fracture surfaces after failure. These analyses are used as a secondary tool to identify the fracture origin.

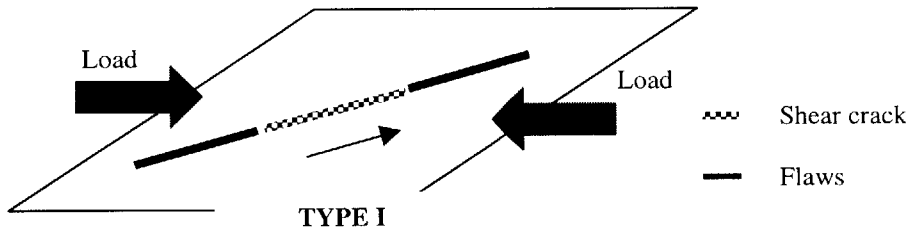
A brief summary of the most important experimental observations from the loading tests and the fractography analyses follows. Specifically, Section 5.1 lists the common results observed in granite and marble, Section 5.2 the specific results for granite and Section 5.3 the results for marble. Section 5.4 compares the observed patterns in natural rocks with those in gypsum. Section 5.5 lists aspects not covered in the present research.

5.1 General results

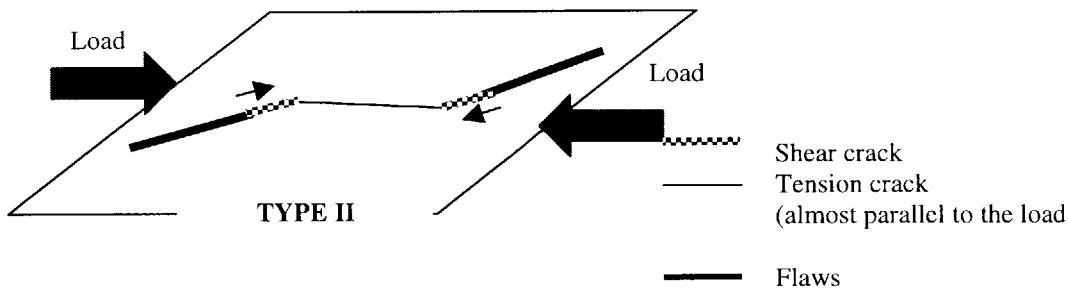
The results are consistent with previous research. In general, similar crack patterns and coalescence types are observed. The different coalescence types observed in granite and marble specimens with non-overlapping flaw geometries are a combination of shear and/or tension crack; they and are summarized in figure 4.1 and repeated in figure 5.1

The main observations for both granite and marble are:

- Typically, the same fracture pattern can be observed on both faces of the specimens. This fact is important since some researchers argue that the fracture process is in fact 3-D and hence the fracture pattern cannot be observed completely by looking at only the face of the specimens.
- Coalescence type I occurs in specimens with coplanar flaws, while coalescence type II occurs for non-coplanar flaws. Other coalescence types occur only in a few geometries and for very few specimens. Coalescence type I is formed by the propagation of one or two internal shear cracks, that develop in the plane of the flaw. Hence, it is logical to expect coalescence type I to occur in specimens with coplanar geometries.



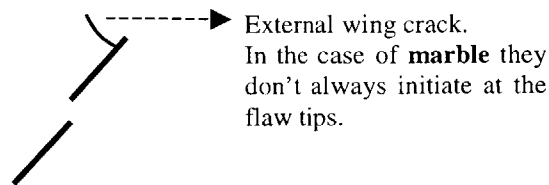
- Specimens with non-coplanar flaws also develop shear cracks at the tips. Then, a tension crack, that usually follows a path aligned with the major principal stress direction (vertical), develops from one internal shear crack to the other, and coalescence type II takes place (note that this vertical crack is a tensile crack but it is not an internal wing crack).



- Both shear and tensile fractures can be distinguished by the relative movement of the crack surfaces. This relative movement can only be adequately detected when

observing the fracture initiation process from 250 to 1,000 times slower (using a high-speed video camera to record during the loading tests). Previous results based only on fractography did not allow one to differentiate shear cracks from tension cracks that slipped afterwards.

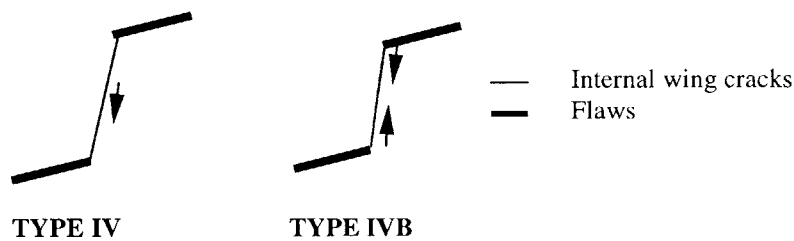
- The crack initiation and propagation processes do not produce leaps or discontinuities in the stress-strain curves. However, the presence of the flaws produces a decrease in the specimen stiffness. In general the flatter the flaws (for a vertical load) the greater the strain and hence the greater the reduction in the stiffness.
- It is generally observed that external and internal wing cracks initiate at about the same stress level and that they both generally develop at a lower stress than coalescence.
- In both granite and marble, tensile cracks have rough, bright surfaces with complete absence of powder and also with exposed grains in the case of granite. Tensile crack surfaces in marble specimens show some plumose structure. On the other hand, shear crack surfaces are smooth, opaque and covered with powder, which is more abundant in the case of marble; slickensides and striations are observed in both granite and marble shear crack surfaces (but are more clearly visible in granite).
- Both internal and external wing cracks initiate at the flaw tips in the case of granite. On the other hand, in marble (for about 25% of the specimens) the wing cracks initiate at about $\frac{1}{4}$ of the flaw length.



5.2 Granite results

- Failure of intact (no flaw) specimens is generally violent, indicating the brittle characteristics of the material.

- Failure of granite flawed specimens is generally caused by external wing cracks that propagate until they reach the specimen boundaries. However, some specimens with coplanar flaws fail due to propagation of internal wing cracks.
- A new type of coalescence is observed in granite specimens. This type of coalescence is a variation of coalescence type IV, observed by Reyes (1991). In the present research, this coalescence type IVB has been observed for granite specimens with flaw geometry 45-a-a, which has a ligament angle of 90° , the boundary between overlapping and non-overlapping geometries.



- Coalescence and failure stresses do not coincide. The relationship between coalescence and failure stress depends on the specimen geometry. The general trend for the failure stress is to increase as the coalescence stress increases.
- It is generally observed at the front face during load testing that cracks go through the grain boundaries. However, when analyzing some crack surfaces, grain breakage is observed; the most probable explanation is that this grain breakage is produced by the slippage of fractures during the loading process.
- In tensile surfaces the different granite minerals can be recognized. Quartz crystals can be found as either hexagonal prisms or with conchoidal fracture. Feldspar grains show cleavage (with planes at or around 90°). On the other hand, shearing produces striations and dust, which makes very difficult the identification of any mineral. Furthermore, in shear crack surfaces thin superposed planes of feldspar with a pointed shape can be observed; these points are aligned with the direction of slippage.
- Cracks typically tend to initiate and propagate through biotite grains (they have a sheet-like shape and are weaker than the other minerals in granite). This process is called zonation. Furthermore, when analyzing both shear and tensile crack surfaces,

biotite grains can be seen on the surface; this is again indicating that the cracks propagate next to them.

5.3 Marble results

- Intact specimens (no flaws) fail by shearing and not as violently as granite.
- In flawed specimens, failure is caused by either external wing cracks or external shear cracks that reach the boundaries of the specimens. As in granite, some specimens that have coalescence type I fail due to internal wing cracks reaching the boundaries.
- Coalescence mode III is much more common in marble than it is in granite and gypsum.
- A brighter area is very visible in the rock bridge between the two flaws when the stress level is about to reach the coalescence stress. This brighter area is also visible in the case of granite but it is not easy to identify due to the material color. This might indicate that the surface is about to be detached.
- In the case of marble specimens with flaw angle $\beta = 30$, closure of the flaws is observed. This process causes more strain, resulting in a lower stiffness. This is observed only in a few granite specimens.

5.4 Comparison with gypsum results

- For granite, a limit for coalescence to occur has been found. Specimens with flaw geometries with ligament lengths equal to or larger than $3a$ do not coalesce. Bobet (1997) observed for molded gypsum specimens that for a ligament length larger than a distance of $3a$ the interaction between flaws is minimal.
- For both granite and marble specimens, the coalescence mode is related to the s/c value in the same way as for gypsum specimens. The relationship (after Bobet 1997) is:

s/c ratio	Type of coalescence
$s/c < 1/3$	I
$1/3 < s/c < 1$	II
> 1	III

- As was already mentioned the coalescence modes observed in this research agree very well with the results presented by Bobet (1997) for gypsum specimens with molded flaws:

Specimen Geometry	COALESCENCE TYPE			
	GYP SUM		GRANITE	MARBLE
	Molded flaws	Cut flaws		
30-0- a	N/A	I	I	NO
30-0-2a	I	N/A	I	NO
30-2a-2a	II	II	II / some III	II
30-a-a	II	II	II	II
30-a-2a	II	II	II	II / III
45-0- a	N/A	I	I	I
45-0-2a	I	I	I / NO ?	I
45-2a-2a	II	N/A	II / some III	II / some III
45-a-2a	II	II	II	III / some II
45-a-a	II	II / III	II / IV / IVB	II/III
60-0-a	N/A	N/A	I	I
60-0-2a	I	N/A	I	I
60-0-3a	I	I	NO	Not Tested
60-a-2a	II	NO	II / some NO	II

N/A: Not Available.


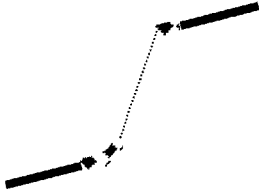

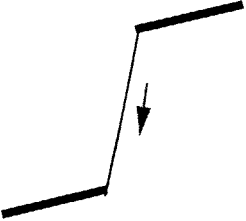
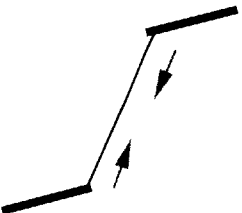
- Initiation angles are around 90° for both internal and external wing cracks. On the other hand, both internal and external shear cracks propagate in the plane of the flaws. Bobet (1997) also observed that internal and external wing cracks have the same initiation angle and that his secondary cracks (shear cracks indeed) were coplanar to the flaws.

- Surface fracture characteristics in molded gypsum specimens were somewhat different than observed in natural rocks. According to Reyes (1991): (1) tension surfaces appeared smooth, and (2) shear surfaces were rough and dusty. In natural rocks the observed roughness is different: (1) tensile crack surfaces are rough, and (2) shear crack surfaces are smooth and also dusty. All the other characteristics of fracture surfaces are to some extent similar (brightness, dust, plumose structure in tensile cracks, slickensides in shear cracks).

5.5 Recommendations for further research

The following is a listing of aspects to be covered in further research:

- Continue testing marble specimens with flaw geometries that have given no completely consistent results.
- Test gypsum specimens with cut flaws in order to evaluate the effect of cutting the flaws with the water jet instead of molding them. This would allow one to better compare results in gypsum, granite, and marble.
- Test other natural rock specimens in order to further observe common patterns within different rocks.
- Study the influence of the flaw length.
- Study the influence that non-parallel flaws would have on the results obtained so far.
- Test specimen with several load-unload cycles in order to evaluate the effect of microcracks developed in the first cycles.
- Further develop numerical models able to accurately predict lab results for different rocks and contrast them with field (large-scale) results.

TYPE I		Produced by the linkage of two internal shear cracks
TYPE II		Produced by the linkage of two internal shear cracks by a vertical tensile crack (not a wing crack)
TYPE III		Produced by the propagation of the internal shear crack from one of the flaws until it reaches the internal wing crack of the other flaw
TYPE IV		Produced by the propagation of an internal wing crack from one flaw until it reaches the other flaw. Observed only for granite.
TYPE IVB		Produced by the linkage of two internal wing cracks that propagate until they joint each other half-way. Observed only for granite.

- ◆◆◆◆◆ Internal Shear crack
- Internal wing crack
- Tension crack (not wings)
- ▬ Flaws

Figure 5.1: Coalescence modes in granite and marble specimens.

Appendix A: LAB PROCEDURE

A.1. Cutting Rock

A.1.1 Overhead saw

The overhead saw is located in room 1-075 (Can be opened with Key # I-31).

Figure A.1.1 shows the main parts. Note that the saw consists of a motor (5), a large diamond embedded saw blade (2), and a sliding table on which the object to be cut should be placed (6). The sliding table surface is very rough and the level of the block should be always checked before cutting (see Section A.1.2). Both the height and the angle of the saw can be adjusted by the appropriate mechanisms on the back (7), which should be checked each time before cutting (the handle there should be placed in one of the holes). There is a single switch on the top (1 in figure A.1.1) that turns on the motor (5).

The saw blade in use is to make “wet” cuts (cooled by water). It is connected to a water supply trough a flexible tube with a valve (4); a valve located on the wall has also to be opened. The saw does not have its own drainage system. It drains through a flexible tube (2 in figure A.1.3) and a bucket has to be placed next to the saw to collect the water. Recently a Plexiglas sheet has been installed in front of the sliding table to serve as chest protection (Not shown in figure A.1.1).

WARNINGS:

- Never put hands close to the saw blade when the motor is on.
- Ensure that a bucket is there to collect the water (otherwise the room will be flooded).
- Always wear noise and eye protection. The overhead saw is very loud, and the noise becomes worse when cutting. The use of goggles is also mandatory as with every cutting tool.
- It is advisable to wear a facemask.
- Do not pour the water from the bucket directly in the sink; otherwise it will become clogged. There is a sedimentation tank next to the sink in the same room for that purpose.

- Do not forget to close all water valves when done. Otherwise, the room may be flooded.

A.1.2 Cutting with the Overhead Saw

The size of the uncut blocks is 14" x 13" x 4" for granite and 12" x 12" x 6" for marble. The overhead saw is limited in the height it can cut. However, greater heights can be cut by changing the saw blade (the one used in the case of granite has a 14" diameter and the one for marble is 21").

In the case of granite the overhead saw is used for the large cross-sectional cut resulting in a 14" x 4" x 1.25" slab and the trimming down to two 3" by 7" blocks. Types and locations of the cuts for granite specimens are indicated in figure A.1.2a. Cutting of marble specimens is done similarly, see figure A.1.2b. Figure A.1.3 shows the block set in the overhead saw.

The first step is to cut a red brick to get the diamond in the saw blade adequately exposed. This step is not necessary each time the saw is used, but it is good practice to do it at least once per week.

To make the first cut in the granite with the overhead saw, place the original block (14" x 13" x 4") on the sliding platform with the line-of-cut parallel to the saw blade (as shown in figure A.1.3). Note that the block is set with its 14" long face parallel to the saw blade. At this point, check that the saw blade is elevated at an appropriate level for cutting granite specimens; when the granite block is on the sliding table, the bottom of the saw blade should be roughly half an inch above it. If the elevation is incorrect, adjust it by pulling out the pin in the back of the saw and placing it in a new notch (7 in figure A.1.1). It is good practice to check that the pin is firmly adjusted in its position each time before cutting. Then, move the granite block on the platform so that the line-of-cut is directly under the saw blade. Do this by pressing down on the foot pedal until the saw blade makes contact with the block, then use the ruler to measure 1.25" from the end of the block to the side of the saw blade (4 in figure A.1.3). The position of the block may have to be adjusted to obtain exactly 1.25". Now, use the level to check that the block's

orientation is perpendicular to the saw blade (see 5 in figure A.1.3). Figure A.1.4 shows the details of this operation and how to measure the slab thickness prior to cutting. Use paper towels to elevate the sides of the block if necessary to have it leveled. Clamp to hold the block and double check the block's position and the level after adjusting the clamp (note that the block shown in figure A.1.3 is not clamped).

Now, the setup for cutting with the overhead saw is complete. To start cutting, turn on the saw and open the water valve, so that there is a good amount of spray, check the amount of spray by looking at it, do not use your hands to check this (**IT IS DANGEROUS**). Lower the saw blade with the foot pedal until it makes contact with the block. Push the platform back and forth while applying constant, but not overly heavy pressure on the foot pedal. The pressure that can be applied by the foot pedal is limited by a spring located over the pedal. Repeat these steps until the first cut is finished.

The second cut trims the slab of granite down to a 3" width that corresponds to the width of the final specimen. Orient the slab on the sliding platform so that the edge with imperfections resulting from the first cut is trimmed off (2 and 5 in figure A.1.2a). Place the line of cut directly under the saw blade, and proceed as in the first cut. For this second cut there is no need to adjust the height of the saw blade (note that now the saw blade will be roughly four inches over the slab surface). Check the leveling and clamp down the slab. Due to the unevenness of the sliding platform, the end of the slab away from the operator might be elevated such that it no longer makes contact with the platform (See figure A.1.5). To solve this problem, pad below the slab with paper towels such that the slab has a firm surface to rest on. Be sure to double check the level after padding. Once all the adjustments have been made, cut by following the same steps described for the first cut.

Finally, the slab is cut in half (see 3 in figure A.1.2a). This last cut need not to be very accurate since it is simply done to fit the specimens in the precision saw, but it is important to ensure that both parts are longer than 6½ inches. Otherwise, the cuts with the precision saw won't be feasible (note that the slab to be trimmed down is 14 inches long).

In the case of marble, the first cut is similar to the first cut in granite (i.e. obtaining a 12" x 6" x 1.25). The second and third cuts (See figure A.1.2b) split this slab in 4 parts obtaining the final specimen. Note that in the case of marble, the final specimen is obtained directly by using the overhead saw (i.e. the precision saw won't be used in this case).

A.1.3 Precision Saw

The precision saw is located in room 1-075. Figure A.1.6 shows its main parts.

It has three wheels controlling the movement of the saw blade (see 3, 6, and 9 in figure A.1.6). The cutting table (2) is attached to the frame of the saw. The wheel at shoulder level (6) controls the height by moving the saw blade. The smallest of the wheels at waist level (3) moves the bed towards and away from the operator; it must not be touched during cutting. Otherwise, the cutting position will change and the saw blade would be damaged. The large wheel at waist level (9) moves the whole frame (including the cutting bed where the specimen is laid) left and right. The cutting bed (2) has a magnet, which is used to fix the guide. The water valve (5) is located above and to the right of the saw blade. It has three positions: when horizontal it is closed. When it is pointing down the water flows straight and does not go to the saw. Finally, when it is pointing up the fluid goes to the saw blade; this is the position to set when cutting (See 1 in figure A.1.7). In this case there is no need to open an extra valve, the switch (8) turns on the saw and also the pump to re-circulate the fluid (water and anti-rust chemicals). There is an oil drop device in the back of the saw (1) for lubricating the axis of the saw blade.

The cutting fluid is a mixture of water and anti-rust agent. This anti-rust agent is usually located under the sink in the same room, and should be used in a 1:40 proportion (Be aware that these proportions may change with the brand). If none is available, see Steven Rudolph.

WARNINGS:

- Before using the precision saw, make sure the re-circulation fluid tank is relatively full, and that there is enough anti-rust chemical (Water in the tank has to be green. But, the color may change with the brand). Check also that there is enough water spray in the saw.
- Never put hands close to the saw blade when the motor is on.
- Always wear noise and eye protection.
- Always wear a facemask. A mask with filters for organic vapor is advisable due to the nature of the anti-rust agent that is diluted in the cooling water.
- Never dispose any mixture of water and anti-rust chemical either in the sink or in the sedimentation tank. (The anti-rust chemical cannot be disposed of directly due to EPA regulations). Contact Steven Rudolph.

A.1.4 Cutting with the Precision Saw

This saw is used only when preparing granite specimens. In the case of marble the final dimension is obtained directly by using the overhead saw, and the faces to load are polished by using a belt sander (Section A.1.6).

The main objective of using the precision saw is to obtain smooth and parallel faces (the ones that will be loaded in a normal uniaxial test) for the granite specimens. Unfortunately, the size of the bed is too small to make both cuts without moving the specimen (see figure A.1.8, which shows the specimen ready to be cut). Hence, the cuts are measured with a ruler instead of with the wheel scale (the smallest at the waist level, 3 in figure A.1.6).

Figure A.1.7 shows the first step when cutting, which is installing the steel guide perpendicular to the saw by using a triangle. Once the guide is set it needs to be fixed. The precision saw has a magnet that is activated by turning to the right the handle located in front of the cutting table (see 4 in figure A.1.7). Figure A.1.8 shows how to set the specimen on the cutting table. There is no

need to check the level since the cutting table is perfectly leveled (i.e. perpendicular to the saw blade) and its surface is smooth.

It is important to set the specimen so that the original upper face of the large block (the one used to level in the first cut with the overhead saw) is aligned with the guide (See 6 in figure A.1.8). This has to be done to ensure that the same surface is used as reference in all of the different cuts; so that, regular prismatic specimens are obtained.

The required length is measured with a ruler (see 2 in figure A.1.8) and the specimen is fixed with a clamp (3 in figure A.1.8).

Turn on the machine (see 8 in figure A.1.6), the recirculating pump for the cutting fluid (water plus anti-rust chemicals) will also turn on. Check that the valve is open and that the spray works by looking at it. **NEVER USE HANDS TO CHECK THIS.**

Right after turning on the saw and before cutting, do the following: open the valve of the oil drop device (See 1 in figure A.1.6). Figure A.1.9 shows in detail this oil drop device. After opening the valve (1) let five drops pass through the visor (3) and close the valve (1) again. If the oil level is low (2), more LIGHT OIL should be added. (Provided by Steven Rudolph).

Two cuts are made per specimen (i.e. the faces to load). For the first cut it is not necessary to measure. However, less than half an inch should be cut in this first step to ensure that there will be enough material for the second cut.

To understand the cutting procedure it is necessary to see again figure A.1.6, which also shows the direction of the wheel movements (i.e. clockwise or counterclockwise) paying special attention to the wheels (3, 6, and 9 in figure A.1.6). Figure A.1.10 shows the typical steps done to cut, which have to be subsequently repeated. The cuts are made by moving the biggest wheel at waist level (see 9 in figure A.1.6) to the left and to the right (see 1 and 3 in figure A.1.10). At the same time the saw has to be lowered using the wheel at the shoulder level (6 in figure A.1.6 and 2 in figure A.1.10). The pace used to move down the saw is very important since it controls the quality of the final surface. During the first half of the cut, the saw is lowered a quarter of a revolution each time it moves over the specimen. After half of the specimen thickness is cut, the pace has to be changed to an eighth of a revolution (i.e. half of before) to obtain a smoother surface.

For the second cut turn over the specimen, so that the same side is against the guide in both cuts, measure 6", clamp, and repeat the cutting procedure.

A.1.5 Belt Sander (For marble).

The belt sander is located in the Machine Shop in room 1-033. Contact Steven Rudolph to obtain access and to operate this machine.

The belt sander is usually used for removing burrs and rough edges from parts. In the present work it used to polish the faces of the marble specimens to be loaded in uniaxial testing.

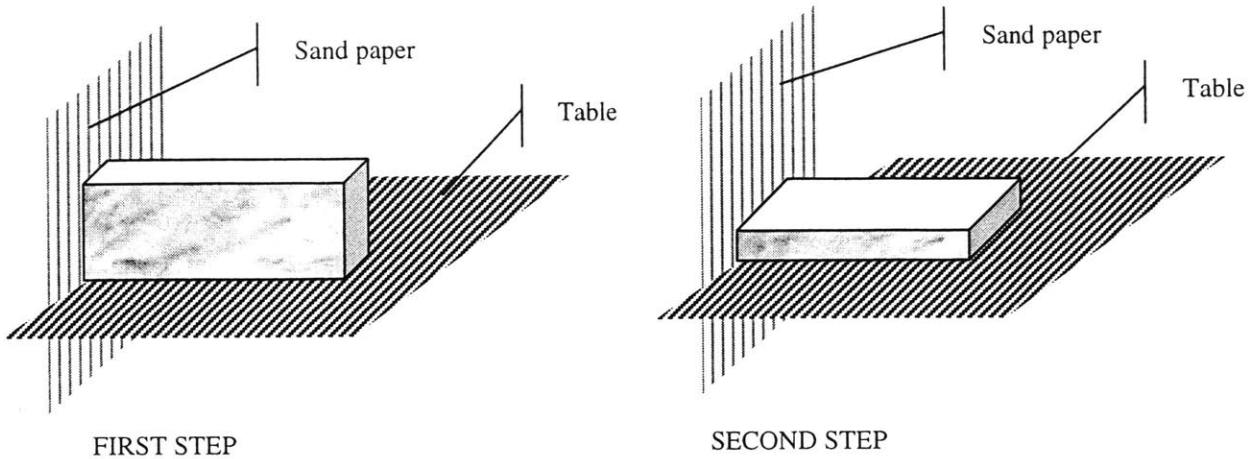
Figure A.1.11 shows its main components. It is composed of a belt coated with abrasive riding on two pulleys. The lower pulley is driven by a motor and the upper pulley follows. The upper pulley allows tensioning the belt if adjustments are necessary.

The small particles generated by the belt sander can be toxic. Hence, always wear a facemask and turn on the extractor over the sander.

A.1.6 Polishing Marble Specimens.

As was mentioned before, the marble specimens are obtained directly by using the overhead saw. Hence, the faces to load might be non parallel and/or rough. In order to solve this problem, the faces to load need to be polished with the belt sander.

First, turn on the extraction fan over the belt sander. Turn on the belt sander (1 in figure A.1.11). Place the marble specimen over the table (2) and start polishing one of the faces to load. The process has to be done in two steps. In these two steps the specimen is polished while lying on the table in the two different possible orientations, as shown in the diagram:



Once the first face is polished (it has to be bright and without any asperity), turn the specimen over to polish the other face to be loaded. The same two steps have to be repeated. It is important to place the specimen on the same faces that were used before to ensure that the polished faces are really parallel. The belt is 6” wide (by 48” long) and the sandpaper to be used is grid 60.

A.2 Making Gypsum Specimens

Two types of gypsum specimens are tested: (1) prefabricated, in which flaws are created at the time of moulding, and (2) cut, in which flaws are cut in after moulding by using the water jet machine. For the cut in type, the flaws are made after moulding and not after drying so that all the “wet” steps are done before drying.

The basic steps in making each type of gypsum specimen are:

Prefabricated Flaws	Cut Flaws
1. Mould Specimen with shims	1. Mould Specimen
2. Polish	2. Polish
3. Curing in the oven	3. Cut the flaws
	4. Curing in the oven

A.2.1 Moulding

a) Machines and Tools

- Gypsum mold

The gypsum mold is located in a drawer in room 1-040. A mold consists of four stainless steel plates bolted together (1, in figure A.2.1) and two Plexiglas plates (PMMA in figure A.2.1), also called Plexiglas patterns, (2 and 3 in figure A.2.1). There are currently 2 different sets of stainless steel plates in the lab (see figure A.2.2), set B appears to be larger but they both create the same sized gypsum specimen. Previously, a set of aluminum plates were used to make the mold, but this material reacted with the gypsum when left over extended periods of time and thus are no longer used. This old mold is in the large green cabinet in 1-040.

The screws to assemble the molds are stored in an open box in the same drawer as the molds. There are five different screw sizes in this box (see figure A.2.3, which also shows the length of each screw size). Size 1 can be used to assemble plate set B (see figure A.2.2) but they are usually more difficult to use. It is advisable not to use these. Size 2 is shorter but of the same diameter as size 1. These are the best to use to assemble plate set B. Size 3 screws are used to assemble plate set A, and of the remaining two sizes (4, and 5), either can be used to assemble the Plexiglas covering.

Spare screws are available in a small white box in the drawers and more can be obtained from Steven Rudolph in the machine shop (1-035) or at Economy Hardware in Central Square. Any other questions concerning molds should also be directed to Steven Rudolph.

- Scales

The scales are located on one of the benches in Room 1-040. There are two scales with different sensitivity and capacity (4400 gr. and 100 gr.). The larger is usually used to measure the 700g of gypsum required to make a specimen, while the smaller is usually used to

measure the 8.00g of celite. If scales are moved, check the levels located on the back or on the side of the scales. If they are unlevelled, turn the two knobs on the bottom of the scales to adjust the tilting.

- Mixer

An ordinary kitchen mixer is used. Be sure to always use the lowest speed i.e., speed number 1 (see figure A.2.4).

b) Materials

These are the raw materials required for molding one (1) gypsum specimen (Size 1" x 3" x 6"):

*NB. Mixture for only **one** specimen can be made at a time.*

- 700.0 g gypsum
- 8.00 g celite
- 280 ml water

c) Equipment

- Gypsum mold
- Plexiglas pattern
- Screws
- Electrical tape
- Masking tape
- Steel shims (for prefabricated specimens with open flaws) or videotape strips (for prefabricated specimens with closed flaw specimens).
- Lithium grease
- Cans for measuring gypsum

- Measuring cylinder
- Timer
- Paper towels
- Level

d) Procedure

1) **Choose Plexiglas pattern** – For each mold there are three pieces of Plexiglas to use. The base (figure A.2.5B), the cover (figure A.2.5A) and the rim (figure A.2.5C). Each pattern has TWO different geometries cut in it and a number written on either face as illustrated by figure A.2.6A. The number written on it is the mold number and it corresponds to a given geometry. A table containing the mold number/geometry specifications should be kept in one of the drawers and a copy is included in this procedure (Table A.1). To obtain the correct geometry the face with the desired mold number should face DOWN and the slots that have a wider opening on top are the correct ones to use (see figure A.2.6B). The other slots should be taped on the face that contains the CORRECT mold number with electric tape to prevent leaking of gypsum. For cut specimens, the blank pattern should be used (the one without any cut space for shims), or any other pattern with all slots taped with electric tape.

The flaw geometry will be explained in Section A.3.2.

2) **Assemble steel plates with screws** – Be sure that the smooth face of the plates faces inside, otherwise the Plexiglas pattern will be difficult to insert.

3) **Insert the Plexiglas base** – Before inserting the base, tape along the sides of the bottom of the mold to ensure that the plate does not fall out (see figure A.2.7A). Insert the base that was chosen in step one. Be sure that the number with the correct geometry faces down or outside of the mold. Be also sure that there is no electric tape inside the mold. Then tape around the edges of the base on the outside to ensure that there is no leakage

and tape close to the center of the base to ensure that there is no “sagging” of the Plexiglas once the gypsum is poured in. There should be three layers of tape along the sides and 2 or 3 pieces close to the center. (See figure A.2.7B).

- 4) **Assemble the plexiglas covering** – Before assembling ensure that all slots for flaws are clear by inserting a shim through them and taking it out again. Using the smallest screws (screws 4 and 5), screw together the Plexiglas pattern and the rim. Note that there is threading only in the pattern so it must always be below the rim (see figure A.2.8). Check that the correct geometry is in the right place.

- 5) **Place mold on stand** – Once the Plexiglas covering is in place, place the completed mold on the aluminum stand on the vibrating machine. (Shown in figure A.2.9 over the vibrating table).

- 6) **Insert the shims** – (NOTE: This is not applicable for cut specimens). First ensure that the assembled plexiglas cover is in place. Apply a thin layer of grease to either side of the steel shims and insert shims into the slots as illustrated in figure A.2.10. It is advisable to first insert the one farthest from the hole in the cover. This may require a bit of practice, but one technique may be to use a finger to reach through the pouring hole of the top to guide the shim down to the bottom plate. Ensure that there is enough length of shim (approximately 1 inch) at the top to allow for slipping during vibration. **NEVER USE RUSTY SHIMS.**

In the case of closed flaws a videotape strip has to be inserted to make the flaws instead of the steel shims. Note that the removing time is also different.

- 7) **Prepare the mixture** – The following are the steps for preparing the mixture. (NOTE: gypsum dries fairly quickly hence it is necessary that these steps be done in quick succession.)

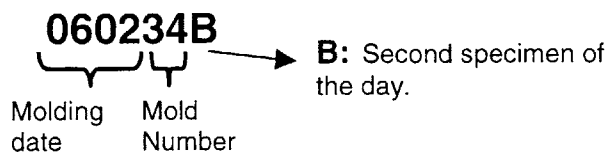
- i) Using a can, tare the larger scale. Fill the can with gypsum from the gypsum bag until it weighs 700g or greater. If there is an excess of gypsum (which is likely), using the spoon and the container, which is usually on the counter, remove excess gypsum from the recipient into the container. This container can remain on the counter with gypsum until it is full. **NEVER** use gypsum from the container on the counter for specimen preparation (since it gets wet from the air moisture), only use it to take off the excess gypsum.
 - ii) Tare the smaller scale with a piece of paper and measure the correct amount of celite on the paper using the beaker of celite on the counter.
 - iii) Measure the correct amount of water using the graduated measuring cylinder and use the water dropper for accuracy.
 - iv) **Mix** celite and water for **20 seconds**.
 - v) **Add** gypsum and mix for **4 minutes**. (always use the lowest speed (#1) for mixing. See figure A.2.4)
- 8) **Pour mixture into mold IMMEDIATELY after mixing** - Pour mixture into mold through the hole in the top. There is a plastic spatula, which is useful for getting the mixture in. The recipe for the mixture results in material for a little bit in excess of the quantity for one specimen. Generally, 80% of the mixture will result in a specimen thickness within the error margin (3.0 cm +/- 0.2cm). However, there is no way of actually measuring this. Knowing the actual amount to pour comes with experience.
- 9) **Vibrate the mold** – First ensure that the vibrating table is leveled. The switch for the table is found on its side (see figure A.2.9). The machine has a 750-RPM motor working at 60 cycles. When vibrating the specimen, use the clamps to ensure that the aluminum stand is firmly clamped to the table, and the mold is firmly clamped to the aluminum stand. **Vibrate for 2 minutes**.
- 10) **Set to dry** - Put the specimen on two blocks standing on their sides making sure that the shims, if any, are not crushed or contorted. Using the leveler, level the mold. When

leveling, use little pieces of paper towels to elevate the appropriate corners of the standing blocks. See figure A.2.10.

In the case of closed flaw specimens the videotape strips have to be pulled out after 30 minutes.

11) **Wash out mixing bowl** - WASH THE MIXING BOWL AS SOON AS THE MOLDS ARE SET TO DRY. Dry gypsum in the bowl can be very difficult to clean up. Wash the bowl in the gypsum sediment bucket and scrape off as much gypsum as possible. Then rinse the inside of the bowl with water and pour into the sediment bucket. Finally, wash the exterior of the bowl and place upside down on paper towels to dry. Also wash the mixer attachment, first in the sediment bucket then rinse off in the sink.

12) **Unmould** - Gypsum specimens solidify within an hour. Thus, after this time, unmould the specimens by first removing the top plate assembly, then the tape, and then the screws. If working with a prefabricated flaws specimen, unmould on top of two blocks so that the shims will not be bent. Note that if working with closed flaw specimens the videotape strips are no longer installed since they were removed 30 minutes earlier (See Step 10). Carefully remove the four sides and remove the gypsum specimen. With a pencil, write the specimen number on the side of the specimen. The usual format for the specimen number is date (mm/dd), mold number (represented as a double digit), and a letter indicating different specimens with the same geometry molded on the same day. An example of a specimen number might be:



This indicates that it was fabricated on June 2, its mold number is 34, and it is the second one for the day. Place it on its sides on top of two blocks to **dry for about 24 hours before polishing.** (See figure A.2.11) If unmolding a prefabricated specimen, **remove the shims the following day** before polishing.

13) **Clean up** - Wash the stainless steel molds and the Plexiglas plates. Be sure to scrape off any gypsum. Use an old steel shim to remove gypsum from molds. Wash also the steel shims and ensure that they are dry before storing them in the drawer. Always be careful not to clog the sink. Place the plates on paper towels to dry. **ALWAYS CLEAN UP WORK AREA AFTER MOLDING.**

A.2.2 Polishing

a) Machines and Tools

- Polishing machine

The polishing machine is located in room 1-075. (See figure A.2.12). It is a table with two round turntables to place the sandpaper and a pair of taps in the center. The turntable on the left is for polishing with removable sandpaper. The polishing turntable on the right is for fixed sandpaper. **ALWAYS CHECK THAT THERE IS A BUCKET UNDER THE DRAINAGE PIPE TO THE LEFT OF THE MACHINE BEFORE OPENING THE TAP.** This collects the water and debris that runs down. There are two settings for the speed. Always use the first speed (the lowest).

b) Equipment

- Gypsum specimens
- Small filler shims (for prefabricated specimens with open flaws)
- Silicon carbide sand paper (circular)

- Paper towels

c) Procedure

Specimens are ready for polishing the day after they are molded.

After molding, the specimen has a smoother face and a coarser face. The smoother face is the one to be concentrated on during polishing because this is the side that will be viewed under the camera when testing. The other side is polished simply for neatness.

To polish prefabricated specimens, place filler shims in flaws remembering not to have the shims protrude out the side you wish to polish while not having them too far in so that the flaws become blocked. To ease this process, lightly grease shims with lithium grease.

To use the polishing machine, remove the cover from the left turntable and place tap above the left turntable. Turn on the water valve on the wall on the upper right. The valve is on when the handle is in the same direction as the pipe (vertical). Turn the faucet nozzle so that it is right over the circular base and drip some water on the base. Place the circular sandpaper on top of the base and secure it with the ring. Finally, put the splashguard in place. Remember to check that there is a bucket in the drainage line before beginning (see figure A.2.12).

Turn on the polishing machine and the water so that it keeps the sandpaper wet. Using both hands, hold both sides of the specimen. Gently place the specimen in the middle of the sandpaper, applying slight pressure and then release. Repeat the process of applying pressure and releasing a few times. Lift the specimen slightly off the sandpaper to wash away the debris and then place back on the sandpaper to polish. Continue this process until one side is polished. The specimen is polished when the entire face appears darker in color and when the face is smooth. To polish the other side, retract the filler shims so that they no longer protrude out of the side that you want to polish and follow the same process described above.

Once completed with polishing all the specimens, remember to clean the polishing machine. Remove the sandpaper and rinse out the inside bowl, ring, and splashguard. Use papers towels to dry all surfaces. Place everything back in its original position, and pour the water from the collection bucket into the sediment tank. The polishing process is now complete.

Prefabricated specimens now go into the oven for three days (See Section A.2.4) and cut specimens are ready to be cut that day (See Section A.2.3) and then go into the oven for drying.

A.2.3 Cutting the flaws

See general cutting procedure (Section 3). (This step does not apply to prefabricated specimens.)

A.2.4 Curing in the oven

a) Machine

- Oven

The oven is located in room 1-040. It should already be set at the appropriate temperature of about 40 degrees Celsius. The corresponding number on the temperature dial is 8.0 (last calibrated by Ariel, 6/6/98). DO NOT change the temperature while there are specimens inside and double check the setting before putting in new specimens.

b) Procedure

After prefabricated specimens are polished, they are placed in the oven to be dried for three days.

For cut specimens, once the flaws are cut, they are placed in the oven to be dried for three days. Always stand specimens on the narrow face when drying. See figure A.2.13.

After three days remove the specimens from the oven. They are ready to be tested **on that day**.

Figure A.2.14 (After A. Bobet) shows in a time line the fabrication (A) and the curing and testing (B) processes for gypsum specimens. Note that the scales are different (A is in minutes and B is in days).

A.3 CUTTING THE FLAWS

A.3.1 Water-jet machine “abrasive-jet”

The Water-Abrasive Jet is located in Building 35 on the 1st Floor in the Materials Processing Lab. This lab is part of the Lab for Manufacturing Process (LMP).

a) Principle :

Figure A.3.1 part 1 shows a cross section of the “cutting tip” of the water-abrasive jet. High-pressure water (40,000-60,000 p.s.i.) passes through a jeweled orifice that ranges from 0.005 to 0.013 inches in diameter. The flow enters through a mixing tube or nozzle that ranges from 0.015 to 0.05 inches in diameter. The speed of the water is about 2,500 feet per second, or about 2½ times the speed of sound (which is 1,108 ft/sec or 1,215 Km/hr). The stream of water causes a vacuum, which draws finely crushed garnet sand (abrasive). Water and abrasive sand go into the mixing tube, exiting through the nozzle and making contact with the material. The jet drags the abrasive through the material in a curved path (See 2 in figure A.3.1) and the resulting centrifugal forces on the particles press them against the work piece. The cutting action is a grinding process where the forces and motions are provided by water, rather than a solid grinding wheel.

The main parameters to be considered in cutting are (explanations regarding these different factors will be given in the following sections):

- Abrasive flow rate
- Mixing tube diameter
- Jewel (orifice) diameter
- Water pressure at nozzle
- Material machineability *
- Material thickness *
- Desired cut "Quality" *
- Pump power
- Part Geometry *
- Others, beyond the scope of the present job

*: These parameters are the ones that can be changed in the OMAX water-jet (The one used in the present research)

b) Main advantages of using an abrasive water-jet:

- Causes very little stress to the material being cut
- Very flexible method for cutting complex pieces
- Does not produce heat-affected zones
- Capability to cut titanium up to 10 inches thick
- Very low side forces during machining. This means the ability to create the flaws without creating too many secondary micro-fractures that would affect the results in the following loading test
- Almost no heat generated, being able to machine without hardening the material, generating poisonous fumes, or recasting. When piercing 2 inches thick steel, temperatures may get as high as 120° F, but otherwise machining is done at room temperature (as it is done to cut granite and gypsum in the present job)

- No start hole is required

c) Disadvantages and imperfection sources:

- Jet Lag: The abrasive jet is a "floppy tool" and it tends to wander while machining. In straight-line cutting, this produces a "lag" as shown in figure A.3.2.

This lag becomes critical when cutting near a corner. As the nozzle approaches the corner, it becomes necessary to slow the motion down so that the bottom of the stream can catch up to the top, and be perpendicular to the material surface. When cutting straight lines (as in the present job) the lag causes a non-vertical end wall if suddenly stopped (Causing the end of the flaws to be irregular).

The easiest way to correct this defect is using a high quality to cut (Section A.3.2 explains how to set the cutting quality). The numbers (indicating cutting quality) shown at the bottom and the curved lines (indicating lag effect) on figure A.3.2 show this. It is clear that increasing cutting quality decreases lag effect. The second way to avoid this when cutting in a straight line is to set some delay to turn the stream off after the end has been reached. This "delay" allows the bottom of the stream to catch up to the upper part. Both of these issues are addressed in detail in Section A.3.2.

- Taper (become narrower): This is certainly one of the most important factors affecting the final quality of the flaws. The main factors causing taper are:
 - Distance of nozzle from material. The closer the nozzle is to the material, the smaller the taper
 - Hardness of material. Usually harder materials exhibit less taper. This is why taper can easily be seen in gypsum specimens (they are softer)
 - Machining speed. Figure A.3.3 shows this effect. This is observed by measuring the flaw dimensions on both faces of the specimen
 - Quality of jet exiting the nozzle. The more focused the nozzle, the less taper exhibited. However, this might vary when the nozzle is changed after approximately 150 hours of use
 - Quality of abrasive used

- Thickness of material
- Piercing: The OMAX machine allows “Wiggle piercing”, which means that the controller wiggles the nozzle back and forth over a short distance (approximately 2 mm) to greatly speed up the piercing process. This can make a big difference in the time it takes to pierce thick materials. This is the main reason why it takes more than 10 minutes to cut 2 flaws in a granite specimen (it also requires more than 4 pounds of abrasive). See Section A.3.2 in order to know how to select the number of wiggles in the OMAX machine.
- What can go wrong? :
 - Wet abrasive may tilt and obstruct the nozzle
 - The nozzle may collide with parts lying on the X-Y table. (The OMAX at MIT has guards in its nozzle to protect it). Section A.3.2 explains how to reduce this risk
 - Parts may deteriorate and need replacing

d) Major components of the OMAX Jet-Machining System: (see figure A.3.4)

- OMAX control system: (see figure A.3.5)

The OMAX is completely controlled using a standard PC (DOS based) running the OMAX control software (Section A.3.2 describes the features of this software). The control system turns the water pump on and off automatically, and moves the abrasive jet on a precise path.

There is also a red emergency stop button (see figure A.3.5) on the front that switches everything off immediately, shutting down the water pump and the motion of the abrasive jet. The computer is not affected by the emergency stop switch, and continues to send pulses to the position controller.

WARNING: in an emergency stop the OMAX loses its home position. The aforementioned emergency stop should be used only in real emergencies. When having just a small problem the space bar should be pressed. By pressing the space bar with the

OMAX machine in operation the motion of the abrasive jet is interrupted and the water pump is shut down. In this case the machining of the same part can easily be restarted. This is the preferred way to stop for other than safety-related reasons (For example when the abrasive tube or the nozzle get clogged).

- High-pressure water pump

The high-pressure water pump pressurizes water that will be used by the OMAX. The OMAX Control System controls all pump operations. When not in use, the switch of the pump is locked; the keys can be obtained from Gerald Wentworth. The pump has this switch only for security reasons (i.e. to allow locking), the pump is actually turned on and off by the control system, and cannot be operated manually.

Old water-abrasive jets had problems in keeping the water pressure constant while cutting. This affected the quality of the piece causing marks on the cut surface. The OMAX machine pump ensures that the pressure will be constant “enough” to get “good” quality cuts without marks. Hence, this would be a problem only when a tolerance of 0.005” is required (not in the case of the present research).

- Precision X-Y table (see figure A.3.6)

The X-Y table consists of a rigid frame with X and Y carriages mounted above a large water tank. The water tank collects the water from the cutting operation and provides a settling tank for spent abrasive and particles of the machined material.

It is possible to retrieve the solid materials from the tank. As long as the machined materials are not hazardous, the spent abrasive and waste material become suitable for land fill. The red color of garnet abrasive looks nice in gardens, but if lots of lead or other hazardous materials are being machined, the waste must be disposed appropriately (according to EPA regulations).

- Abrasive jet system (see figure A.3.7)

In the abrasive jet nozzle, high-pressure water is forced through a sapphire orifice to create a narrow stream moving in excess of 2500 feet per second (1700 mph). This stream

causes suction that draws air and abrasive material through a plastic feed tube. When cutting, it is important to ensure that this plastic tube does not get clogged. If that happens, the machine has to be stopped, and the entire abrasive feeding system has to be cleaned with pressurized air. This feeding tube can get clogged if the abrasive gets wet.

WARNINGS:

- The space bar (used to pause the machine) sometimes fails due to keyboard malfunction. Be ready to press it more than once when pausing the machine.
- Always be sure that there is enough abrasive.
- Check that the nozzle does not hit anything in its way. (Section A.3.2 explains that while cutting, the specimen has to be kept in place by heavy lead blocks).
- Wear eye protection (mandatory in this lab).
- The water jet manufacturer recommends wearing noise protection only when cutting non-submerged pieces (which is not the case in this job, since the rocks must be cut submerged as explained in Section A.3.2). However, noise protection is advisable since usually more than one machine is running in this lab.
- The X-Y table bottom consists of steel bars. These steel bars have been cut in previous use of the machine, and hence have very sharp edges. Avoid physical injury by being careful when placing the specimen.

A.3.2 Cutting with the Water Jet Machine

a) Starting

One should bring a disk to store necessary data (CAD files) when using the water-jet machine (saving data on the hard drive is not allowed). Open the two water valves in the wall. Check that the abrasive valve close to the ceiling (over the water jet) is open, this valve is usually open and

does not have to be closed after finishing (it allows the compressed air to get into the water jet). Unlock and turn on the pump. Turn on the switch on the front of the control (See **figure A.3.5**). The procedure for cutting consists of several steps. These steps must be followed also by looking at the referenced numbers in the figures.

Figure A.3.8 shows the first screen (“Welcome to the water jet”).

b) Drawing

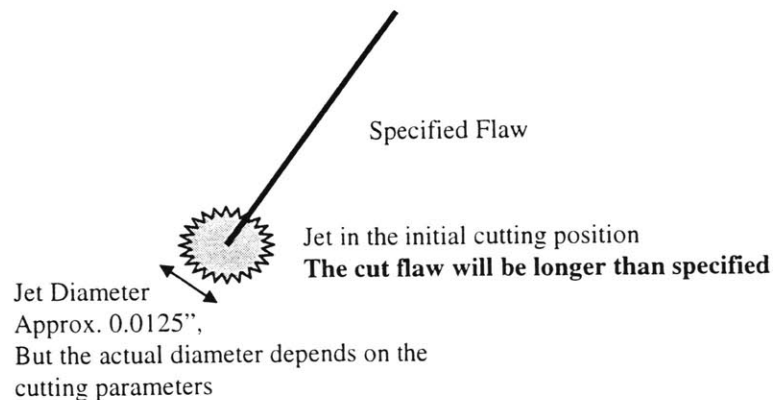
By pressing the “Go to Layout” button the Layout program is started. Figure A.3.9 shows the “Layout” screen:

The task of drawing is facilitated by the existence of a 1” by 1” grid (Drawn in dashed lines in figure A.3.9). This grid is yellow in the actual screen. Note that the units by default are inches.

Figure A.3.10 shows the notation used to identify the geometry. For example, a geometry called “**30-a-2a**” means $\beta=30^\circ$, $s = 2a$, and $c = 2a$. Where “a” is half of the flaw length (in all the present work $a = 0.25$ ” since the flaw length is always 0.5”).

In order to draw the flaws the coordinates of the flaw tips are computed using a spreadsheet (See figure A.3.11). The coordinates were computed with a spreadsheet so that they are available beforehand, making possible to save time when using the water jet. (The charges for the water jet usage are by the hour).

The computed coordinates assume a null thickness of the flaw and if these values were used directly the obtained flaws would be larger than the required length (which is half an inch):



In order to get the correct flaw length, the specified flaws should be shortened; in the case of granite 0.03” at each end (See figure A.3.12), in the case of marble 0.04” at each end, and in the case of gypsum 0.0431” outside and 0.03227” inside (See figure A.3.13). These correction values were obtained by trial and error (i.e. shortening by different values until the correct flaw length was obtained).

The fastest way to shorten the drawn flaws is by drawing circles (also shown in figures A.3.12 and A.3.13) with the aforementioned radii and using the command “I-divide”:



The steps to prepare the drawing are summarized in figure A.3.14. Note that the cut path is a segmented line, which includes the flaws and starts in the bottom left corner of the specimen (called the zero user position). Both the dashed and the continuous lines have to be drawn. The difference is the specified cutting quality (see next step for the actual procedure to set the cutting the quality). The dashed lines have only “traverse quality” which means that no cut will be done there, while the continuous lines have quality 5 (maximum cutting quality of the OMAX machine) in the position of the flaws.

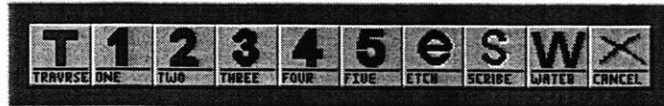
Note that the path is drawn so that the cut in both flaws starts from the outside tip. There are two reasons for that. First, it was previously discussed that the water jet can affect the initial point of cut (see Piercing). Second, the overall objective of the present job is to observe what happens between the flaws (existence and mode of coalescence).

c) Setting the cutting quality

Once the drawing is done the quality of the cut has to be defined. Five cutting qualities are available, quality number 5 (the best) is used to cut the flaws. By default all the drawing is in quality 0 or “traverse” (color green), which means no cutting. Hence, the two lines representing the flaws are the only ones to change. To start, click on the “cut quality” button:



Then, the cut quality bar appears:



Also the explanation of the differences among the qualities is displayed in the state bar (bottom of the screen):

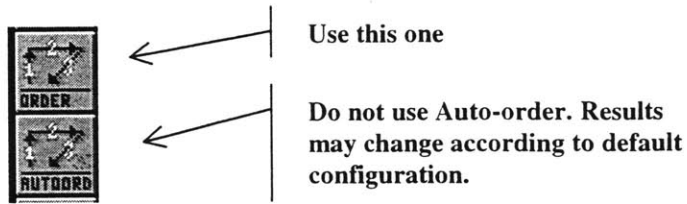
Pick a Quality
0 is rapid traverse. 1 = Cut fast, low quality 5 = Machine slowly
Etch = Traverse with pump and abrasive on. Scribe = Etch without abrasive.
Water lets you cut soft materials without abrasives (rubber, foam, etc.)

Select quality 5 (Quality 5 will show in the screen as electric blue color) and select the two flow lines with the cursor.

Note that cutting quality takes into account the geometry of the part, and it varies the feedrate continuously to adjust for every corner, curve, or straight section of the part (i.e. it corrects for the previously explained Jet Lag effect). Also "Quality" is independent of material and thickness. If one machines a part with quality 1 in a 3" thick aluminum piece, the surface will look very similar to a quality 1 part machined in a 1/4" brass piece.

d) Setting the path order

Once the cutting qualities have been set, the order has to be predetermined. There are actually two buttons to set the cut order. Do not use the Auto-order button:



When this button is pressed the file is saved and the program goes to a screen where only the drawing can be seen. The first thing to mark is the starting point, which is the left bottom corner (It is the local zero for the x-y table when cutting. See figure A.3.15). Then, the offset has to be indicated. It can be either left or right (In the present job, this step is irrelevant and either option can be selected since offset zero is used,). Next, the program asks to save the order file and it returns to the “layout screen”.

Figure A.3.15 shows a typical finished cut path, as well as some references to the “order” set.

e) Starting the “make” screen and entering settings

After the order file is created, select “MAKE”:



The first thing that appears is the setting screen shown in **figure A.3.16**.

The settings to be entered are:

	GYPSUM	GRANITE	MARBLE
Thickness:	1.00”	2.75”	2”
Machineability:	1,000	90	450
Tool offset:	0”	0”	0

Note that the thickness is not the actual dimension (1.25”), and that the machineability is not the value recommended in the water jet list (shown in figure A.3.16, which is 322 for granite). If the real values were entered the quality of the flaws would be very poor. The setting values to be entered were obtained by trial and error in order to get a good quality cut. (i.e. same flaw geometry in both faces of the specimen, and flaws with the required length). The entered values (greater thickness and smaller machineability) cause the nozzle to move slower in order to obtain a better quality flaw (See taper in Section A.3.1 and figure A.3.3).

Once the settings are accepted a screen asking for the number of wiggles appears. The values to enter are:

	GYPSUM	GRANITE	MARBLE
Wiggles:	2	8	4

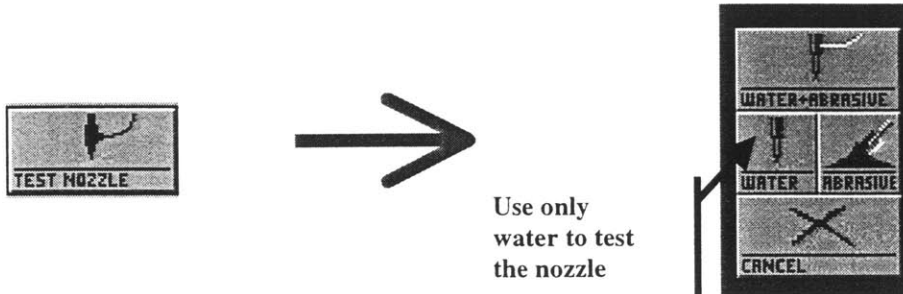
After this is accepted the actual “Make” screen appears (see figure A.3.17).

There is still one preset value to change. The “abrasive off” delay has to be set to 6 seconds in the case of granite and marble, and 1 second in the case of gypsum. The “water off” delay has to be set to one second more than the “abrasive off” delay, so that the nozzle does not get clogged. Both off delays are changed by using the “Set-up” Button:



This last step is important to ensure a good quality in the last part of the flaws (internal tips) by minimizing the Lag (in addition to setting a good quality to cut). Figure A.3.18 shows how this lag effect would intensify if the nozzle were suddenly stopped. These extra 6 seconds are required to allow the bottom part of the jet to catch up with the upper part (See also previous explanation of Jet Lag Effect in Section A.3.1).

Before putting the specimen on the X-Y table and only for the first time every day test the pump with only water (done by pushing the “test” button).



This step will help avoid getting the nozzle clogged.

f) Adjusting the height of the nozzle

The next step is adjusting the height of the nozzle (see figure A.3.19). The important distance to set is the standoff (distance between the nozzle and the material). If it is too small, the water jet gets clogged. If it is too great, frosting (a haze on the material) occurs and the required quality would become difficult to maintain.

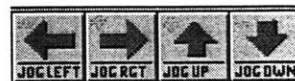
This standoff distance must be set before putting anything on the X-Y table to ensure that the nozzle does not hit any object there. In order to adjust the height the lever should be pulled up, the height is adjusted by rotating the horizontal wheel so that the standoff is about 2-3 mm. This distance should be always maintained. Before going on be sure that the handle is pulled down to lock the nozzle again.

Figure A.3.17 shows the “make” screen. The following steps will explain how to use its different features.

g) Setting the specimen to cut

The first step here is to coordinate the actual position of the specimen on the X-Y table and the drawing. The following list explains the steps to do this:

1. Figure A.3.20 shows the buttons for the “MAKE” screen (see figure 3.17) that are used.
2. Only local (USER) coordinates are used (the ones in the lower row).
3. The specimen is installed on the x-y table (see figures A.3.6 and A.3.21). The specimen is not set directly in contact with the border of the X-Y table. A piece of steel is placed to separate it from the border. It is important to check that this piece’s borders are parallel. The specimen is laid next to the steel piece and three or four “heavy” lead blocks are laid over it (without covering the place where the flaws are to be cut) to ensure that the specimen does not move during machining. Place the heavy blocks as close to the edges of specimen as possible to minimize the risk of hitting them with the nozzle (see figure A.3.21).
4. The nozzle is moved by using the arrows on the screen (By clicking on them) until it is located over the corner designated as the zero position (see figure A.3.21).



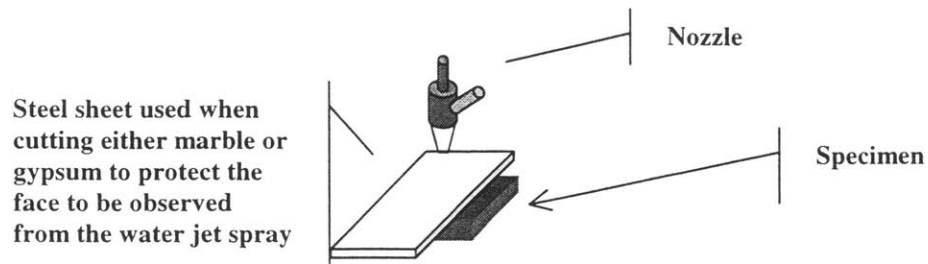
5. Once the nozzle is over the bottom left corner press the button “Zero User”.



Now, the zero in the drawing and the zero in the specimen are coordinated. Note that the zero is set by eye (when positioning the nozzle over the specimen corner), and that this fact introduces an error in the order of 1 mm. in the absolute position of the flaws. However, the relative position between flaws is not affected.

The last step before cutting is to ensure that the level of water in the catcher tank is high enough to cover the specimen. This helps to reduce the damage on the surface due to the spray and will also reduce the noise produced while cutting. In the case of marble and


gypsum there is a further step; a steel sheet should be installed over the specimen to be cut and held with the blocks. This steel sheet protects the specimen surface from being damaged.



h) Cutting

To start cutting click the “BEGIN” button and next the ”Continue” button. For the first few times it is useful to see the path in a segmented fashion, which is done by selecting “ahead” instead of “Continue” (after pressing “BEGIN”).



If something goes wrong just pause with the space key (on the PC keyboard). This bar:  will appear again. The cutting process can be continued (provided that the specimen has not been moved).

Operational issues:

- Always set an appointment to use the water jet 2 or 3 working days in advance. By e-mailing Gerald Wentworth (gerwent@mit.edu).

- A requisition form should always be carried and delivered to Gerald Wentworth (preferably in person). The price for using the water jet is \$50 per hour. Try to plan the time carefully and not to use partial hours (they have to be paid as complete ones).
- All the surroundings of the tank should always be left clean (no matter how it was before using it), and the program should be exited properly (i.e. by pressing the “Exit OMAX” button):



- The pump has to be turned off and locked, and the two wall water valves in the wall behind the water jet closed. Do not close the valve close to the ceiling (the one for compressed air), it must remain open.

A.4 LOAD TESTING

A.4.1 TV, VCR, Standard Camera, Microscope, and Optic Fiber Light

The standard camera, microscope, and lights are always kept in the cabinet in 1-040 (combination of lock 3-5-2). The cabinet can be opened with key #3. The TV and VCR are usually on a cart either in the Centrifuge lab 1-079 (can be opened -with general key 153L) or in room 1-040. Tapes for the VCR are stored either in the drawers in 1-040 or in the cabinet with the camera and microscope. Videotapes should be Hi-Fi.

The devices used for the loading tests are (see figure A.4.1):

- TV Monitor
- VCR
- Fiber Optic illumination device and its base
- Video Camera
- Microscope (Mounted on a platform not shown here)

- Testing machine with control P.C. (with required software)
- Loading control and Data Acquisition. (Installed also on the control P.C.)

Figure A.4.1 shows the aforementioned devices and their set-up. The main parts are: a low power microscope that is used to amplify the image, so that fractures can be identified. A video camera attached to the microscope and connected to the TV monitor that displays the images. At the same time a VCR is recording on normal VHS videotapes (in the case of granite it is advisable to use Hi-Fi tapes to get a sharper image). The microscope and the camera are installed on a platform that allows vertical and horizontal movements to scan the specimen surface. The microscope can be set with the following amplifications: 6.5, 10, 16, 25 or 40. The greater the amplification, the smaller the scope (area that can be seen) and hence the more the time needed to see the whole specimen (see explanation of the loading test in the next section). The focus can be corrected on the microscope, it is important to have the images clear enough to identify fractures. The fiber optic illumination system is completely independent and does not need to be moved during testing. Note that figure A.4.1 is not to scale and that the relative position of the instruments is not the one shown there (See figure A.4.2 and A.4.3 for the actual layout).

The connections to make are:

- The camera has to be connected to the VCR using the plug labeled "Video In", and to the power source (See 8 in figure A.4.2)
- The TV has to be connected to the VCR using the plug labeled "Video Out", and to the power source
- The fiber optic light is connected through a flexible tube to its base, which is in turn plugged to the power

Figure A.4.2 shows in detail the illumination device and the platform, holding both the microscope (2) and the camera (7). Two fiber optic lights are used (4), usually one directed to each flaw. The intensity control of the light (13) is in the base (5), next to the switch (12). Also shown, are the focus controller (1) and the amplification controller of the microscope (6) (Barely visible in the picture). Number (10) indicates the knob that controls the vertical movement of the

platform. It also indicates the location (but it is not visible) of the knob which controls the horizontal movements of the platform (9). The platform (14) has two more knobs that DO NOT have to be touched in regular testing, since they are only used to loosen and/or to replace parts of the platform.

WARNINGS:

- After testing the lights are hot (Both the fiber optics and their base), avoid burning yourself by waiting 5 or 10 minutes to let them cool down (note that the base has a fan for that purpose).
- It is important to set the TV to its maximum brightness, and set it to black & white (i.e. not color); otherwise a lot of small multi-color lines will appear on the screen.
- Move the cart with the TV and VCR carefully, since the floor in the basement is very rough.
- Never test any specimen without installing a protective shield (See figure A.4.3 and later explanation).
- Connect the camera with its switch in the off position. Failure to do so may result in burning the connectors. Also be sure that the wires in the camera are loose so that they do not get pulled out.

A.4.2 Baldwin 200 Kip Loading Machine

The Baldwin 200 Kip loading machine is located in room 1-034. Keys to the power box and the computer that controls the machine may be obtained from Steven Rudolph or Professor H. H. Einstein.

In order to power the machine, turn the switch in the very upper left of the power box located behind the lab door. (The switch is labeled 200 K). Note that in the box next to the machine there is a **red** button. This is the **emergency button**, which stops the pump instantaneously.

This is a computer controlled universal testing machine that allows one to run either compression or tension tests (this is why it is called universal). The upper space is for tension testing, and is not used in the present work (See figure A.4.4B).

Figure A.4.3 shows the set-up of the loading machine for testing. A switch (7) (above a box at the side of the machine, between it and the computer) turns on the pump (8). The two buttons (6) above the platform raise and lower the upper crosshead by an electric motor (5), allowing one to adjust the height in order to fit the specimen before testing (Note that this upper head remains fixed while testing). The computer (9) starts on a menu with several options; the option "MTest2" has to be selected to start the appropriate software for testing. Mtest2 is the software loaded in the P.C. that controls the loading machine.

Figure A.4.4A shows the movements of the machine during loading; note that the upper crosshead (3 in figure A.4.4A) is fixed and that the lower plate (5) is moved up during loading. A pump (see 8 in figure A.4.3) provides the required pressure to lift the piston (6 in figure A.4.4A). The upper crosshead (3 in figure A.4.4A) remains fixed while testing but has to be moved to set-up the specimen by using the electric motor (5 in figure A.4.3).

Readings of the vertical load and vertical displacement of the machine crosshead are taken during testing by a data acquisition system, recording data every two seconds. The program MTest2 plots displacement versus load on the screen while testing. More features about the MTest2 software as well as how to use it and configure it will be detailed in Section A.4.4. Also by using this software, the data are saved in "text only" files, which can be retrieved by any spreadsheet program (Excel, Easyplot, Kaleidograph, Lotus, etc.).

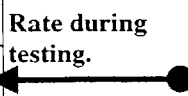
A.4.3 Other Issues Affecting Load Testing

a) Load Rate

As in every load test the load rate (or displacement rate) is a very important factor and should be kept constant in different tests in order to have consistent results. For testing granite, gypsum, and marble the settings are already fixed in the program MTest2. These settings fix a segmented displacement rate and sometimes a load rate. The machine works essentially by imposing displacement on the specimen and measuring the reaction force to this imposed displacement. Section A.4.4 explains how to check or change these settings.

The present settings are:

GRANITE and MARBLE		GYPSUM	
LOAD [lb.]	RATE	LOAD [lb.]	RATE
0 – 1000	0.10 in/min	0 – 1000	0.10 in/min
1000 – 5000	0.05 in/min	1000 – 2500	0.015 in/min
5000 to $\Delta L = 0.40$ in (Failure)	0.0047 in/min	2500 to $\Delta L = 0.40$ in (Failure)	2300 lb./min



For all cases, it can be seen that the first part is faster. This is done to accelerate the process by which the specimen “takes load”. The second step is slowing down until the chosen testing rate (shown in the third row) is reached. The actual rate during testing (third row value shown in the table) should be low enough to allow the observation of crack initiation and coalescence. This is why A. Bobet chose half a value of the “normal” rate. In the case of gypsum a load rate is defined. This was so done to keep the load constant during “holding” (See Section A.4.4). However, fixing a load rate makes impossible to observe any strain softening effect (The machine can take readings only while the load is increasing). The values of the strain rate during this last step are comparable for both gypsum and granite. In order to make the comparison the load rate used for gypsum must be converted into strain rate. This is done using an elastic modulus (for gypsum) of 5,800 MPa (= 58,000 Kg/cm² = 830,000 Lb/in²). The result is a strain

rate of 4.3 %/hour for gypsum, while for granite is 4.7 %/hour (result from the last row of the former table). Note that displacement rate can be converted into strain rates by dividing the length of the specimen (6" for both granite and gypsum), and this strain rate is usually presented as a percentage. The details on how to specify these rates in the Mtest2 software will be given in Section A.4.4.

b) Displacement Recording and Machine Compressibility

As was mentioned before, the data acquisition system takes readings of the vertical displacement of the machine crosshead during testing. The quality of the collected displacement data is however obscured by the compressibility of the machine. Figure A.4.5 shows data collected for compression tests on a dummy (steel piece). The steel piece used has the same dimensions as the granite, gypsum, and marble specimens, i.e. 6"x3"x1.25". The curves shown in figure A.4.5 are different due to the machine compressibility, which is changing in every test. The testing machine compressibility changes according to how both the crosshead and the piston were moved before testing. It also depends on the position of the piston. If more accurate displacement data are necessary, an LVDT should be attached to the specimen (adequately protected in the case of granite). Other option, for measuring deformations is to use strain gauges. However, this last option would be very time consuming if done for every specimen.

Video extensometers are something to consider in the future. At the moment the resolution is not enough, and the software does not allow one to view the data while testing (it is a post-mortem analysis).

c) Testing dry specimens

Testing saturated specimens can yield a different stress strain behavior than dry specimens. Hence, always test dry specimens. Do not test the specimens right after cutting the flaws in the

water jet (it is a “wet process”). Allow at least one day for drying. In the case of gypsum, the specimens are tested after three days in the oven.

A.4.4 Load Testing

The setting-up and testing subsections apply when testing with both the standard camera + microscope and with the high-speed camera.

a) Setting up

Before testing, three measurements of each dimension of the specimen (i.e. thickness, width, and length) are taken and recorded in the data sheet. The measurements should be taken by using a caliper. In the case of gypsum, only thickness measurements need to be taken (the specimens are molded and hence the length and the width are constant). These dimensions have to be recorded in the appropriate place on the data sheet (See figure A.4.16 and A.4.17).

The specimens are loaded in the formerly described load-testing machine until either failure or coalescence occurs. Figure A.4.6 shows the direction of the load with respect to the specimen.

The specimen is placed between two steel platens (See figure A.4.7). These steel platens can be found in the same cabinet as the microscope and camera (in room 1-040, and can be opened by cabinet key #3). In fact the two steel platens are different, the upper one has a chain that has to be wrapped around the screw in the crosshead (3 in figure A.4.4A), so that the upper platen does not fall after the specimen fails. The chain is clearly shown in figure A.4.7.

The influence of these rigid platens on the stress state in the specimen (the border effect) is compensated by a height to width ratio of two (the specimen size is 3” by 6”).

A Plexiglas sheet should always be installed between the specimen and the microscope (See figure A.4.2) and can be clamped to the biaxial load frame. This is necessary since many

specimens literally explode at failure. This could cause injury to the operator and damage to the equipment.

b) Testing

When the computer is started, three options are displayed: DOS, Windows, or MTest2. Select Mtest2. The MTest2 screen appears (See figure A.4.8). The screen has several areas: in the upper left corner the load value is indicated. The load rate, peak load and peak stress are indicated in the upper right corner. Disregard these last values. The stress values are not correct since the cross section of the specimen changes for each specimen. There is a load versus displacement (of the crosshead) chart with different scales according to the setting (This scale can also be changed when defining a new setting). Figure A.4.8 shows the chart for gypsum, while figure A.4.9 shows this chart for the granite setting. The lower part of the screen shows the control bar. The left bar, which is indicated in figure A.4.8; it actually has red buttons and contains all the commands to configure the program (covered later in this section). The right bar has the commands necessary to do load testing, which are “**Start**”, “**Home**”, “**Preload**”, “**Hold**” (This buttons are green and turn to brown when pressed). The preload option is not used in the present job. The “**hold**” function is the one used while scanning the surface looking for fractures (see explanation of surface scanning later on this section).

The necessary steps to perform in every test are:

1. Turn on the computer.
2. Select the MTest2 option (from the initial screen menu).
3. Press “**Utils**” in the left bar (See figure A.4.8).
4. After pressing “**Utils**” the bar changes (All the other parts of the screen remain unchanged). The new left bar that appears is shown in figure A.4.10. Press the “**Setup**” button.

5. After pressing “**Setup**” the bar changes again (All other parts of the screen remain unchanged). The new left bar that appears is shown in figure A.4.11. Press the “**Recall Setup**” button.
6. After pressing “**Recall Setup**” a new window opens (See figure A.4.12), which allows browsing the hard drive (or the floppy disk) to find the setting file. The setting files that are used in the present job are called “granite.set” and “gypsum.set”. These setting files have information about displacement rates and the scale in the chart displayed in screen (See figures A.4.8 and A.4.9). Find the files and press “**OK**”. After that press “**Exit**” twice (it will go through the same bars as before, first the one in figure A.4.11 and then the one in figure A.4.10).
7. Once the set-up of the specimen and platens is done press “**Zero**” in the MTEST2 screen (+**enter** to zero every channel).
8. Turn on the loading machine (See 7 in figure A.4.3).
9. Press “**Start**”. After a few seconds the load (in the upper left corner of the screen) will start increasing. If after one or two minutes the load has not increased, turn off the machine and be sure that there is no gap between the upper platen and the upper plate of the load machine. If there is such a gap move this upper crosshead down with the electric motor (See 6 in figure A.4.3), then come back to step g). The test is performed stepwise, as it will be explained in the next paragraph. Observe the upper left corner in the Mtest2 screen to see the load, and the right bar (green buttons) to manage the computer while testing.

c) Loading Process

This paragraph applies when testing with the standard camera.

Figure A.4.13 shows the loading process. The specimen is loaded up to a first level of stress low enough to ensure that no fractures are created. The next phase of the test is done stepwise, after each load step the surface is scanned with the microscope for new fractures. To pause loading, select the button “**Hold**” from the right bar. (See figure A.4.8).

Both the initial stress step and the step increments depend on the material (i.e. gypsum or granite) and are indicated in the table below:

TESTING STEPS			
	GRANITE	GYPSUM	MARBLE
First step load [lb.] :	20,000	4000	Never tested with the std. camera
Increments [lb.] :	2,500 to 3,000	1000	

d) Surface Scanning

This paragraph applies when testing with the standard camera. Figure A.4.14 shows why the process has to be done in steps. Only a small portion of the surface is visible through the microscope (See figure A.4.15 for examples). The complete scanning process takes about two or three minutes (per step). During this process the load is being held. Theoretically, a constant load is kept. However, instability of the pump causes the load not to be constant, and hence introduces a small error in the load in the order of 500 Lb. (This is why A. Bobet chose to control load rate and not displacement rate).

e) Taking Data

This paragraph and the following ones, apply when testing with both the standard and the high-speed camera.

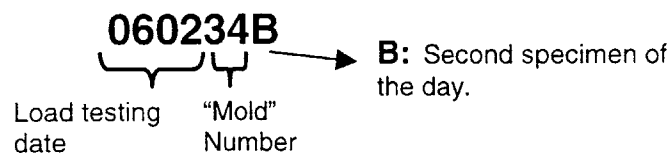
All introductory information in the data sheets (See figures A.4.16 and A.4.17) must be filled before testing (date, data file, tape number, etc.). Load measurements, as well as the detailed crack pattern observations are made during the loading process. When any crack is observed it is sketched in the space of the data sheet labeled “detailed sketch” (See figures A.4.16 and A.4.17). The initiation angles can also be recorded at this stage in the same place (see figure A.4.16). Note that the values circled in figure A.4.16 are indicating the load in KN.

The specimen is loaded until it either reaches failure or the flaws coalesce (whichever happens first). A. Bobet used to measure the angles between the new cracks and the flaws after coalescence (i.e. postmortem analysis). Now, and for testing granite and marble, the angles are estimated during the loading process, this can lead to an error of around 10 degrees (due to the fact that the camera is not exactly perpendicular to the face of the specimen). It is very important to be consistent when recording initiation angles. Figure A.4.16 shows a gypsum data sheet and the correct way of recording the initiation angles. Figure A.4.17 shows a granite data sheet. All of the specimen measurement, as well as the observed data (cracks and loads) are recorded there.

In the case of gypsum, coalescence is usually accompanied by a cracking noise and is indicated by a crack joining both flaws. As soon as coalescence or failure occurs pause the loading and write down the load on the data sheet in the space provided for “observations” (See figures A.4.16 and A.4.17). After either failure or coalescence testing is complete, the next step is to save the load displacement data to a text file.

f) Saving Load Displacement Data

Stop the machine and then save the data to a file (**if this isn't done at this time the data is lost**) before beginning a new test. After either failure or coalescence testing is complete, press “**Home**” in the MTest2 screen (See figure A.4.8), this causes the head to move to its original. Turn off the machine (See 7 in figure A.4.3) and press “**Store**” to save the data. After pressing “**Store**” the left bar changes to the one shown in figure A.4.18. Press “**Raw Data**”, a new window will open, which allows searching for a directory in the hard disk to save the file (or in a floppy disk). The files are named following the same criteria as for gypsum specimens. Here is an example of how to name gypsum specimens:



This notation means that the gypsum specimen was fabricated on June 2, it is mold number 34 and the second one for the day. In the case of granite or marble the format is the same, but the date corresponds to the load testing date. Granite and marble specimens are labeled in a similar fashion. This is done to facilitate future comparison of results. The “**B**” at the end of a granite file means that it is the second one tested on the same day with the same geometry. After selecting the file name in the correct folder, press “**OK**” and come back to the initial screen (By pressing “**Exit**” once). Be aware that the old DOS does not allow saving files with names larger than eight characters, if the name is larger it will be truncated and some data may be lost. The text files are saved with extension “raw” (*.raw).

Before setting up a new specimen be sure that the machine is off. After all the load tests for the day are done, turn off the loading machine, Press **ALT+X** in the MTest2 main screen to exit the program (NEVER RESET THE PC WHILE THE PROGRAM IS RUNNING). Then turn off the PC and the key in the power box.

After finishing testing be sure to clean up all the rock pieces around the testing machine and lock both the general power box and the CPU cabinet.

g) Changing the Settings in Mtest2

Each time either gypsum, granite or marble is tested the aforementioned settings must be used. However, the steps necessary to either check these setting or change them will be explained here:

1. In the general MTest2 screen (See figure A.4.8) press “**Servo**”. The left bar will change (see figure A.4.19).
2. In the new left bar press “**Segmented**” (The rate set is segmented as it was explained in Section A.4.3). After pressing “**Segmented**” a new window is opened showing the values that have been described in Section A.4.3. Figure A.4.20 shows the “segmented servo parameters for granite and figure A.4.21 shows the same parameters for gypsum. The values can be changed right in this window. Before changing anything, be sure to check

the units and the channel numbers. The channel numbers are explained in the box at the upper left corner. Use channel #5 to set displacement rates (since Channel #5 corresponds to the head position) and channel #1 to set load rates (since Channel #1 corresponds to the vertical load).

Once again, do not change these setting for regular testing.

WARNINGS:

- NEVER go to the backside of the machine when the pump is on.
- Remember to zero the machine each time before testing, this can be done either before or right after turning the pump on.
- In case of malfunction do not try to “repair” anything without consulting Steven Rudolph.
- In case of EMERGENCY push the RED KNOB next to the switch box between load frame and computer (7 in figure A.4.3).

A.4.5 High Speed Camera

The high-speed camera belongs to the Edgerton Center at MIT, which is located in Strobe Alley (the fourth floor of Building 4). In order to reserve the camera; contact Anthony J. Caloggero (Technical Instructor) at acalogge@mit.edu. E-mail him at least one week in advance.

The equipment consists of two carts. The first one has the high-speed camera, the image processor, a VCR, and the high-resolution monitor. The second cart carries the lights, the tripod, and a suitcase containing all the necessary lenses, close-ups, and amplifier lenses. There is a third cart available, which carries a PC with a PCI digital video card, and a frame grabber, which can be used to digitize the image after testing. Since the camera is available only for a limited time it is advisable to do the frame grabbing (digitizing the images from the video) some other day (See Section A.4.6). Hence, only the two first mentioned carts are used.

The name of the system is "KODAK EKTAPRO Hi-Spec Motion Analyzer, Model 1012", and it is designed to record high-speed events and to provide immediate, slow motion playback.

The system consists of two main parts (See figure A.4.22A and A.4.22B): first, a high-speed camera that can record up to 1,000 full frames per second. With split screen or partial framing the exposure rate can be increased to 1/12000 second. This last option is not used, since the obtained resolution is too low to identify fractures. The second part is a processor that can store up to 2,400 full frames of information retained in dynamic memory and stored in a digital format with up to 256 gray scales.

RECORDING TIMES: 50, 125, 250, 500, 1000 full frames per second.

EXPOSURE RATES: 1/50, 1/125, 1/250, 1/500 & 1/1000 second, or 2000, 3000, 4000, 6000 & 12000 per second when using split images.

The camera is relatively compact (9"x4"x5" or 23cm x 10cm x 12cm) and lightweight (5 lbs. or 2.3kg). As a result, it is easily transportable, and easy to mount where space is limited.

The solid state memory design eliminates the need for a built-in tape drive. Consequently, there are no moving parts to clog. There is no "ramp-up" time required to bring tape up to speed, and there is greater tolerance for extreme temperatures.

The system incorporates a dynamic memory, which can store up to 2,400 full frames. This "revolving" buffer, which continually replaces old frames with new ones, is the key to capturing unpredictable events (such as fracture coalescence). The 2,400 frames that can be stored in the image processor represent 2.4 seconds of real time when recording at a 1,000 frames /sec. Speed, or 4.8 seconds of real time at 500 frames/sec.

Upon receiving a signal from an external trigger, the analyser will store the frames into a buffer and continue recording until its memory is full (See “How the processor stores images in high-speed camera user guide). In this way, the analyser can capture both the pre-event and post-event frames of an uncontrolled occurrence. The system can be triggered by virtually any kind of sensor, including optical, acoustical, impact, acceleration, temperature and proximity sensor. The manual option for unpredictable events is used (since the coalescence or failures events are not predictable). In addition, to trigger signal input, the analyser accepts both analogue and digital input through the KODAK EKTAPRO Multi-Channel Data Link accessory. With this capability, signals such as voltages and switch closures can be recorded and displayed along with the images. Dual image overlay is also possible using two KODAK EKTAPRO Imagers to record different views of the same event simultaneously (Dual image overlay). This last option is not used, however, since only one camera is available. There is also a built in XY electronic reticule (see figure A.4.23) with a reference marker. Hence, it is possible to calculate the distance between the reticule and the reference mark. This feature allows, for example, measuring speeds of events (by knowing the distance and the time).

The captured frames can be reviewed in slow motion for on-the-spot analysis. The available playback speeds are 1,2, 3, 4, 5, 6, and 8. 12, 25, 50, 75, 100, 200, 400 & 1000 frames per second.

Once captured by the analyzer, electronic images can be transferred to standard videotape or to a computer for post-event digital processing and analysis. As was mentioned before, the images are downloaded to a VCR for posterior processing and digitizing. Currently a professional VCR is used and recording is done in normal NTSC/PAL format, so that the recorded videotapes can be seen in normal VCRs.

The recorded images include date, ID number, recording rate, exposure, image split, elapsed time, playback rate, frame number, pixel depth, reticule coordinates & real time (see figures A.4.23 and A.4.28).

The operator manages the whole operation (including the playback of the images) by using a keypad (see figure A.4.24). This keypad has 15 feet of wire and is connected to the image processor.

This system is widely used in applications ranging from automotive safety testing to biological research and flame/fluid visualization studies.

A.4.6 Using the High Speed Camera

This section covers the necessary steps to test using the high-speed camera. Setting up the specimen is done in the same way as with the “normal” speed camera. Hence, these first steps are just mentioned here. For a detailed explanation see Section A.4.4.

Turn on the PC and start Mtest2 (7 in figure A.4.3). Measure the specimen and fill in the data sheets (see figure A.4.17). Set up the specimen and the steel platens as shown in figure A.4.7. Clean the Plexiglas sheet and put it between the specimen and where the camera will be installed. Prepare the videotape to record and write down the starting recording time in the data sheet.

Now, the image processor and the camera have to be connected and set up. First, place the tripod next to the loading machine. Level it, and check that the legs are firm. Install the camera on the tripod before connecting; be sure that it is correctly fixed.

All the motion analyzer connections are indicated in figure A.4.25: (1) connect the keypad (See figure A.4.24) to the controller. (2A) Connect the controller to the VCR. (2B) Connect the VCR to the video monitor. (3) Connect the camera (referred as imagers in figure A.4.25).

Plug and turn on the controller (4 in figure A.4.25), VCR, and video monitor.

600-Watt lamps standing on tripods are used. Install, and plug the lights. Be sure that the light tripod is standing firmly. Also try not to plug the lights to the same power supply (it is not convenient to overload only one power line). For testing granite, two 600-Watt halogen lamps are used. When testing marble, only one of them is necessary. Usually the more light the better since

the brighter the object the more the diaphragm (which controls lens aperture) can be closed and the better the resolution.

Press “**live**” in the keypad. Now the image has to be obtained. The lens and accessories to be used depends on the target, the distance to the object, and the light. Since the light and the distance to the object are constant (Distance is approximately 20 inches), the lens and accessories to use depends only on the target area.

Figure A.4.26 shows the different lenses, close-ups, and amplifiers available at the moment at the Edgerton lab.

The lenses are identified according to their focal length in millimeters. Lenses come either with fixed focal lengths (primes) or multiple, adjustable focal lengths (zooms). The ones used here are all zooms.

If there are problems to obtain a clear image, check both the focus and the diaphragm (it allows more light to enter).





These lenses also allow adjusting the aperture. The aperture of a lens is the open space through which the light passes on its way to the chip (this is a digital camera). By means of the lens diaphragm it is possible to adjust the size of the aperture. This size is then referred to as the f-number (or f-stop). The shown f-number is a ratio of the size of the aperture to the focal length of the lens. Hence, a lens with f2.8 has a focal length that is 2.8 times the size of the aperture (1:2.8). It is customary to refer to, for example, f2.8 rather than 1:2.8. Because of this, smaller numbers are used to refer to larger apertures.

A larger aperture allows more light to pass through. Hence, a larger aperture allows one to use a faster shutter speed. In general, this is a good thing. However, it may not always be desirable to use a large aperture. By varying the size of the aperture it is possible to vary the Depth of Field. Depth of field is the term for the distance that is in focus in front of and behind the point of focus of the lens. For example, if the lens is focused on a tree, things at a certain distance in front of and behind the tree will also be in focus. This has been a problem when the specimens fail (since

the object is no longer in a plane). The distance changes with the aperture used. Larger apertures give a shallow depth of field. Smaller apertures give a longer depth of field.

The close-up attachment lenses are attached to the front of the lens to allow focusing closer. However, in order to be used effectively, the distance from the lens to the object needs to be small (about 10 inches), and hence they are rarely used in the present work.

The lenses and accessories to be used according to the target area:

GEOMETRIES	AREA	LENS (Zoom)	Magnifier	Close ups	NOTES
60-0-a 30-0-a 30-0- 2a 45-0-a		200 mm	2x	1:2 or 1:4	Use either magnifiers or close ups. Do not use both.
30-a-a 45-a-a 30-a-2a 45-0-2a 60-0-2a 45-a-2a		200 mm	NO	NO	If the image is not clear, try a 90-mm lens with a 2x magnifier.
30-2a-2a 45-2a-2a 60-0-3a 60-a-2a		90 mm	Optional 2x. Use to get only the coalescence area.	NO	
Intact		50 mm	Optional 2x according to the working distance.	NO	It can also be used to observe the global failure of pre-cracked specimens

If a blurry image is obtained, try to check the cleanliness of the lenses and other optic parts.

Once the image is obtained, focus the zoom. At this moment the image to be recorded is in the screen of the video monitor. There is one more thing to take into account. The high-speed camera is mounted on the tripod (I.e. static), while the object (specimen to be tested) is mounted on the loading machine and hence is moving up during testing. Thus, It might be necessary to adjust the

image in the middle of the test or to allow some space over the specimen in the screen. (See figure A.4.27):

Check (See figure A.4.28) the recording rate in the monitor (500 frames per second are used for granite, and 250 Fr/sec for marble).

Now, prepare the loading machine for testing. Recall the appropriate setup file (according to the material to be tested) and zero the machine. Turn on the machine and press “**Start**” in the Mtest2 software (see detailed instructions in Section A.4.4).

At this point the load testing has started, but nothing is being recorded (usually there is no useful information at the beginning of the test). Check in the keypad the recording mode. The one to be used is the record stop mode, which means that an unpredictable event is about to be recorded. The images will be recorded till the camera is stopped. The last 2400 frames can be recovered. Refer to the camera user manual for an explanation on how the processor stores the images (taken from the camera user’s manual). The explanation of this record mode (called “**record stop**” mode) is on page 6.5 of this user guide.

Also with the keypad, select the recording speed. Usually 500 frames per second are enough for granite, and 250 frames per second for marble.

In the camera keypad press “**Ready**” and then “**Record**”. Now the images are being stored in the image processor but not in the VCR.

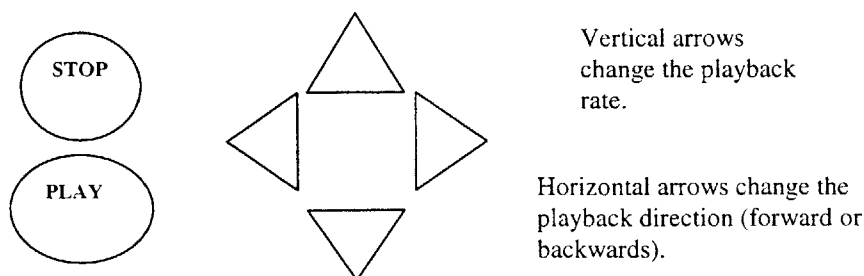
At a load value of 15,000 Lb. for granite and 5,000 Lb. for marble start recording in the VCR (these load values are low enough to ensure that no cracks are formed under them).

There are two interesting events to be recorded with the high-speed camera. One of them is the coalescence and the other one is the failure. The possibility of playing back the events at a lower speed lets us observe relative displacement when the fractures are created. Hence is easy to identify the cause of the fractures (E.g. shear or tension).

Right after the event (either coalescence or failure), press “**Stop**” on the keypad. It is important to be ready for that. Stop the VCR recording. At this moment turn off the lights (otherwise they overheat).

Store the “raw data” in the Mtest2 software and press home. Turn off the loading machine. Move up the upper head of the loading machine to remove the specimen (when testing granite the specimen has already exploded, but this step is still necessary to fit the next specimen to be tested).

Now it is possible to play back the recorded event (either coalescence or failure) at a lower speed. The image processor has stored 2,400 frames, which can be replayed at a lower speed. First, start recording on the VCR (so that the event at a lower speed is recorded in the videotape). Press “**Play**” on the keypad, at this moment the arrows located in the bottom of the keypad let one select different features:



The event can be played-back as many times as necessary to ensure that it is properly recorded on the videotape. Press “**Stop**” on the keypad. Stop recording on the VCR and write down end of recording time in the data sheet.

The image processor works as a carrousel to store slides. When “play” is pressed the carrousel starts rotating and the 2,400 stored frames can be viewed as many times and necessary. If the VCR is recording while the event is played back the images will be stored in the videotape.

Finally, recover as many specimen pieces as possible and draw the failure mode in the data sheet, by looking at these pieces and the recorded images. Also write down the zoom and magnifiers used to test.

After finishing, the lab has to be cleaned and the equipment disassembled. Before touching any of the connections, remember to unplug everything.

WARNINGS:

- Treat the equipment with care, and never push more than one cart at a time.
- Always install a Plexiglas sheet to ensure that no rock pieces damage the equipment, or harm the operator.
- Make all the necessary connections in the image analyzer before connecting it to the power.
- Avoid burning yourself when handling the lights. Try to wait at least 45 minutes after testing before disassembling the lights.
- Be extremely careful when cleaning the lenses. If in doubt contact Tony Caloggero.
- Try to start using the camera with someone familiar with the equipment. Since it is a very expensive and delicate. There are many other features not explained here. It is also a good idea to read the complete user's manual before starting (available at the Edgerton Lab).

A.4.7 Processing data

This processing data section applies when testing with both the standard and the high-speed camera.

The data acquisition information is stored in a text file by using the MTest2 software. The criterion to name files is explained in Section A.4.4. The text file has DOS extension RAW and its configuration is shown in figure A.4.29.

The Macintosh used for plotting and data processing is located in the Civil Engineering computer cluster on the second floor (1-252). The combination is 15-4-3.

It is not necessary to use the Kaleidograph or a Macintosh to process the results of the experiments. That computer was used to process all the information in A. Bobet thesis. However, all the new data (for both gypsum and granite) is being processed in a new Excel template. Essentially both templates transform the data coming in Load/displacement form to stress/strain form and plot it. Beware that the new template changes units automatically (from pounds and inches to SI units, stresses in MPa and strains in %).

The processed data is formatted as shown in figure A.4.30. The new template requires entering the specimen number and date of loading test (1 in figure A.4.30), the geometry (2) and the actual dimensions of each specimen. However, to avoid mistakes (in case of forgetting entering the actual dimensions of the specimen), the theoretical dimensions (6"x3"x1.25") are set as default values (7). Note that the units to enter the dimensions are millimeters. The data coming from the data sheet regarding type of cracks and load have to be entered (in Lb.) (4). The columns of displacement and load (5) are copied from the text file (saved in the program Mtest2). Stress/strain data are computed (6) automatically by the template.

The stress-strain data are plotted as shown in figure A.4.31A for granite, A.4.31B for gypsum, and A.4.31C for marble. Note the scales used are different for each material. Also note that the geometry, and the stress level for crack initiation have to be clearly indicated in the plot. It is important to preserve the same scale in different tests on the same material in order to make the comparison easier.

Since the new template is in Excel and in a user file in the CEE-Net it can be accessed from whichever terminal (a total of approximately 30 P.C. based on Windows NT) in that net. The CEE-NET clusters are in rooms 1-051, 1-341, and 1-252 at MIT building 1. The following is a list some useful URL/e-mail address regarding CEE-Net:

- Introduction to computer lab:
<http://web.mit.edu/civenv/courses/cee-net/>

- Having hard time on CEE-Net workstations?
<http://web.mit.edu/civenv/courses/cee-net/report-problem.html>
- Complaints, suggestions?
E-mail to: cee-net@mit.edu
- Need a new account?
<http://web.mit.edu/civenv/courses/cee-net/account-request.html>

A.4.8 Image Processing

This section explains how to obtain digital images from videotapes. This procedure can be followed independently of how the images were recorded on the videotapes (I.e. it is applicable to both the high speed and the standard camera videotapes). The equipment to be used is in the Edgerton Lab. (image processing room 4-408). To gain access to that facility contact Tony Caloggero or Cindy (3-4629). Be sure to take to the Edgerton lab the VCR, the appropriate videotapes (the ones with the information to be digitized), and Zip disks.

Plug the VCR (Video out) to the PC (it has a RCA plug “video in”). Figure A.4.32 shows the connections. Installing the TV is optional since the images will be seen on the PC monitor.

The computer to be used is the smallest Macintosh. After turning the computer on select the icon “*Apple Video Player*” two new windows with gray backgrounds will appear. One of the windows is simply like the TV screen (See figure A.4.33). It has a screen area, a counter (for the videotape), and a volume control (not used in the present work).

The second window is the one that has the controls. It has two possible configurations according to what button is pressed in the left half. There are two buttons:

- a) If the TV button is pressed in the left half of the screen, the right half is as shown in Figure A.4.34A. These controls allow one to adjust the image. Note that the better the frame

grabber, the more controls available to adjust the image. When the TV button is pressed the adjustments will be made in the connected TV (which is optional to connect). In order to adjust the image in the PC monitor screen (the window shown in figure A.4.33) the button “Video” has to be pressed. Finally the button “S-Video” is never used with our configuration.

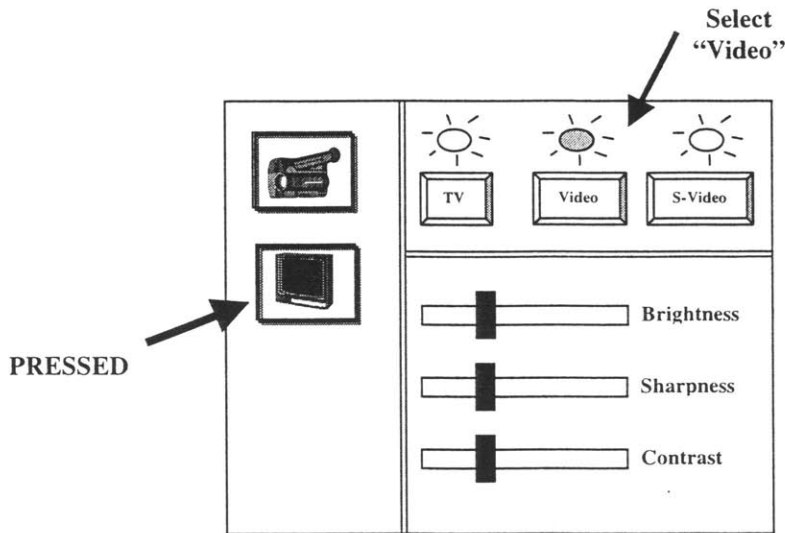


Figure A.4.34A: Adjusting the image.

- b) When the button with the Video Camera icon in the half left is selected the right half is as shown in Figure A.4.34B. Here, according to the right half of the window, there are two options: capturing pictures or capturing movies.

To capture pictures, turn the VCR on, press “play”, the video will be displayed in the screen window (figure A.4.33). Press the TV button in the left half of the second window (the one shown in figure A.4.34A) and adjust the image. At this moment, the screen is like a TV monitor (In a small screen). When the image to capture is in the screen **press “freeze”**, the screen window will be interrupted (but the VCR will continue playing). See the image, make any necessary last adjustments and press save. A normal “save” dialog box will open asking for the location to save files. Select Zip Drive and save the file (this is a Macintosh do not use more than 8 characters for file names). To save another image press the “freeze” button again, and repeat the aforementioned steps.

Note that the buttons in the screen can only control what is being shown in the screen. Hence when “freeze” is pressed the image will be interrupted only in the screen, but the VCR will keep on playing the videotape. To pause or stop the VCR use its own buttons (or the remote control).

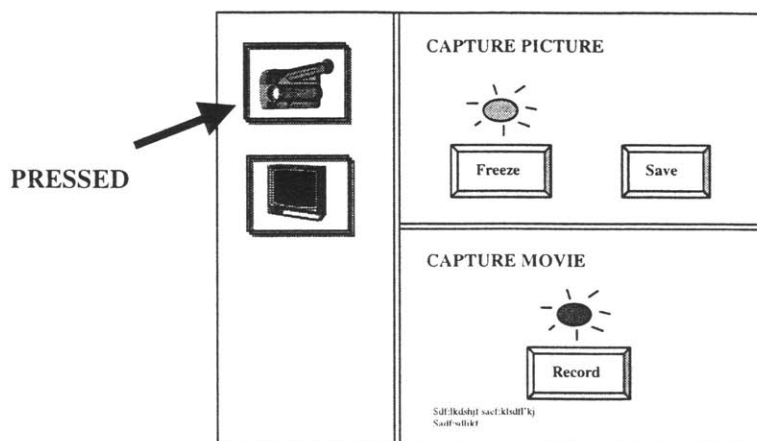


Figure A.4.34B: Capturing Pictures and Movies.

To capture movies press the button “record” in the bottom right of the screen shown in figure A.4.34B. While recording the red light over the “record” button is on. To stop recording press “record” again. Then a dialog box to save the video file will open. Save the file on the Zip drive. Use a small screen to obtain a better resolution. Be aware that the digital video files can be very big (10 seconds of video can take more than 100 Mbytes).

Mold Number	Geometry angle-spacing-continuity (β - s - c)
12*	30-0-2a
2	30-0-3a
3	30-0-4a
4	30-a-a
5	30-a-2a
6	30-a-3a
7	30-a-4a
8	30-2a-2a
9	30-2a-3a
10	30-2a-4a
11	30-3a-2a
12	30-3a-3a
13	30-3a-4a
14	30-4a-3a
15	30-4a-4a
25*	45-0-2a
16	45-0-3a
17	45-0-4a
18	45-a-a
19	45-a-2a
20	45-a-3a
21	45-a-4a
22	45-2a-2a
23	45-2a-3a
24	45-2a-4a
25	45-3a-3a
26	45-3a-4a
27	45-4a-4a
34	60-0-2a
28	60-0-3a
29	60-0-4a
30	60-a-2a
31	60-a-3a
32	60-a-4a
33	60-2a-4a
35	30-0-a
36	45-0-a
37	60-0-a

Table A.1: Mold number-geometry for gypsum specimens

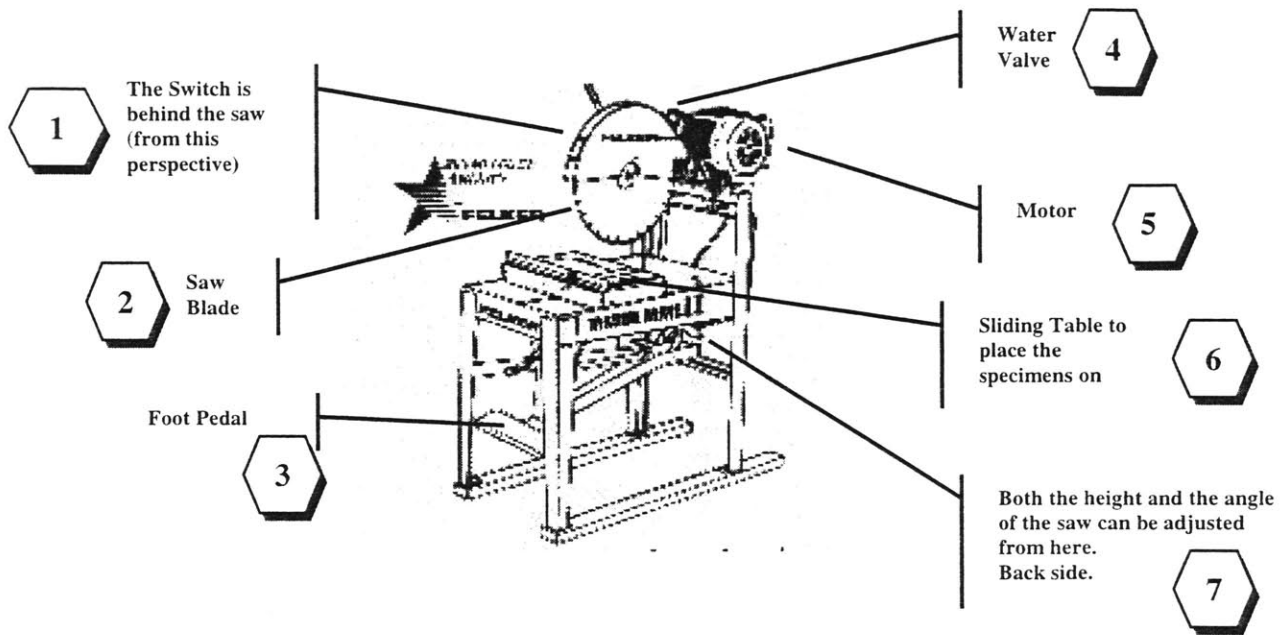
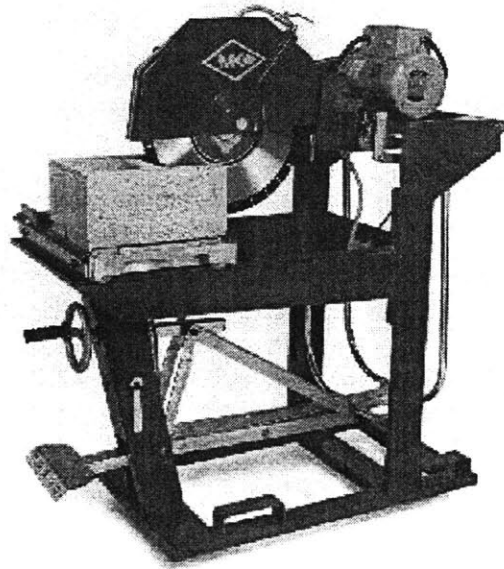


Figure A.1.1: Overhead Saw - Main Parts



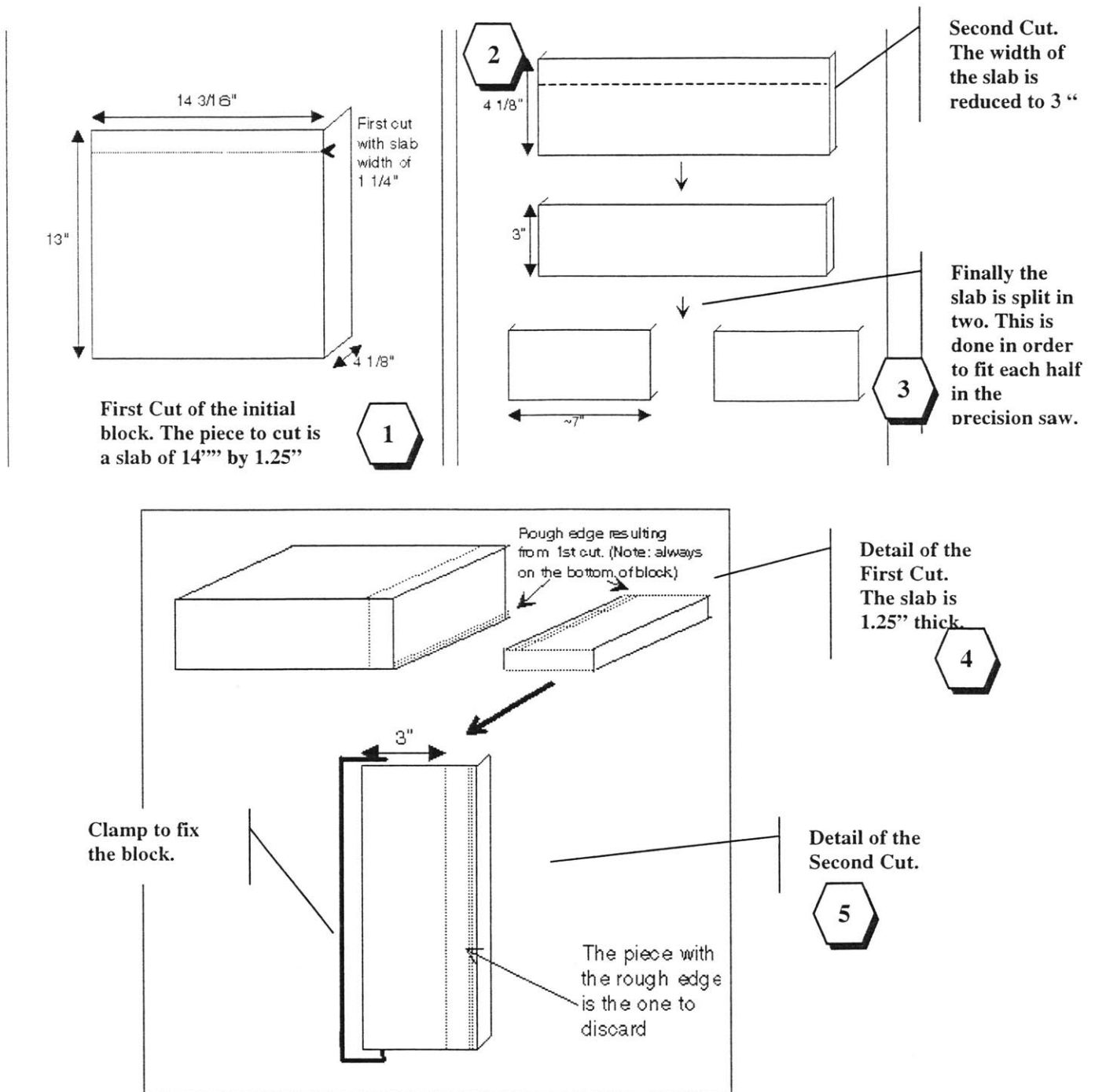


Figure A.1.2a: Detail of the cuts done on granite specimens with the overhead saw.

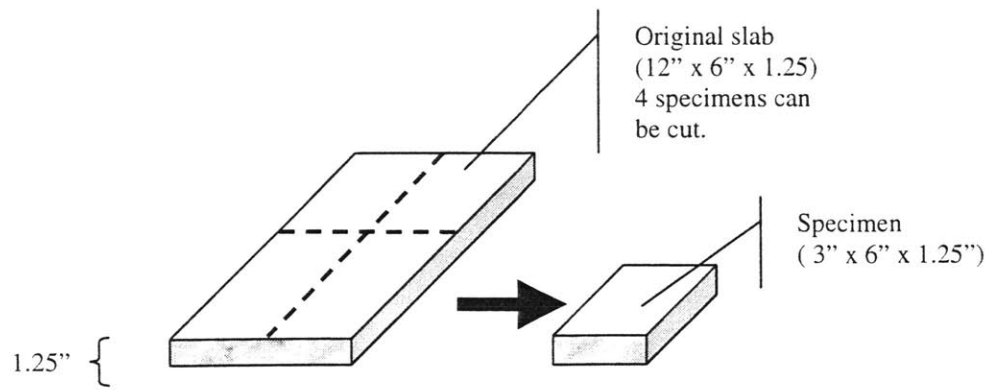


Figure A.1.2b: Second and third cut to be done in marble.

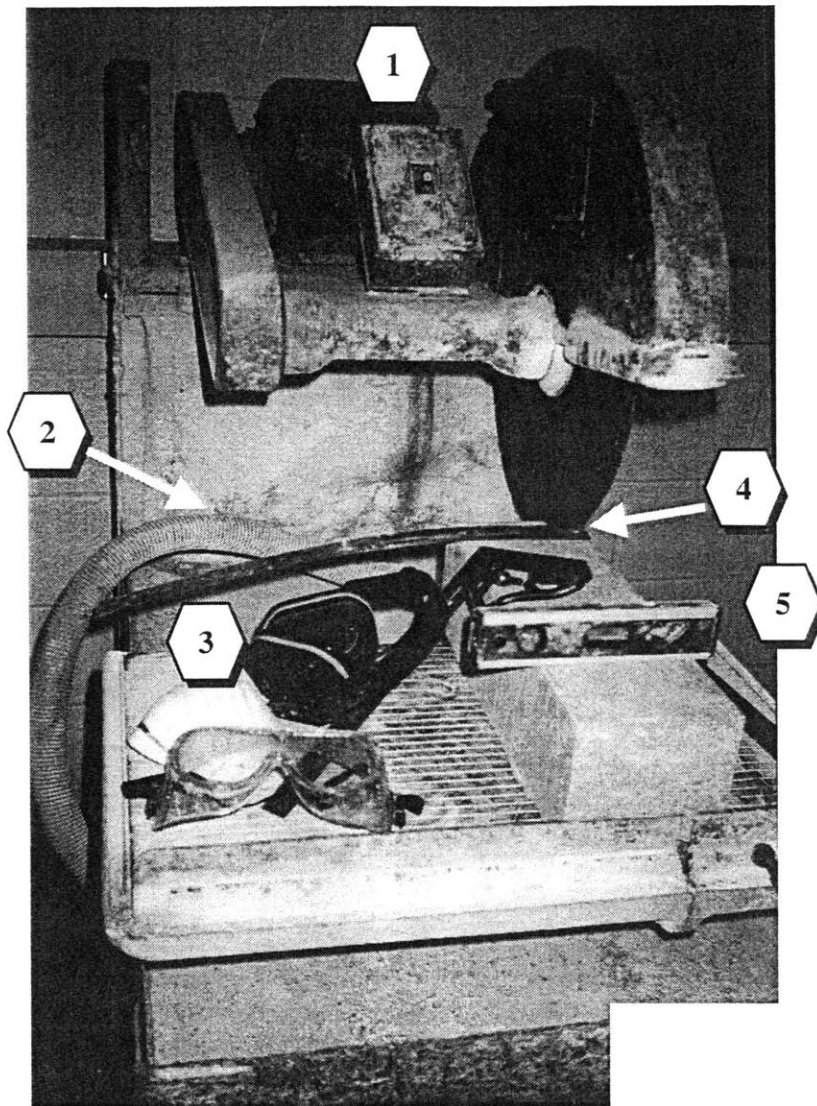


Figure A.1.3: Set up of specimen in the overhead saw. (Ready for the first cut)

- 1 Switch (turns on the motor)
- 2 Flexible Drain Pipe. Drop water into a bucket
- 3 Mask, ear and eye protection
- 4 Ruler measuring 1.25" (thickness of the slab to cut in the first cut)
- 5 Level, (set it perpendicularly to the saw blade)

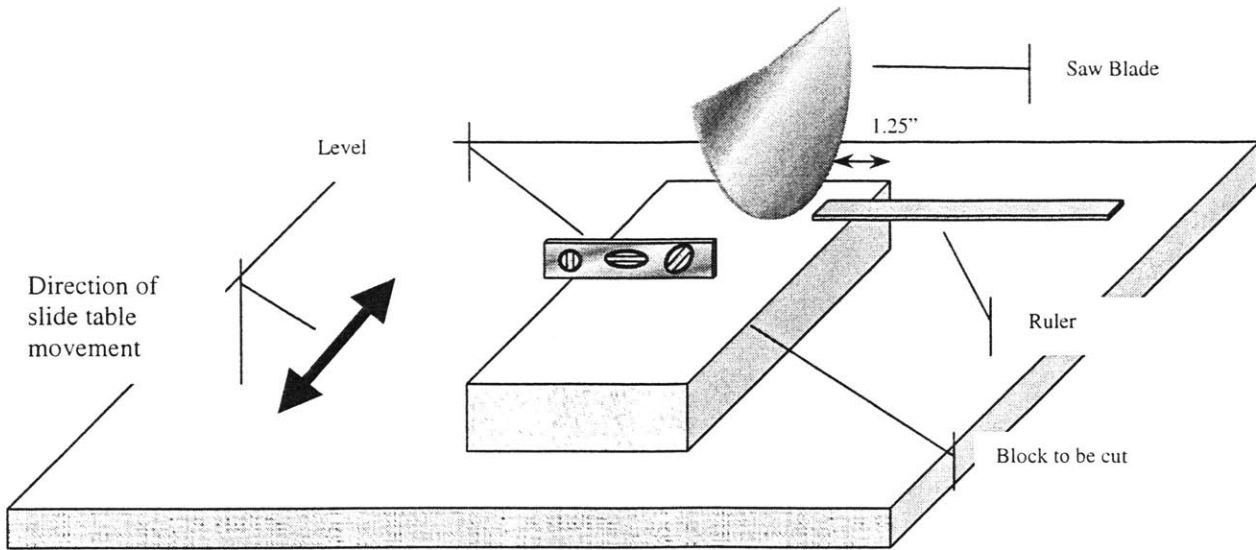


Figure A.1.4: Measuring and leveling to make the first cut.

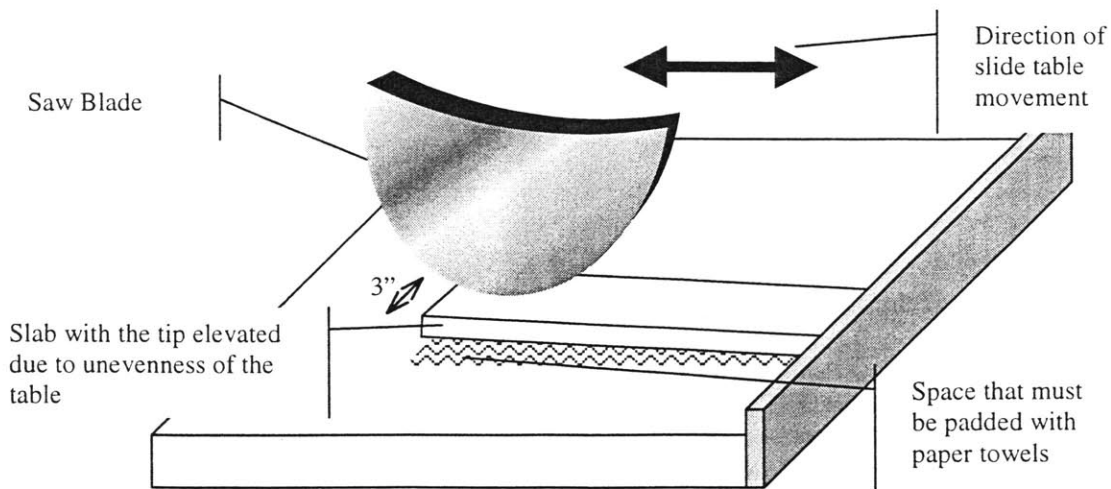


Figure A.1.5: Making the second cut. Note elevation of the back part of the slab.

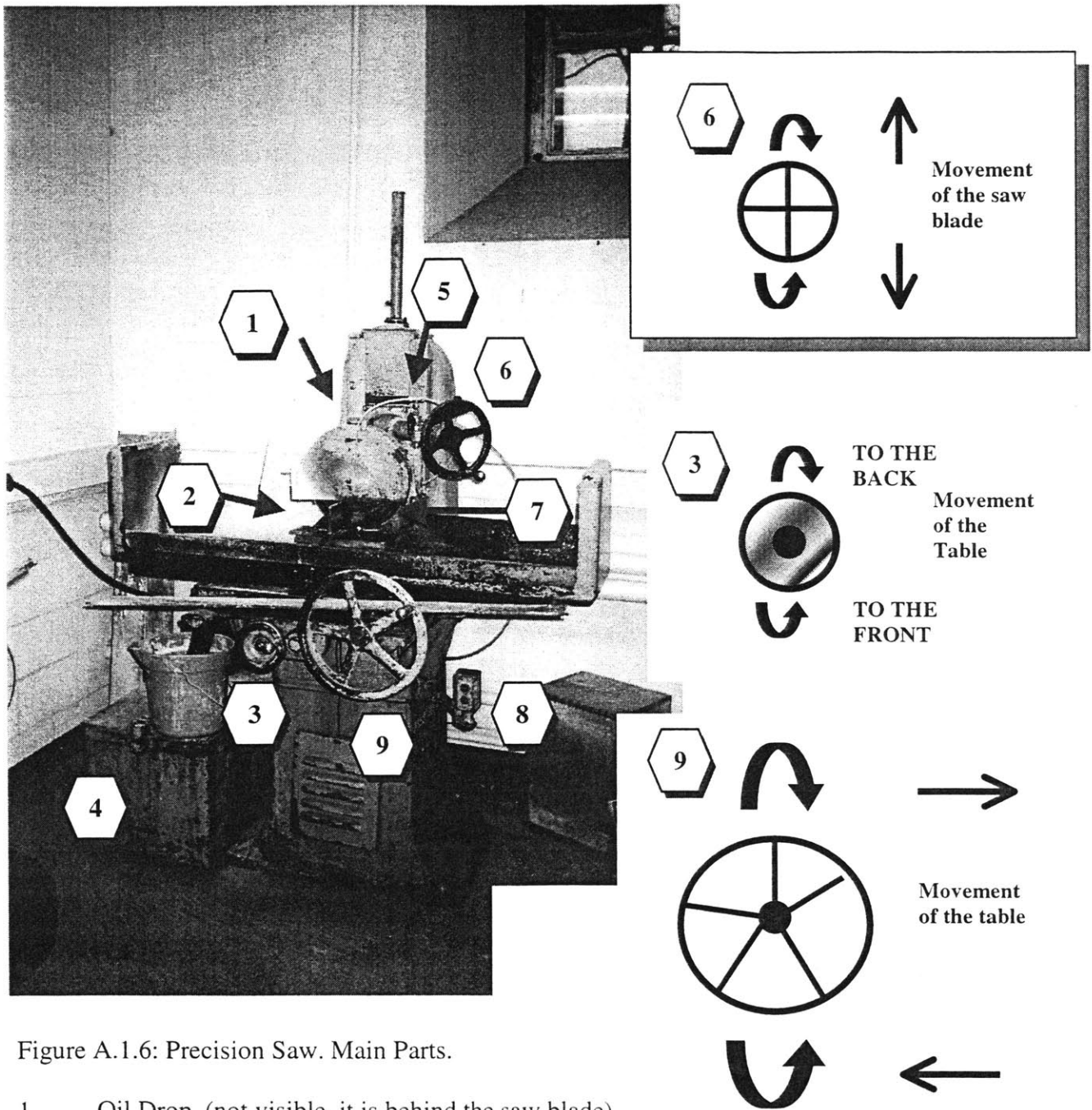


Figure A.1.6: Precision Saw. Main Parts.

- 1 Oil Drop, (not visible, it is behind the saw blade)
- 2 Magnet Table (to put the piece to be cut)
- 3 Back and Forth Wheel. (DO NOT TOUCH IT WHILE CUTTING)
- 4 Recirculation Tank
- 5 Water Valve
- 6 Vertical Movement Wheel
- 7 Saw Blade
- 8 On/Off Switch (turns on motor + recirculation pump)
- 9 Lateral Movement Wheel

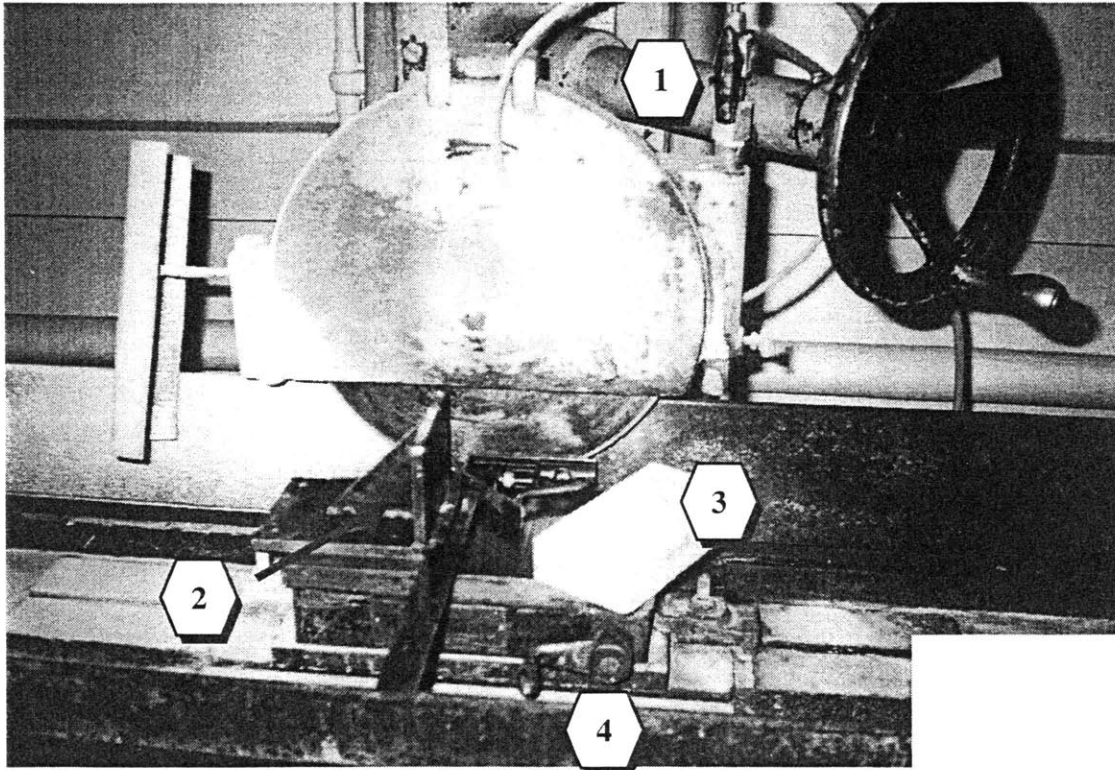


Figure A.1.7: Setting the guide in the precision saw.

- 1 Water valve in position to cut.
- 2 Guide at 90° from the Saw Blade.
- 3 Piece to be cut.
- 4 Handle to activate the magnet, which will fix the guide.

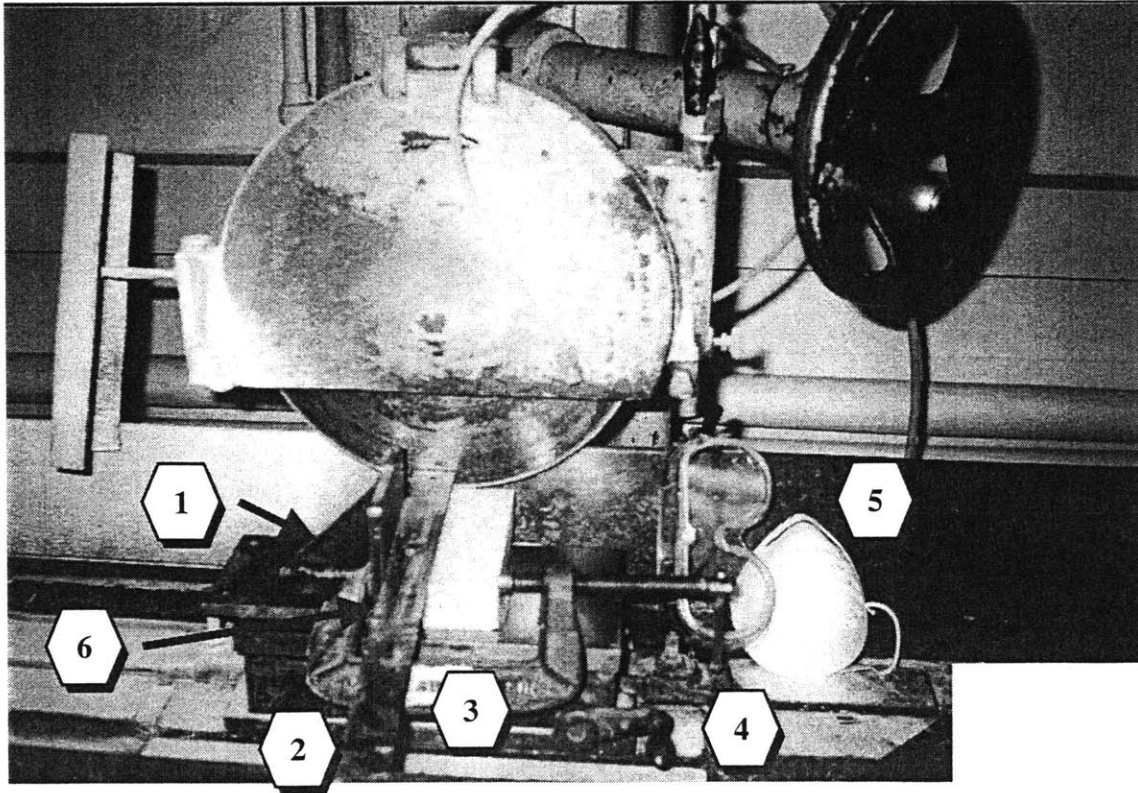


Figure A.1.8: Setting the specimen to cut in the precision saw.

- 1 Guide fixed by the magnet.
- 2 Ruler measuring 6".
- 3 Clamp.
- 4 Handle. Note the position to lock the magnet.
- 5 Eye protection and mask.
- 6 The side against the guide has to be the same face of the original block used to level when cutting with the overhead saw.

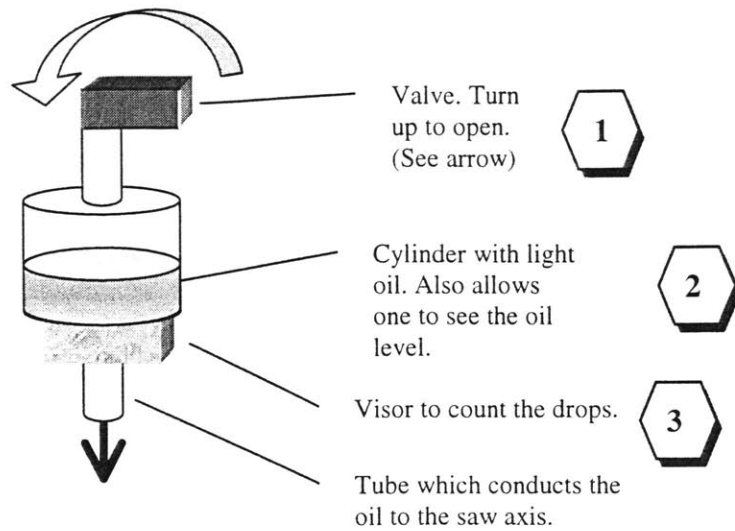


Figure A.1.9: Oil drop device in the precision saw.

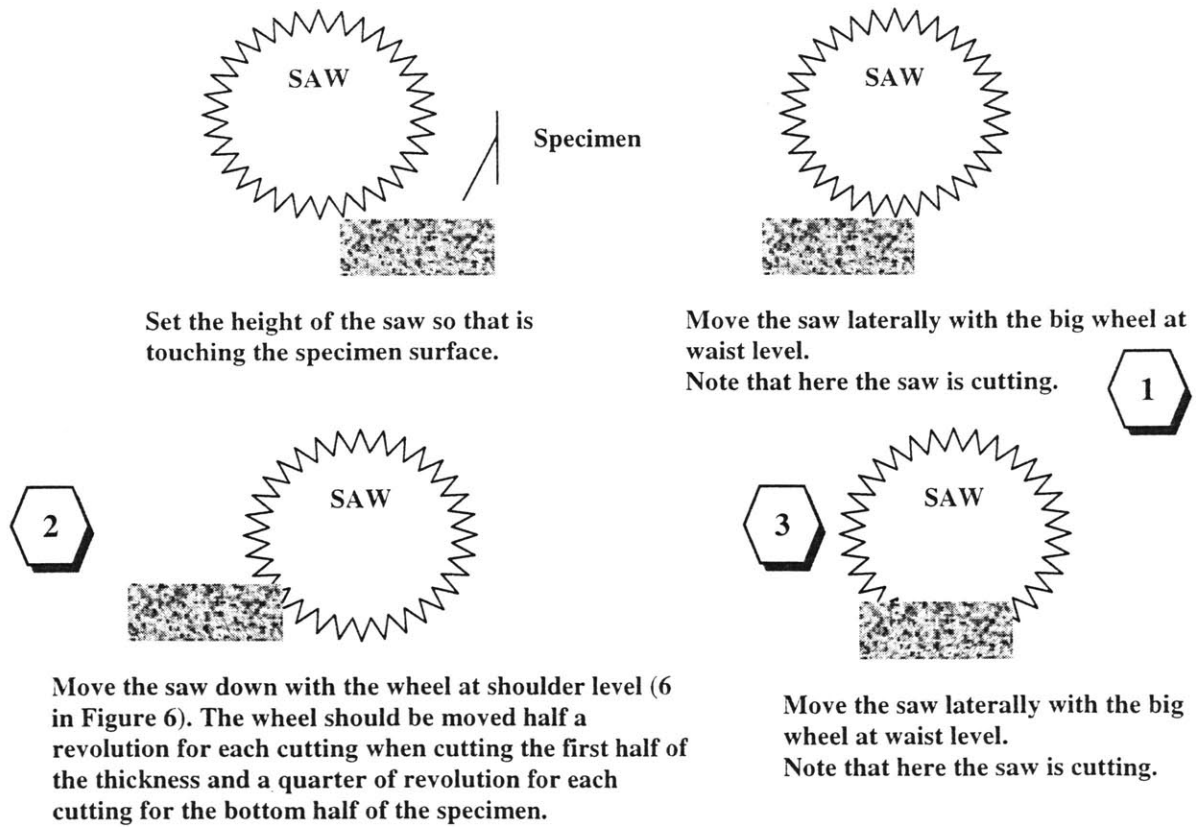


Figure A.1.10: Steps to cut with the precision saw.

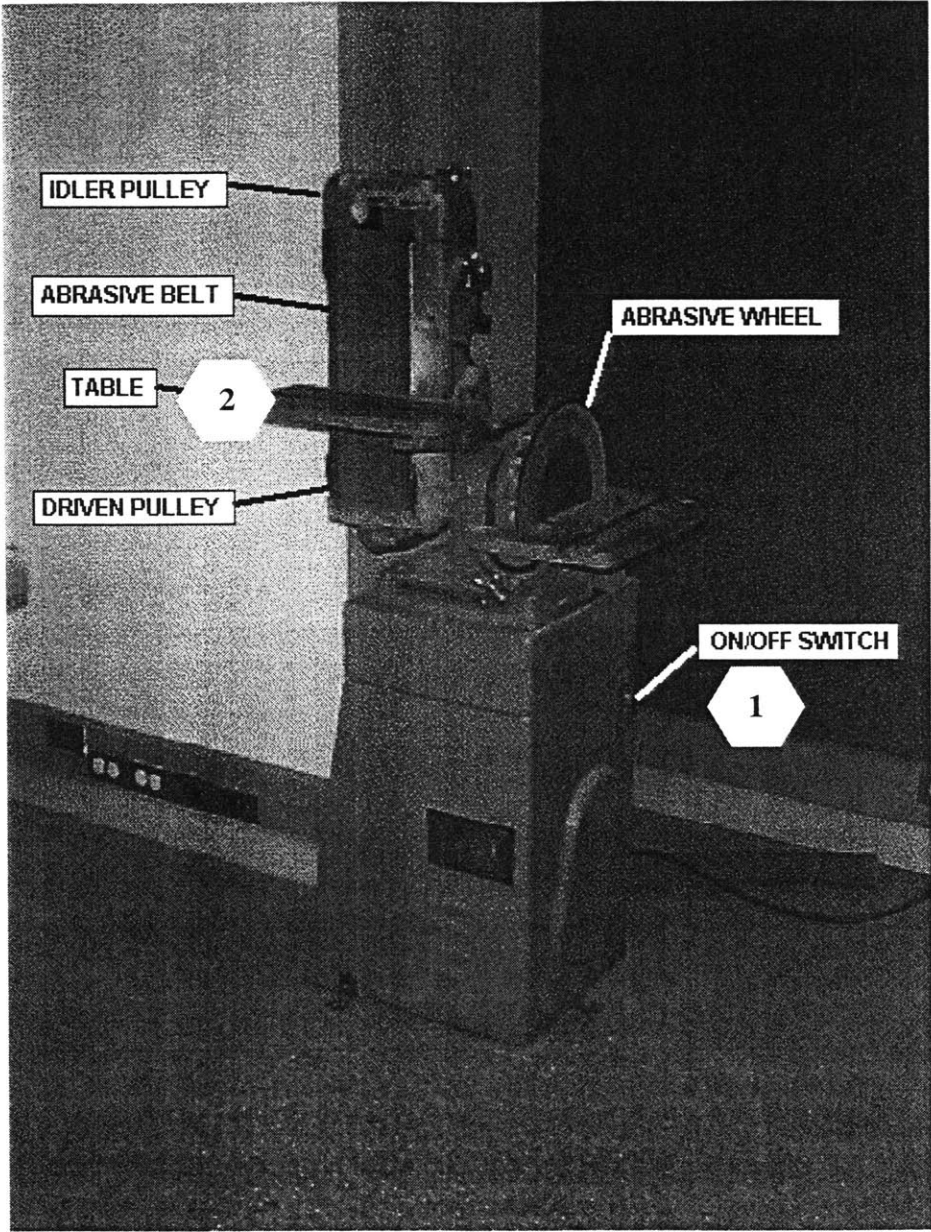


Figure A.1.11: Belt Sander. Main Components (used to polish marble specimens)

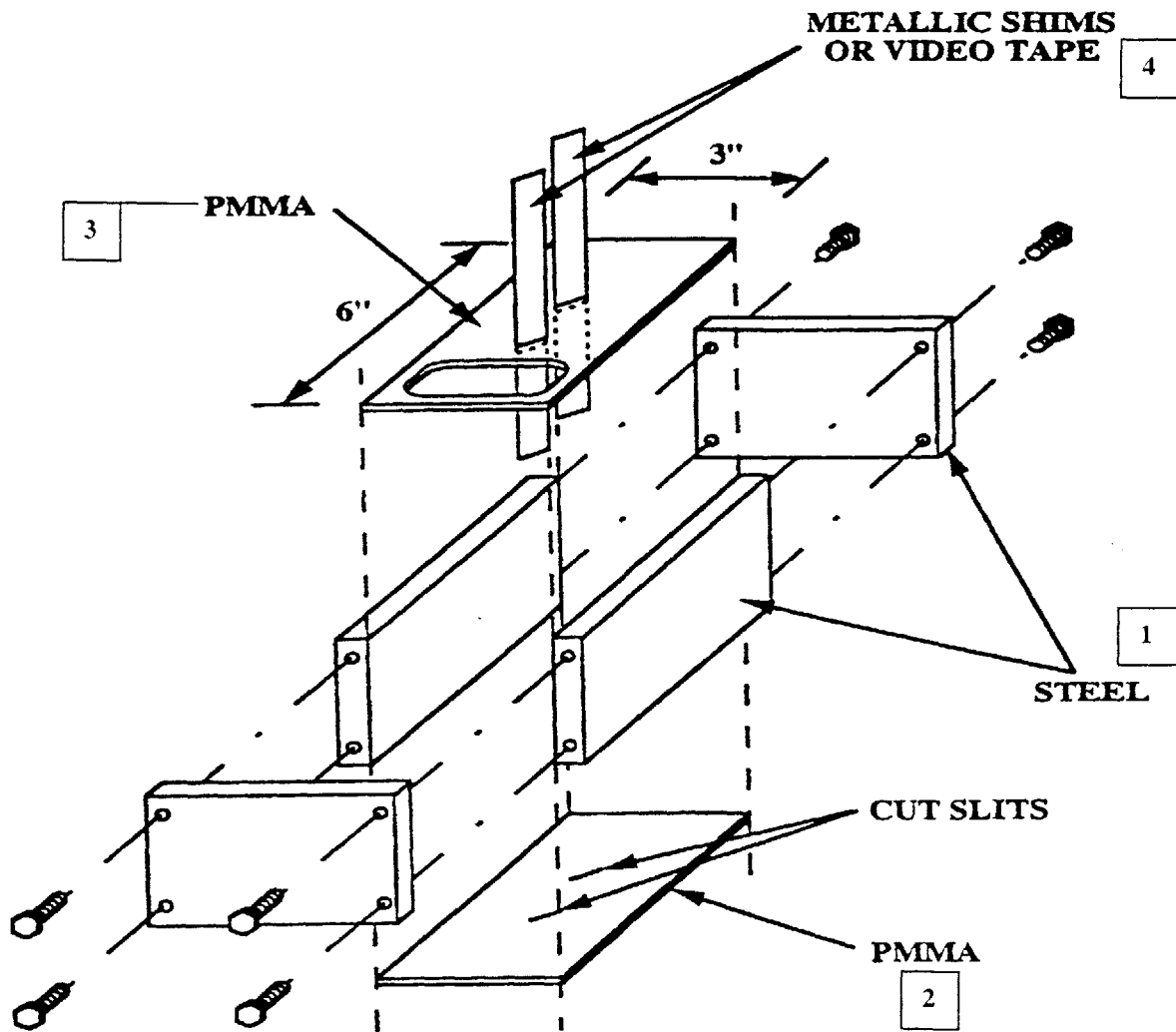


Figure A.2.1: Gypsum Mold, from Bobet (1997)

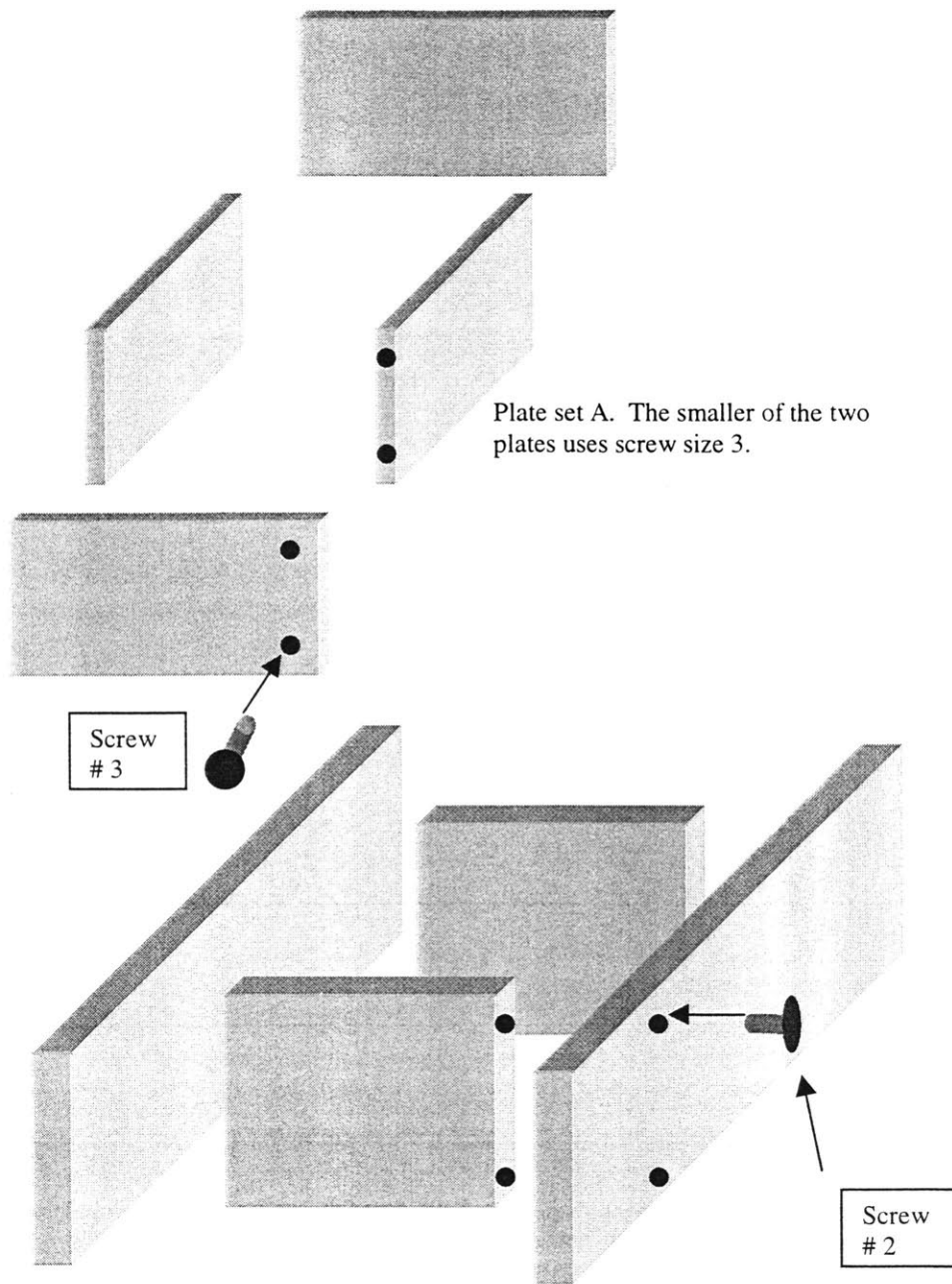


Plate set A. The smaller of the two plates uses screw size 3.

Screw # 3

Screw # 2

Plate set B. Larger plates that use screw size 1 or 2. Preferably use size 2.

Figure A.2.2: Plate sets

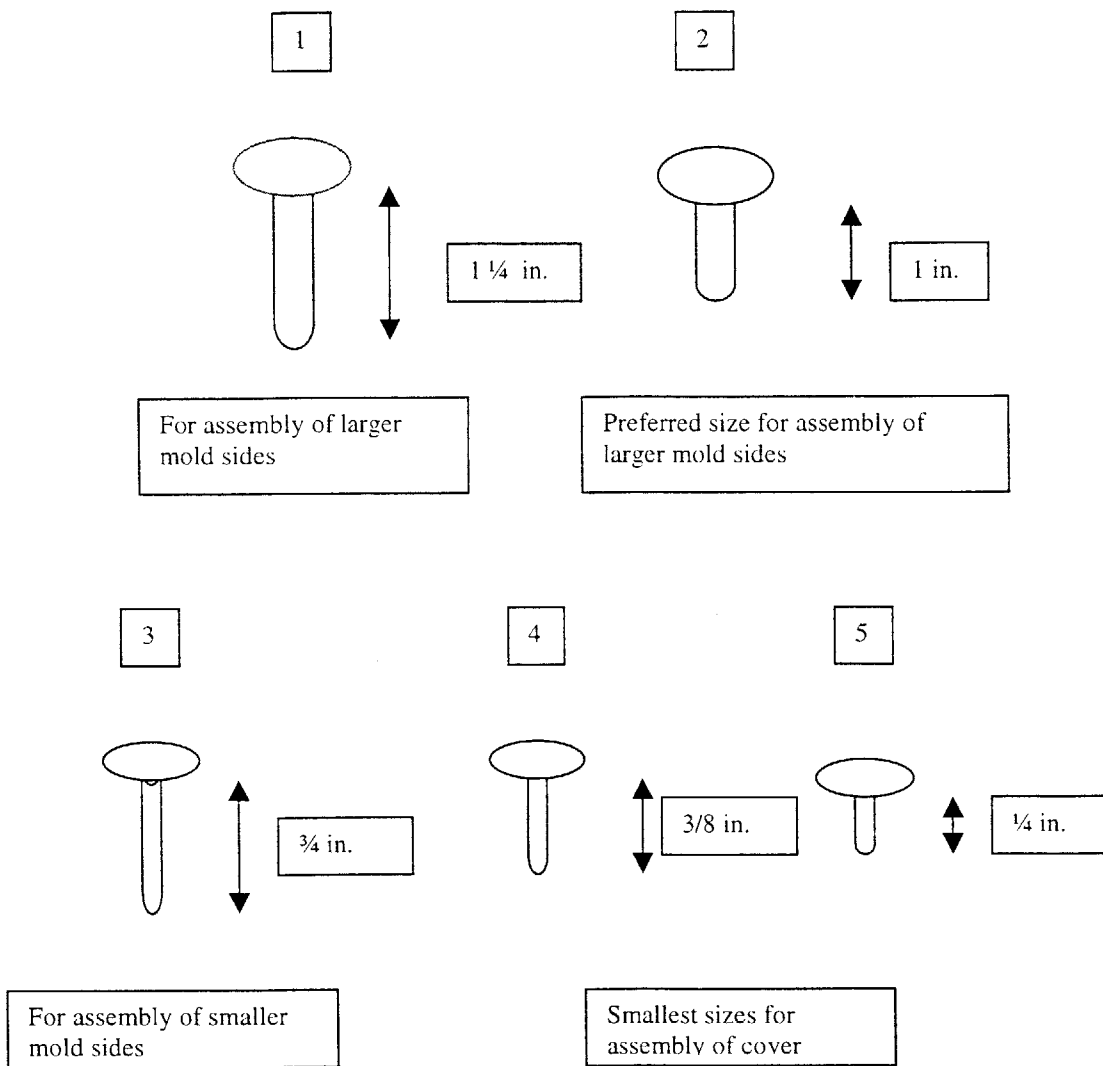


Figure A.2.3: Screw sizes

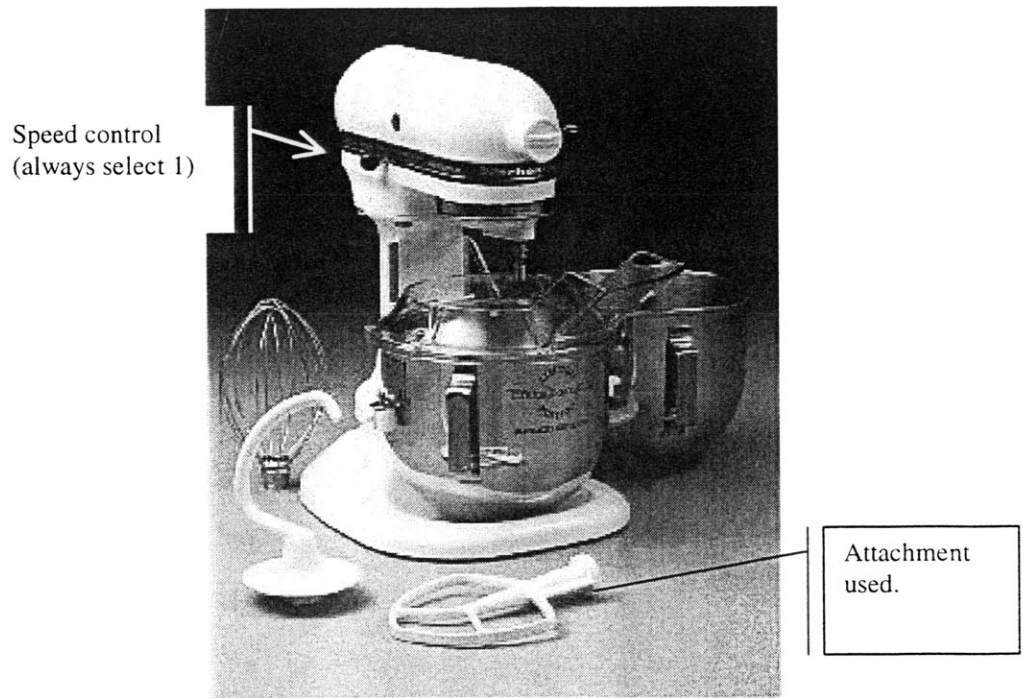
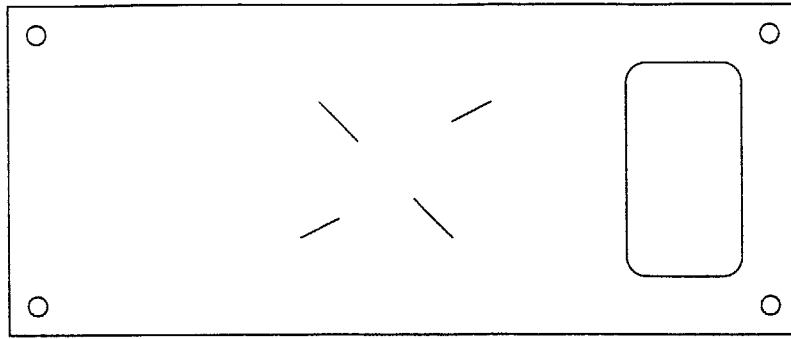
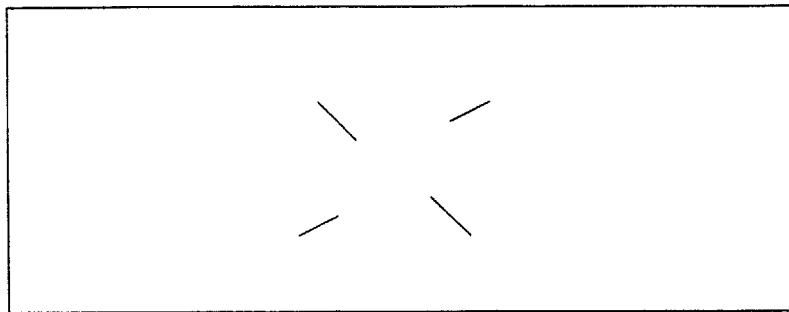


Figure A.2.4 :Mixer used to mix gypsum and celite



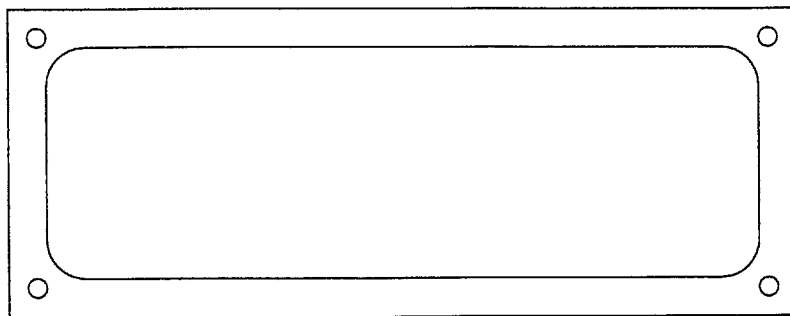
A

Plexiglas cover



B

Plexiglas base

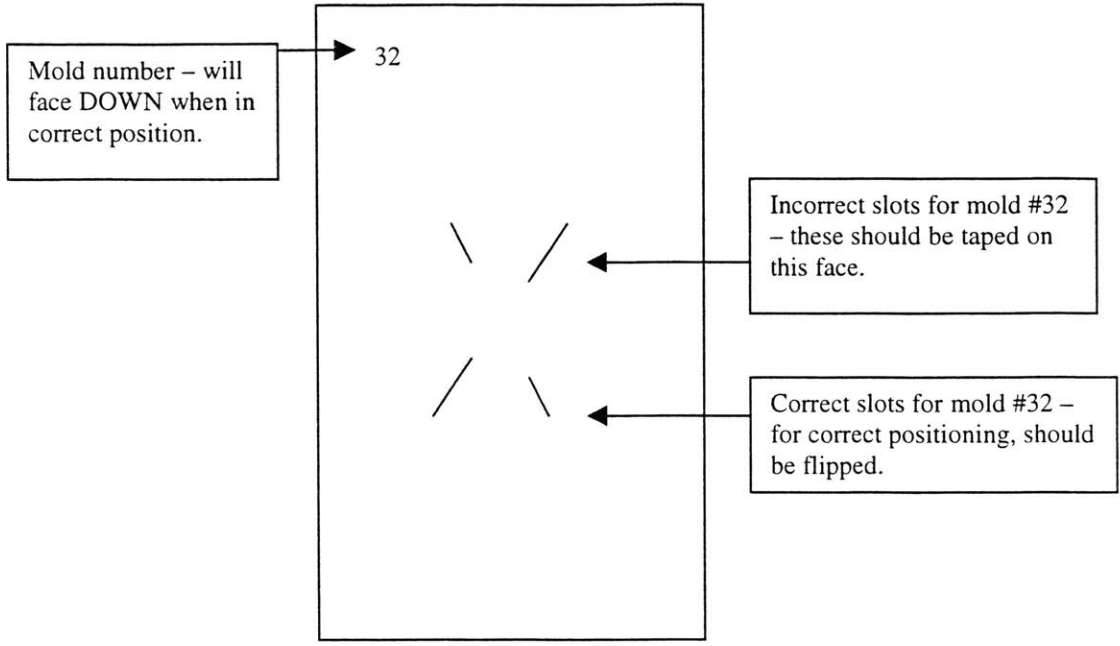


C

Plexiglas rim

Figure A.2.5: Plexiglas pattern/plates. Refer to Figure A.2.8 to see their relative position.

A



B

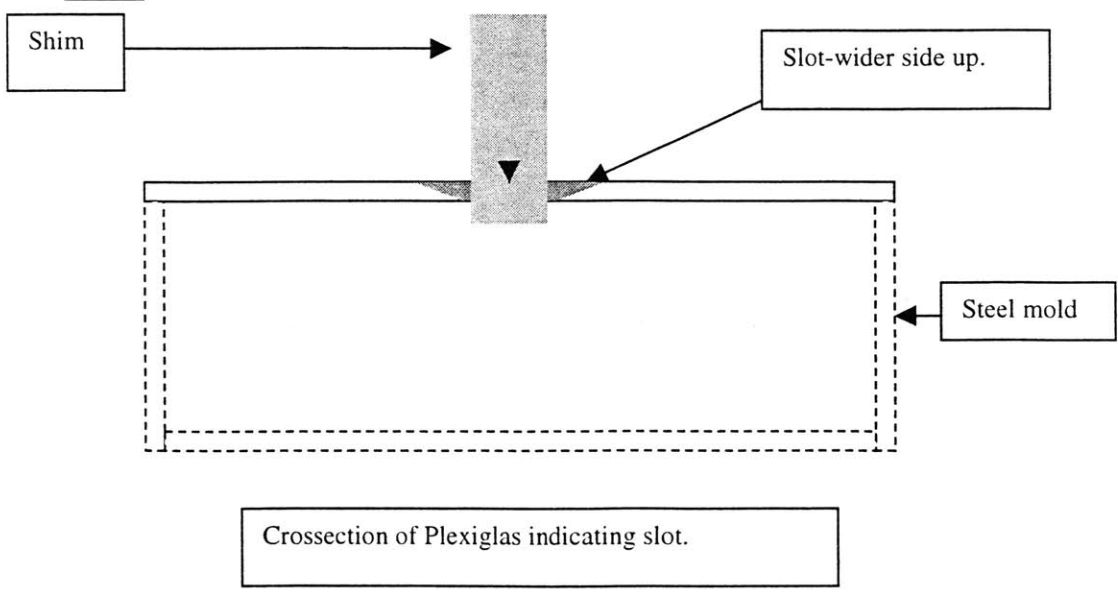


Figure A.2.6: Plexiglas Pattern

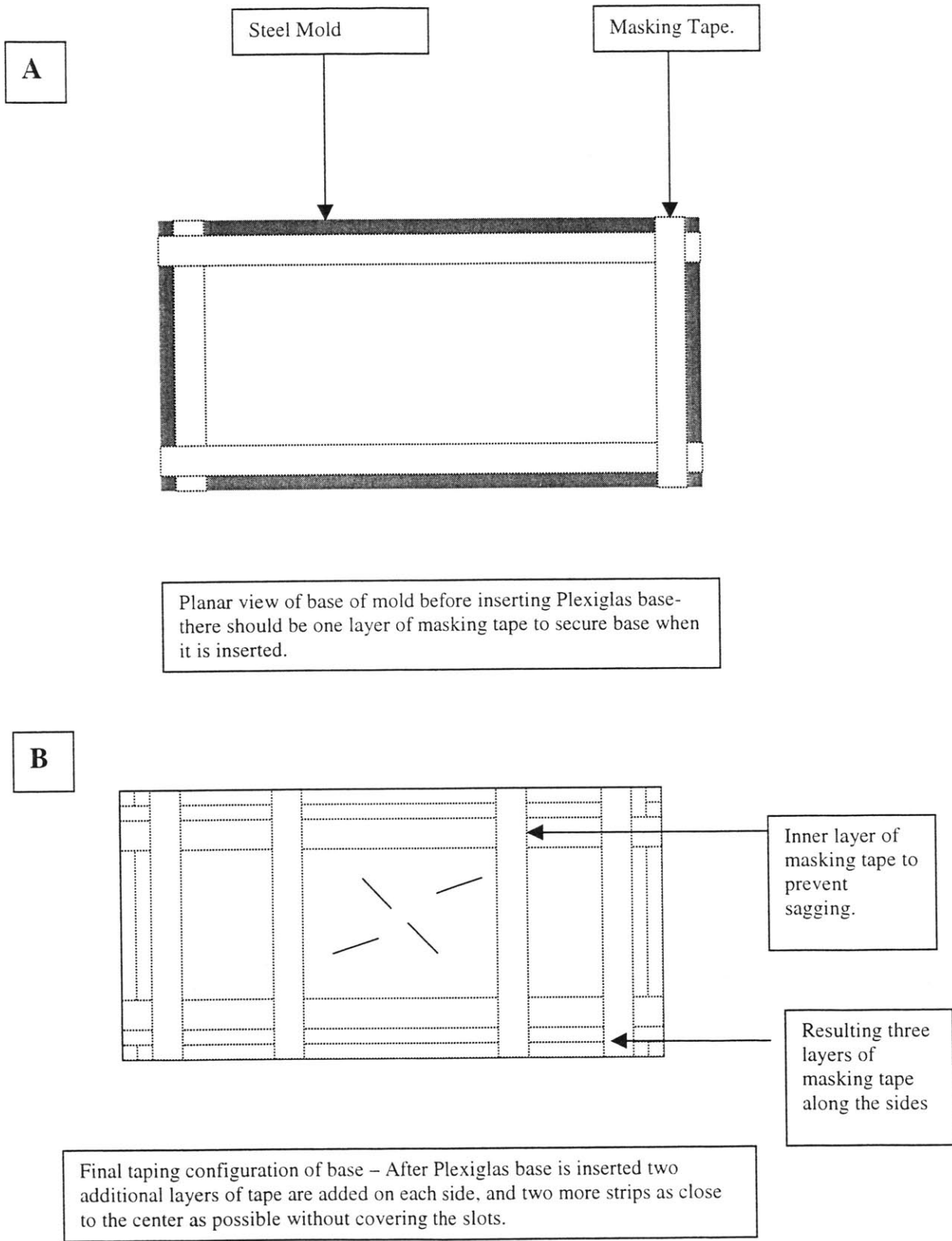


Figure A.2.7: Taping base of mold

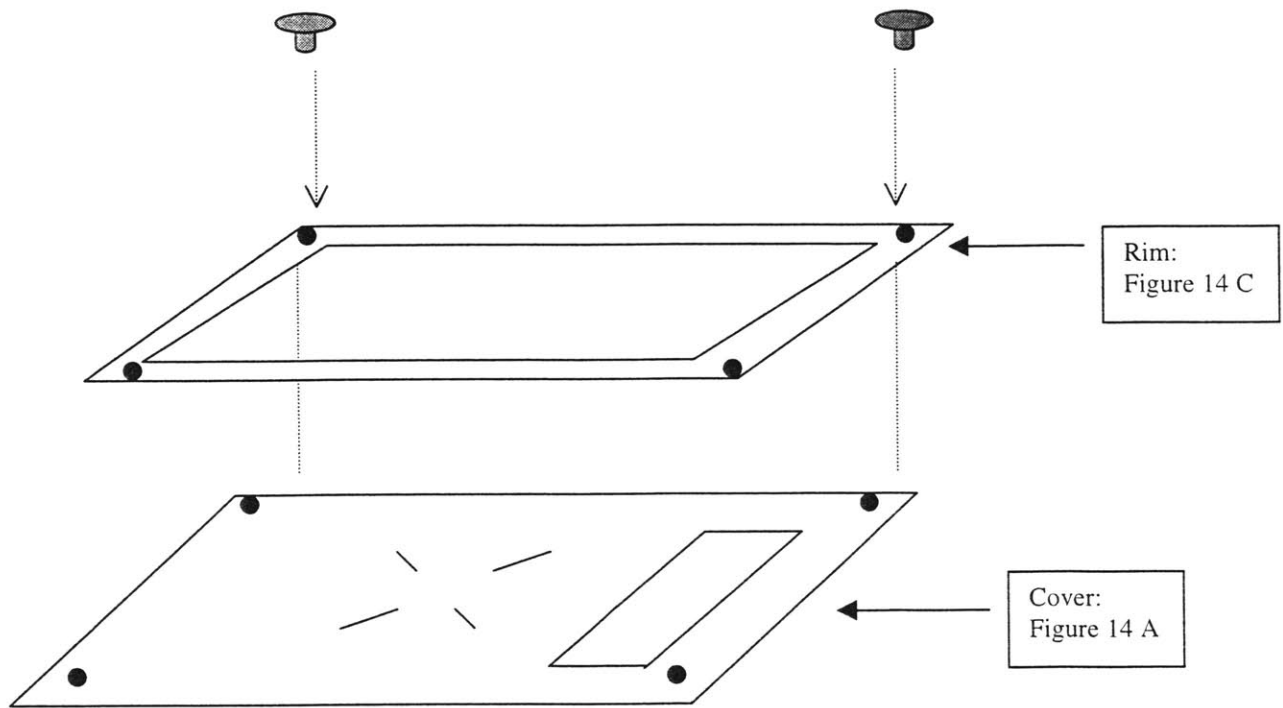


Figure A.2.8: Correct way to assemble Plexiglas covering

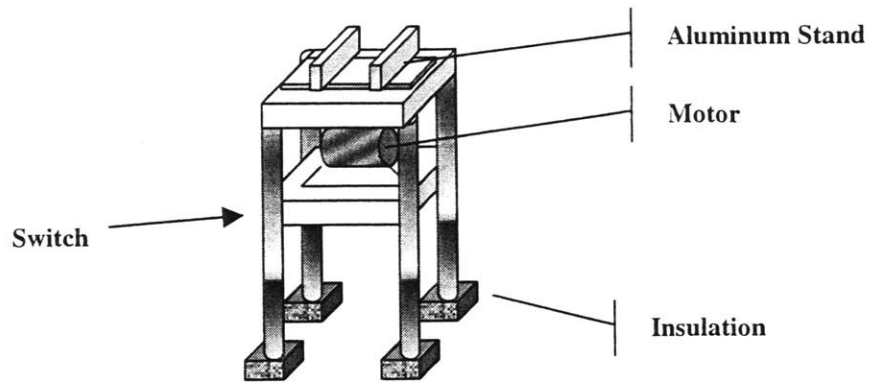


Figure A.2.9: Vibrating Table

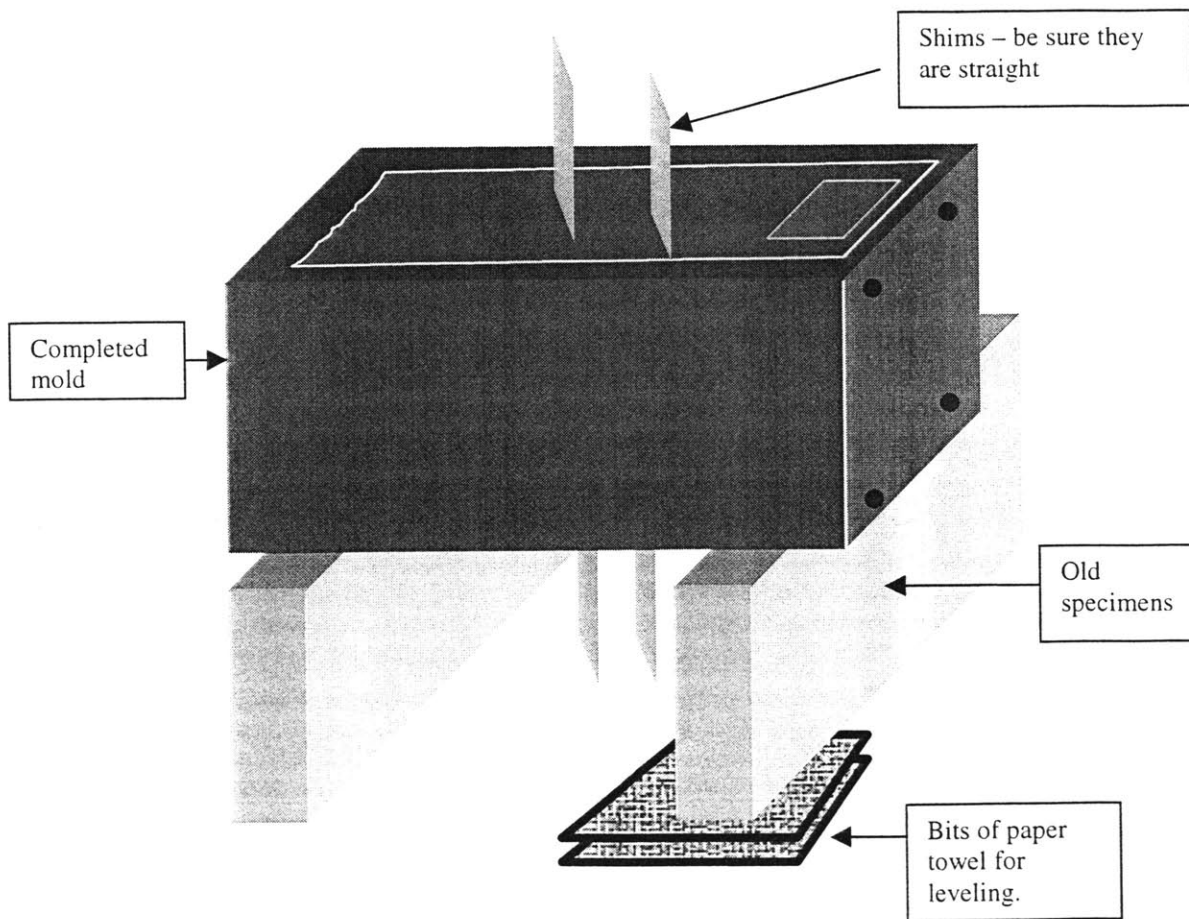


Figure A.2.10: Mold set to dry

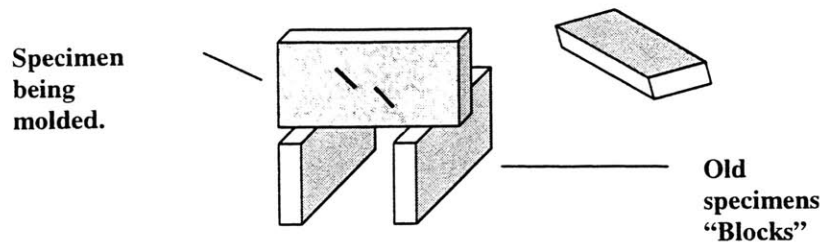


Figure A.2.11: Specimen set after unmolding

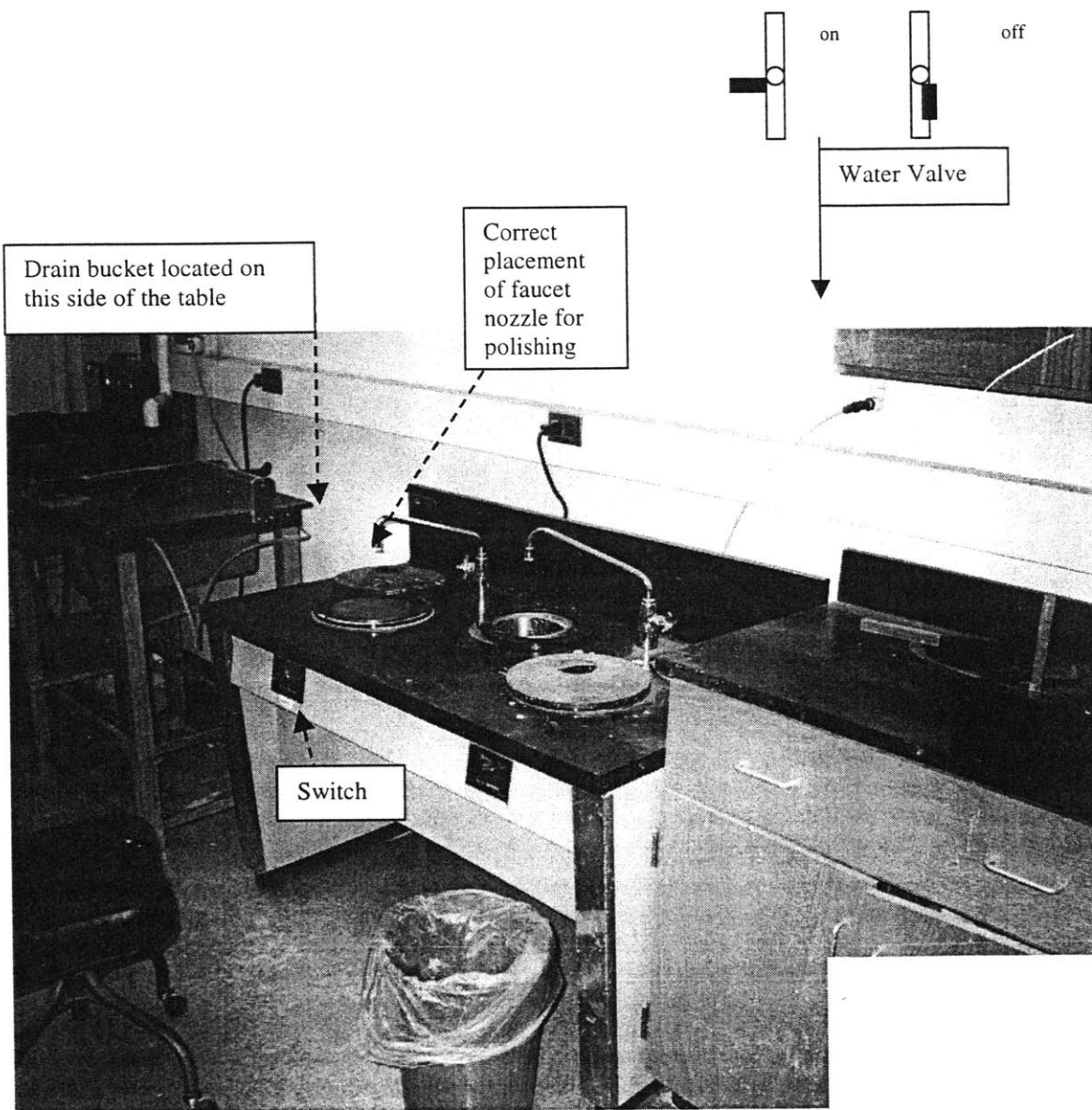
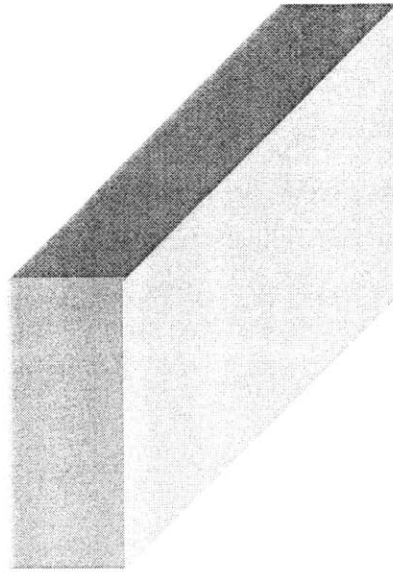


Figure A.2.12: Polishing Table



Correct

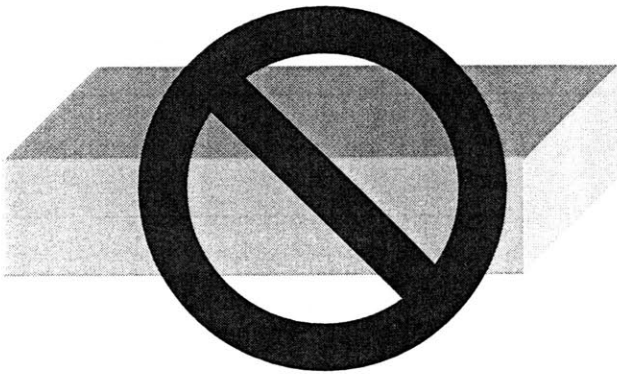


Figure A.2.13: How to place gypsum molds in the oven when curing

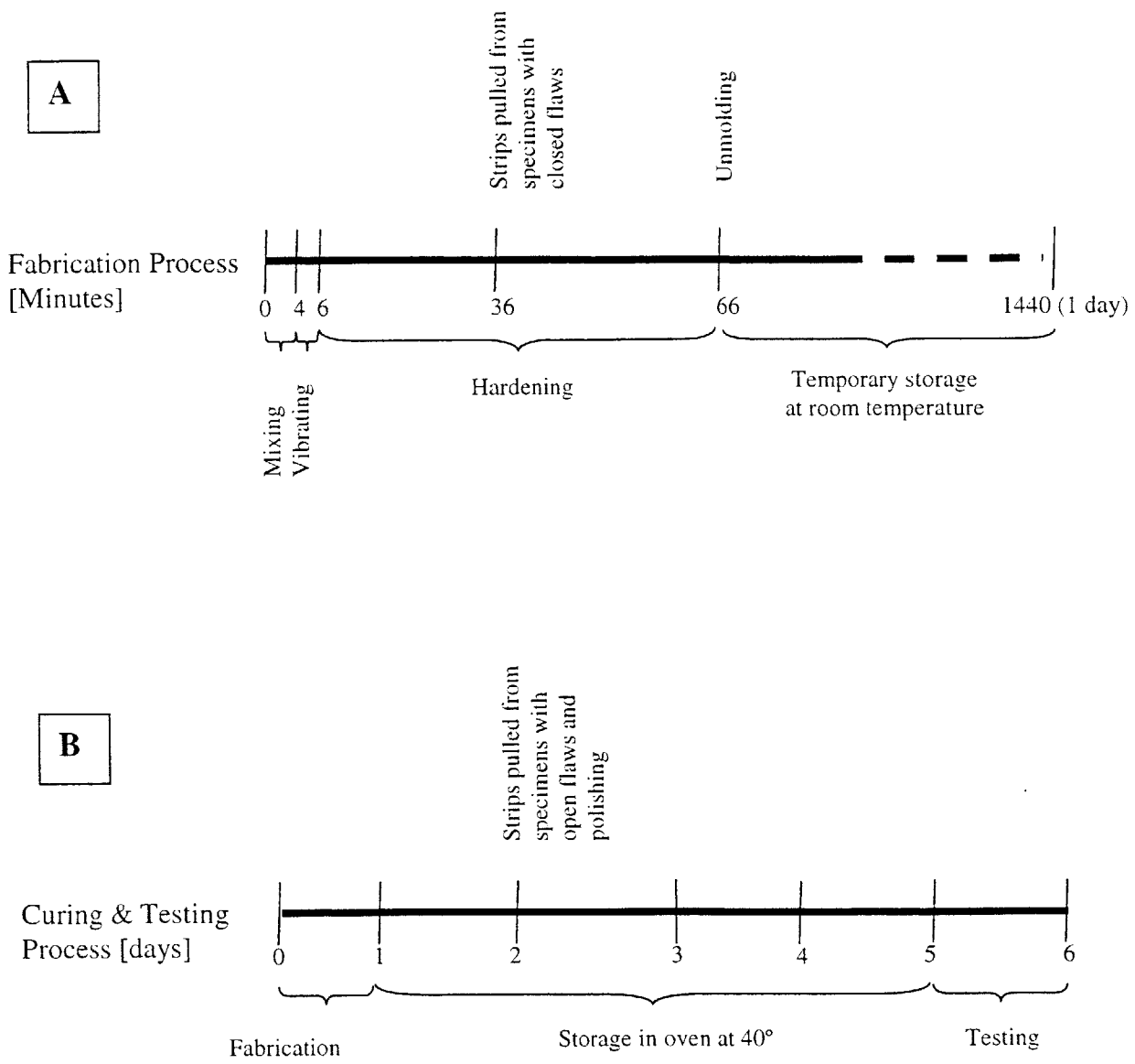


Figure A.2.14: Timelines for gypsum specimens fabrication, curing and testing.

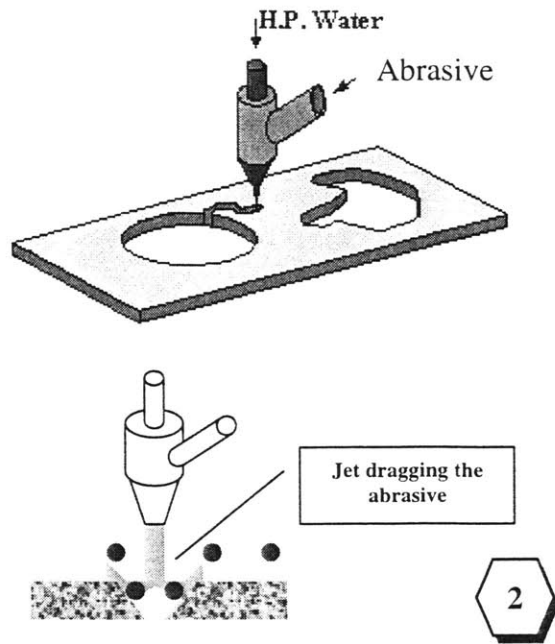
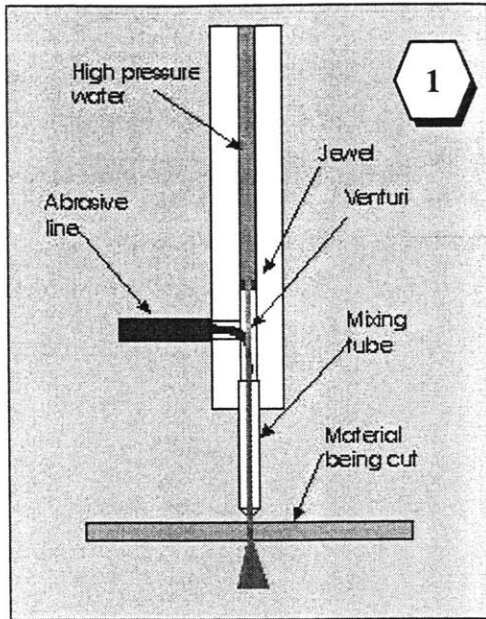


Figure A.3.1: Operation principle of a water-abrasive jet

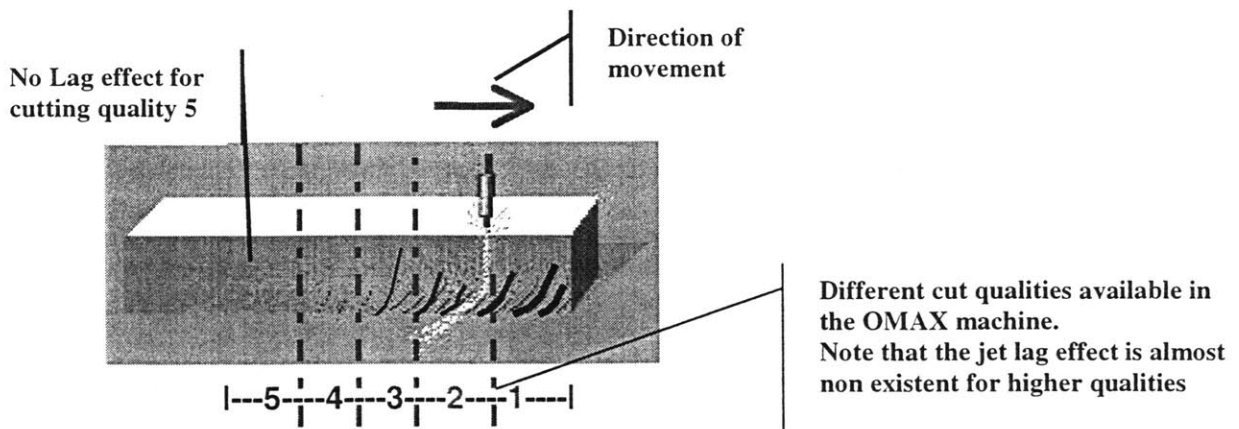


Figure A.3.2: Jet Lag defects

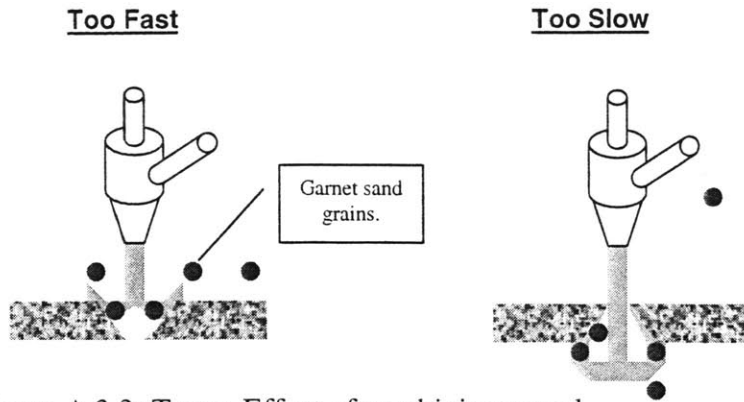


Figure A.3.3: Taper. Effect of machining speed

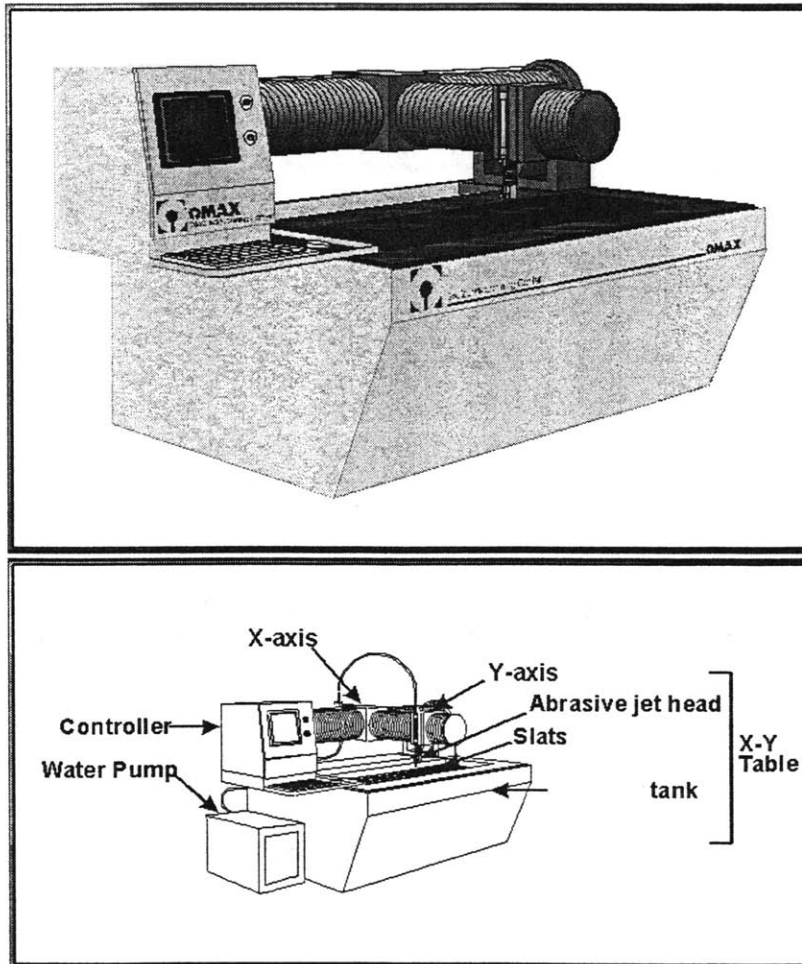


Figure A.3.4: Main parts of the OMAX water-abrasive jet

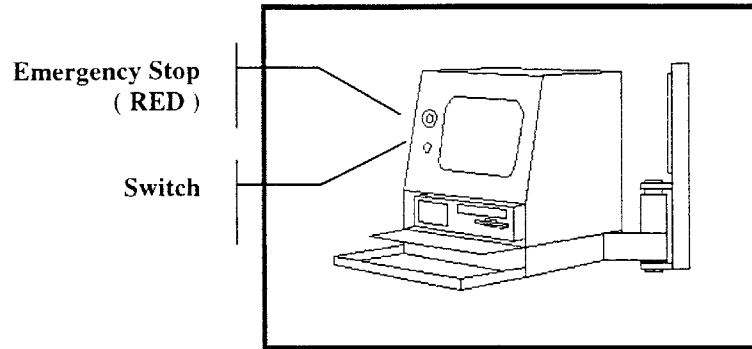


Figure A.3.5: OMAX Control System

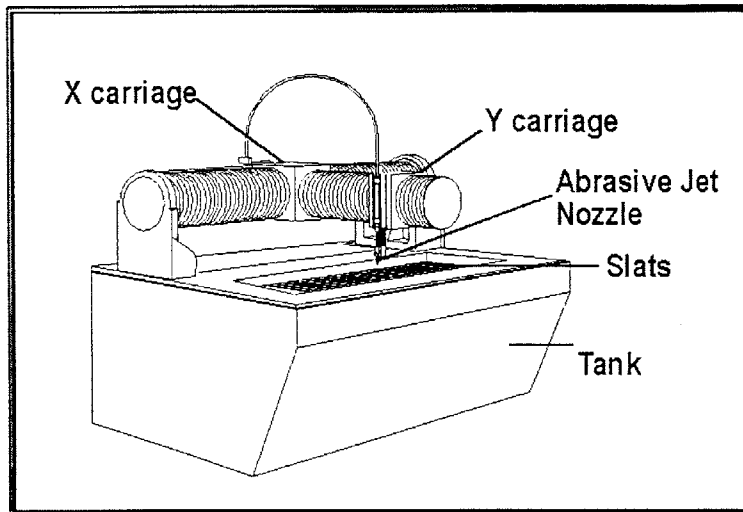


Figure A.3.6: Precision X-Y Table

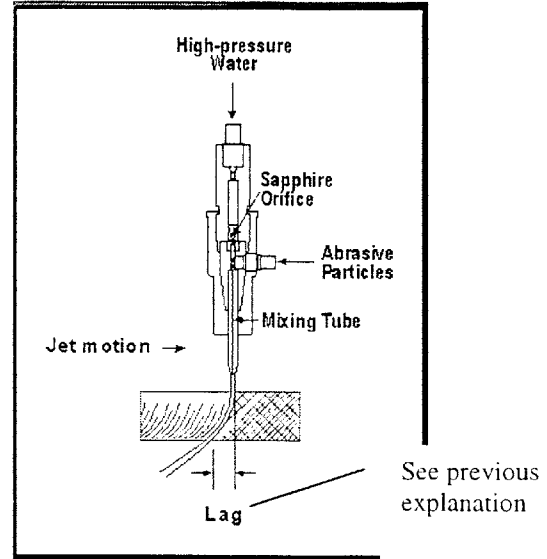
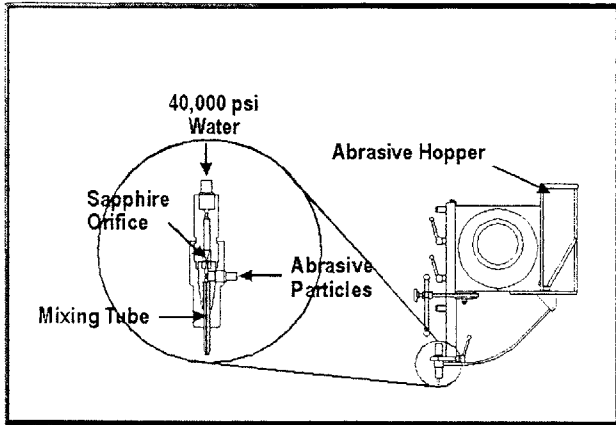
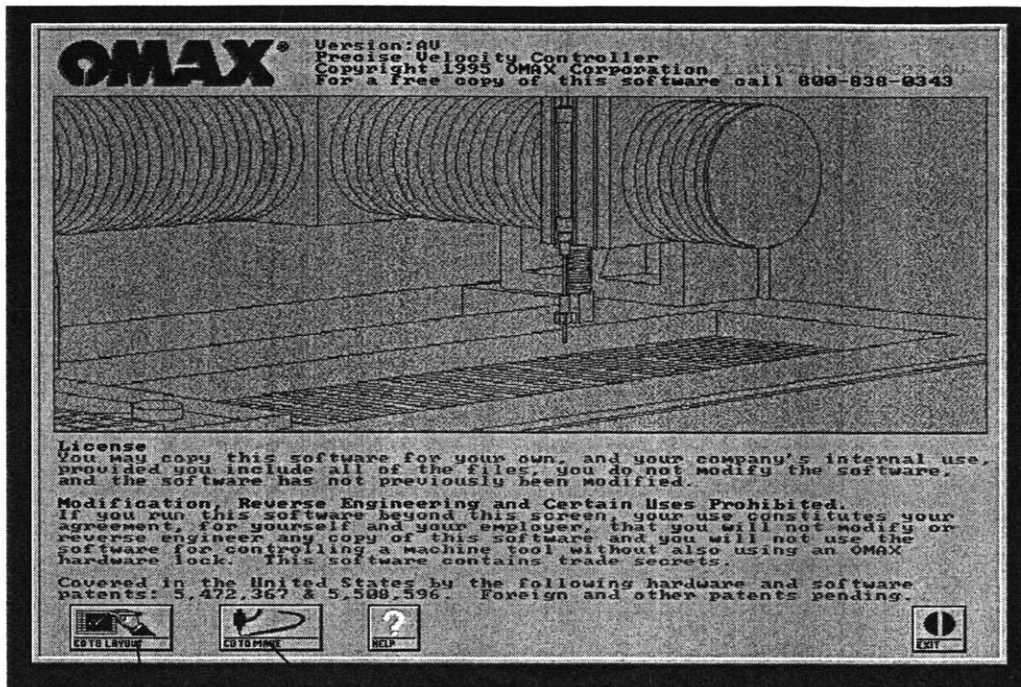


Figure A.3.7: Abrasive jet system



GO TO MAKE. Only use when the dxf file is done, the quality of the cut is set and the order file generated.

GO TO LAYOUT: Is the usual first step.

Figure A.3.8: Welcome screen on the water jet controller

Draw. (Here is just an example, not our specimen).

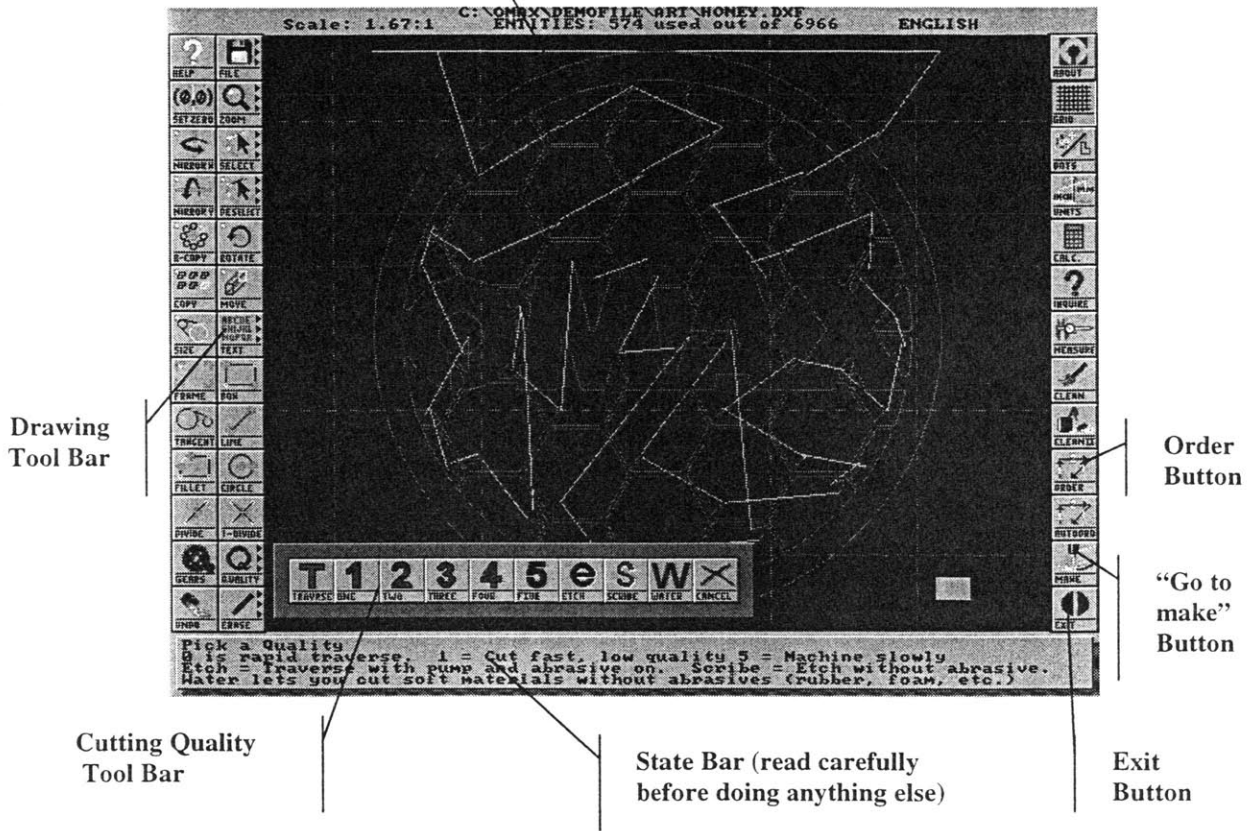


Figure A.3.9: Layout Screen on the water jet controller

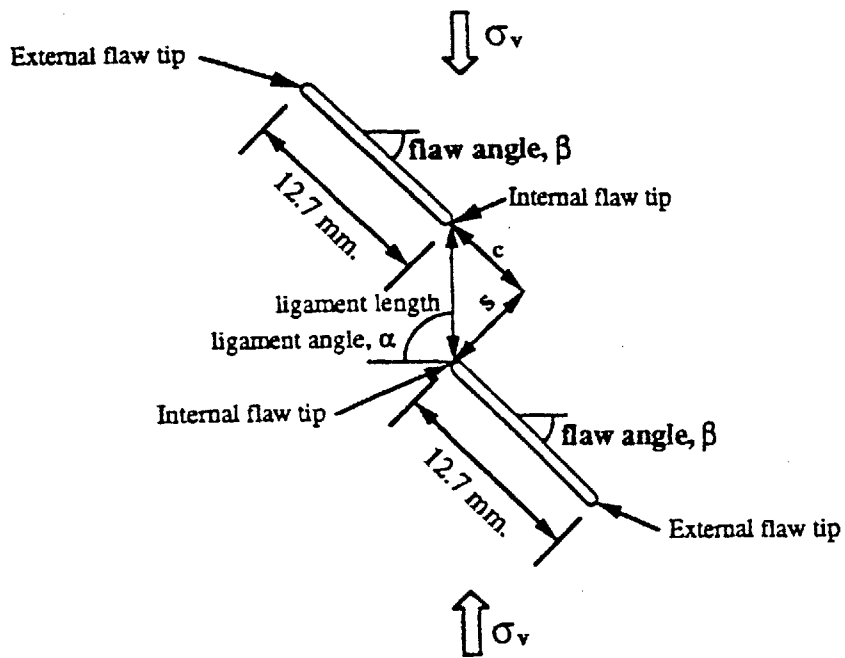
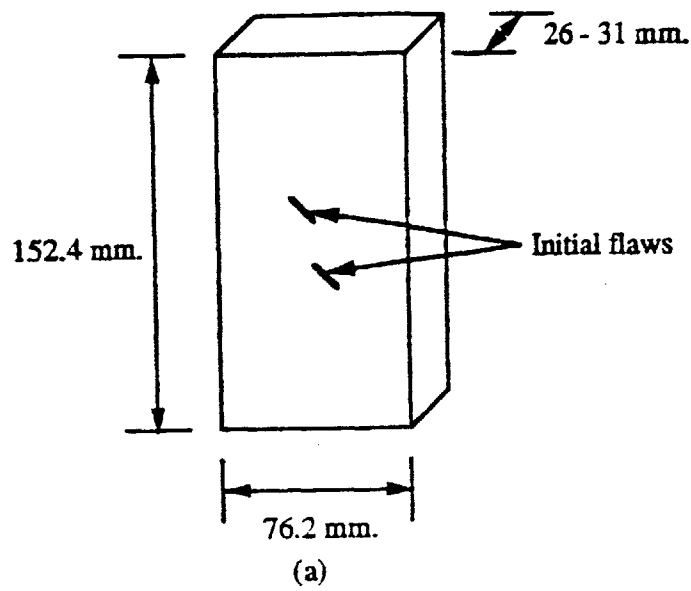


Figure A.3.10: Notation used to identify geometry, after Bobet (1997)

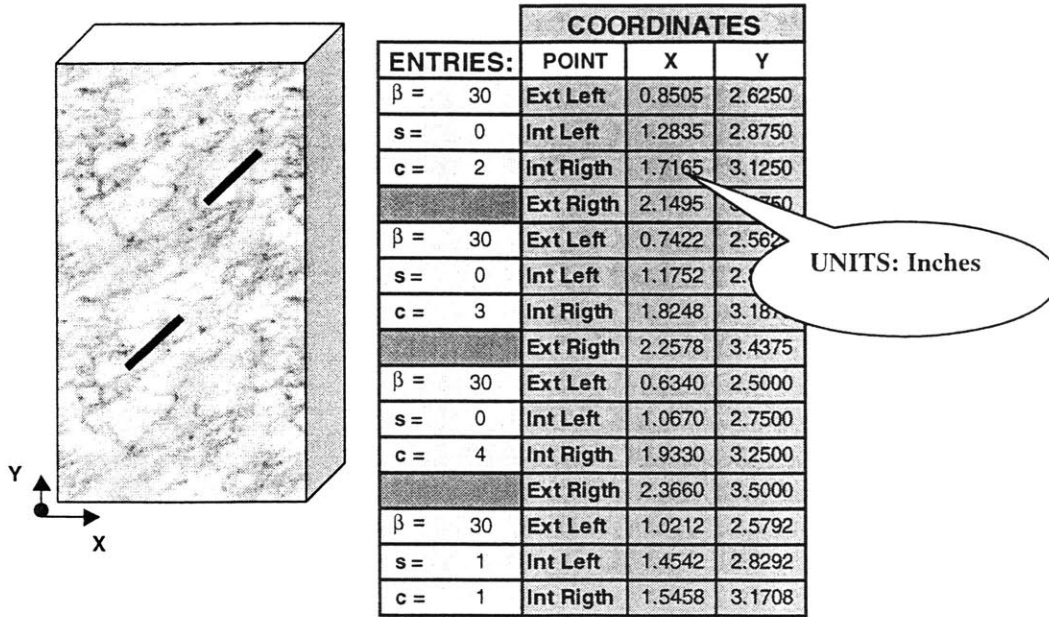


Figure A.3.11: Spreadsheet done to compute the flaw tips coordinates

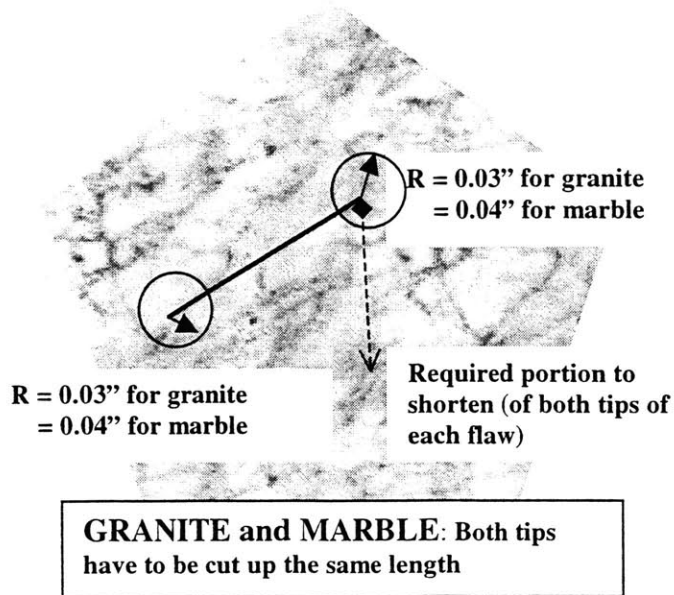


Figure A.3.12: Correction of the flaw length for granite and marble

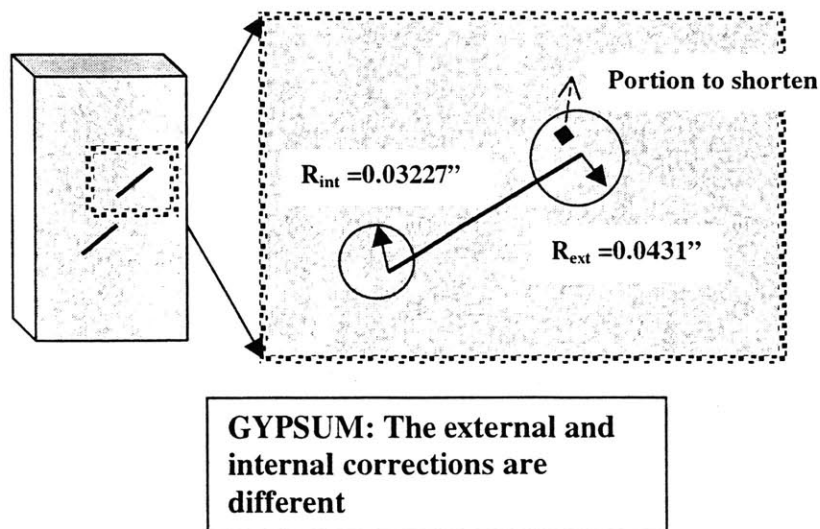


Figure A.3.13: Correction of the flaw length for gypsum.

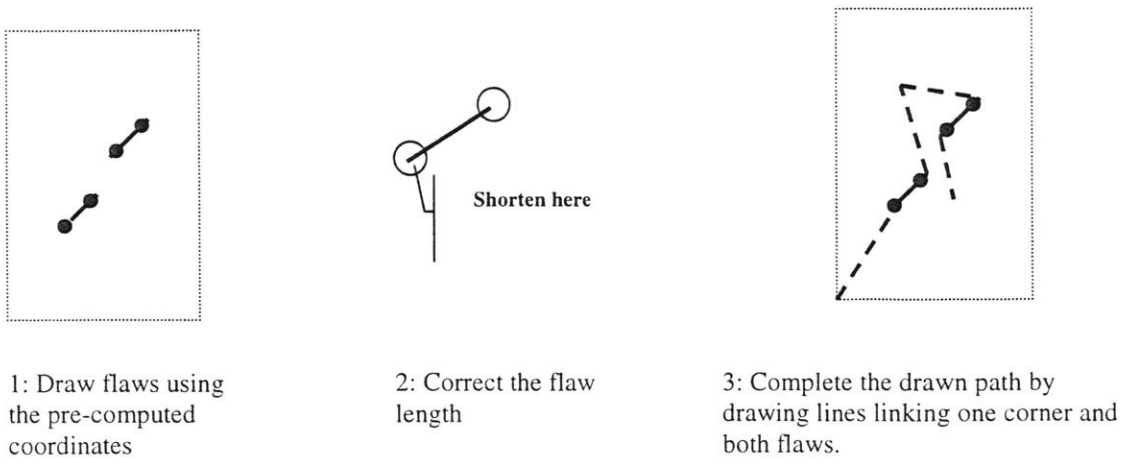


Figure A.3.14: Summary of the necessary steps to draw the geometry

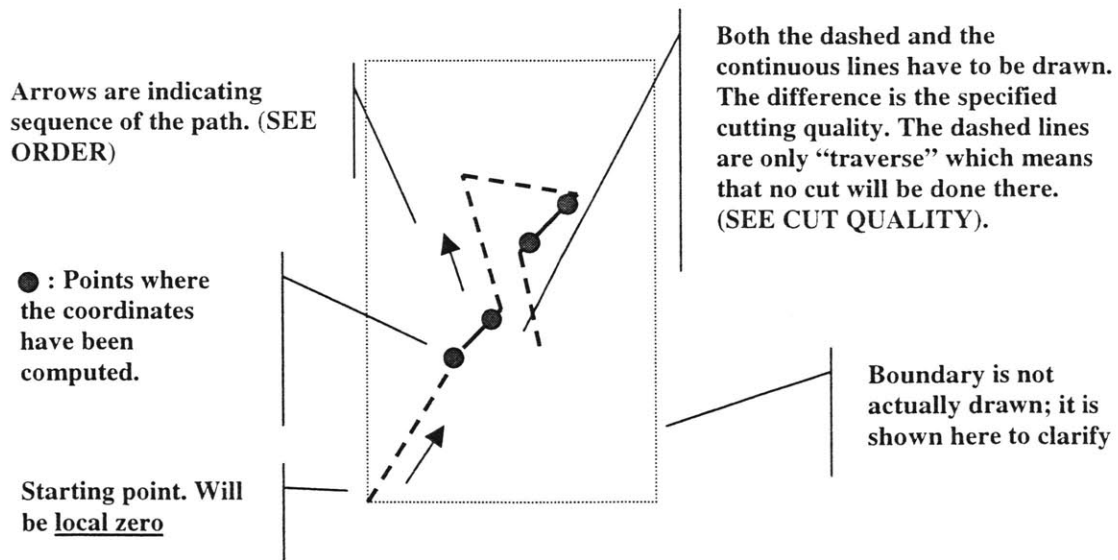


Figure A.3.15: Typical cut path finished

Note
recommended
workability
for granite
= 322

THICKNESS:
Enter 2.75"

MACHINEABILITY:
Enter 90

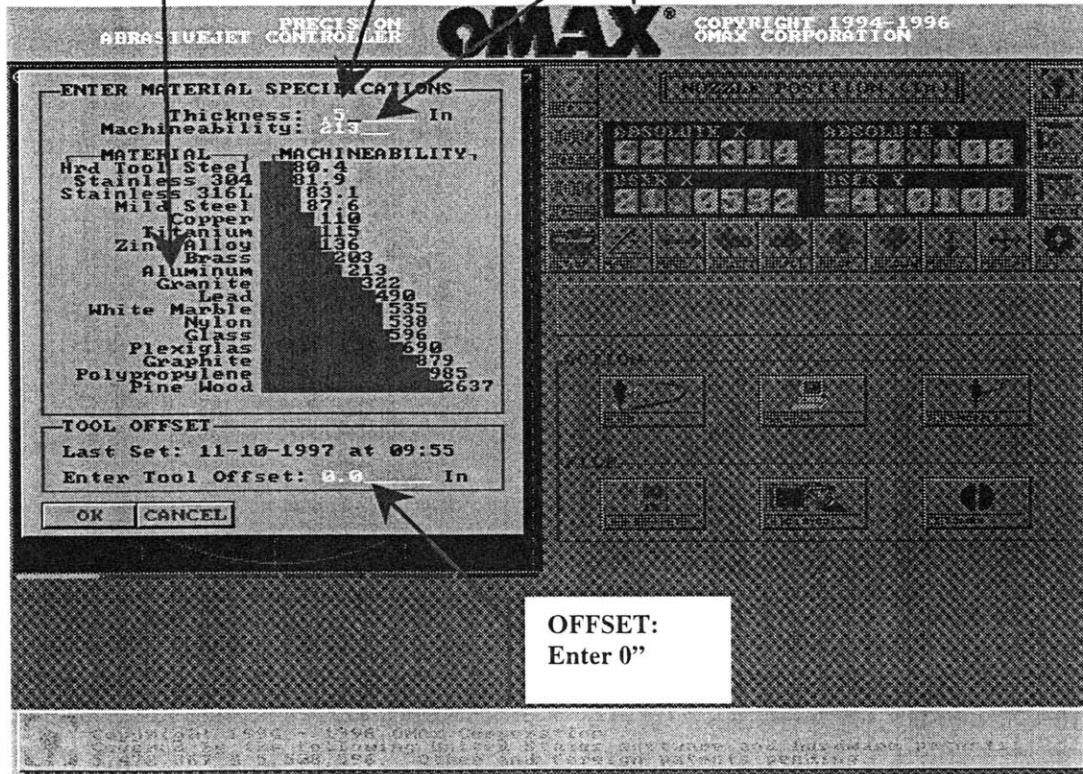


Figure A.3.16: Setting Screen in the water jet controller

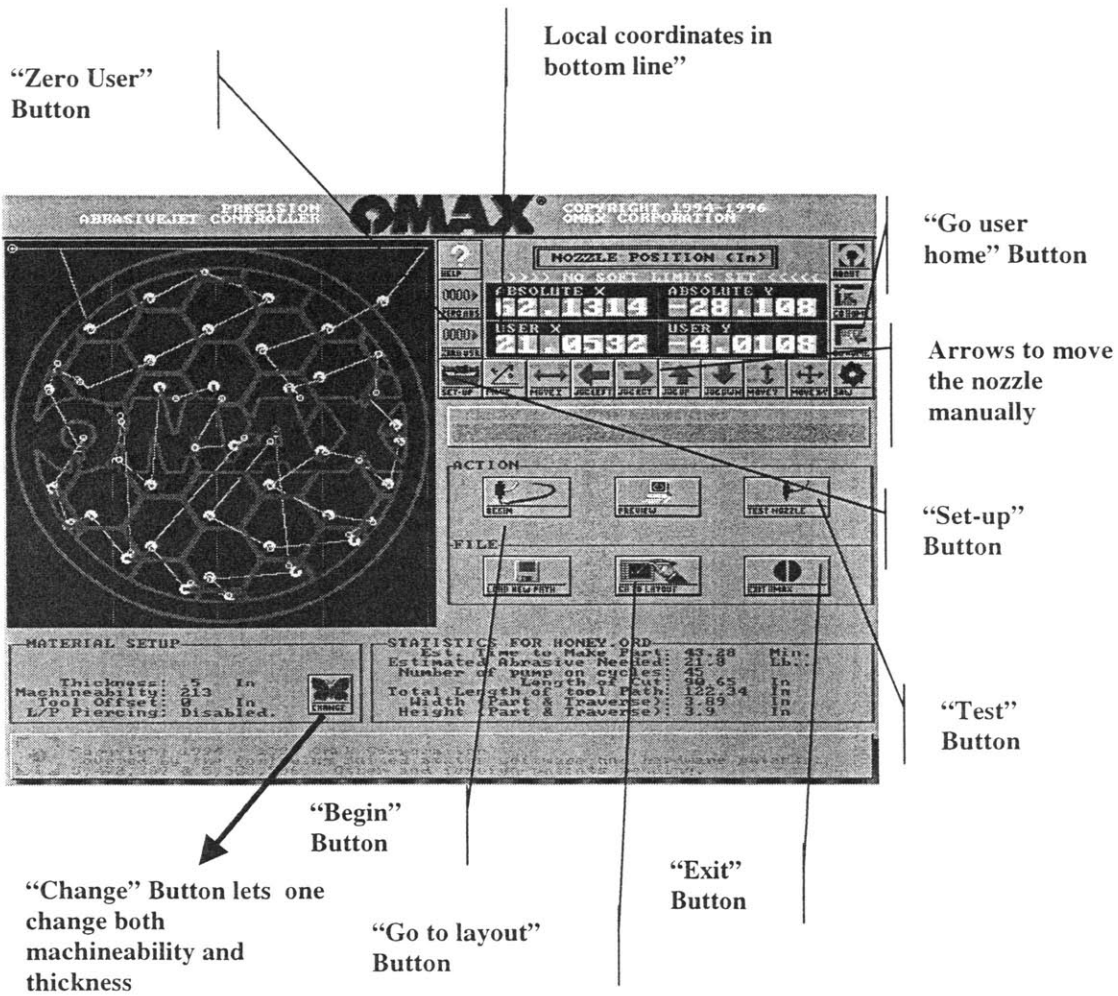


Figure A.3.17: "Make" Screen on the water jet controller

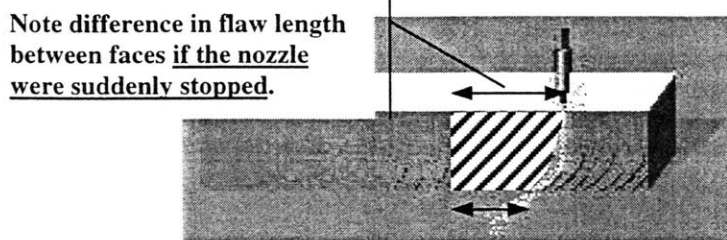


Figure A.3.18: Correction of the lag effect by setting an "Off Delay"

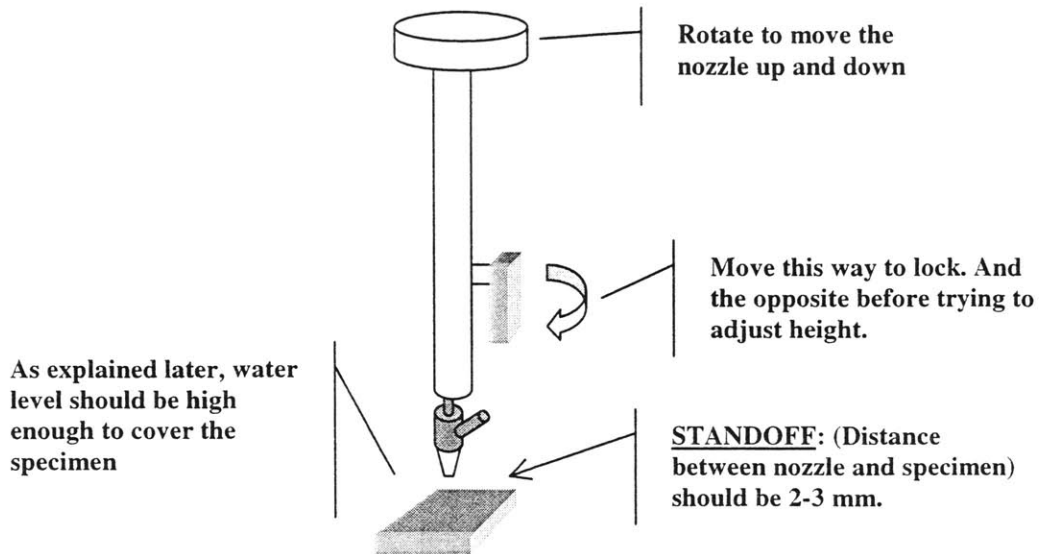


Figure A.3.19: Adjusting the height of the nozzle (Standoff Distance)

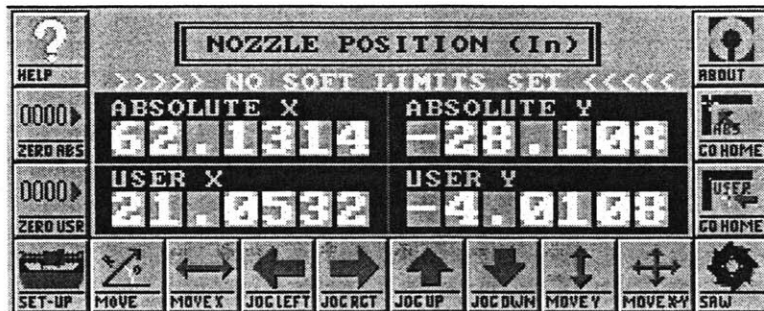


Figure A.3.20: Buttons on the “Make” Screen used to coordinate the actual position of the specimen in the X-Y table and the drawing

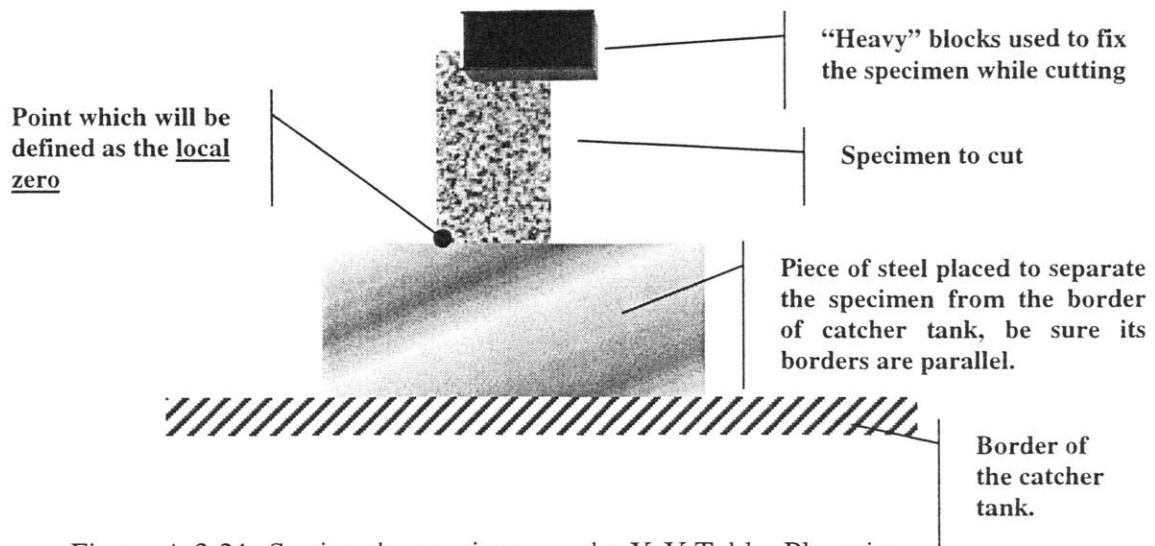


Figure A.3.21: Setting the specimen on the X-Y Table. Plan view

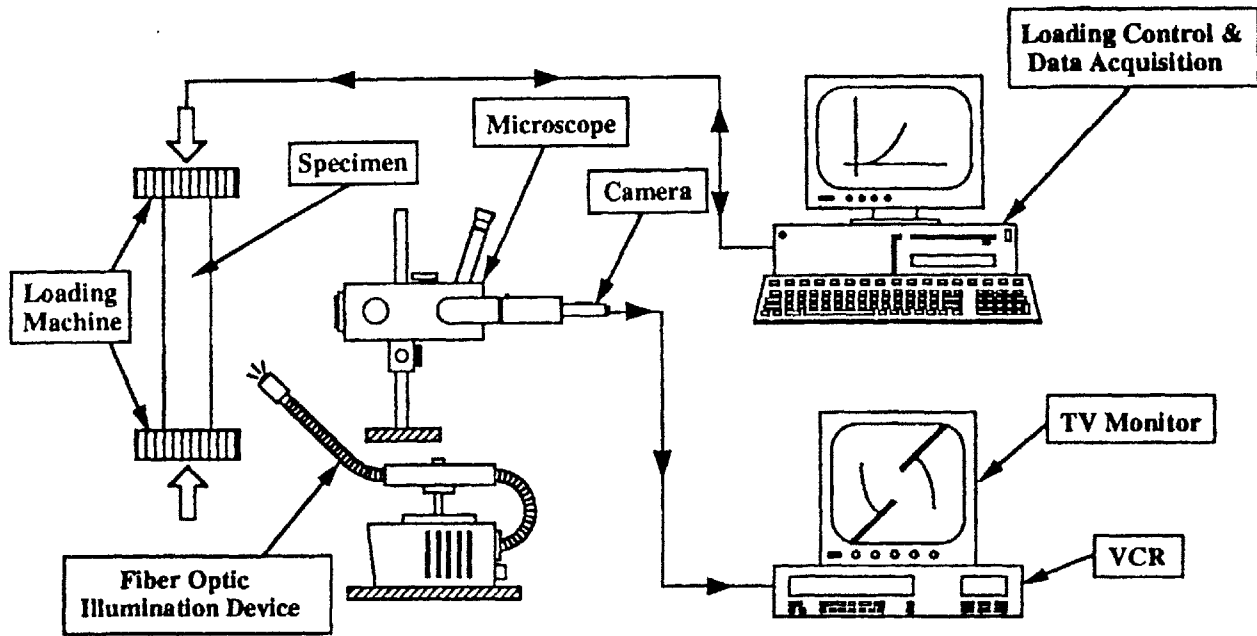


Figure A.4.1: Schematic of the set-up for loading test, after Bobet (1997)

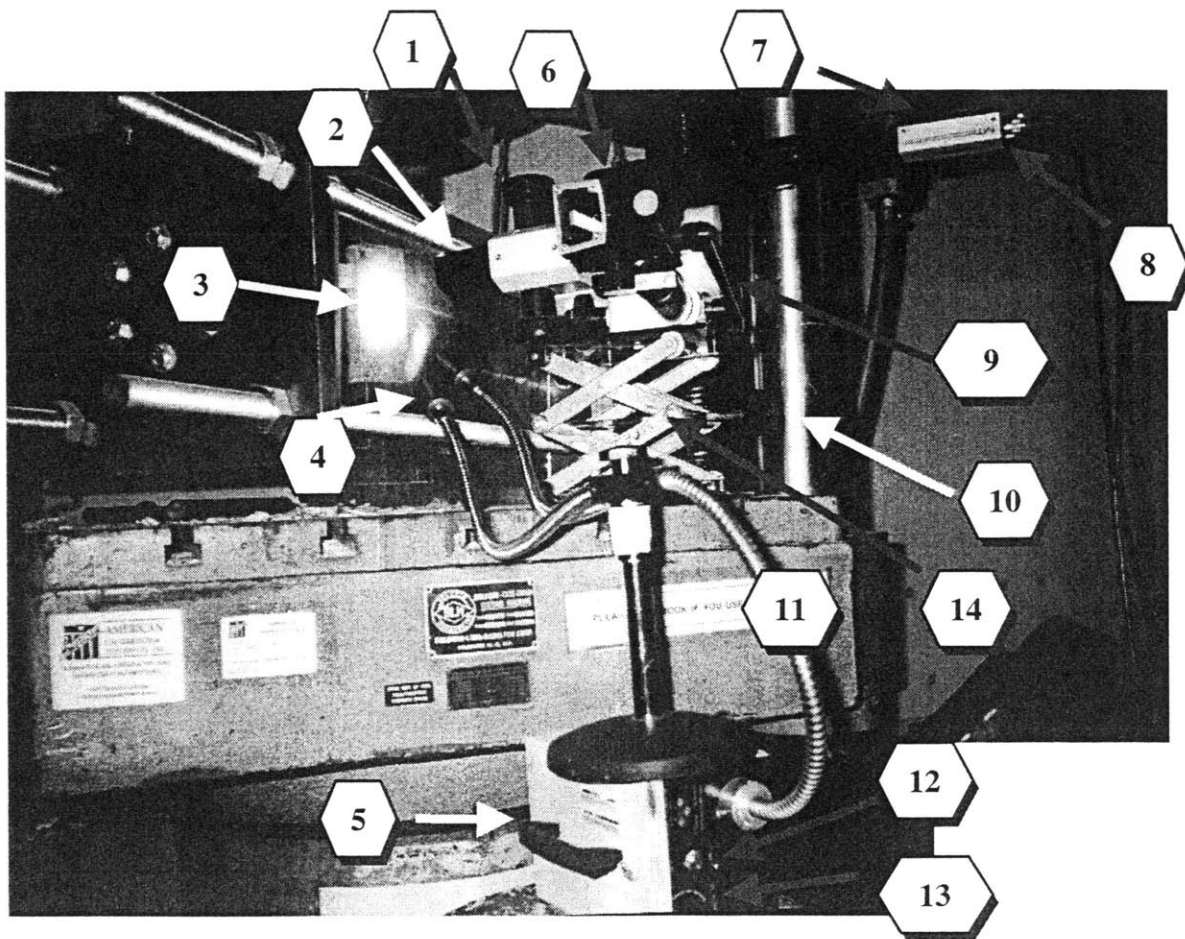


Figure A.4.2: Detail of the Loading Test Set-up

- 1 Focus control of the microscope
- 2 Low power microscope
- 3 Specimen. (granite in this picture)
- 4 Fiber Optic. (There are 2 of them; one per flaw)
- 5 Base of light
- 6 Control of microscope amplification (barely visible)
- 7 Video Camera
- 8 Connections (One to the V.C.R, and one to Power)
- 9 Knob to move the platform horizontally (it's on the not visible side)
- 10 Knob to move the platform vertically
- 11 Flexible connection of the lights to their base
- 12 Switch of the light system.
- 13 Intensity control (set it at maximum when testing granite)
- 14 Platform

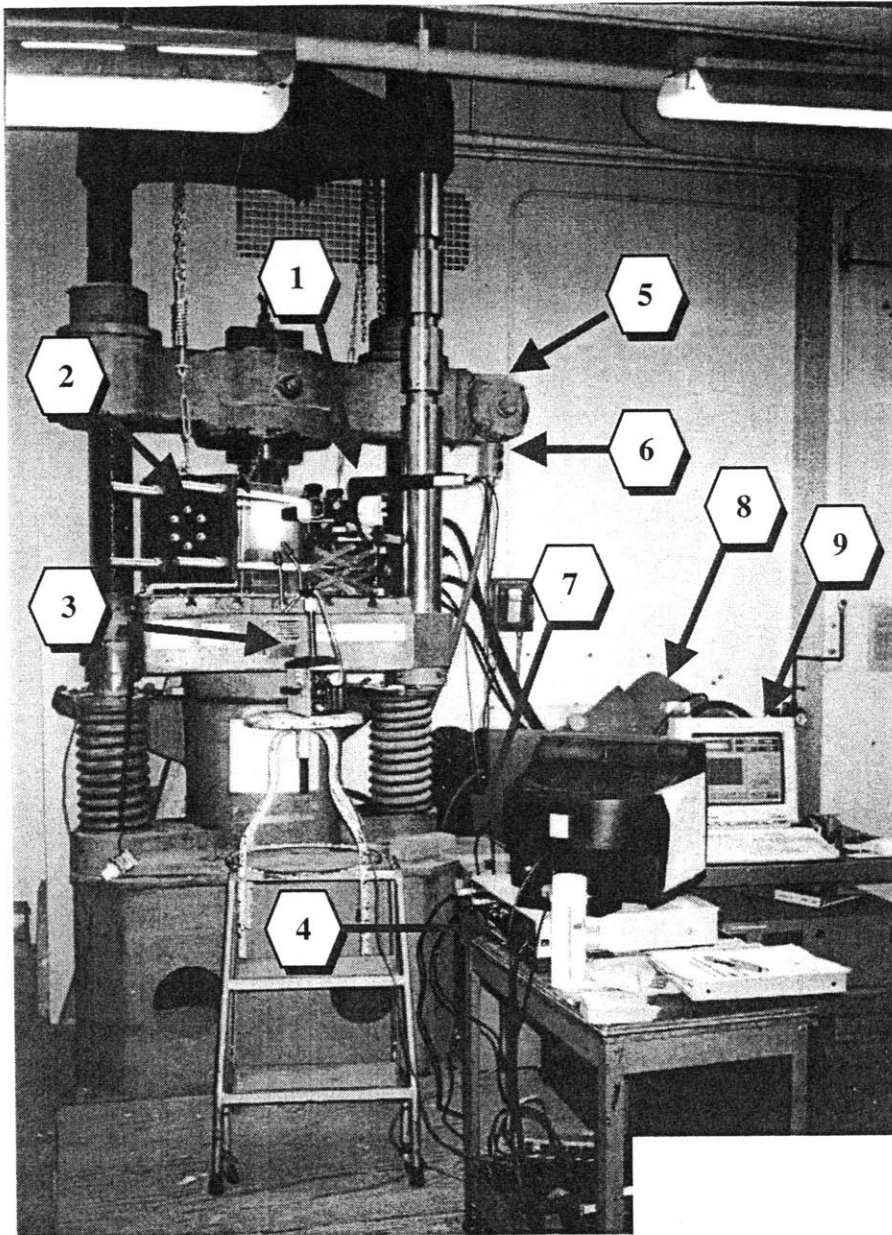


Figure A.4.3: Set-up for loading test

- 1 Camera and Microscope on their Platform
- 2 Frame for horizontal loading (not being used right now)
- 3 Optic fiber light system (lights over their base)
- 4 TV and VCR cart
- 5 Electric motor to move the upper head
- 6 Control switch of the electric motor (up and down)
- 7 General Switch
- 8 Pump, which provides the oil pressure for the loading machine
- 9 P.C. that controls the loading machine. It is displaying a force vs. displacement chart

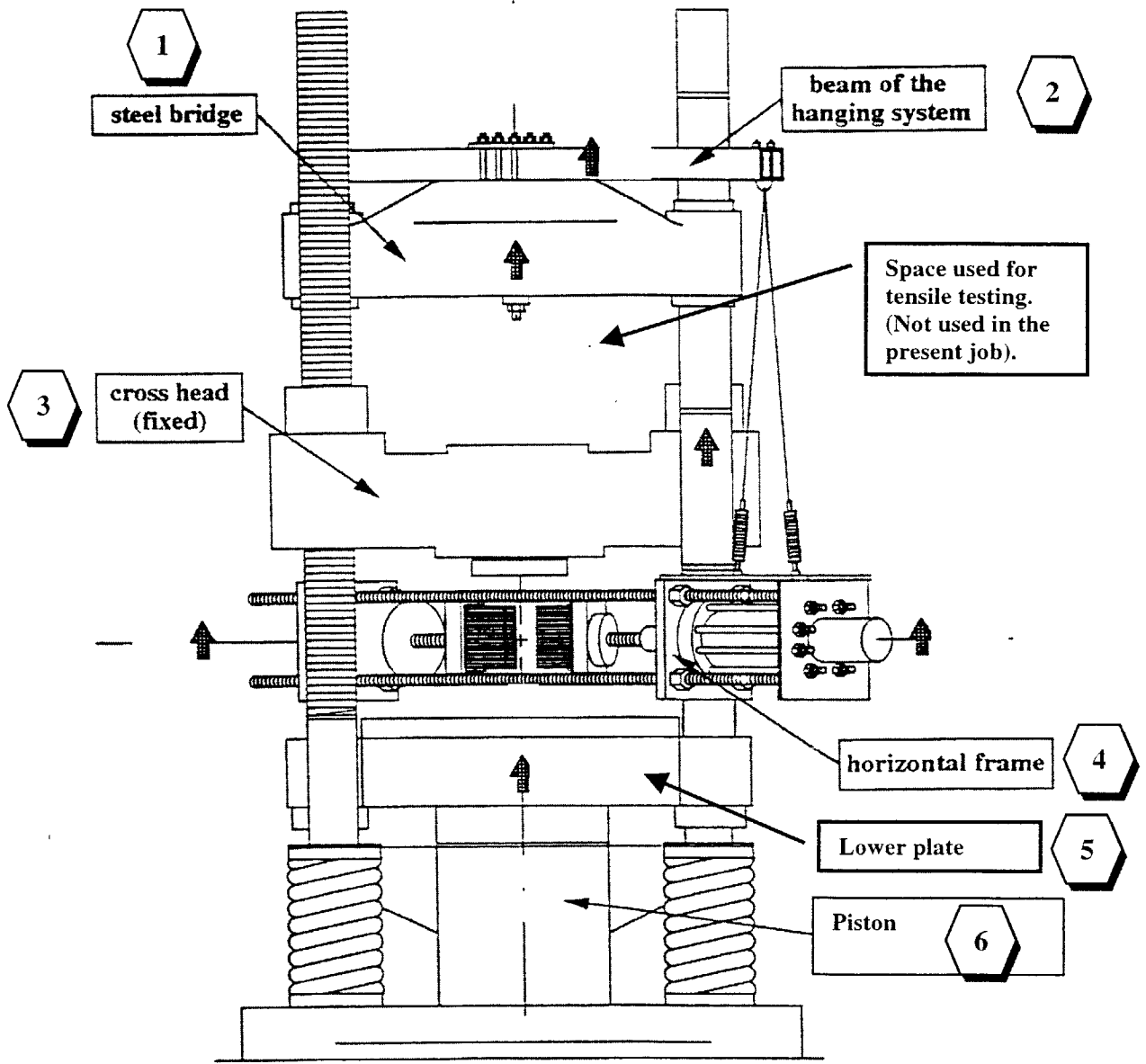


Figure A.4.4A: Load Testing Machine. Movement of the different parts when testing After Bobet (1997)

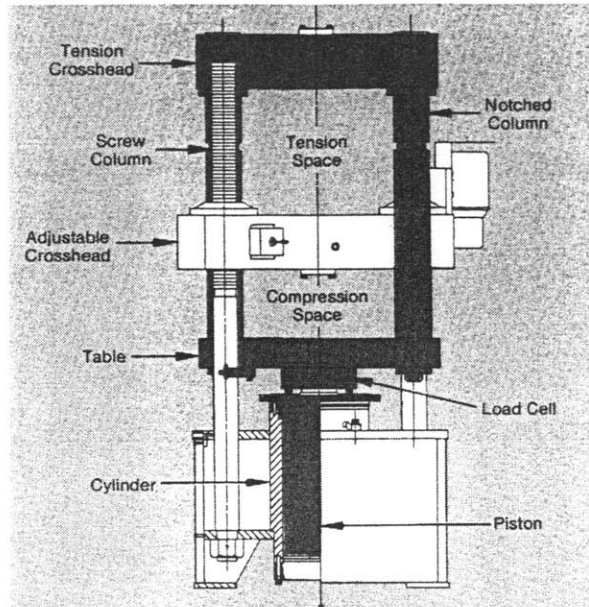


Figure A.4.4B: Main component of a universal loading machine, from SATEC catalogue

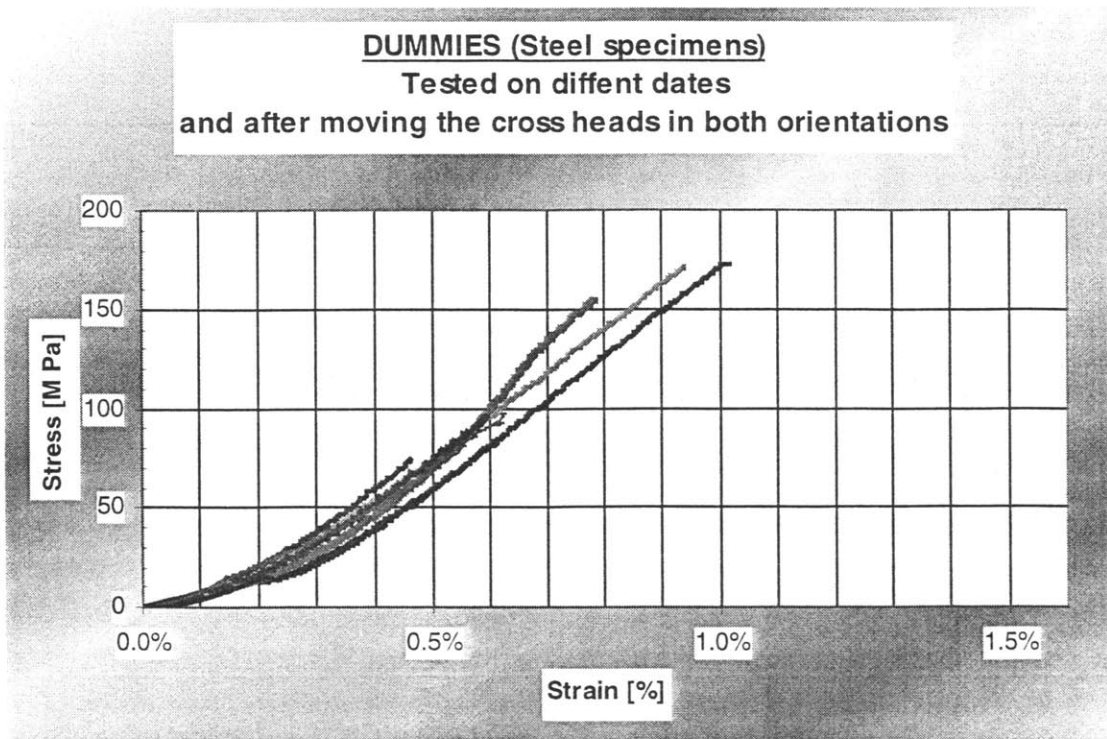


Figure A.4.5: Data collected on compression tests run on a dummy (steel piece). Note difference in machine compressibility among the different tests

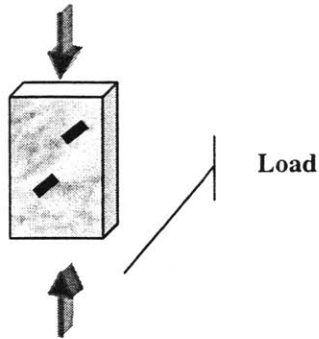


Figure A.4.6: Direction of the load in uniaxial testing

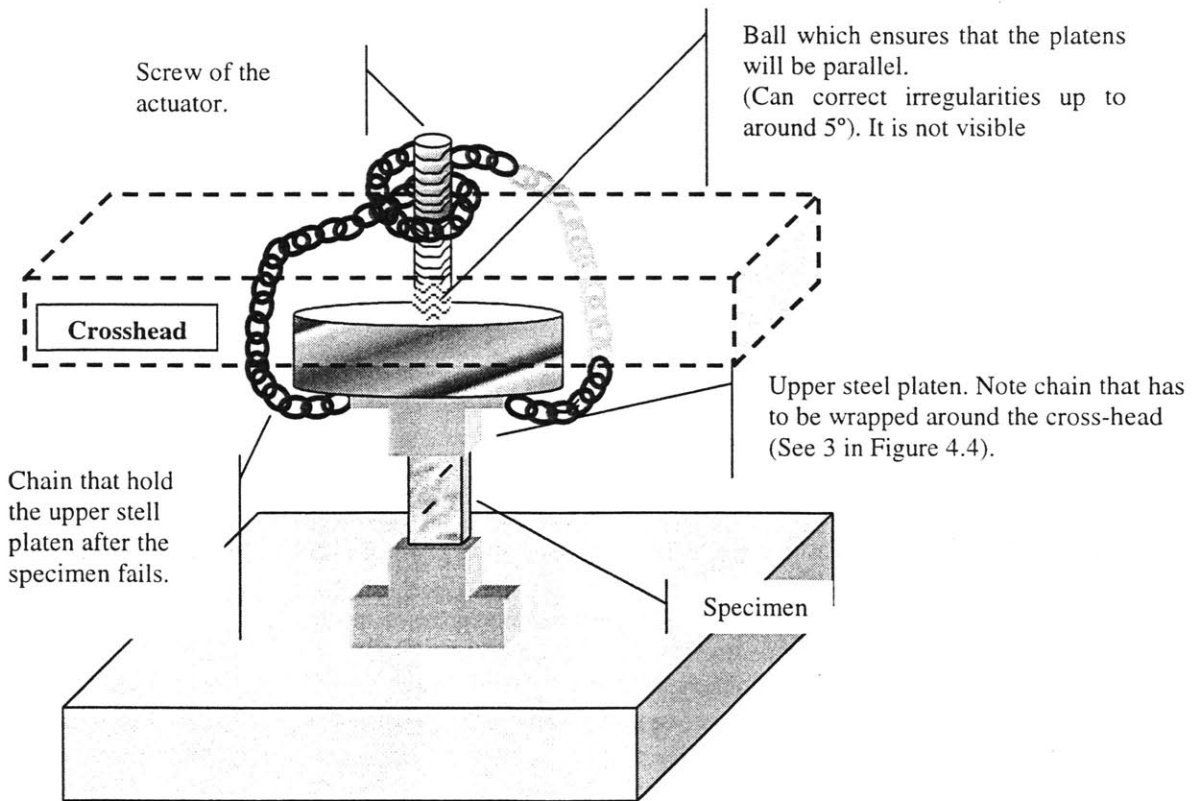


Figure A.4.7: Set-up of specimen and steel platens for uniaxial load testing

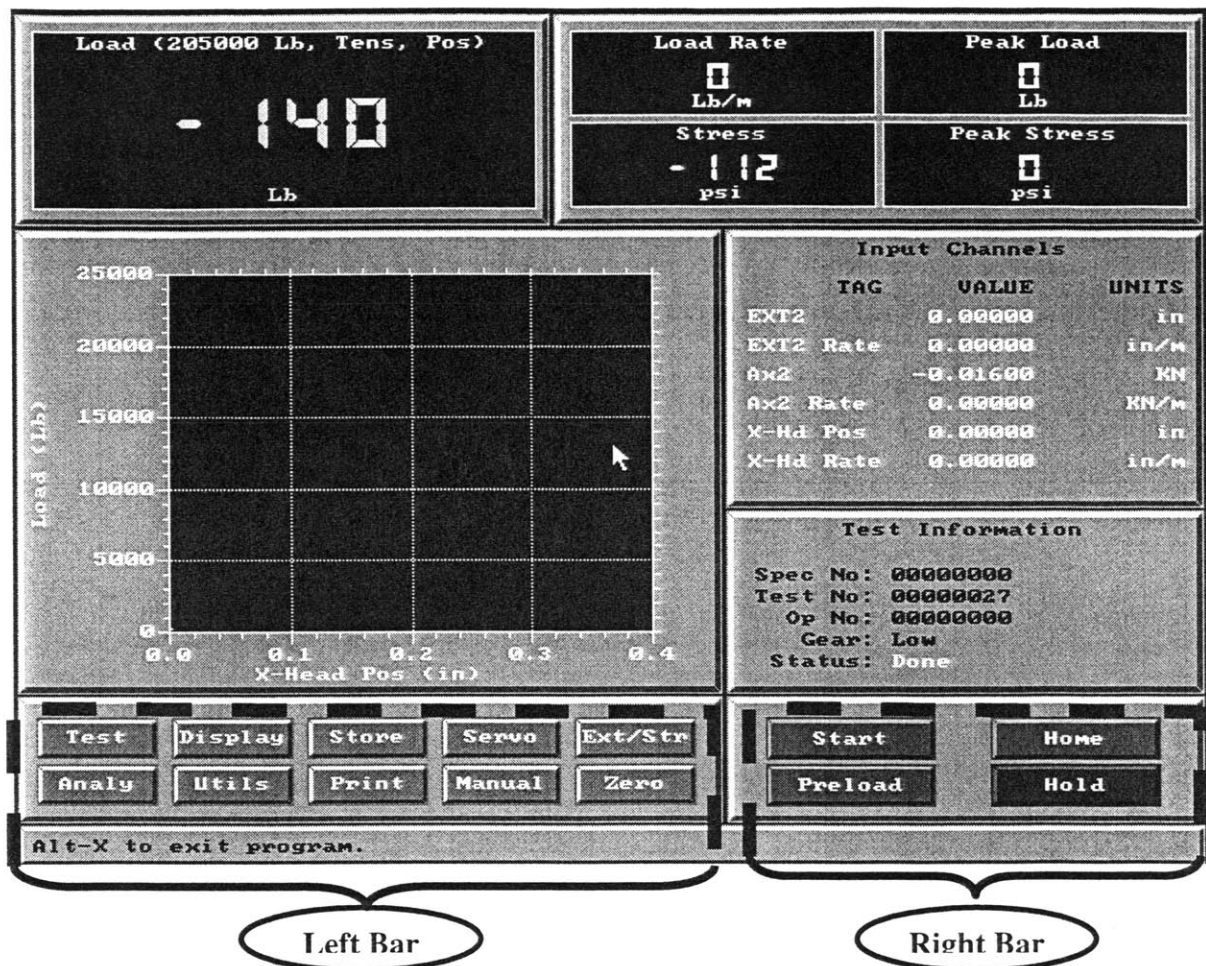


Figure A.4.8: MTEST2 screen (the chart has the appropriate scale for gypsum)

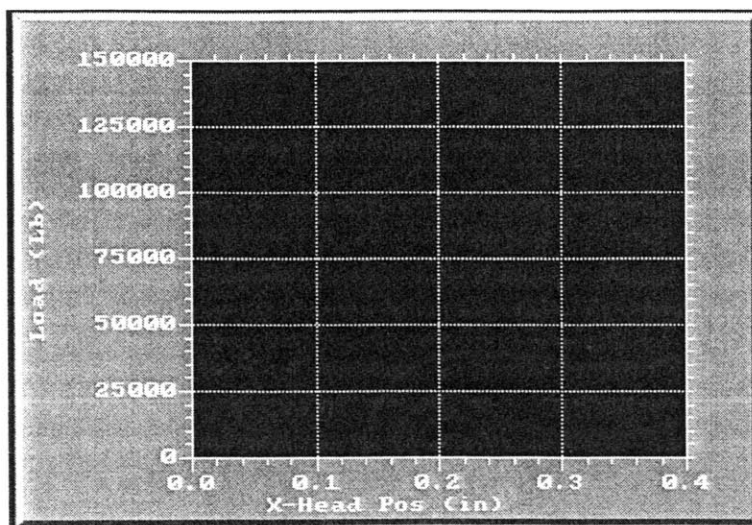


Figure A.4.9: MTEST2 chart area (set for testing granite)

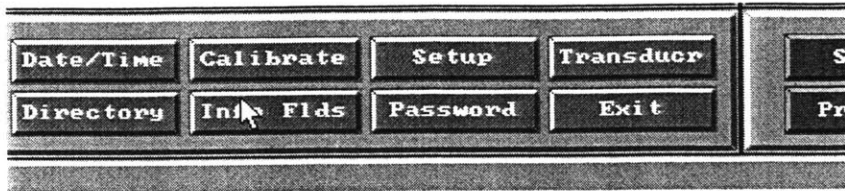


Figure A.4.10: Left bar after pressing "Utils"

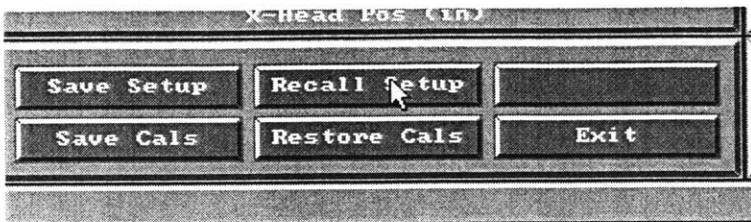


Figure A.4.11: Left bar after pressing "Setup"

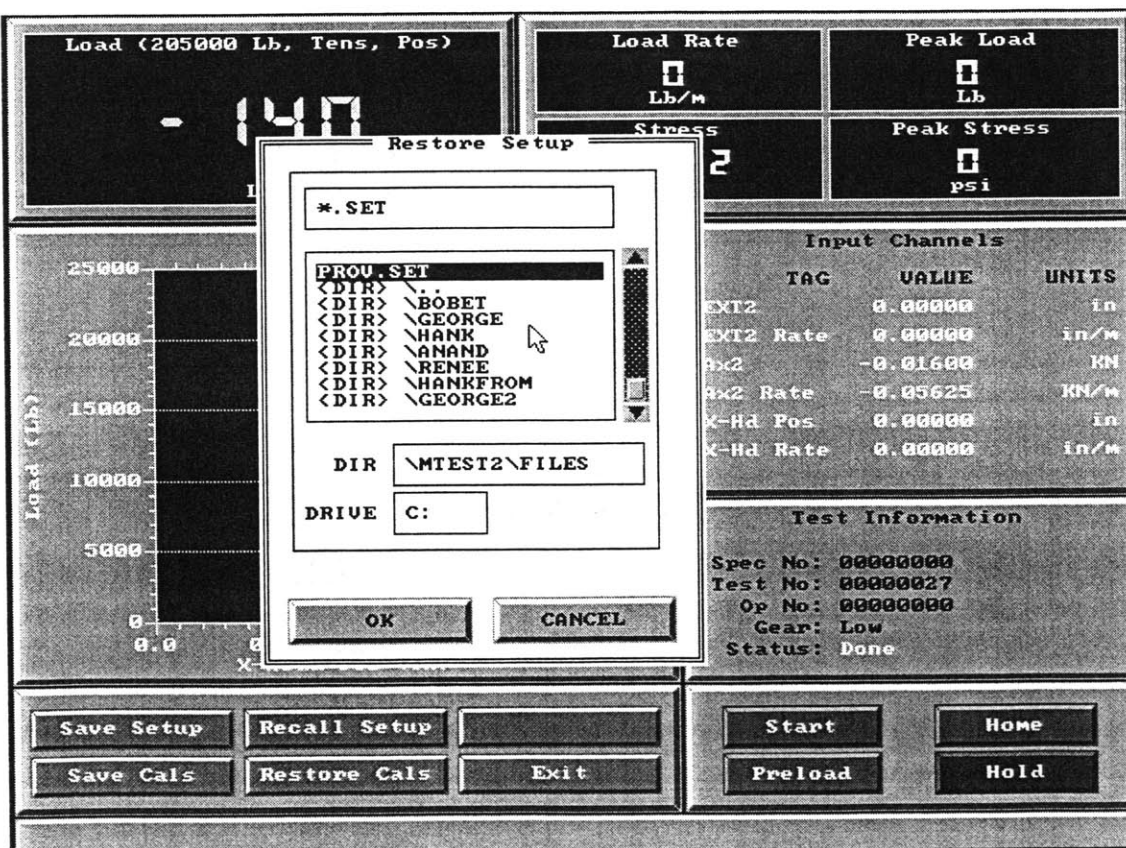


Figure A.4.12: New window that appears to search for the setting file after pressing "Recall Setup"

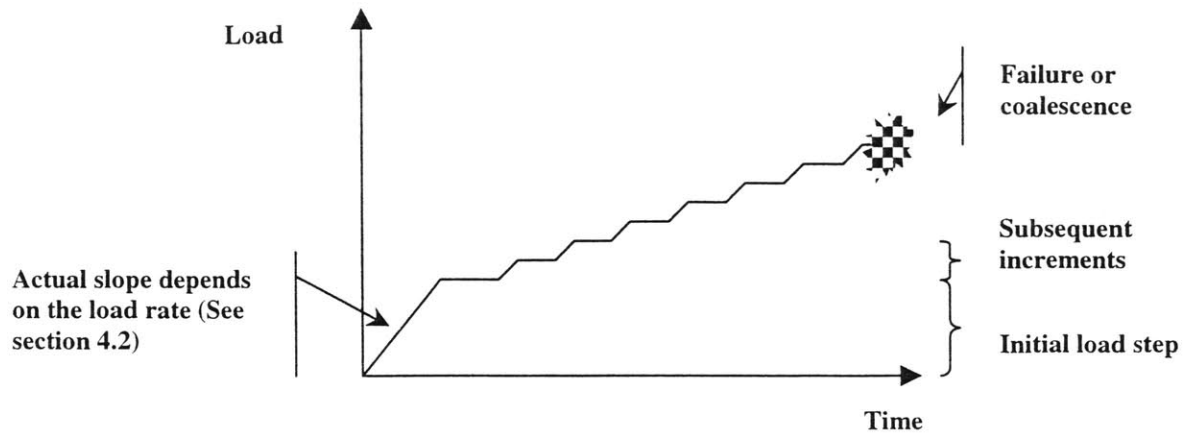


Figure A.4.13: Loading Process

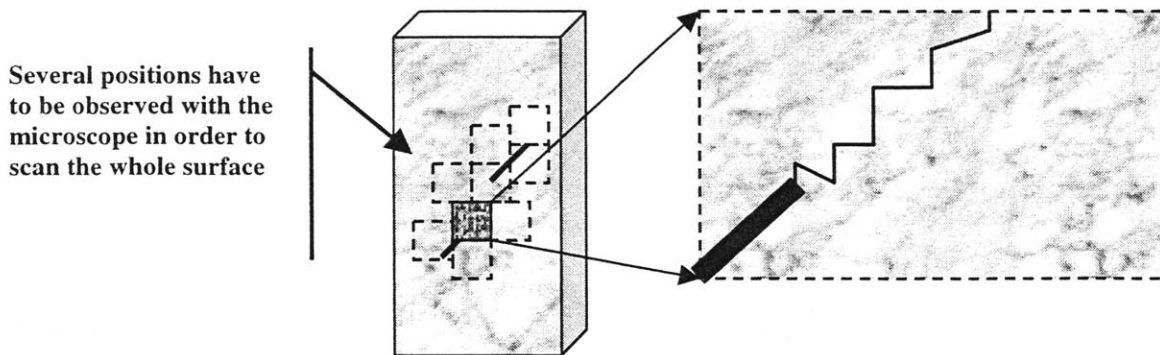


Figure A.4.14: Amplification needed to identify fractures. Note that the scope is greatly reduced and that more than one observation is required to cover the entire area

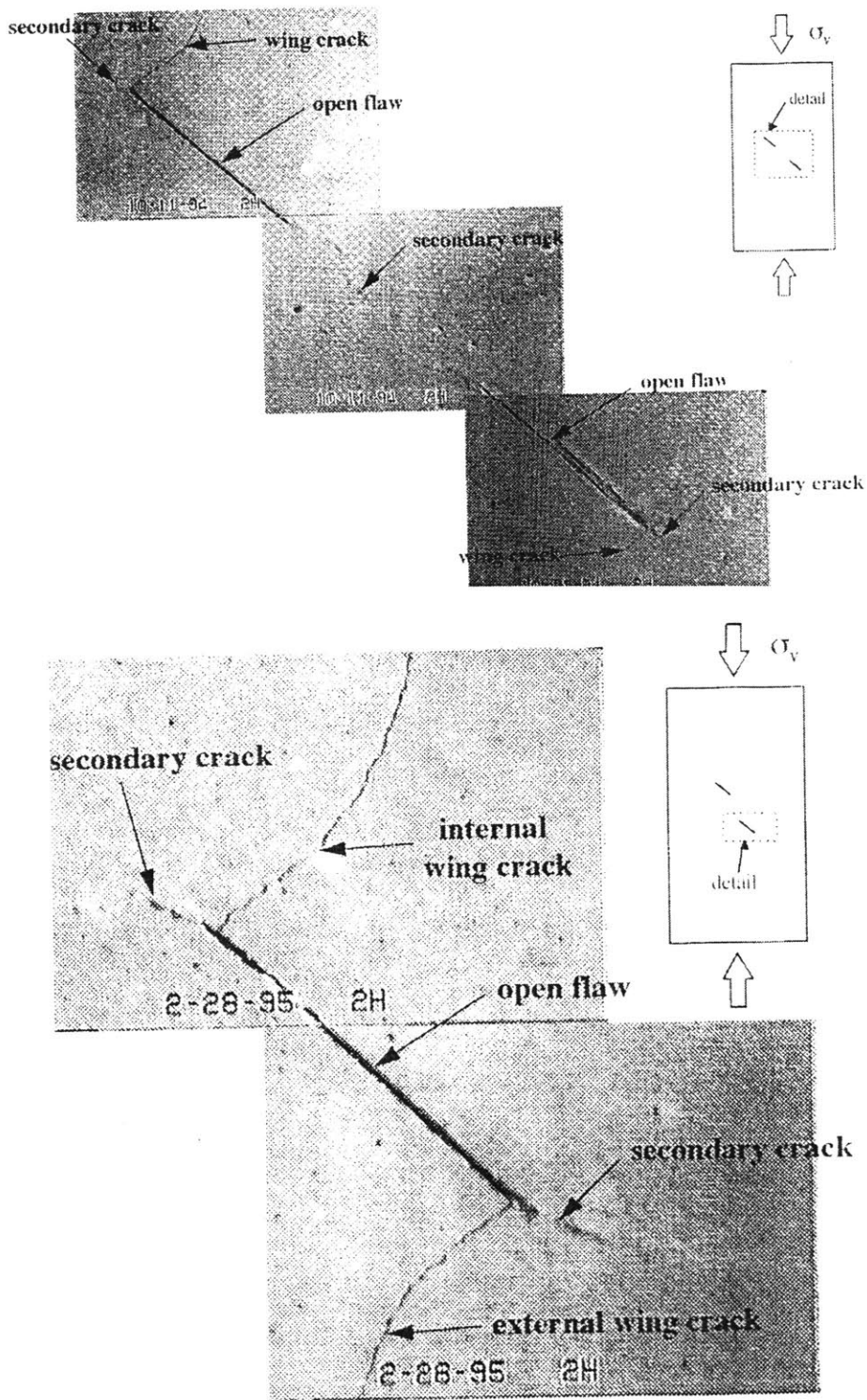
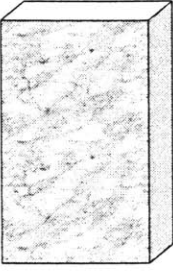
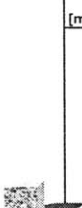


Figure A.4.15: Examples of amplification needed to identify fractures.
From Bobet (1997)

SPECIMEN NUMBER: _____			
SAMPLE DESCRIPTION: $\beta =$ $s =$ $c =$			
MOLD NUMBER:		LOAD TEST DATE:	
DONE BY:		DATA FILE NAME:	
	1 st	2 nd	3 rd
Thickness:			TAPE NUMBER:
Width:			START:
Length:			END:
LOAD (KN)	DESCRIPTION	ANGLE	DESCRIPTION
GENERAL SKETCH		THE FLAWS	
			
OBSERVATIONS:		[mm] DETAILED SKETCH	

DO NOT FORGET to identify specimen number and geometry

Indicate here actual dimensions of the specimen

Indicate here any imperfection in the flaws

Figure A.4.17: Granite Data Sheet

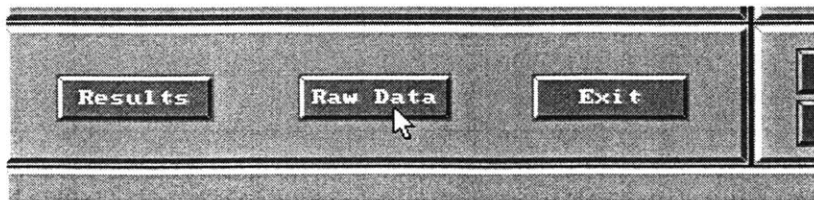


Figure A.4.18: Left bar shown after pressing “Store”

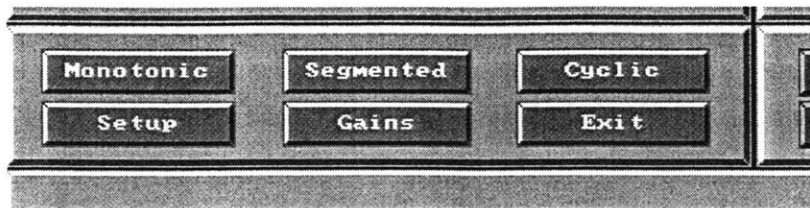


Figure A.4.19: Left bar shown after pressing “Servo”

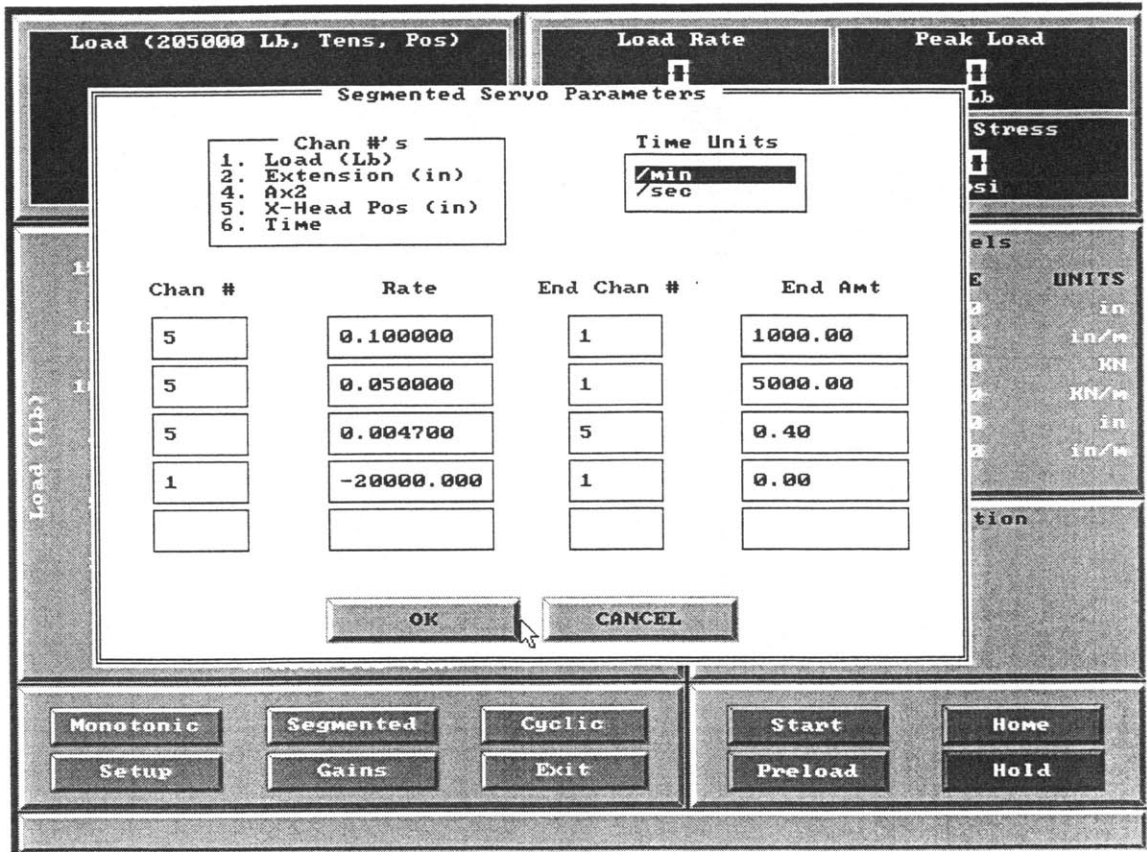


Figure A.4.20: Segmented displacement rate parameters (or segmented servo parameters) for granite

Note:

Channel #1 is used to set a load rate (or stress rate)

Channel #5 is used to set a displacement rate (or strain rate)

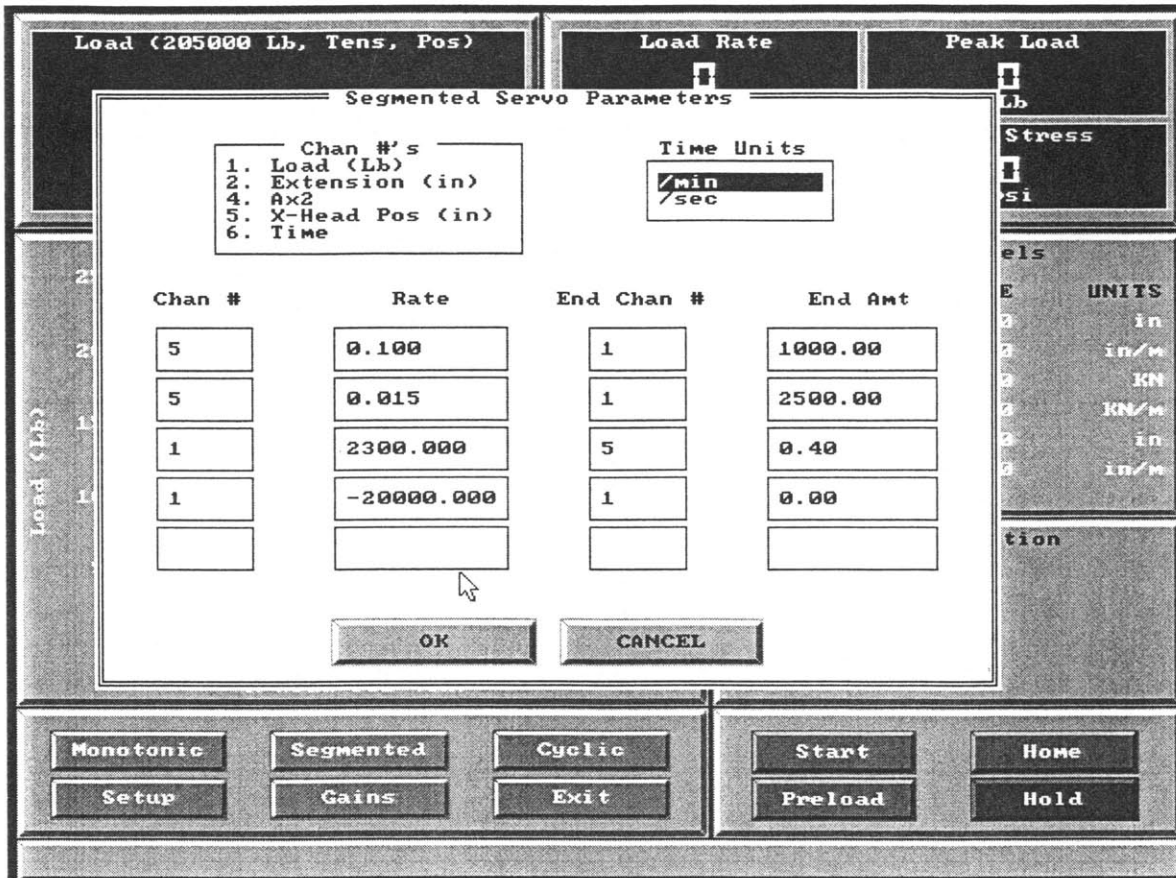


Figure A.4.21: Segmented displacement rate parameters (or segmented servo parameters) for gypsum

Note:

Channel #1 is used to set a load rate (or stress rate)

Channel #5 is used to set a displacement rate (or strain rate)

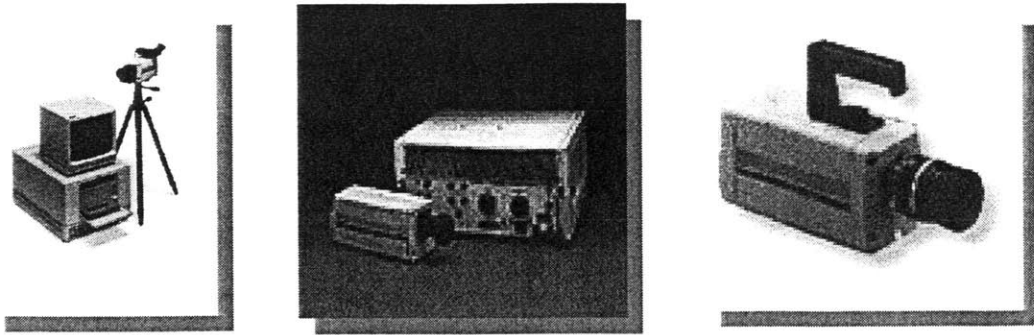


Figure A.4.22A: Main parts of the Kodak Ektapro. (high-speed camera + motion analyzer)

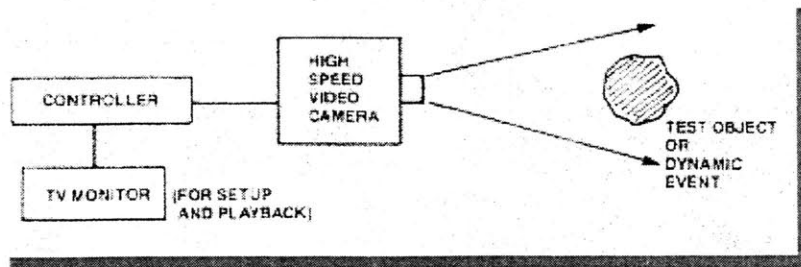


Figure A.4.22B: Main parts of a motion analyzer

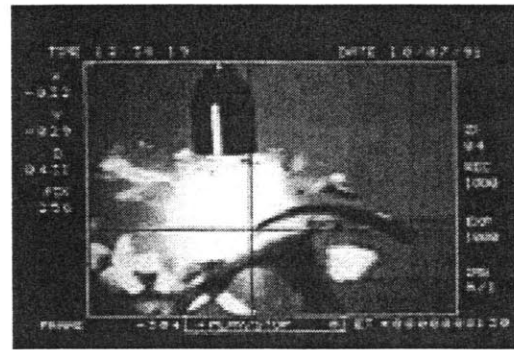
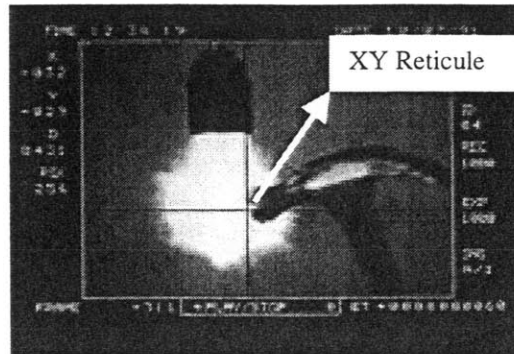


Figure A.4.23: Example of recorded images



Figure A.4.24: Keypad to operate the motion analyzer

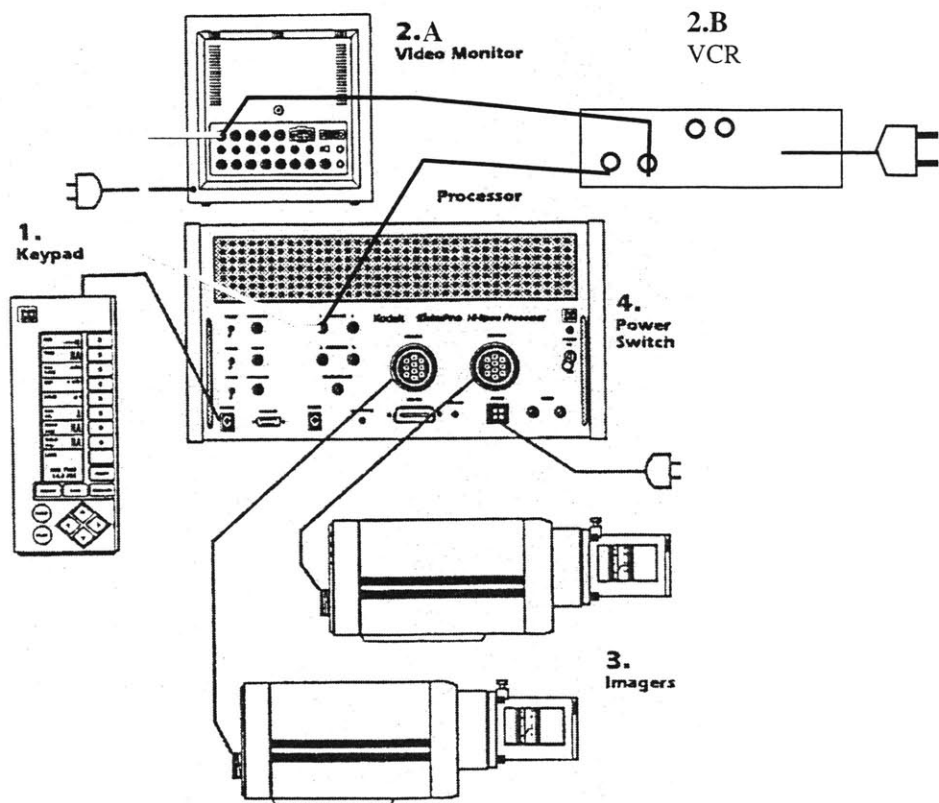


Figure A.4.25: Connections to make

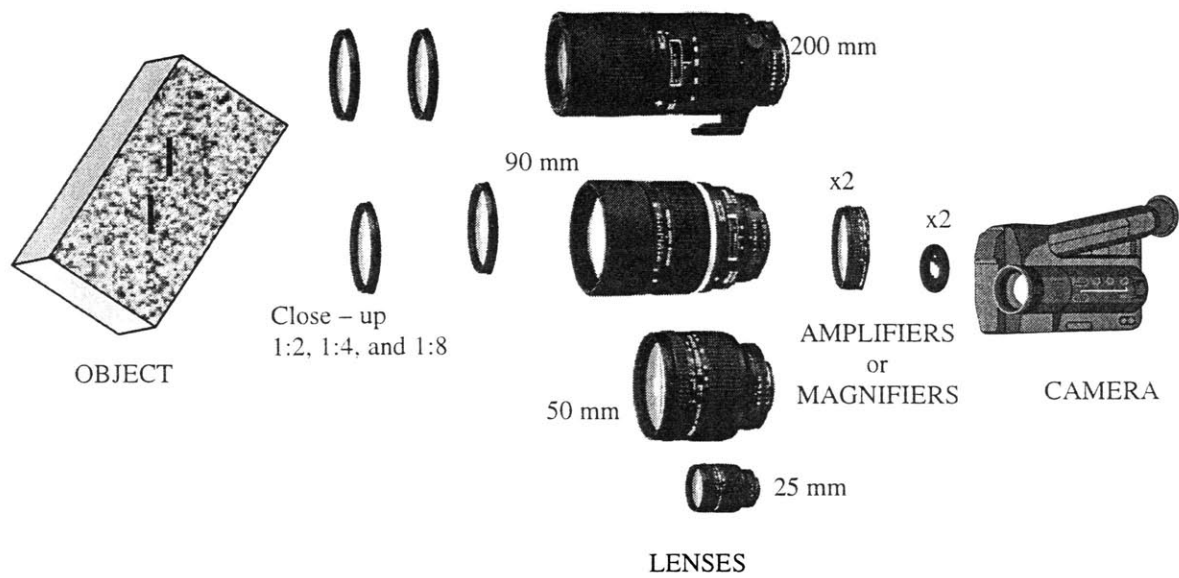


Figure A.4.26: Lenses, close-ups, and amplifiers

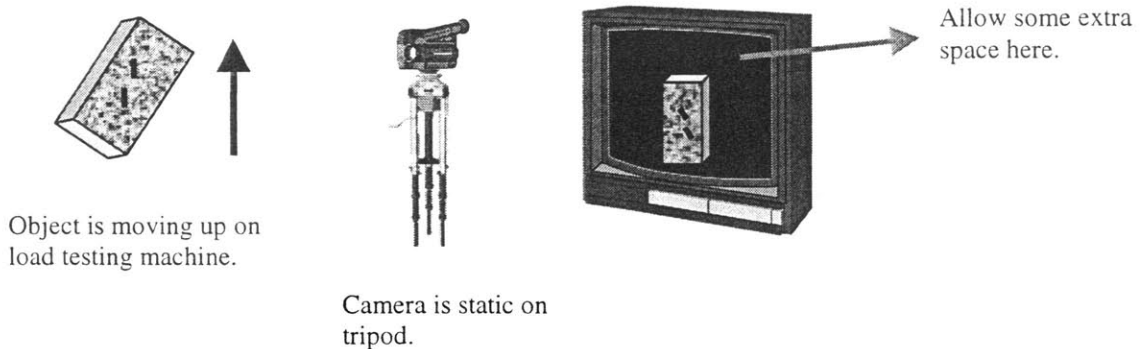


Figure A.4.27: Adjusting the image due to loading machine movement

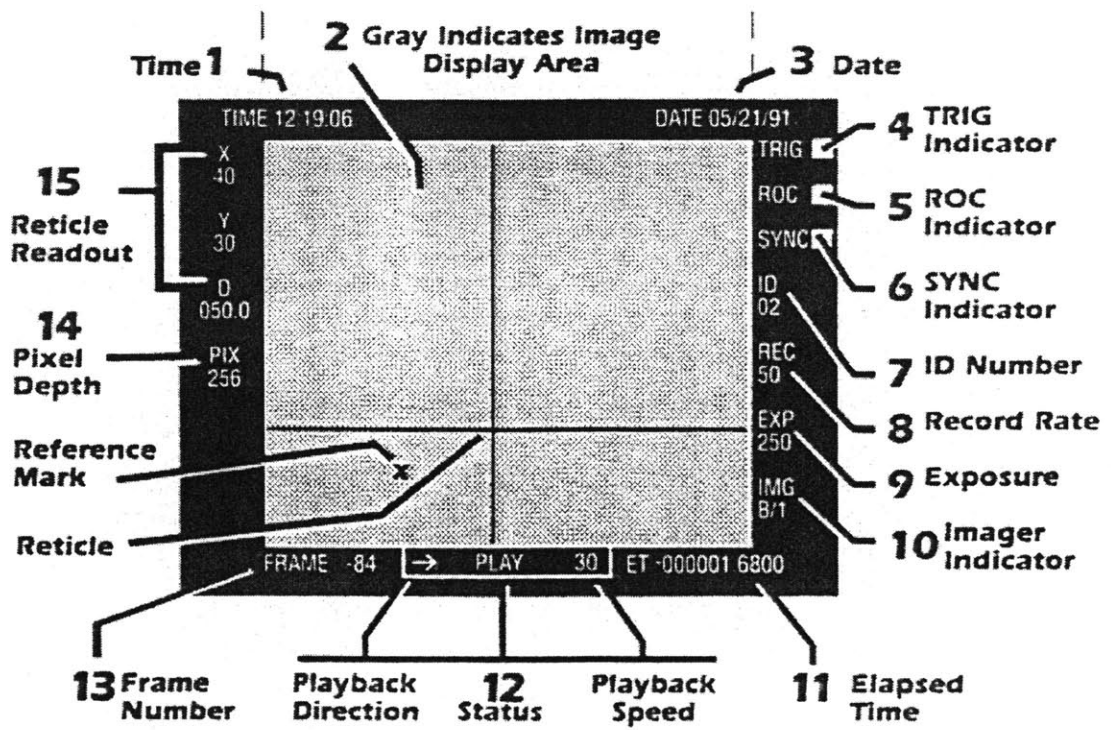


Figure A.4.28: Video Display

Date	Time	Test	Spec	Oper	Peak	Peak
		No	No	No	(Lb)	(psi)

02/28/98	18:18:02	39	0	0	61510	49208
Area (in^2): 1.250000, Flat 2.5 0.5						
Gage Len (in): 5.000000						
Log Rate (sec): 1.999964						
	220	-0.01	0	-0.025	0.00425	
	1310	-0.01	0	-0.024	0.005	
	1350	-0.01	0	-0.025	0.005	
	1350	-0.01	0	-0.025	0.005	
	1370	-0.01	0	-0.027	0.005	



Load [Lb.] 
Displacements [in] 

Figure A.4.29: Format of the "Text Only" file created by the MTEST2 controlling software

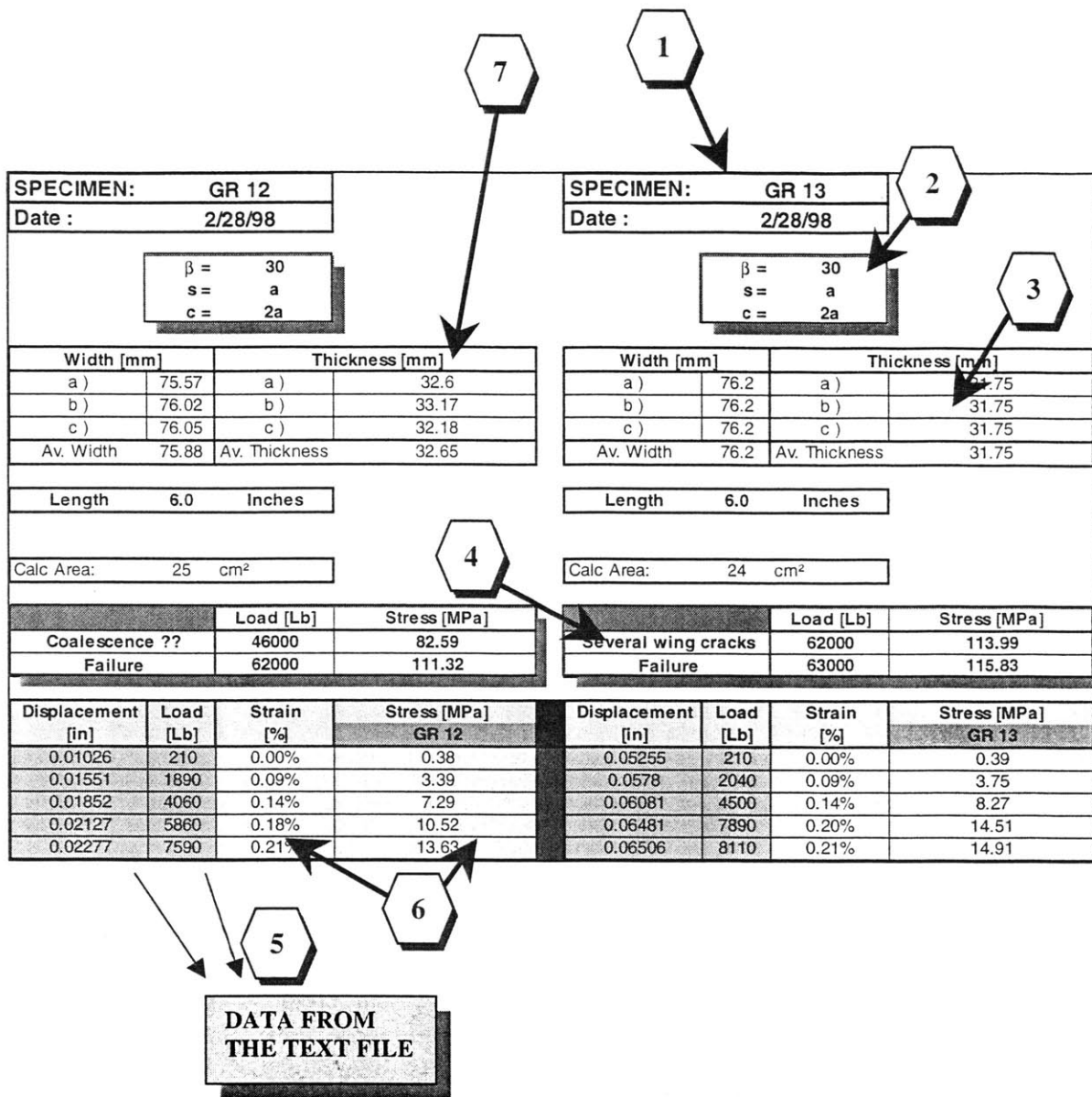


Figure A.4.30: Processed data in the “new” Excel template

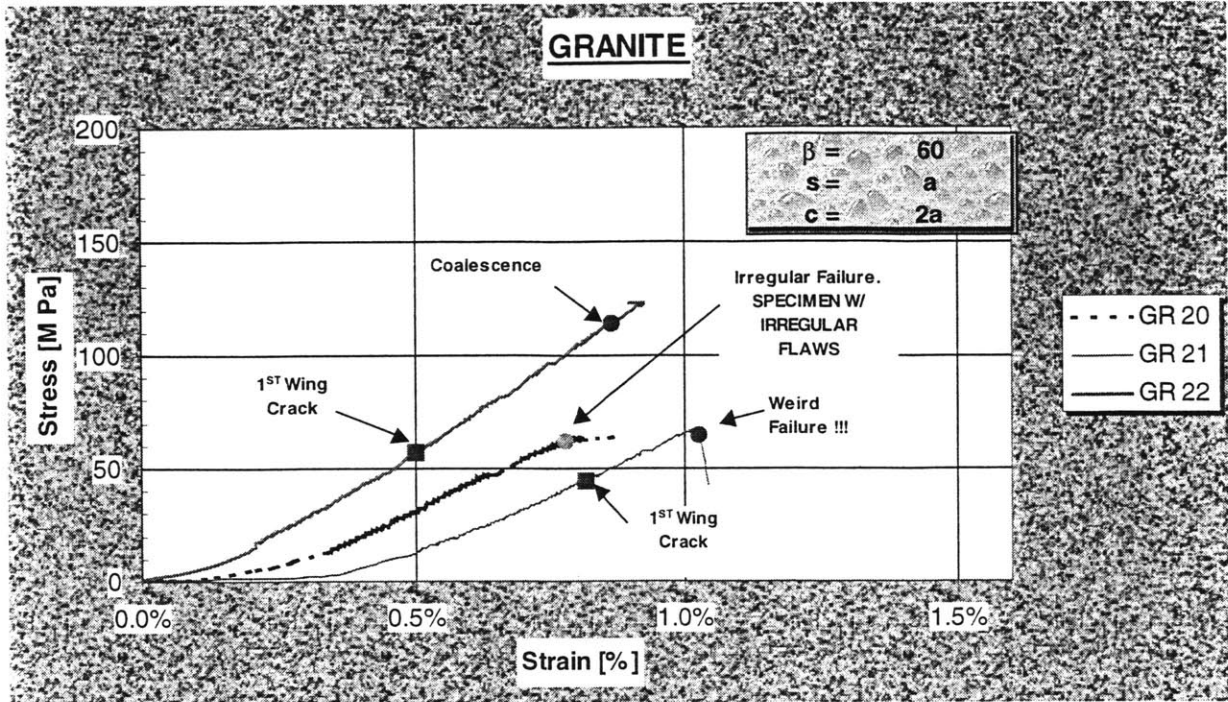


Figure A.4.31A: Plotted data for granite specimens

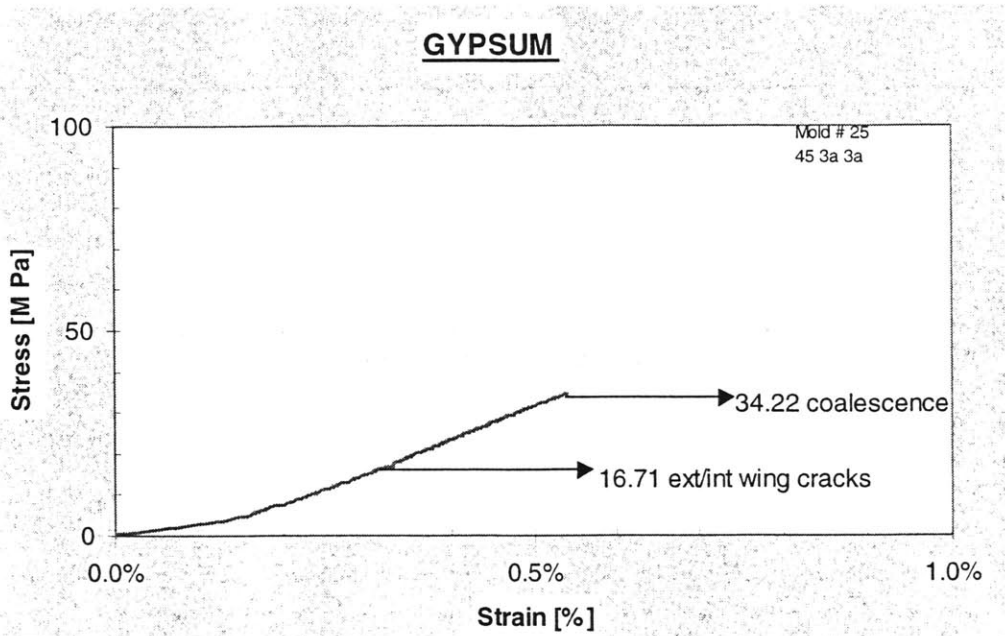


Figure A.4.31B: Plotted data for gypsum specimens

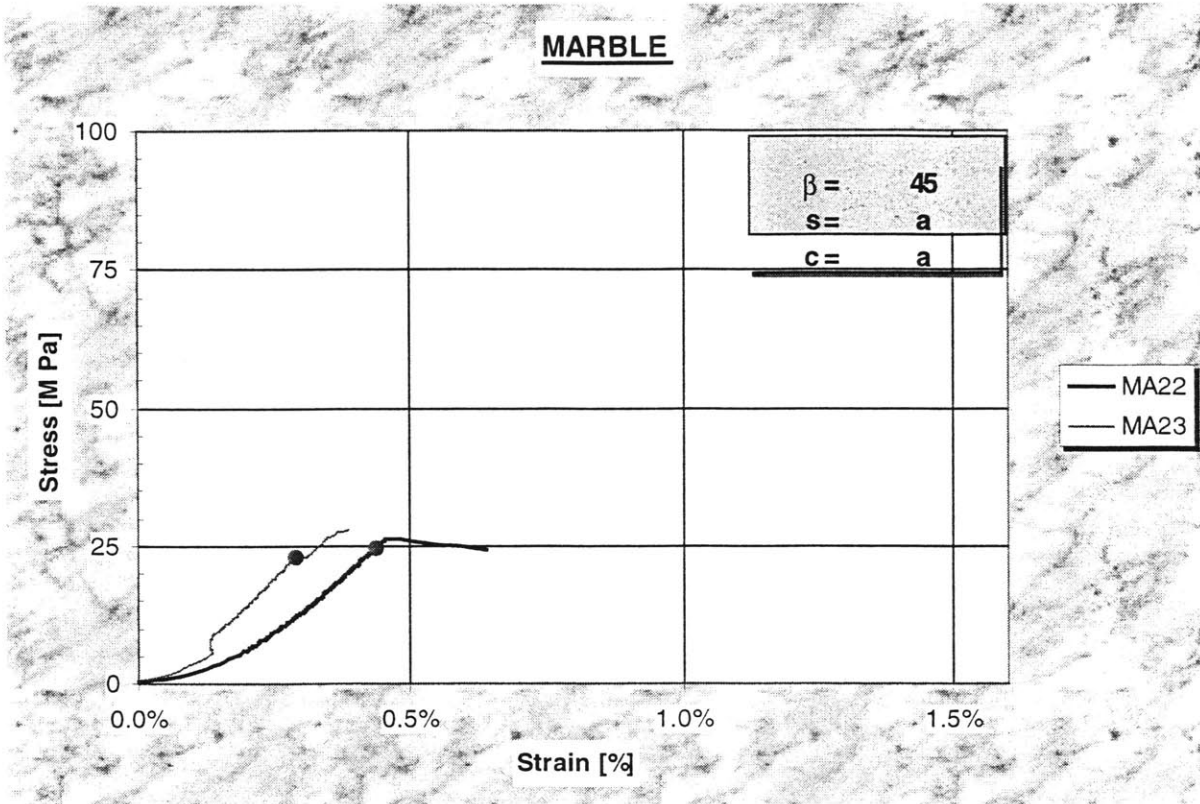


Figure A.4.31C: Plotted data for Marble Specimens

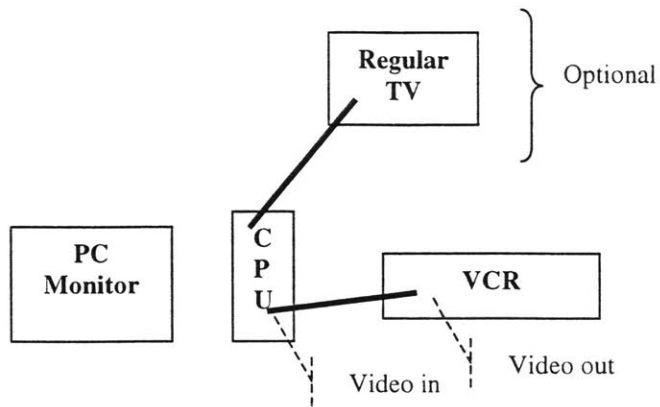


Figure A.4.32: Connecting the VCR to the PC to use the frame grabber

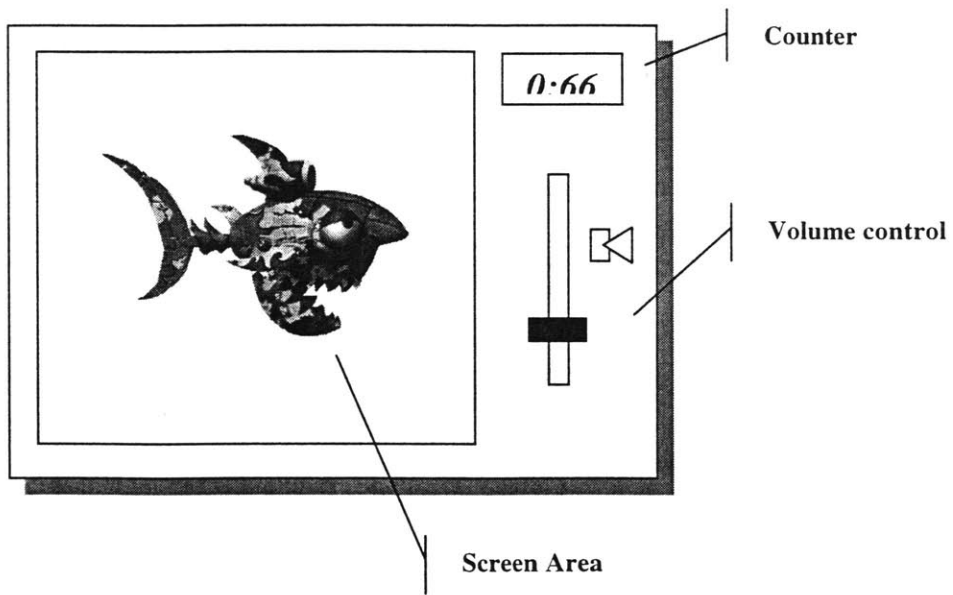


Figure A.4.33: Screen window in the frame grabber

Appendix B: STRESS STRAIN PLOTS IN GRANITE

This Appendix contains stress-strain curves for prismatic granite specimens prepared as detailed in Appendix A. All the specimens have two parallel flaws cut through the thickness. Each of the presented figures includes several plots that correspond to different specimens with the same flaw geometry arrangement. Note that the machine deformability is included in the plotted strain. The black dots in some of the plots indicate coalescence.

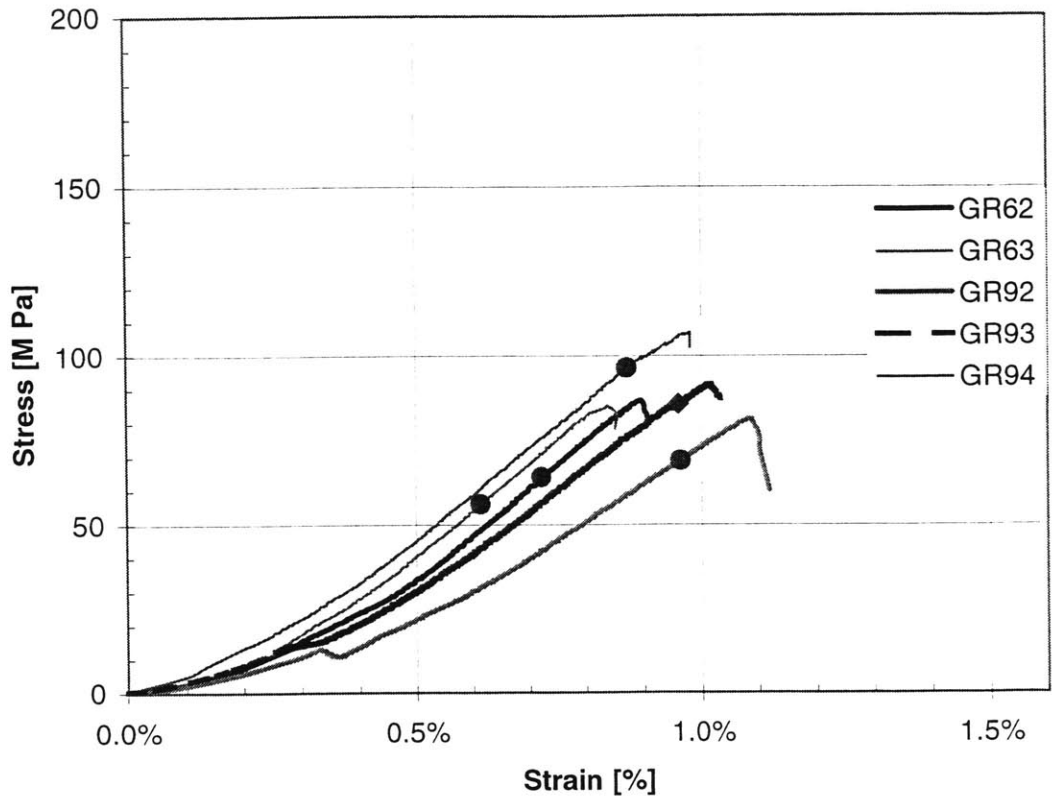


Figure B.1: Stress-strain curves for granite specimens with geometry 30-0-a.

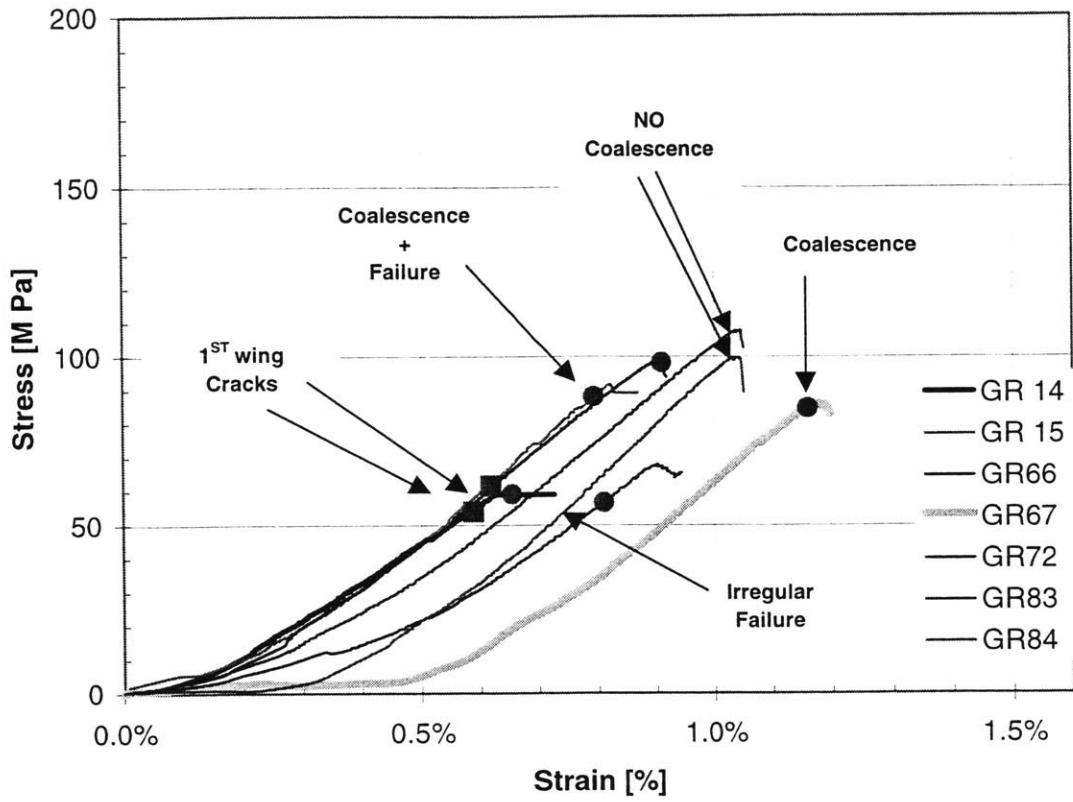


Figure B.2: Stress-strain curves for granite specimens with geometry 30-0-2a.

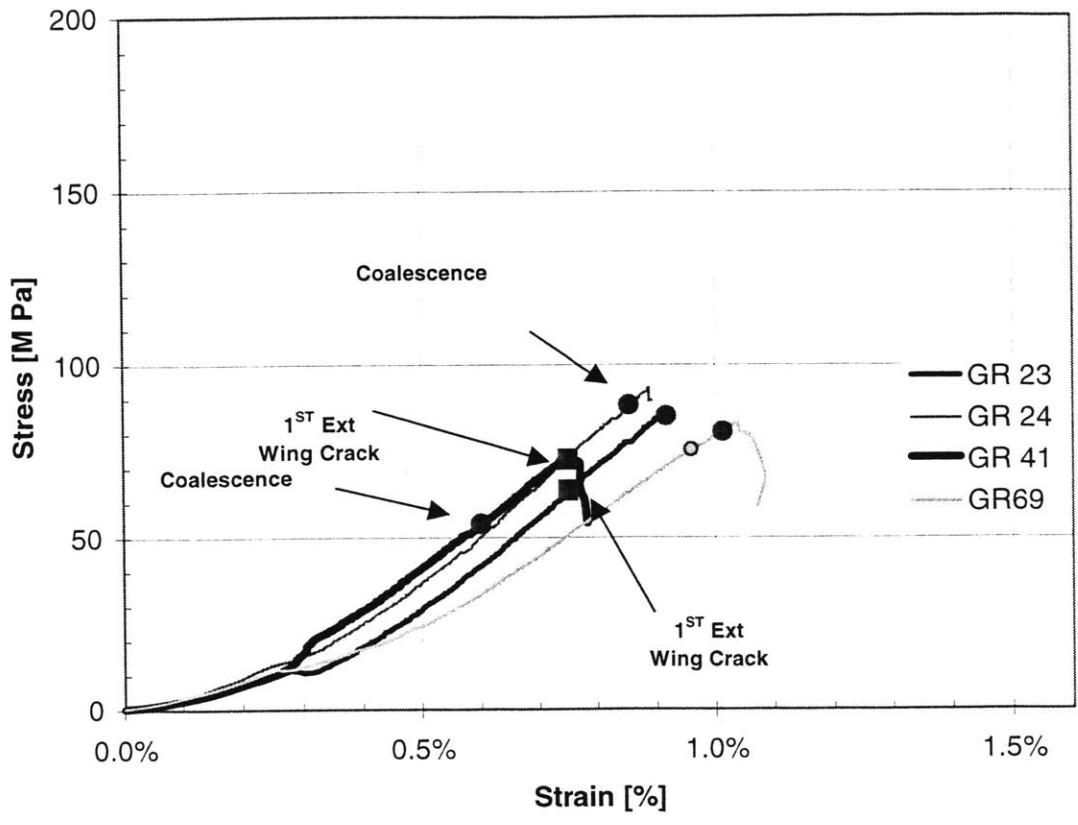


Figure B.3: Stress-strain curves for granite specimens with geometry 30-2a-2a.

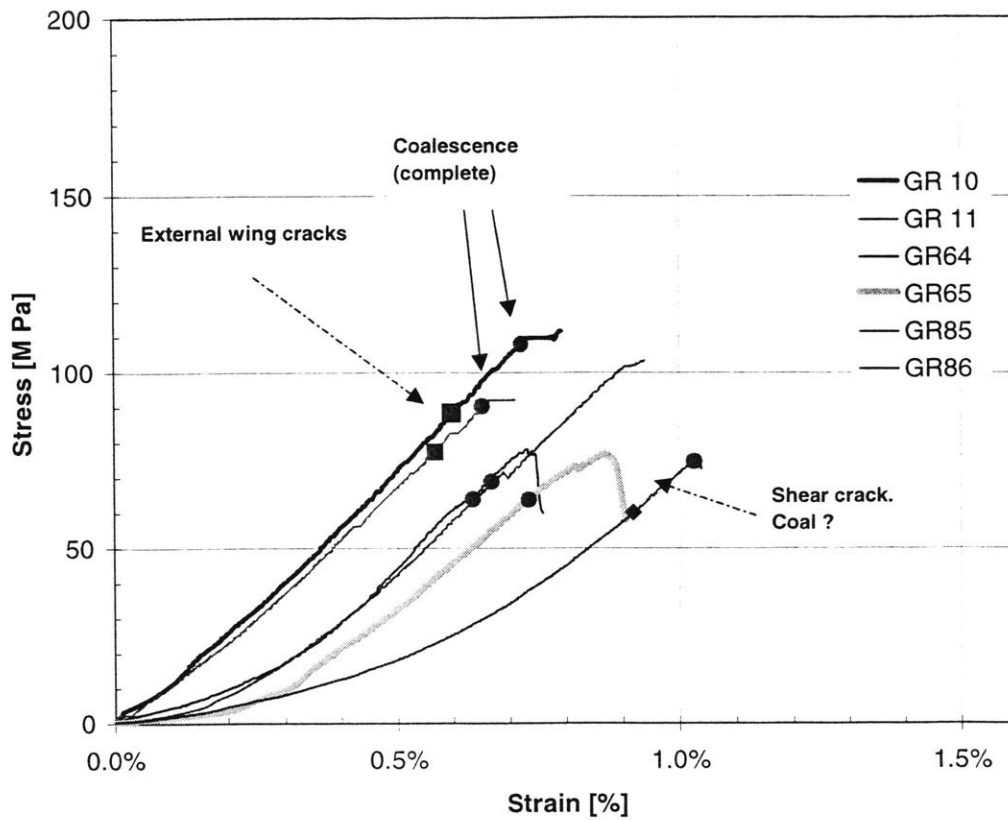


Figure B.4: Stress-strain curves for granite specimens with geometry 30-a-a.

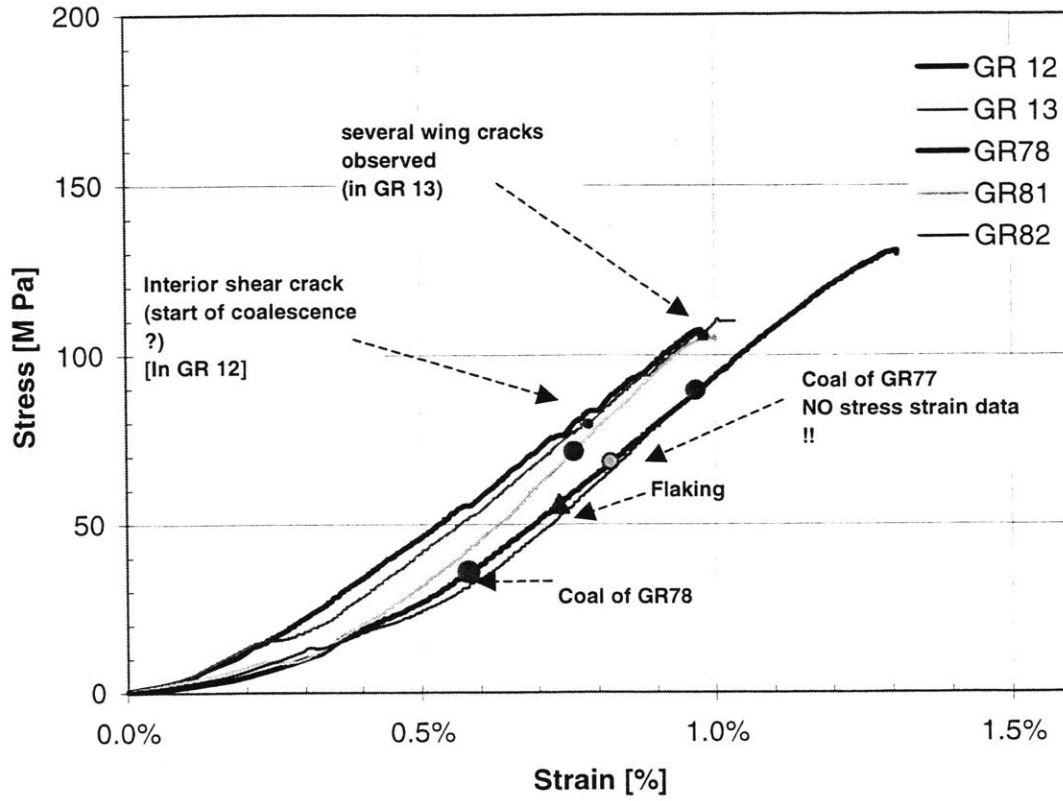


Figure B.5: Stress-strain curves for granite specimens with geometry 30-a-2a.

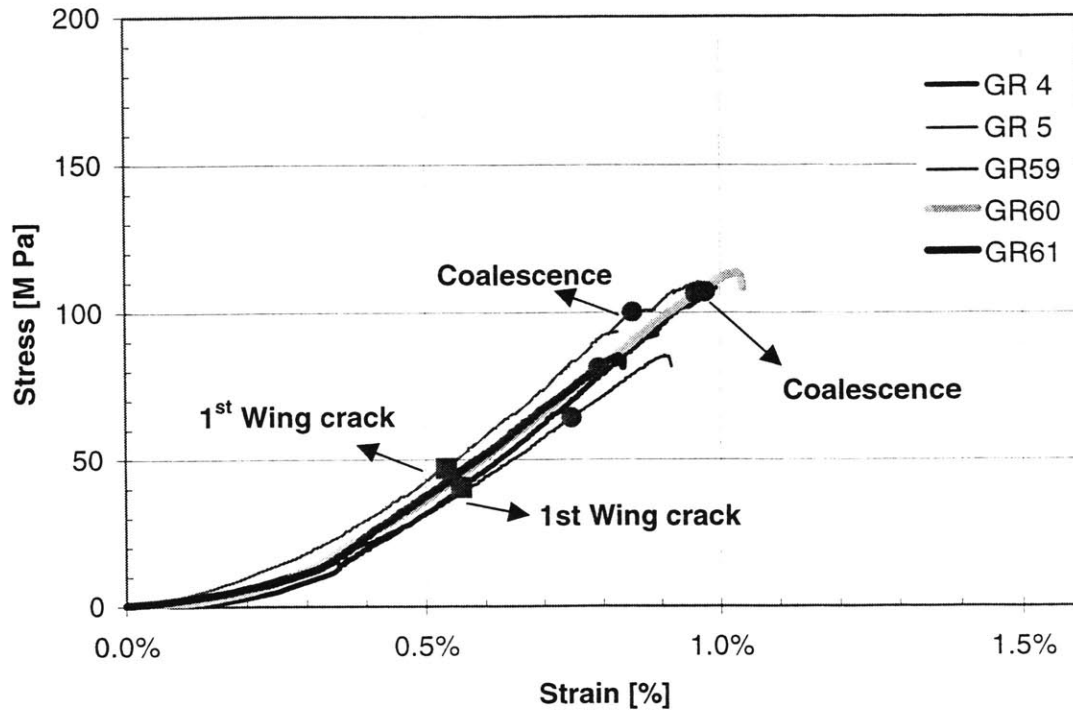


Figure B.6: Stress-strain curves for granite specimens with geometry 45-0-a.

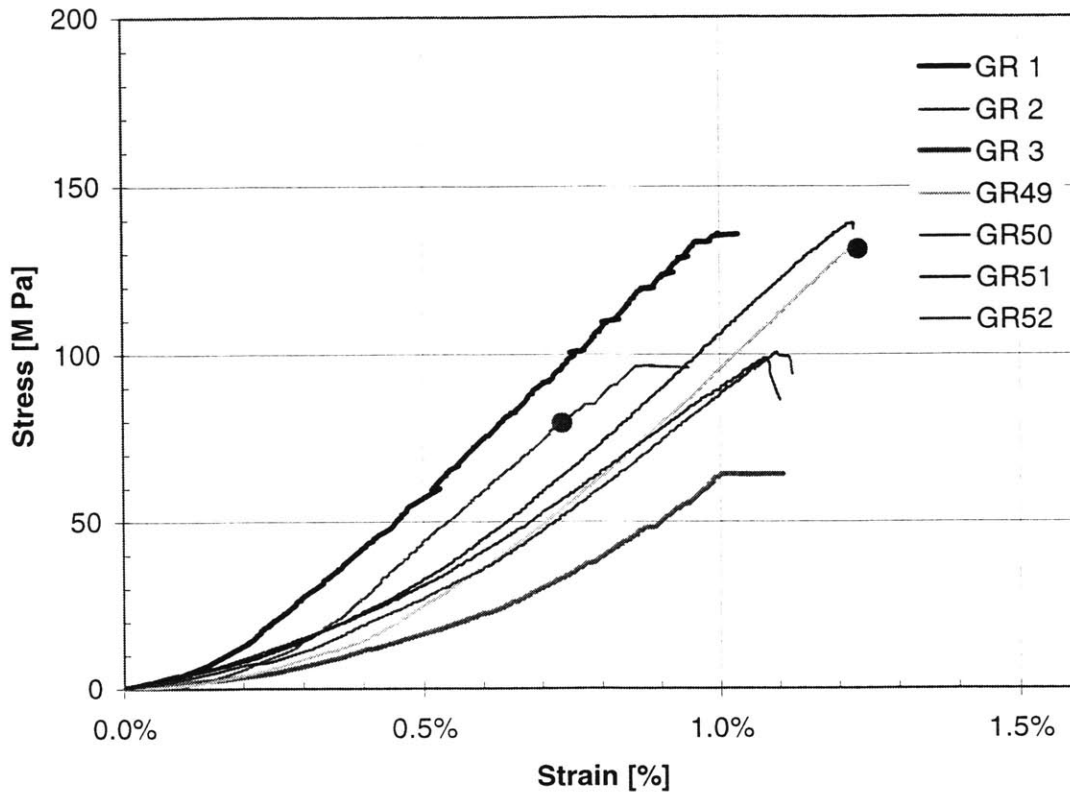


Figure B.7: Stress-strain curves for granite specimens with geometry 45-0-2a.

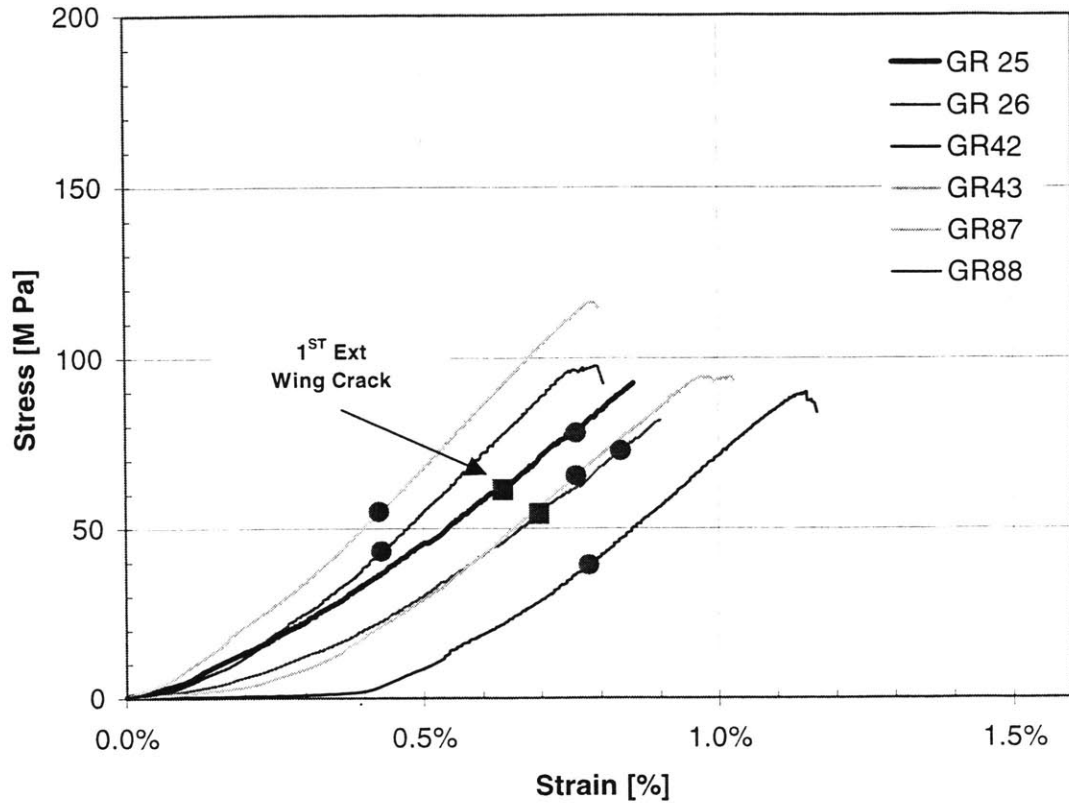


Figure B.8: Stress-strain curves for granite specimens with geometry 45-2a-2a.

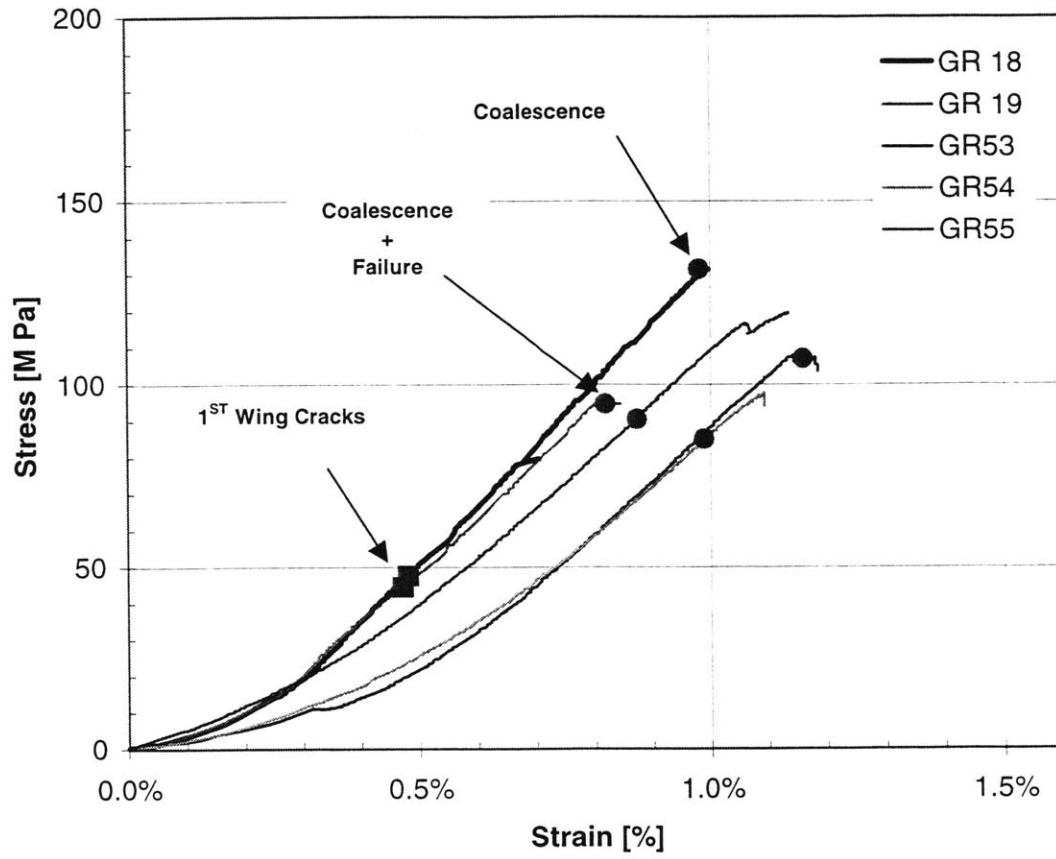


Figure B.9: Stress-strain curves for granite specimens with geometry 45-a-2a.

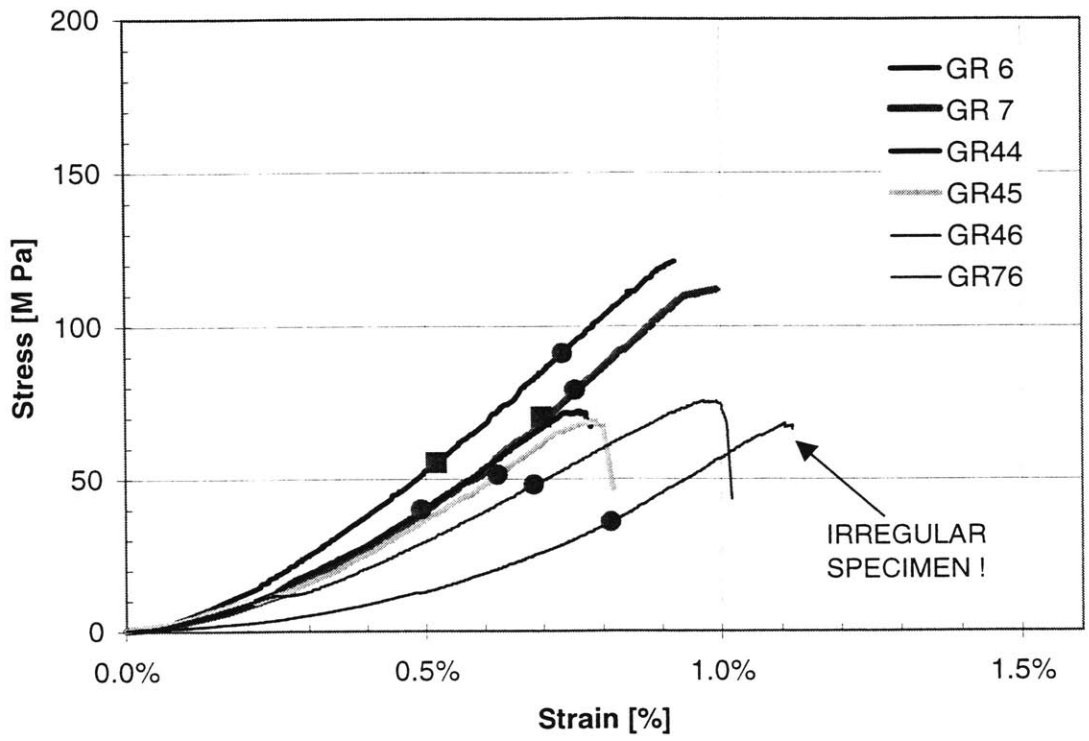


Figure B.10: Stress-strain curves for granite specimens with geometry 45-a-a.

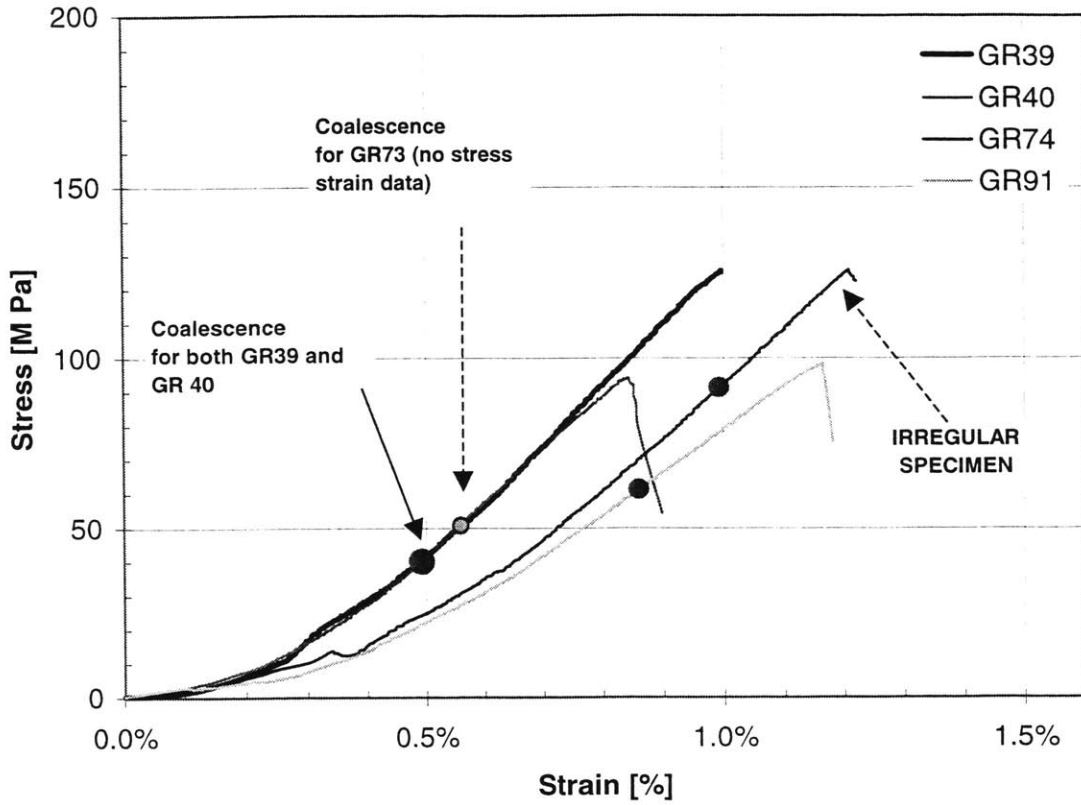


Figure B.11: Stress-strain curves for granite specimens with geometry 60-0-a.

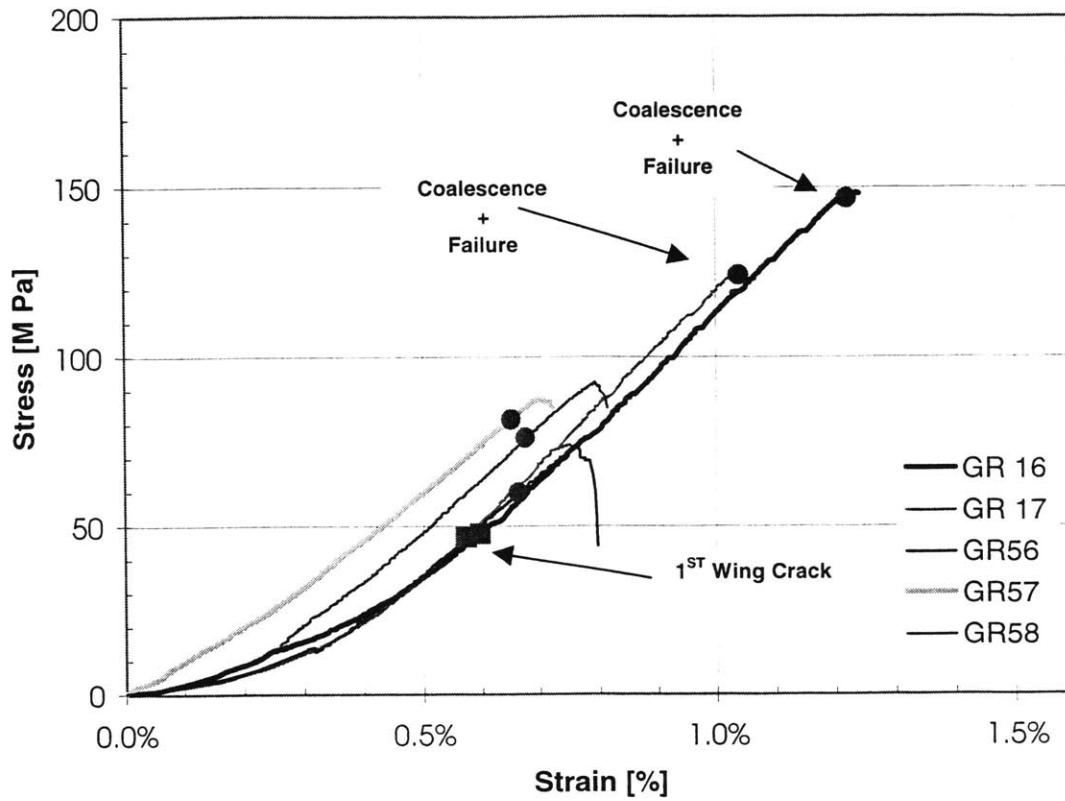


Figure B.12: Stress-strain curves for granite specimens with geometry 60-0-2a.

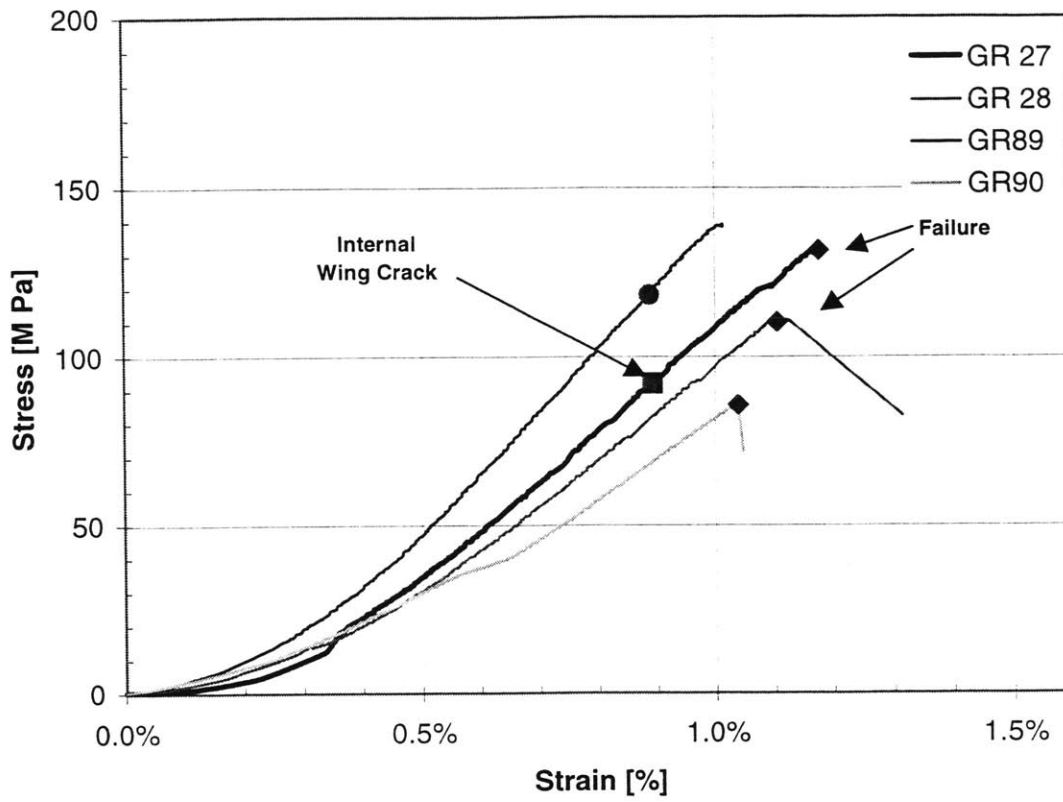


Figure B.13: Stress-strain curves for granite specimens with geometry 60-0-3a.

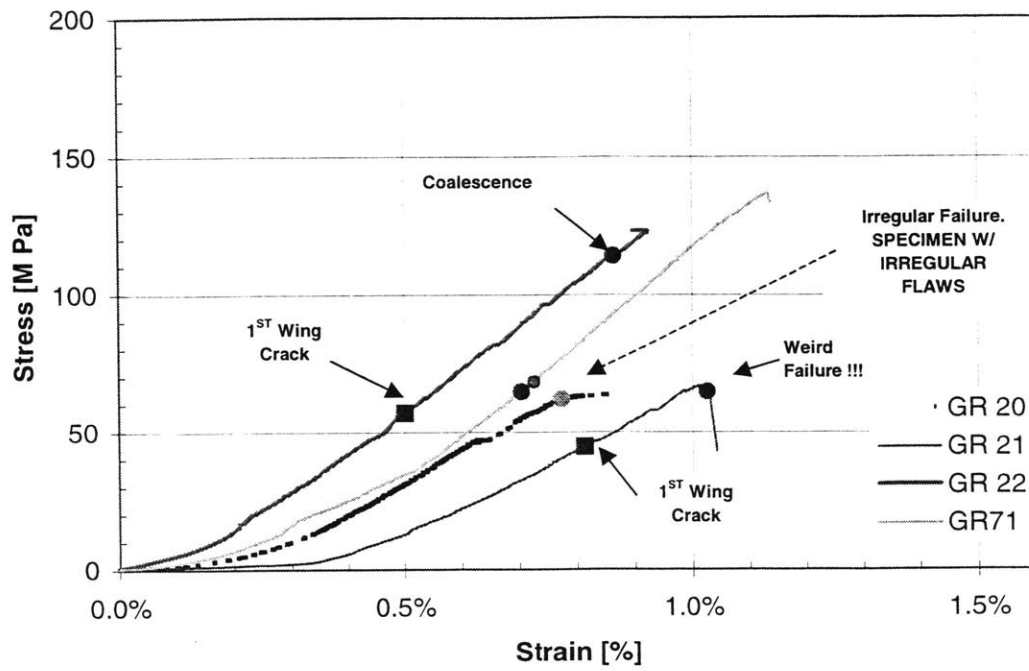


Figure B.14: Stress-strain curves for granite specimens with geometry 60-a-2a.

Appendix C: STRESS STRAIN PLOTS IN MARBLE

This Appendix contains stress-strain curves for prismatic marble specimens prepared as detailed in Appendix A. All the specimens have two parallel flaws cut through the thickness. Each of the presented figures includes several plots that correspond to different specimens with the same flaw geometry arrangement. Note that the machine deformability is included in the plotted strain. The black dots in some of the plots indicate coalescence.

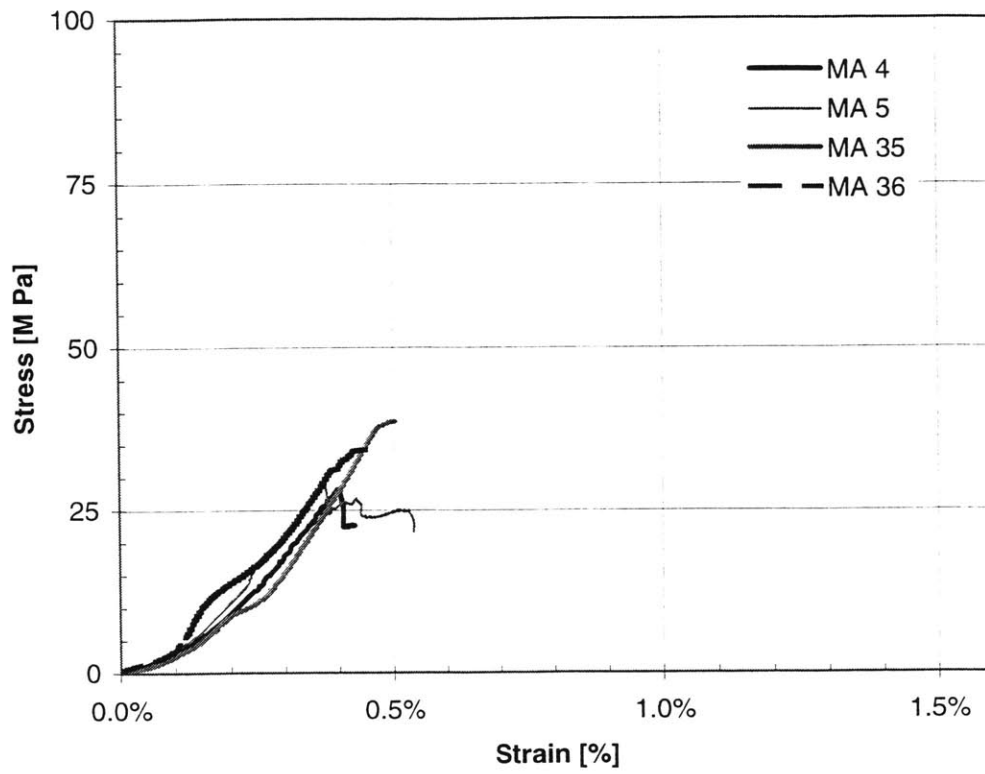


Figure C.1: Stress-strain curves for marble specimens with geometry 30-0-a.

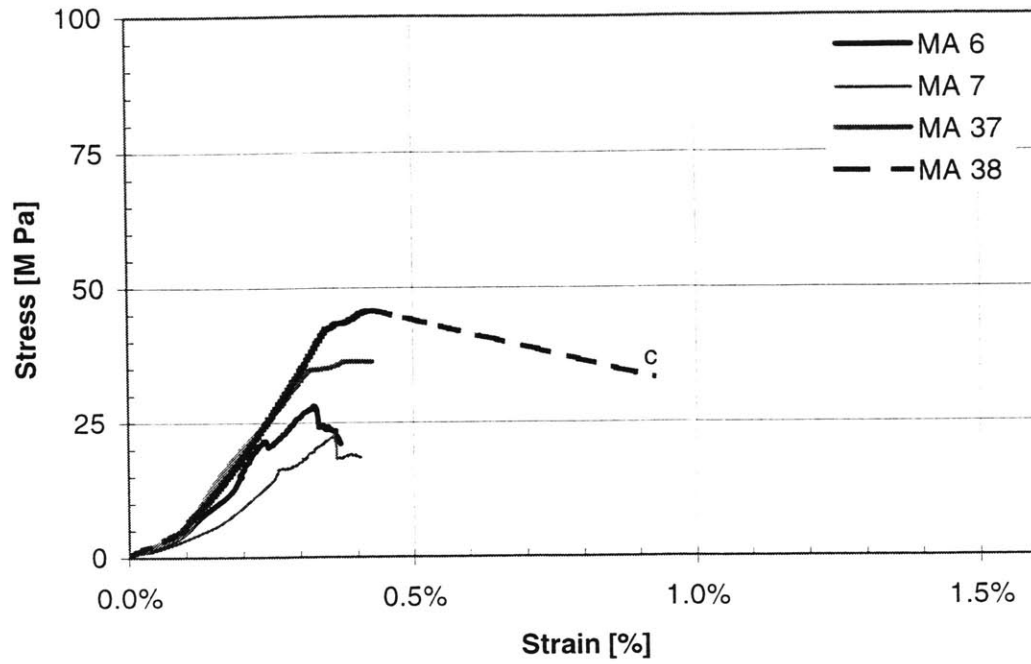


Figure C.2: Stress-strain curves for marble specimens with geometry 30-0-2a.

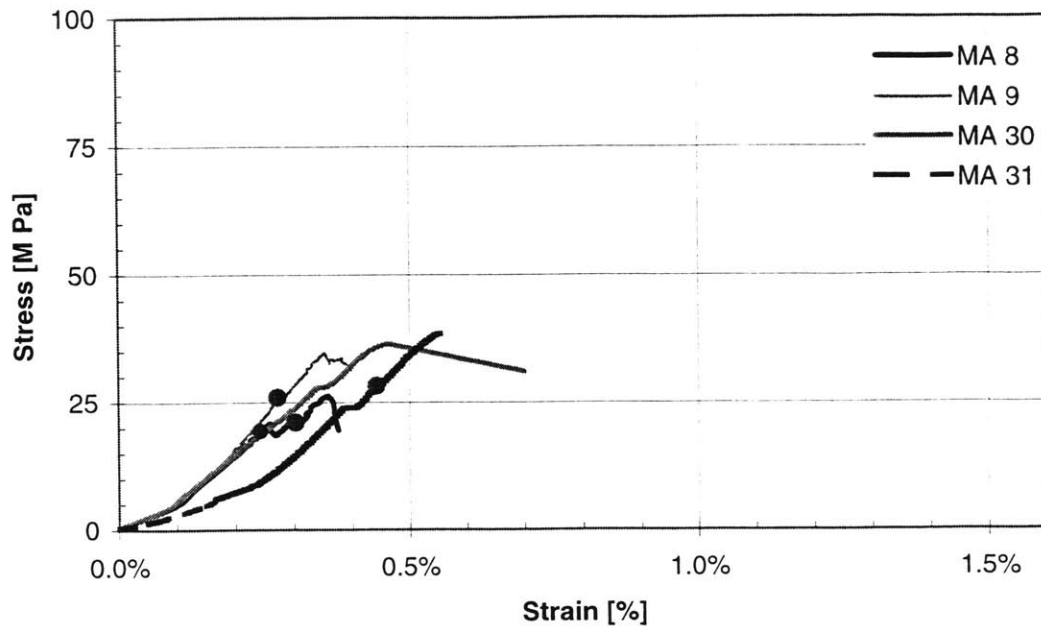


Figure C.3: Stress-strain curves for marble specimens with geometry 30-2a-2a.

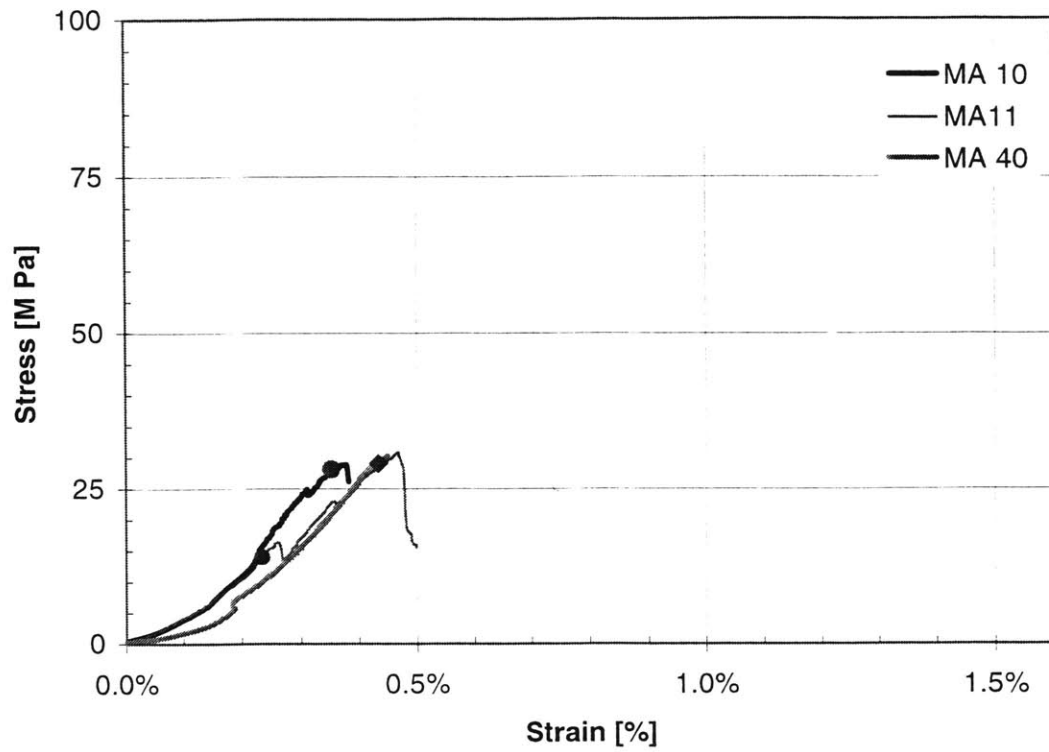


Figure C.4: Stress-strain curves for marble specimens with geometry 30-a-a.

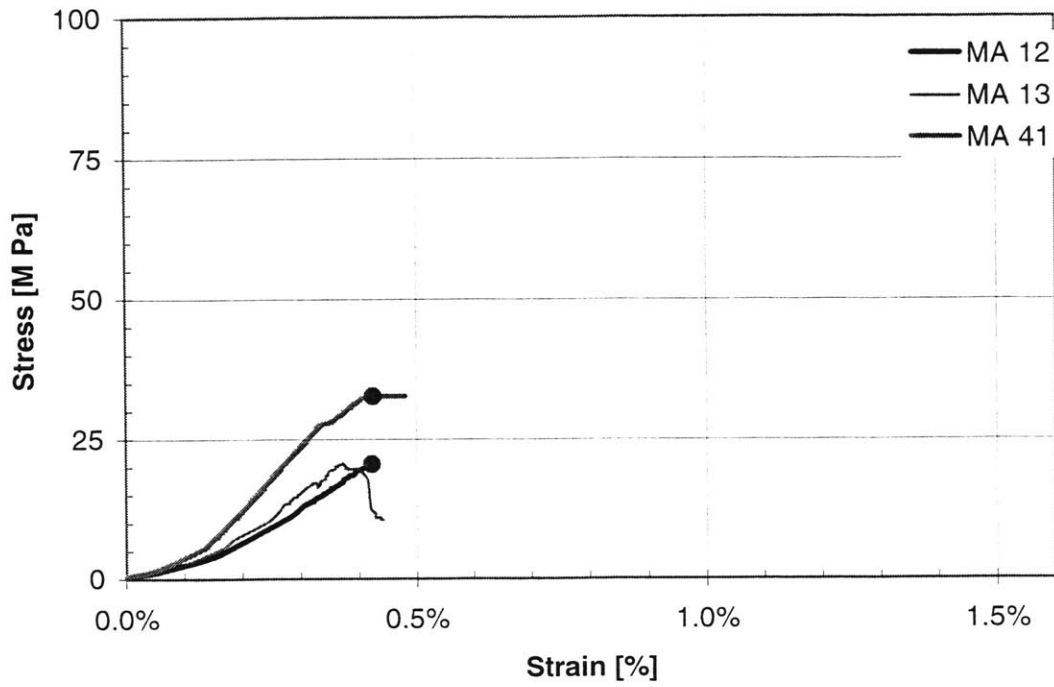


Figure C.5: Stress-strain curves for marble specimens with geometry 30-a-2a.

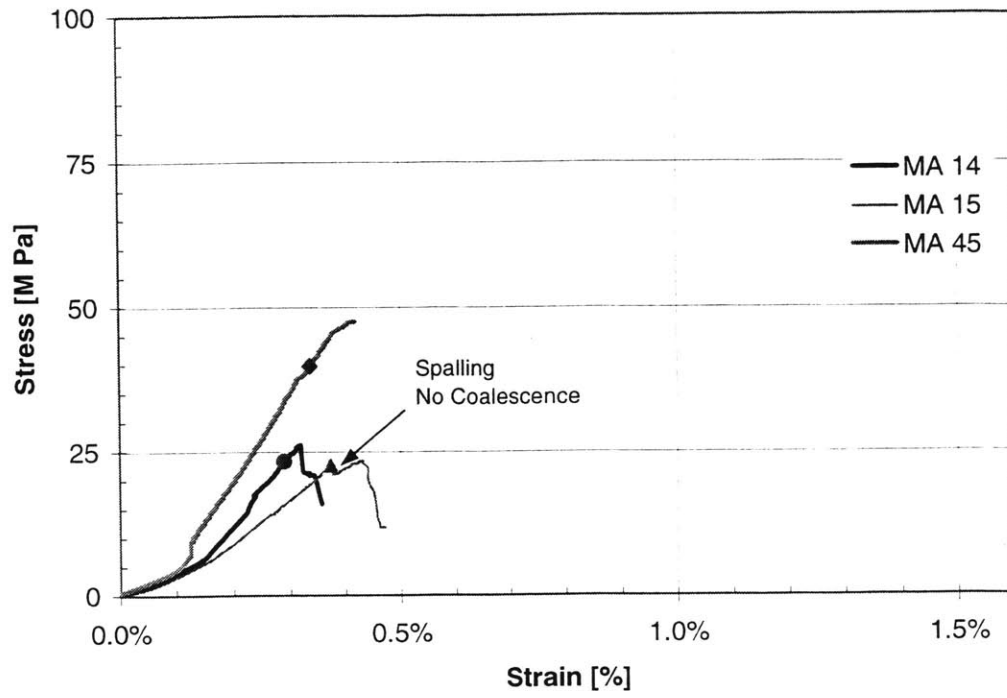


Figure C.6: Stress-strain curves for marble specimens with geometry 45-0-a.

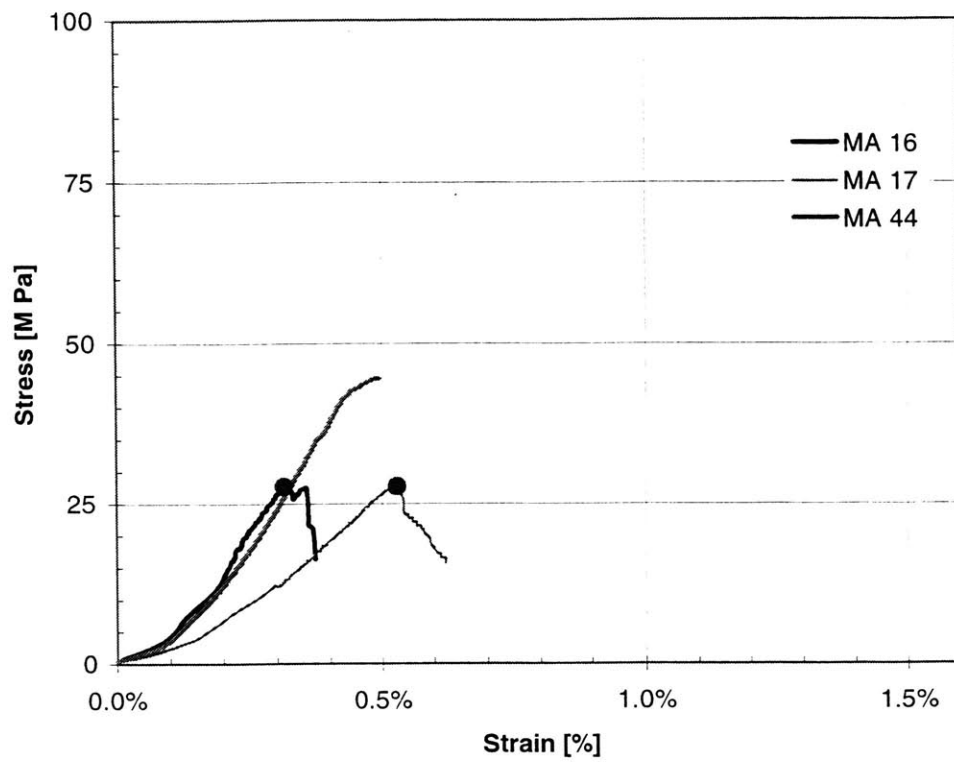


Figure C.7: Stress-strain curves for marble specimens with geometry 45-0-2a.

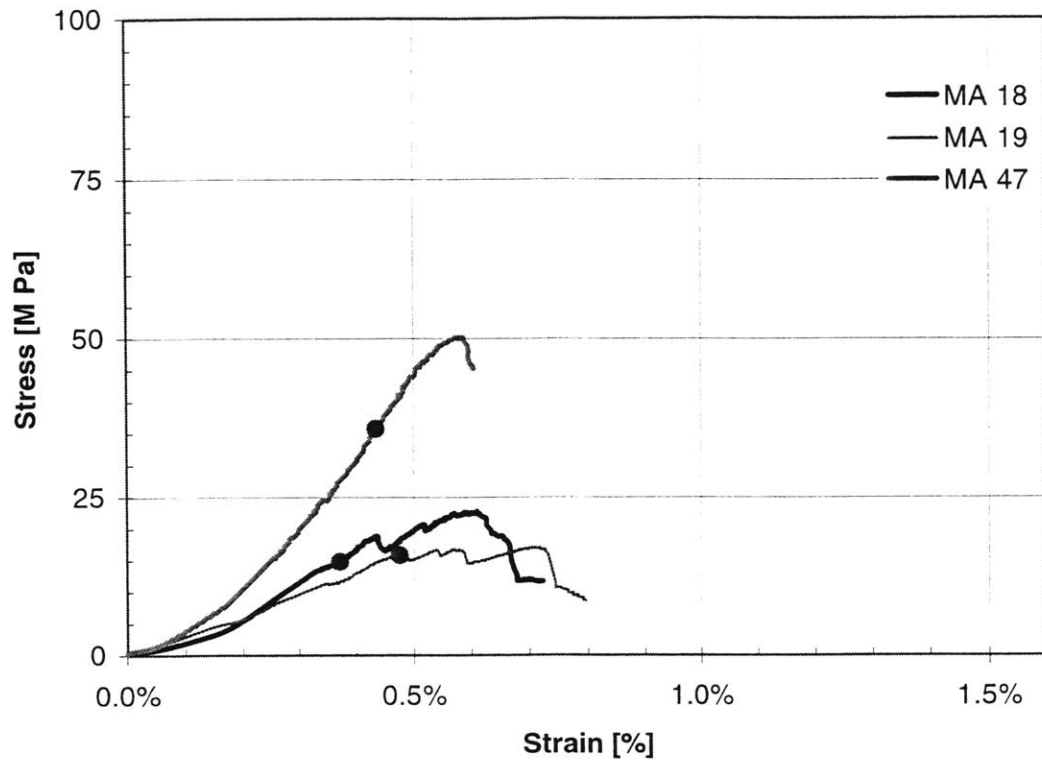


Figure C.8: Stress-strain curves for marble specimens with geometry 45-2a-2a.

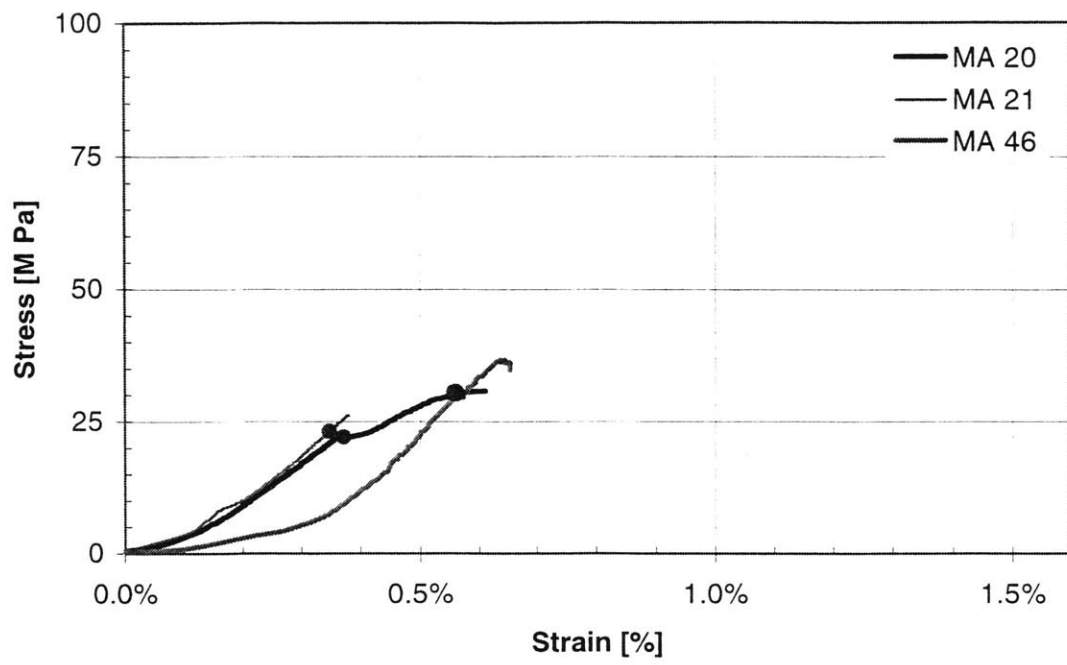


Figure C.9: Stress-strain curves for marble specimens with geometry 45-a-2a.

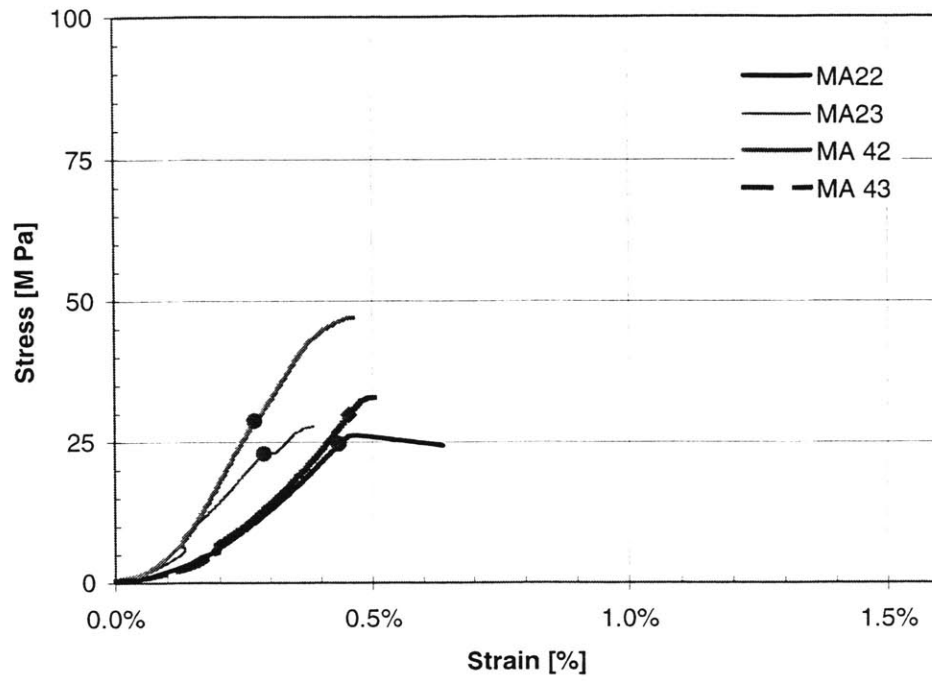


Figure C.10: Stress-strain curves for marble specimens with geometry 45-a-a.

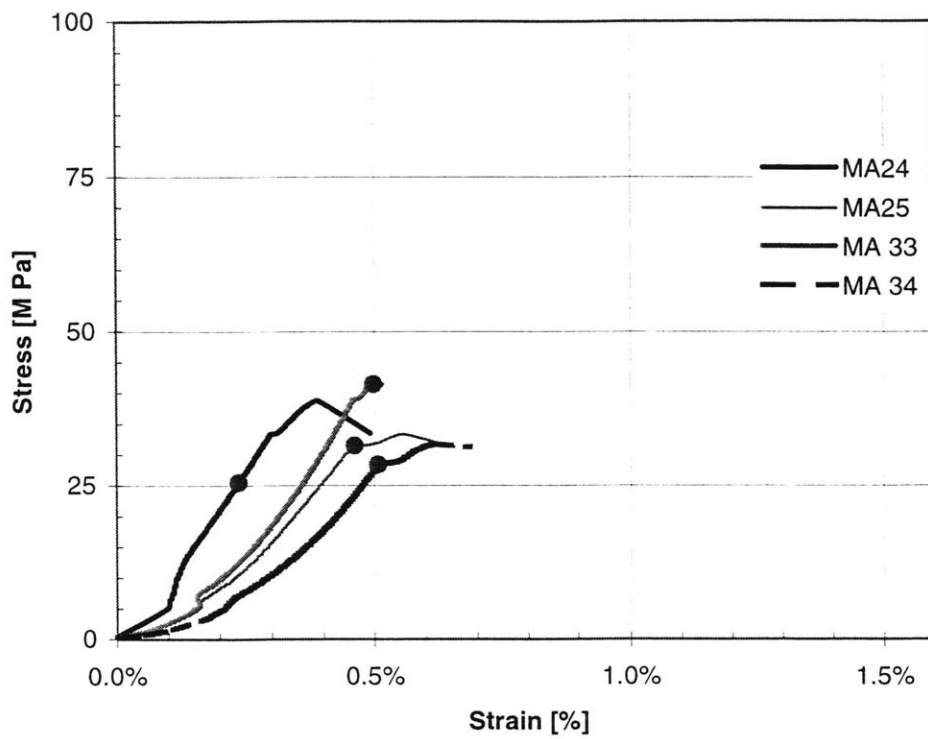


Figure C.11: Stress-strain curves for marble specimens with geometry 60-0-a.

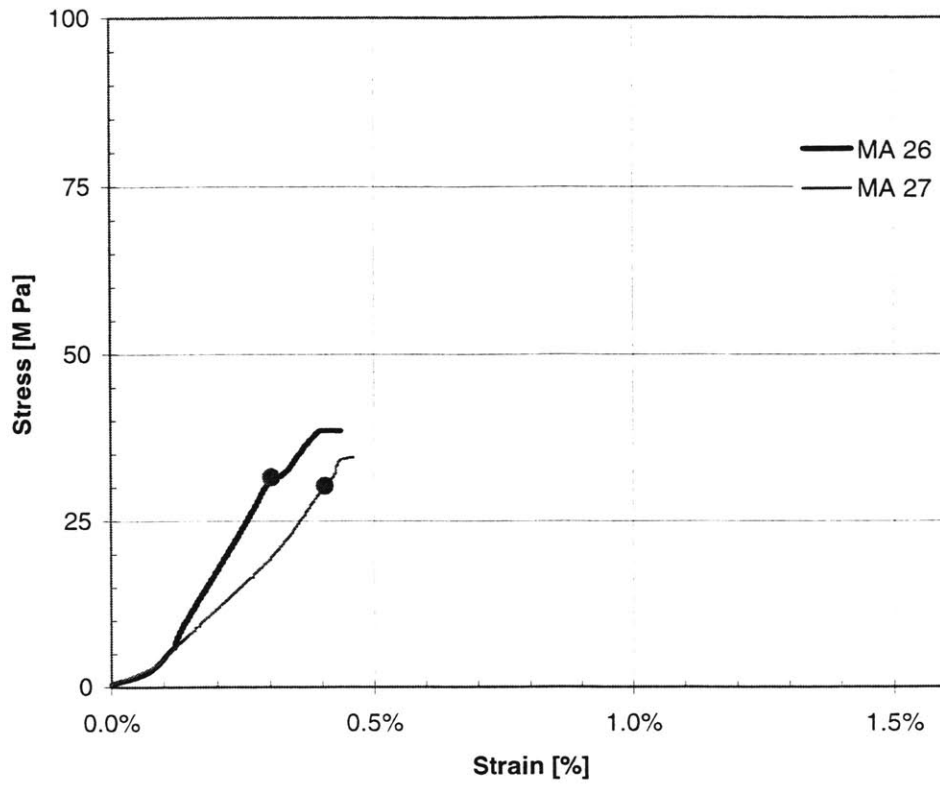


Figure C.12: Stress-strain curves for marble specimens with geometry 60-0-2a.

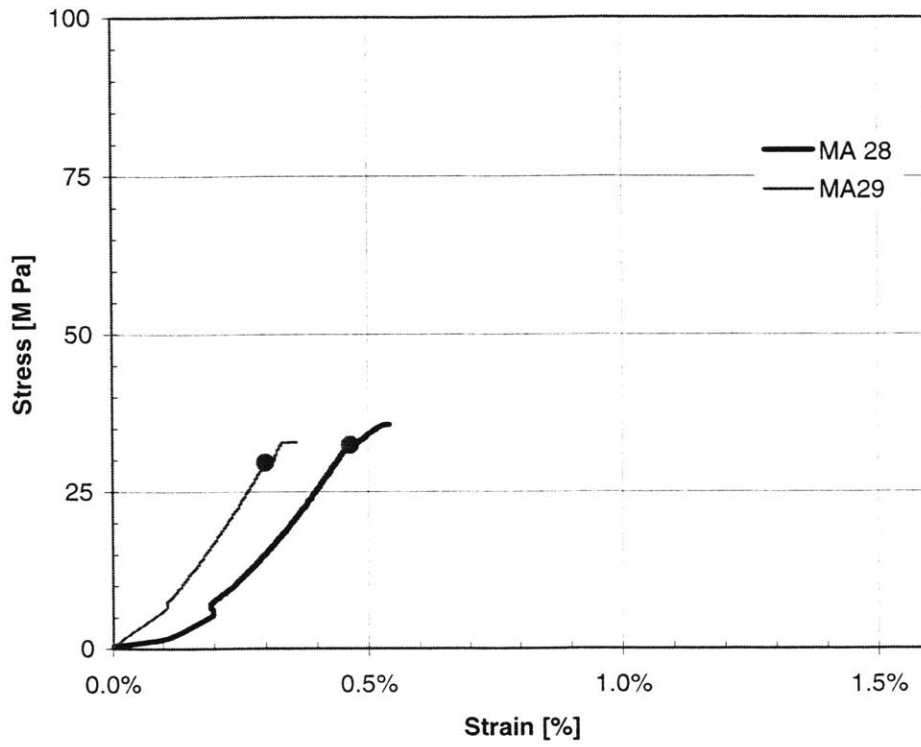


Figure C.13: Stress-strain curves for marble specimens with geometry 60-a-2a

APPENDIX D: Lab Equipment Improvement Alternatives

D.1 Introduction:

The objective of this appendix is to discuss different alternatives to improve the existent lab equipment for rock testing, data and image acquisition by acquiring new technologies and/or retrofitting some of the existent equipment.

The new equipment will be able to improve and coordinate the present capabilities.

D.2 Overview of the existing equipment

The Lab Procedure in Appendix A has a detailed description of the present equipment, the functions and limitations.

In essence, the present equipment contains two different data flows as indicated in figure D.1. These are: The data coming from the data acquisition system (1) that are stored in a data file in the PC that operates the loading machine, and (2) the image acquired with either the high speed camera (2A), or the standard camera (2A), or both. In the case of the high-speed camera the images are first stored in solid memory in the image processor; from there, they can be transferred to either a VCR or, in digital format, into a PC. The standard camera records directly into a VCR (2B). In both cases, after the images are stored on videotape, they are digitized using a frame grabber and its software.

The high-speed camera currently in use (Kodak Ektapro 1000 Motion System) belongs to the Edgerton Lab (see Appendix A for a description).

The next subsections cover the elements that should be bought. Different alternatives, advantages, disadvantages and relative costs are given.

D.3. Equipment to be acquired

This section describes different pieces of equipment. These pieces are part of the upgrade alternatives discussed in Section D.4.

D.3.1. High-Speed Camera:

Three acquisition choices have been evaluated:

A. Tech Imaging: **MotionScope 1,000S**. This is a fully integrated, high-speed CCD video system with a built-in digital memory storage, 5” monochrome monitor and integral keypad system operation. The system includes a power cable, extended record software, camera head with 15 feet video cable, and the operator manual. A “Maximum Memory” upgrade is necessary to have the necessary recording time at different recording rates. Table D.1 shows the advantage of having a “maximum memory” upgrade; the table lists both the “real” recorded time at high speed and the number of frames. Note that the number of stored frames remains constant for the same memory capacity. Just for reference, is convenient to mention that a standard camera records at 30 or 36 frames per second.

An accessory kit is available (to be bought separately), which includes a tripod, lights, lenses, etc. In addition, a 1,000 watt halogen lamp is necessary.

- Disadvantage: Analog video. There is no way to coordinate the images with the data acquisition data. This equipment has the same capabilities as the available now.
- Advantages: Better resolution.
- Approximate cost: \$ 23,000
- Contact: Len D’Avolio at Tech Imaging: (617) 539-0099 to set a demo.

B. Tech Imaging: **MotionScope PCI 1,000**: This analysis system has simplified high-speed image acquisition for in-depth image analysis. Designed as a PC peripheral for capturing high-speed images directly into the PC. The system consists of a high-speed camera, a full size PCI camera control frame store board (onboard memory), installation and user interface software. Up to four MotionScope PCI cameras can be operated with a single PC, providing multiple views of a high-speed event. The board is provided with RCA output for display or storage in videotapes. An option to acquire images of both sides of the specimens at the same time would be having two cameras (for example a 1,000 and 500 frames per second), connected to one board.

- Disadvantage: The included software has to be personalized to coordinate the images with the data acquisition system. This job is done by the provider (they are not sure if it is possible) at an extra charge.
- Advantage: Digital video. Compact system (there is no separated video monitor, the images are seen directly in the computer monitor).
- Approximate cost: \$ 25,000 for one MotionScope PCI 1,000.
\$ 38,000 for two MotionScope PCI (a 1,000 and a 500)
- Contact: Len D'Avolio at Tech Imaging: (617) 539-0099 to set a demo.

C. KODAK: **Motion Corder Analyzer. Model SR-1000 + Multi-Channel Data Link.**

(See figure D.2). This is a high-speed motion analysis system. It has been evaluated as an alternative, since is the only system (as of to date) that provides the possibility to connect other signals into the video monitor. (Through a “Multi-Channel Data Link”). The captured images may be transferred to videotape or downloaded as TIFF files directly to a PC via a SCSI-2 port. Note that this Multi-Channel Data Link is an accessory of this camera and hence cannot be used with any other high-speed camera from either Kodak or other manufacturer.

The “Multi-Channel Data Link” can measure analog voltage levels of transducers such as actuators, sensors, and other dynamic devices and **simultaneously** record this data along with the video image of a high-speed event. As shown in figure D.3 and

during playback, the data are displayed on the monitor screen, adjacent to the actual images of the event. Digital data are displayed in up to six boxes in the screen. Analog data are displayed in up to two charts at the bottom of the screen.

- Disadvantage: Analog video. Resolution is 256X 256 pixels (The same as the one in use now). Adding an extra camera would be expensive since it is necessary to buy another image processor.
- Advantage: No necessity to buy a new PC, to modify, or touch anything in the data acquisition + feedback loop control of the testing machine. No need to personalize or deal with any software.
- Approximate cost: \$ 25,000.
Extra camera: add \$ 19,000 (too expensive).
- Contact: 1-800-462-4307 (7AM to 4PM PST).

D.3.2. PC (with monitor):

Some of the improvement alternatives require a new PC. It has to be at least a 450Mhz processor (or better as available). The RAM (read access memory) should be as big as possible (128 Mb), since is where the images are stored (besides in the PCI boards).

- Approximate cost: \$2,500 + software licenses.
- Contact: CompUSA, or Micro Center. Both in Cambridge.

D.3.3 (Postmortem) Image processing software

Some of the options require a postmortem image processing software to digitize and analyze the images from the videotapes. The best two found alternatives are:

A. **IMAQ Vision (+ LabView)**: see description in National Instruments handbook. This software can be used to both acquire and process the images. Either digital cameras or analog cameras (connected through a PCI board or a normal frame grabber board) may be used.

- Approximate cost :\$ 995 (Base version) + LabView (\$1,000 extra)
- Contact: www.natinst.com

B. **Leica QWin Image Processing and Analysis Software**: This system combines higher speed image acquisition, better resolution, and sophisticated image processing techniques (might be in fact too sophisticated fracture mechanics testing). This software can be used for post-mortem image processing (i.e. after finish testing).

- Approximate cost :\$ 2,000
- Contact: www.leica.co.uk

D.4. Alternatives

This section contains a brief description of the studied alternatives for complete lab upgrades; also relative advantages and disadvantages are discussed (note that this section shows complete alternatives and not only isolated equipment). The costs include everything to have the equipment running, but not installation costs. The installation can be easily done. The costs do not include any accessories (see Section D.5).

D.4.1 Just buy a high-speed camera and leave everything else as it is now.

This alternative is the cheapest, but for a little more money is possible to access to alternative D.4.4. The options are:

- Options + cost: Buy camera option D.3.1.A → \$23,000
Buy camera option D.3.2.B + PC → \$28,000
- Advantages: Cheapest alternatives
- Disadvantages: Needs coordination. It would be the same as the equipment be have (and borrow) now.

D.4.2 Plug two cameras in the same frame grabber card and coordinate everything with real time after testing.

Figure D.4 shows this alternative using the standard camera already available plus one high-speed camera.

The video data can be stored either in drives or in videotapes (or both). The postmortem image processing software (i.e. Leica Qwin or the other option described in D.3.3) is necessary to process images in order to obtain good quality prints. It would also be very good to perform fractography analysis. (See Section 4.6). During testing only the Mtest2 software and the high-speed camera software are running. The only difficult point in this alternative is that the PCI card, which comes with the high-speed camera, allows one to plug two high-speed cameras (not one high-speed + a standard camera, unless the software is modified, at an extra cost).

- cost: of buying 1 high-speed camera and personalize software →\$37,000
(Approximate)
- Advantages: Everything is visible in the PC monitor
- Disadvantages: Needs coordination. It is expensive.

D.4.3 Same as D.4.2 but coordinates everything by using LabView. It will require programming time (Best estimate: 2 months).

- Cost: \$ 44,000

- Advantages: Everything is visible and is coordinated in the PC monitor
- Disadvantages: Needs **a lot** of programming time. Still needs image postmortem analysis.

D.4.4 Use Multi-Channel data link (KODAK) to get everything in the high-speed camera monitor. This high-speed motion system is described in subsection D.3.1C (see also figures D.2 and D.3). It is the **best alternative** in terms of cost, ease of installation, and features, besides having good technical support. It allows one to coordinate all the information in the monitor of the high-speed camera. The stress strain data are connected also to the monitor through the “Multi Channel Data Link” (see figure D.5). A new PC is not necessary. However, it would be convenient to buy a 15” high-resolution monitor, and a frame grabber card to be installed in any of the CEE PC to allow image processing.

- Cost: \$ 27,000 (cam + data link + monitor + accessories)
- Advantages: Everything is visible in the high-speed camera monitor (Specimen shots, and stress strain data). Cheap. Only one provider.
- Disadvantages: Needs postmortem image analysis. Acquiring a second high-speed camera to obtain images of both faces is possible, but it would be expensive (\$19,000).

D.4.5 Use video strain extensometer software + LabView + high-speed camera.

This alternative is using the same elements as alternative D.4.3, but it adds video extensometers (available from Instron). This is only software that allows one to compute 2-d strains by using video images. Note that this would be very useful since the initiation of cracks tend to affect horizontal strains, Wong and Chau (1998). This analysis software may even use the images from the high-speed camera. At the moment this software only allows postmortem strain analysis and could even have some problems in being

coordinated with LabView. The Instron service Center promises that these problems will be solved by 1999.

- Cost: \$54,000
- Advantages: Complete coordination + good quality strain recording
- Disadvantages: It is still not available. Also same disadvantages as alternative D.4.3. Very expensive now, but cost will decrease.

D.5. Accesories

This is a list of secondary things to be obtained. They have low cost and can make a difference in terms of productivity and data quality.

- Caliper with laser output: It allows up to three readings to be downloaded directly to the PC through an infrared device. It helps reducing the occurrence of mistakes.
- Laser printer set in photo quality. This can make a big difference in terms of the obtained printed quality, which is very poor with the printers in the CEE net (at least with the actual configuration).
- Zip or Ditto drives. They allow storage of big amounts of data. They can be external or internal drivers installed in the PC (Now available also in the CEE-net).
- Net connection. This would simplify the transfer of information, and reduce the possibility of errors due to different software versions

The total cost of these secondary items is about \$ 2,000.

Record Rate [frames/sec]	Std Memory [sec]/[frames]	Maximum Memory [sec]/[frames]
60	8.5/512	34.1/2,048
125	4.1/512	16.4/2,048
250	2.0/512	8.2/2,048
500	2.0/1024	8.2/4,096
1000	2.0/2048	8.2/8192

Table D.1: Recording time [Seconds] and Frame Storage capacity of Motion Scope 1000 S motion system

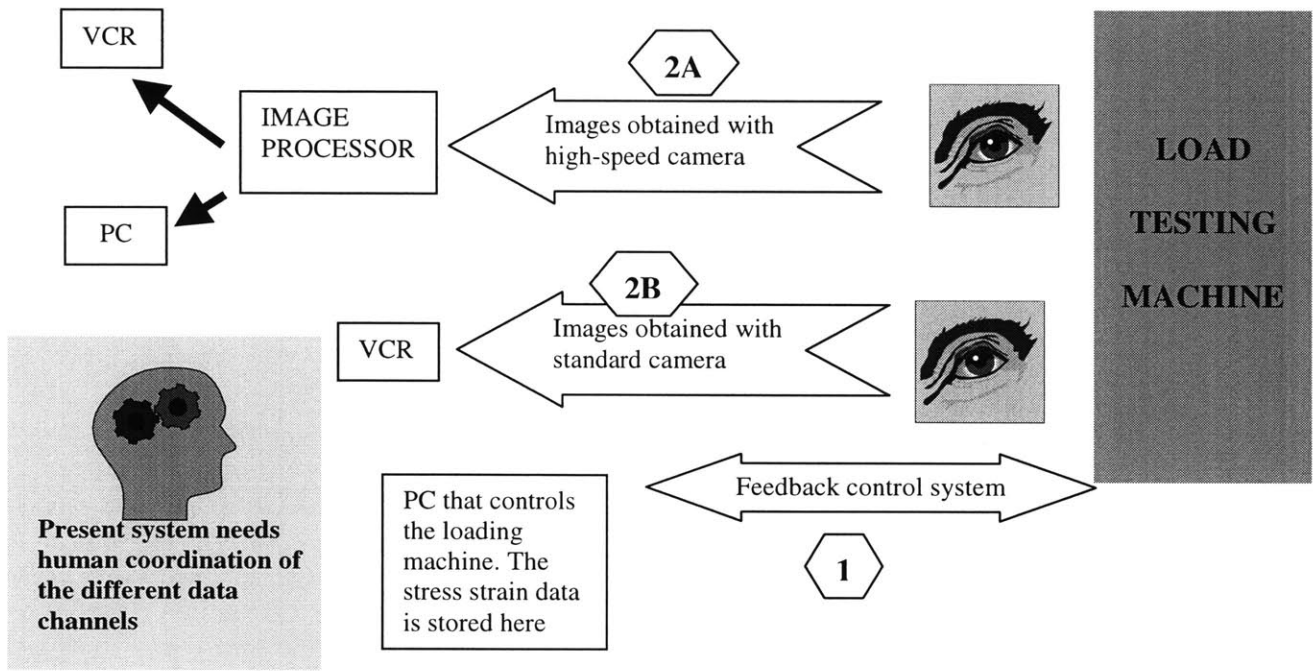


Figure D.1: Data flow with the existent lab equipment.



Figure D.2: Kodak SR-1000. High-speed motion system.

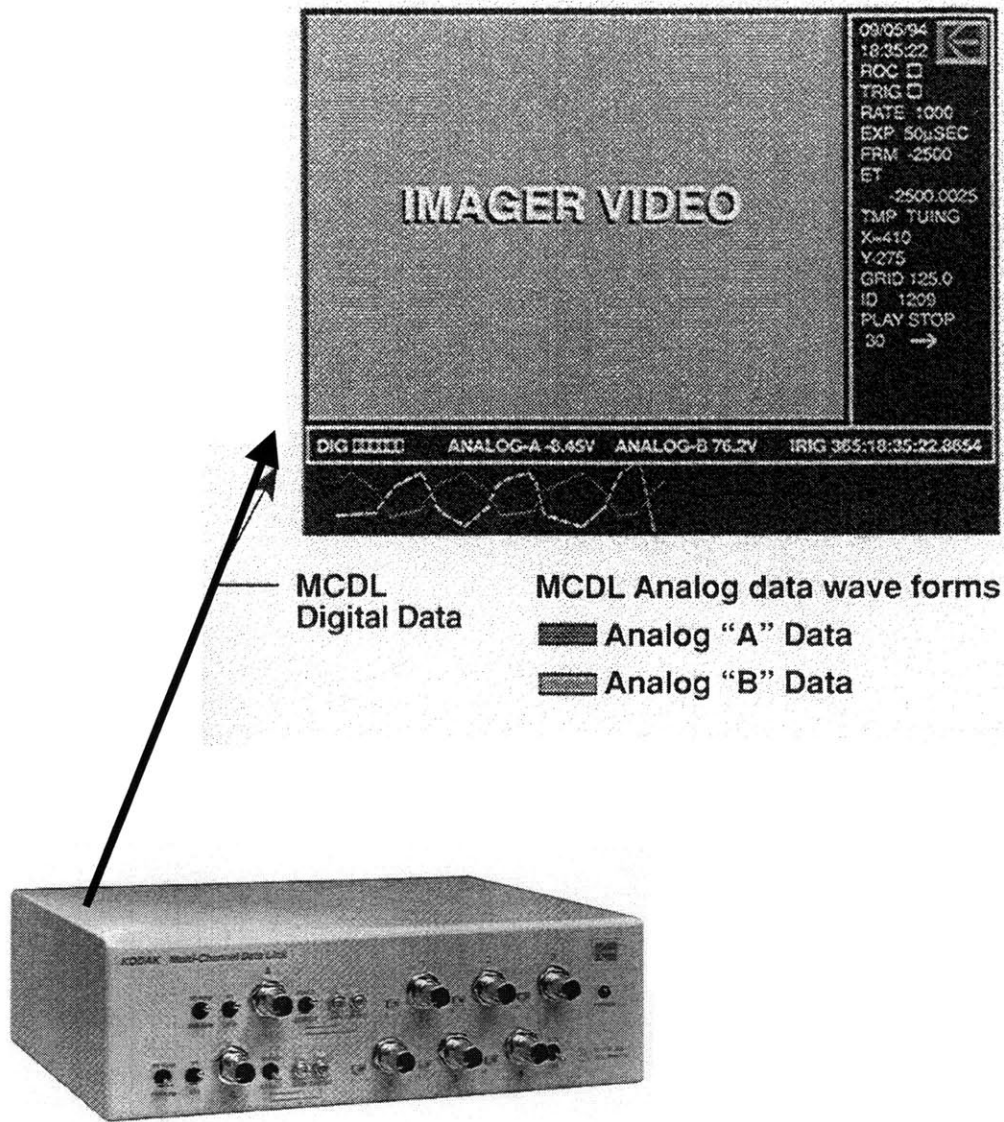


Figure D.3: Multi channel data link. Note how the data is displayed in the video monitor allowing one to observe the images and data (stresses) at the same time

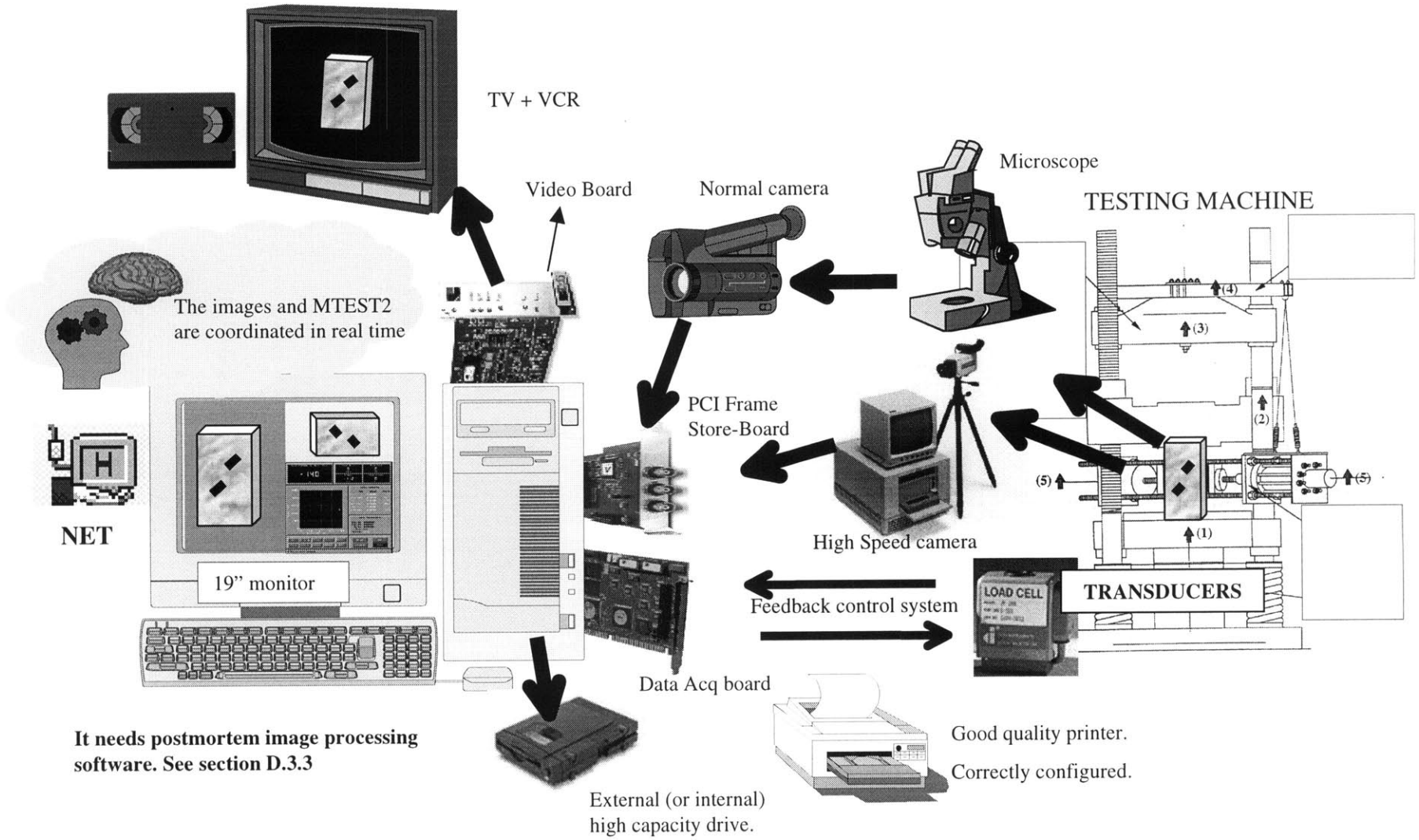


Figure D.4: Alternative showing the use of the std camera + one high speed camera.

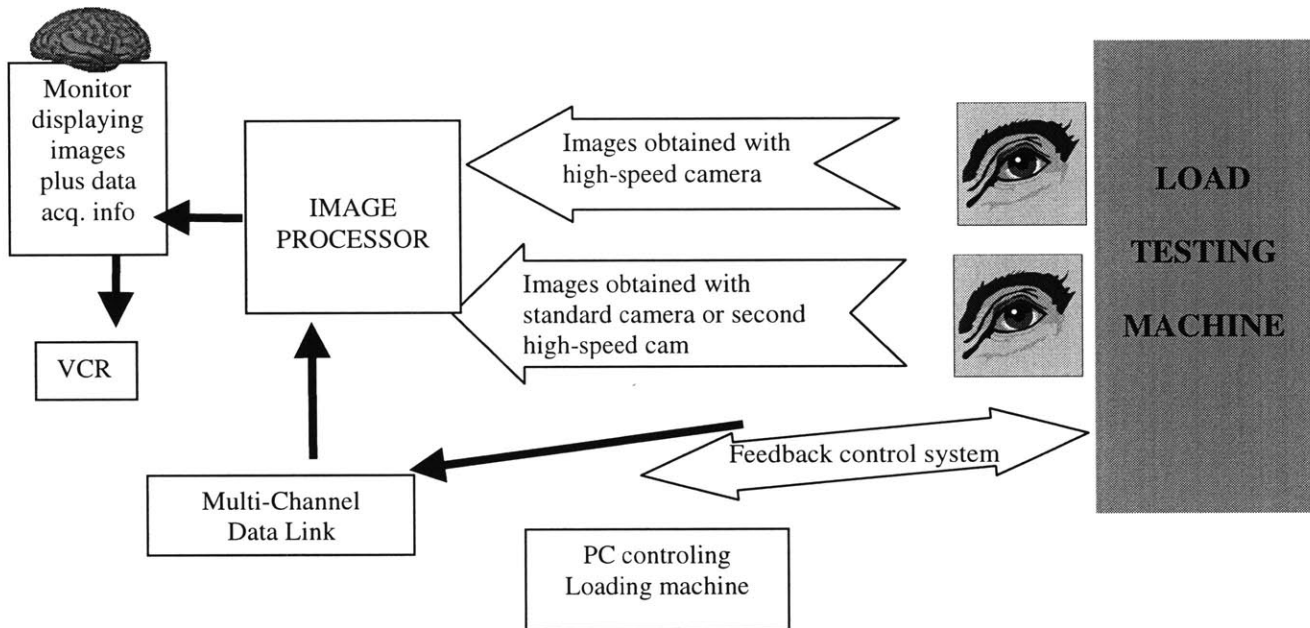


Figure D.5: Lab data flow using the Kodak SR-1000 high-speed motion system. Note use of multi-channel data link

References

- Ameen, M.S. Fractography: Fracture Topography as a Tool in Fracture Mechanics and Stress Analysis. Geological Society Special Publication No. 92, pp 1- 10, 59-83, 1995
- Atkinson, B.K. Fracture Mechanics of Rocks. Harcourt Brace Jovanovich, pp. 1-23, 27-59, 74-90, 1987.
- Aydan, O. N. et. al. Deformability and Strength of Discontinuous Rock Masses. Fractured and Jointed Rock Masses. Myer, Cook, Goodman, and Tsang (eds.), pp. 255-262, 1996.
- Bles, J.L. and Feuga, B. The Fracture of Rocks. Elsevier, 1986.
- Bobet A. Fracture Coalescence in Rock Material: Experimental Observations and Numerical Predictions. Ph.D. Thesis, Massachusetts Institute of Technology, Cambridge, MA, USA. 1997.
- Broek, D. Elementary Engineering Fracture Mechanics. Kluwer Academic Publisher, Norwell, MA, USA, 1991.
- Chen, G.J. et. al. Fracture Propagation and Coalescence in Marble Plates with Pre-Cut Notches under Compression, Symposium on Fractured and Jointed Rock Mass, Lake Tahoe, CA, pp. 443-448, 1992.
- Chernyshev, S.N. and Dearman, W.R. Rock Fractures. Butterworth-Heinemann (eds.), 1991.
- Coates, D.F. Rock Mechanics Principles, pp. 1-128, 1981.
- Deere, D.U. Rock Mechanics in Engineering Practice, by Stagg, KG. and Zienkiewicz, O.C. Wiley & Sons, 1968.
- Dyskin, A. V. et. al. Modeling Crack Propagation in Compression. Rock Mechanics, Nelson and Laubach (eds.), pp. 451-460, 1994.
- Dyskin, A.V. et. al. Some Experimental Results on Three-Dimensional Crack Propagation in Compression. Mechanics of Jointed and Faulted Rock, Rossmannith (ed) Rotterdam, 91-96, 1995.
- Einstein, H.H. and Dershowitz, W.S. Tensile and Shear Fracturing in Predominantly Compressive Stress Fields- a Review. Engineering Geology, 29. Elsevier Science Publishers, B. V. Amsterdam, pp. 149-171, 1990.

Eshwaraiyah, H.V. and Upadhyaya. Influence of Rock Joints in the Performance of Major Civil Engineering Structures. Mechanics of Jointed and Faulted Rock. pp. 951-958, Rossmanith (ed.) Rotterdam, 1990.

Fidalgo Valverde, B. Fracture Coalescence in Rocks under Uniaxial Compression. M.Sc. Thesis, Camborne School of Mines, University of Exeter, 1998.

Gramberg, J. A Non-Conventional View on Rock Mechanics and Fracture Mechanics. A.A. Balkema, Rotterdam, 1989.

Griffith, A.A. The Phenomenon of Rupture and Flow in Solids. Philosophical Transactions of the Royal Society of London, Series A, 221, pp. 163-198, 1921.

Hakami, E. and Einstein, H.H. Characterization of Fracture Apertures- Methods and Parameters. Proceeding Pre-print for the 8th International Conference of the IRMS, International Society of Rock Mechanics.

Harrison, J.P. Engineering Rock Mechanics. An Introduction to the Principles, 1997.

Hoek, E. Brittle Failure of Rock. Imperial College Rock Mechanics Research Report No 2. 1967.

Hoek, E. and Bieniawski. Brittle Fracture Propagation in Rock under Compression. International Journal of Fracture 26. Pp. 276-294, 1984

Hoek, E. and Bray, J.W. Rock Slope Engineering. Institute of Mining and Metall, 3rd edition, 1981.

Hoek, E. and Brown, E.T. Underground Excavations in Rock. McGraw-Hill Book Co. USA, 1980.

Hudson, J.A. Engineering Rock Mechanics. An Introduction to the Principles. Pergamon, pp. 13-115, 1997.

Ingraffea, A.R., Heuze, F.E. An Analysis of Discrete Fracture Propagation in Rock Loaded in Compression. Proceedings of the 18th U.S. Symposium on Rock Mechanics, Keystone, Colorado, pp. 2A4-1 to 2A4-7, 1977.

Jiefan, H. et. al. An Experimental Study of the Strain Field Development Prior to Failure of a Marble Plate under Compression. Tectonophysics, Vol. 175, pp. 283-290, 1990

Karaka, M. et. al. Mechanics of Failure around Shallow Tunnels in Jointed Rock. Mechanics of Jointed and Faulted Rock. pp. 771-776, Rossmanith (ed.) Balkema Rotterdam, 1995.

Kessler, D.W. et. al. Physical, Mineralogical, and Durability Studies on the Building and Monumental Granites of the United States. Journal of Research of the National Bureau of Standards, Vol 25, No 2, Paper RPI1320, August 1940.

Lajtai, E.Z. Brittle Fracture in Compression. International Journal of Fracture, Vol 10 N4, pp. 525-536, 1974.

Li, C.O. et. al. Behavior of Rock Joints and rock Bridges in Shearing Testing. Rock Joints, Barton and Stephanson (eds.), pp. 259-266, 1990.

Mtest2, Material Testing System User Manual. Advanced Machine Technology, Inc. 767 Concord Av. Cambridge, MA, USA.

Moore, D.E. et. al. Deformation of Granite During Triaxial Load Friction tests. Mechanics of Jointed and Faulted Rock, Rotterdam, pp. 345-352, 1990.

Petit, J. and Barquins, M. Can Natural Faults Propagate Under Mode II Conditions?. Tectonics, Vol 7, N6, pp. 1246-1265, 1988.

Pollard, D.D. et. al. Understanding the Process of Jointing in Brittle Rock Masses. Proceedings: 31st U.S. Symposium on Rock Mechanics, A.A. Balkema (ed.), Rotterdam, pp. 447-454, 1990.

Pusch, R. Rock Mechanics on a Geological Base. Developments in Geotechnical Engineering 77. Elsevier, 1995.

Reyes, O. M. Experimental Study an Analytical Modeling of Compressive Fracture in Brittle Materials. Ph.D. Thesis, Massachusetts Institute of Technology, Cambridge, MA, USA. 1991.

Reyes, O. and Einstein, H.H. Failure Mechanism of Fractured Rock- A Fracture Coalescence Model. Proceedings 7th International Congress of Rock Mechanics, Vol. 1, pp. 333-340, 1991.

Shen, B. and Stephansson, O. Deformation and Propagation of Finite Joints in Rock Masses, Symposium on Fractured and Jointed Rock Mass, Lake Tahoe, CA. Pp. 303-309, 1995.

Shen, B. et al. Coalescence of Fractures under Shear Stress experiments. Journal of Geophysical Research, 100, pp. 5975-5990, 1995.

Stokes, W.L. and D.J. Varnes. Glossary of Selected Geology Terms. Colorado School of Mines, 1955.

Takeuchi, K. Mixed-mode Fracture Initiation in Granular Brittle Materials. Ph.D. Thesis, Massachusetts Institute of Technology, Cambridge, MA, USA. 1991.

Tarbut, E.J. and Lutgens, F. R. Earth an Introduction to Physical Geology. Prentice Hall, 1996.

Vallejo, L. The Influence of Fissures in a Stiff Clay Subjected to Direct Shear. Geotechnique 37, No1, 69-82, 1987.

Wade, F.A. and Mattox, R. B. Elements of Crystallography and Mineralogy. Pp. 103-112, 1960.

Wong, H. C. and Chau, K. T. Crack Coalescence in a Rock-Like Material Containing Two Cracks, Proceedings, International J. Rock Mechanics Min. Science, Vol. 35, N2, pp.147-164, 1998.

Biographical Note

Name: Ariel R. Martinez

Born: 1972 in Cordoba, Argentina.

EDUCATION:

- | | |
|-----------|---|
| 1997-1999 | Master of Science in Civil Engineering.
Massachusetts Institute of Technology. |
| 1991-1996 | Ingeniero Civil (6 year degree).
Universidad de Buenos Aires, Argentina. |

RESEARCH AND TEACHING EXPERIENCE

- | | |
|-----------|---|
| 1992-1995 | Teaching Assistant: Algebra II. |
| 1994-1997 | Teaching Assistant: Behavior of Engineering Materials |
| 1994-1995 | Research Assistant – Materials and Structures Lab.
University of Buenos Aires, Argentina. |
| 1998-1999 | Research Assistant-Civil and Environmental Engineering
Massachusetts Institute of Technology |

PROFESSIONAL EXPERIENCE

- | | |
|------------|---|
| 1997 | Global Retail Image Supervisor
SHELL (Buenos Aires, Argentina) |
| 1996- 1997 | Assistant Design Engineer.
GIC Consultant Engineers. Buenos Aires, Argentina |

AWARDS:

- | | |
|------|---|
| 1996 | Argentine Structural Engineers Association Annual Award . |
|------|---|

PROFESSIONAL MEMBERSHIPS

ASCE, American Society of Civil Engineers.